Modes dégradés résultant de l'utilisation multi constellation du GNSS

Christophe Ouzeau

THÈSE

En vue de l'obtention du

DOCTORAT DE L'UNIVERSITÉ DE TOULOUSE

Délivré par *l'Institut National Polytechnique de Toulouse*
Discipline ou spécialité : *télécommunications* - SIAO
Ecole doctorale : *Mathématiques Informatique Télécommunications de Toulouse*

Présentée et soutenue par *Christophe OUZEAU*
Le *08/04/2010*

Titre : *Modes dégradés résultant de l'utilisation multi constellation du GNSS*
Title : *Degraded Modes Resulting From the Multi Constellation Use of GNSS*

JURY
Pr Francis Castanié (Président)
Pr Igor Nikiforov (Rapporteur)
Pr Bernd Eissfeller (Rapporteur)
Dr Christophe Macabiau (Directeur)
Dr Benoît Roturier (Examinateur)

Résumé

Actuellement, on constate dans le domaine de la navigation, un besoin croissant de localisation par satellites. Après une course à l'amélioration de la précision (maintenant proche de quelques centimètres grâce à des techniques de lever d'ambiguïté sur des mesures de phase), la relève du nouveau défi de l'amélioration de l'intégrité du GNSS (GPS, Galileo) est à présent engagée. L'intégrité représente le degré de confiance que l'on peut placer dans l'exactitude des informations fournies par le système, ainsi que la capacité à avertir l'utilisateur d'un dysfonctionnement du GNSS dans un délai raisonnable.
Le concept d'intégrité du GNSS multi-constellation nécessite une coordination au niveau de l'architecture des futurs récepteurs combinés (GPS-Galileo). Le fonctionnement d'un tel récepteur dans le cas de passage du système multi-constellation en mode dégradé est un problème très important pour l'intégrité de navigation.

Cette thèse se focalise sur les problèmes liés à la navigation aéronautique multi-constellation et multi-système GNSS. En particulier, les conditions de fourniture de solution de navigation intègre sont évaluées durant la phase d'approche APV I (avec guidage vertical). En disposant du GPS existant, du système Galileo et d'un système complémentaire géostationnaire (SBAS), dont les satellites émettent sur des fréquences aéronautiques en bande ARNS, la question fondamentale est comment tirer tous les bénéfices d'un tel système multi-constellation pour un récepteur embarqué à bord d'un avion civil. En particulier, la question du maintien du niveau de performance durant cette phase de vol APV, en termes de précision, continuité, intégrité et disponibilité, lorsque l'une des composantes du système est dégradée ou perdu, doit être résolue.

L'objectif de ce travail de thèse est donc d'étudier la capacité d'un récepteur combiné avionique d'effectuer la tâche de reconfiguration de l'algorithme de traitement après l'apparition de pannes ou d'interférences dans une partie du système GNSS multi-constellation et d'émettre un signal d'alarme dans le cas où les performances de la partie du système non contaminée ne sont pas suffisantes pour continuer l'opération en cours en respectant les exigences de l'aviation civile. Egalement, l'objectif de ce travail est d'étudier les méthodes associées à l'exécution de cette reconfiguration pour garantir l'utilisation de la partie du système GNSS multi-constellation non contaminée dans les meilleures conditions.
Cette étude a donc un intérêt pour les constructeurs des futurs récepteurs avioniques multi-constellation.

Abstract

The International Civil Aviation Organization (ICAO) has defined the concept of Global Navigation Satellite System (GNSS), which corresponds to the set of systems allowing to perform satellite-based navigation while fulfilling ICAO requirements.

The US Global Positioning Sysem (GPS) is a satellite-based navigation system which constitutes one of the components of the GNSS. Currently, this system broadcasts a civil signal, called L1 C/A, within an Aeronautical Radio Navigation Services (ARNS) band. The GPS is being modernized and will broadcast two new civil signals: L2C (not in an ARNS band) and L5 in another ARNS band.

Galileo is the European counterpart of GPS. It will broadcast three signals in an ARNS band: Galileo E1 OS (Open Service) will be transmitted in the GPS L1 frequency band and Galileo E5a and E5b will be broadcasted in the same 960-1215 MHz ARNS band than that of GPS L5.

GPS L5 and Galileo E1, E5a, E5b components are expected to provide operational benefits for civil aviation use. However, civil aviation requirements are very stringent and up to now, the bare systems alone cannot be used as a means of navigation. For instance, the GPS standalone does not implement sufficient integrity monitoring.
Therefore, in order to ensure the levels of performance required by civil aviation in terms of accuracy, integrity, continuity of service and availability, ICAO standards define different systems/algorithms to augment the basic constellations. GPS, Galileo and the augmentation systems could be combined to comply with the ICAO requirements and complete the lack of GPS or Galileo standalone performance.

In order to take benefits of new GNSS signals, and to provide the service level required by the ICAO, the architecture of future combined GNSS receivers must be standardized. The European Organization for Civil Aviation Equipment (EUROCAE) Working Group 62, which is in charge of Galileo standardization for civil aviation in Europe, proposes new combined receivers architectures, in coordination with the Radio Technical Commission for Aeronautics (RTCA).

The main objective of this thesis is to contribute to the efforts made by the WG 62 by providing inputs necessary to build future receivers architecture to take benefits of GPS, Galileo and augmentation systems. In this report, we propose some key elements of the combined receivers' architecture to comply with approach phases of flight requirements.

In case of perturbation preventing one of the needed GNSS components to meet a phase of flight required performance, it is necessary to be able to switch to another available component in order to try to maintain if possible the level of performance in terms of continuity, integrity, availability and accuracy. That is why future combined receivers must be capable of detecting the impact of perturbations that may lead to the loss of one GNSS component, in order to be able to initiate a switch. These perturbations are mainly atmospheric disturbances, interferences and multipath. In this thesis we focus on the particular cases of interferences and ionosphere perturbations.

The interferences are among the most feared events in civil aviation use of GNSS. Detection, estimation and removal of the effect of interference on GNSS signals remain open issues and may affect pseudorange measurements accuracy, as well as integrity, continuity and availability of these measurements. In literature, many different interference detection algorithms have been proposed, at the receiver antenna level, at the front-end level. Detection within tracking loops is not widely studied to our knowledge. That is why, in this thesis, we address the problem of interference detection at the correlators outputs. The particular case of CW interferences detection on the GPS L1 C/A and Galileo E1 OS signals processing is proposed.

Nominal dual frequency measurements provide a good estimation of ionospheric delay. In addition, the combination of GPS or GALILEO navigation signals processing at the receiver level is expected to provide important improvements for civil aviation. It could, potentially with augmentations, provide better accuracy and availability of ionospheric correction measurements. Indeed, GPS users will be able to combine GPS L1 and L5 frequencies, and future GALILEO E1 and E5 signals will bring their contribution. However, if affected by a Radio Frequency Interference, a receiver can lose one or more frequencies leading to the use of only one frequency to estimate the ionospheric code delay.
Therefore, it is felt by the authors as an important task to investigate techniques aimed at sustaining multi-frequency performance when a multi constellation receiver installed in an aircraft is suddenly affected by radiofrequency interference, during critical phases of flight. This problem is identified for instance in [NATS, 2003]. Consequently, in this thesis, we investigate techniques to maintain dual frequency performances when a frequency is lost (L1 C/A or E1 OS for instance) after an interference occurrence.

Remerciements / Acknowledgments

Je tiens tout d'abord à remercier mon directeur de thèse, Christophe Macabiau. Tu m'as permis de commencer cette thèse dans de bonnes conditions. Tes conseils précieux m'ont permis d'améliorer considérablement mon travail. De plus, je te remercie pour avoir relu à plusieurs reprises ce rapport. Merci aussi pour tes qualités humaines et tes rires bruyants.

Merci à Benoît d'avoir cru en ce travail et m'avoir permis de mener à bout ces travaux de recherche.

Merci à Frédéric Bastide pour la qualité de son encadrement et ses conseils avisés lors des premiers mois de cette thèse.

I thank all the EUROCAE members for their remarks about this thesis. I was really pleased to work with you. I'd like to thanks in particular, Benoît, Mikael, Laurent and Eric. It was really a pleasure to work with you!

Merci au Professeur Igor Nikiforov pour avoir accepté d'être rapporteur de cette thèse et merci pour tous ses conseils.

I would like also to thank Pr Bernd Eissfeller for being my reviewer and for its remarks and advices during my PhD defense.

Merci à Francis Castanié pour avoir été mon président de jury de thèse, pour sa sympathie, mais aussi pour toutes les discussions intéressantes que nous avons eues tout au long des mon séjour au TéSA.

Je remercie tous mes anciens collègues du LTST dans l'ordre alphabétique : Axel, Damien, Damien, Emilie, Hanaa, Anais, Mathieu, Na, Olivier, Anne-Christine, Paul, Philippe et Gaël. Merci à vous tous pour ces excellentes conditions de travail. Ce fut un plaisir de travailler en votre compagnie.

Je tiens à remercier Hanaa, Na et Cyril pour leurs relectures de ce rapport et leurs conseils avisés.

J'ai été très heureux de pouvoir travailler en compagnie de nombreux collègues d'une grande sympathie et d'une grande générosité à l'ENAC. Je ne peux malheureusement tous vous citer tant vous êtes nombreux ! Merci à Coco et Cathy pour leur soutien administratif mais aussi humain.

Un grand merci aussi à tous les collègues du TéSA. Je pense en particulier à Marie-Jo et Sarah, dont la bonne humeur a ensoleillé chaque matin de mes passages au TéSA. Merci aussi les filles pour la préparation de mes nombreuses missions parfois un peu compliquées !

I really thank Chris Hegarty for giving me advices about ionospheric code delay estimations and for our pleasant discussions about my thesis and some professional points.

Je fais une grosse bise à toute ma famille pour tout ;).

Sommaire / Outline

List of figures

List of tables

Glossary

AAIM	Aircraft-based Autonomous Integrity Monitoring
ABAS	Aircraft Based Augmentation System
AIC	Aeronautical Information Circular
AIP	Aeronautical Information Publication
AIRAC	Aeronautical Information Regulation And Control
AMC	Acceptable Means of Compliance
ANP	Actual Navigation Performance
APV	Approach with Vertical Guidance
ARNS	Aeronautical Radio Navigation Services
ARINC	Aeronautical Radio Incorporated
ATC	Air Traffic Control
BER	Bit Error Rate
CDI	Course Deviation Indicator
CDU	Cockpit Display Unit
CONUS	CONtinental United States
DAC	Direction de l'Aviation Civile
DLL	Delay Lock Loop
DTK	Desired Track
DER	Departure End of the Runway
DME	Distance Measuring Equipment
EASA	European Aviation Safety Agency
ECAC	European Civil Aviation Conference
EGNOS	European Global Navigation Overlay Service
EPE	Estimated Position Error
EPU	Estimated Position Uncertainty
ETA	Estimated Time of Arrival
EUROCAE	European Organization for Civil Aviation Equipment
FAF	Final Approach Fix
FAS	Final Approach Segment
FDE	Fault Detection and Exclusion
FFS	Full Flight Simulator
FMC	Flight Management Computer
FMS	Flight Management System
FNPT	Flight Navigation and Procedure Trainer
FTD	Flight Training Device
FTE	Flight Technical Error
GBAS	Ground Based Augmentation System
GLONASS	GLObal NAvigation Satellite System
GNSS	Global Navigation Satellite System (OACI terminology)
GPS	Global Positioning System
GGTO	GPS Galileo Time Offset
IAF	Initial Approach Fix
ICAO	International Civil Aviation Organisation

ICD	Interface Control Document
IF	Intermediate Fix
IF	Initial Fix (in ARINC 424 terminology)
IFR	Instrument Flight Rules
ILS	Instrument Landing System
IMC	Instrument Meteorological Conditions
IRS	Inertial Reference System
JAA	Joint Aviation Authorities
LNAV	Lateral Navigation
LOA	Letter Of Acceptance
MA	Missed Approach
MAP	Missed Approach Point
MDH	Minimum Descent Height
MEL	Minimum Equipment List (Liste Minimale d'Equipements)
MOPS	Minimum Operational Performance Specification
NDB	Non Directional Beacon
NOTAM	NOtice To AirMen
NPA	Non Precision Approach
OACI	Organisation de l'Aviation Civile Internationale
OCH	Obstacle Clearance Height (hauteur de franchissement d'obstacle)
OCP	Obstacle Clearance Panel (OACI)
PANS-OPS	Procedures for Air Navigation Services – Aircraft Operations
P_{FA}	False alarm rate
P_{FD}	Probability of false detection
P_{FE}	Probability of failed detection
P_{MA}	Missed alert rate
P_{MD}	Probability of missed detection
PLL	Phase Lock Loop
QFU	Direction magnétique de la piste
RAIM	Receiver Autonomous Integrity Monitoring
RNAV	Area Navigation
RTCA	Radio Technical Commission for Aeronautics
RVR	Runway Visual Range
SBAS	Satellite Based Augmentation System
SIS	Signal In Space
SOL	Safety Of Life
TAA	Terminal Arrival Altitude
TF	Track to Fix
TSO	Technical Service Order
VMC	Visual Meteorological Conditions
VOR VHF	Omni-directional Range
WAAS	Wide Area Augmentation System (United Stated of America)
WGS 84	World Geodetic System 1984
WP	Waypoint (point de cheminement)
XTE	Cross Track Error

Chapter 1

Introduction

Contents

1. Introduction

1.1. Background and motivations

With the multiplication of the satellite radio navigation systems (Global Navigation Satellite System: GNSS), the variety of radio navigation signals increases greatly. The development of GNSS is of interest for aeronautical applications.

Amongst the existing navigation systems, the Global Positioning System (GPS) provides an accurate positioning service but its standalone use cannot meet the civil aviation requirements (particularly for the demanding aircraft phases of flight). The GPS is modernized progressively with new signals transmitted by new satellites (block II-R, II-F and block III). Galileo is the European positioning system and will be operational in the next years.

The future Galileo E1, E5a/E5b and GPS L1 C/A, L1C, L5 signals are of particular interest for civil aviation community since they will be broadcasted in Aeronautical Radio Navigation Services (ARNS) frequency bands.

The constellation, the signals and the augmentation systems are all GNSS components that must be taken into account for aviation applications. If combined, these components are expected to provide operational benefits for civil aviation community.

The future civil aviation combined receivers must provide accurate, integrity-compliant and continuous measurements in concordance with the International Civil Aviation Organization (ICAO) requirements concerning the aircraft phases of flight.

For a targeted phase of flight, the GNSS components needed to meet the civil aviation requirements must be identified, and, in case of loss of component needed for perform the phase of flight, the receiver must be capable of switching to other available components to maintain, if possible, the level of performance. Indeed, the receiver must fully benefit from most of the available GNSS components. That is why receiver architecture must be established in compliance with the ICAO requirements.

For the purposes of civil aviation, many groups and organisms are in charge of validations and certifications of future civil aviation combined receivers. Amongst them, the EUROCAE (EURopean Organization for Civil Aviation Equipment) Working Group 62, in coordination with the RTCA (Radio Technical Commission for Aeronautics), proposes a Concept of Operation document (ConOps), which contains specifications for GPS/Galileo civil aviation receivers.

This thesis falls within the framework of the EUROCAE WG 62 ongoing work and is sponsored by the DTI (Direction de la Technique et de l'Innovation), which is a DGAC (Direction Générale de l'Aviation Civile) service.

Two points of interest are addressed in this thesis work:

- The capability of a combined receiver to initiate a switch between GNSS components combinations during aircraft operations, when it is necessary;
- After a loss of component, if the remaining components are not sufficient to reach the required performance level for a targeted phase of flight, the receiver must be capable to sign alert and to maintain as long as possible the level of performance required continuing an operation.

The first point implies to implement detection algorithms that will enable the receiver to detect a degradation of performance and thus, a loss of component. In the second point, the alert is mandatory in order to decide to use the combined receiver or not.

1.2. Thesis outline

The future receivers' architecture proposed by the EUROCAE Working Group 62 is the baseline of this thesis work. This document is organized as follows.

Chapter 2 presents the main GNSS components that are planned to be used for civil aviation, that is to say the GPS and Galileo constellations with a set of signals (L1 C/A, L5, E1 and E5) and augmentation systems. The different services provided by these components are described. Then, signals characteristics are recalled and signal processing within civil aviation receivers is detailed. A budget of the perturbations affecting the GNSS measurements is made. Finally, the civil aviation requirements are described.

Chapter 3 starts with the definition of aircraft navigation modes provided in [RTCA, 2006] or in [EUROCAE, 2007]. The identified GNSS components combinations are then classified by modes of operation. In coordination with the DTI, a global and generic combined receiver architecture is proposed in this chapter and is based on a switching logic between operational GNSS components combinations.

Chapter 4 describes in details the switching strategy between the GNSS components combinations, for the different modes of operation. The strategy proposed depends upon the availability of each GNSS component. Since the ICAO performance requirements are related to the phase of flight of the aircraft, the WG 62 decided to propose different switching strategies for two kinds of phases of flight (En route down to NPA and APV). Chapter 4 describes each strategy investigated in coordination with the DTI, and proposed to the WG62.

To initiate a switch between the GNSS components it is necessary to be able to detect performances degradations that lead to insufficient performances to perform a phase of flight. This concerns not only the integrity monitoring but also the continuity and the accuracy of the GNSS measurements.

Amongst the most feared physical phenomena which lead to degradation, and thus, a loss of component availability, the interferences impacts on ARNS signals processing have to

be monitored. Indeed, this phenomenon can affect simultaneously several GNSS measurements. Future combined GNSS receivers should be robust against interferences.

From a signal processing point of view, interference is one of the most feared event because it can caught simultaneously several GNSS frequencies. It can affect signals reception at front end level and can lead to a loss of lock in tracking loops. For this reason, Chapter 5 focuses on interference detection.

For civil aviation applications, interferences with power level below the masks defined in [EUROCAE, 2007] are expected to generate tracking errors within a low margin, so that it does not affect significantly the resulting pseudoranges and thus the navigation solution. In this study, it is shown that, even below the Radio Frequency Interference (RFI) masks, with low Doppler rate between the jammer and the incoming signal, the tracking errors induced by a Cosine Wave (CW) interference can be larger than expected in [EUROCAE, 2007]. This is all the more important for highly restrictive approach phases of flight in terms of accuracy. That is why this study focuses on detection of CW during a demanding approach phase of flight which requires vertical guidance (APV I).

After a RFI area crossing, the aircraft embedded receiver can lose one or more frequencies. In particular, the receiver can revert to a single frequency mode.

Amongst the sources of propagation errors, the ionosphere is a dispersive medium that can strongly affect the GPS and Galileo signals and thus, the resulting GNSS receiver measurements. It is the larger source of ranging error, if left uncorrected. In addition, this perturbation is difficult to model and thus difficult to predict. Indeed, it is dependent upon the aircraft location and the atmosphere behaviour which present a high variability.

A multi-frequency receiver can identify and correct errors induced by the ionosphere. Indeed, two frequencies are needed to determine precisely the ionospheric code delay. However, if affected by a radio frequency interference, a receiver can lose one or more frequencies leading to the use of only one frequency to estimate the ionospheric code delay. Therefore, it is identified by the WG62, in [NATS, 2003] and [Shau-Shiun Jan, 2003] as an important task to investigate techniques aimed at sustaining multi-frequency performance when a multi-constellation receiver installed onboard an aircraft is suddenly affected by radiofrequency interference, during critical phases of flight.

When only one frequency is available, one way to use single frequency measurements is to use code and carrier phase measurements to deduce the delay induced by the ionosphere. This method is called code-carrier divergence technique and is described in Chapter 6.

The case of a loss of all GNSS components but one frequency is studied in [Shau-Shiun Jan, 2003]. In this case, the code-carrier divergence technique can be used. It consists in computing the difference between the signal code and the carrier phase measurements. This difference is twice the ionospheric delay plus the carrier phase ambiguity plus errors, from which the ionospheric code delay can be extracted. If a cycle slip occurs on phase measurements, the integer ambiguity appearing as a constant offset in the code-carrier

difference can make this technique not accurate enough to meet the ICAO requirements. For this reason, it is necessary to be able to detect cycle slips. The used detection algorithm must be compliant with APV I integrity and continuity requirements.

In Chapter 6, the problem of maintaining the dual frequency performances is addressed without any use of augmentation system (the hypothesis is that the SBAS: Satellite Based Augmentation System is unavailable). For instance, for a dual frequency GPS L1 C/A / L5 receiver, the loss of L1 or L5 implies the use of the remaining L1 or L5 frequency. The same remark can be made for Galileo E1 and E5 signals.

Finally, Chapter 7 summarises the main PhD work results and concludes on it. Some remaining issues are discussed and propositions are made for future works.

1.3. Thesis original contributions

The main original contributions of this thesis, detailed all along this dissertation, are enumerated below:

- Proposition of a generic global receiver architecture taking into account switches between GNSS components and degradation detection algorithms (Chapters 3 and 4), in coordination with the DTI

- Proposition and analysis of interference detection algorithms. They are implemented and tested on CW detection taking into account the interference masks defined in [EUROCAE, 2008]. Their impact is studied on both the GPS and Galileo signals on the L1 frequency band. The performances obtained during the approach phases of flight are analysed in terms of integrity and continuity. (Chapter 5)

- Proposition of an algorithm capable of estimating the interferences characteristics. The accuracy of this algorithm is discussed (Chapter 5).

- Development of an algorithm capable of estimating the ionospheric code delay (in a single frequency case without any augmentation system) thanks to GNSS single frequency measurements and a Kalman filter (Chapter 6).

- A cycle slip detection algorithm is proposed and tested on the measurements. The compliance of this detection algorithm with required integrity for the APV I phase of flight is discussed. The availability of the cycle slip detection technique is provided by means of availability maps over Europe for both GPS and Galileo constellations (Chapter 6).

Chapter 2

GNSS applied to Civil Aviation operations

Contents

Résumé

Le chapitre 2 présente le GNSS appliqué à l'aviation civile tant au niveau signal, services que sur des aspects récepteur, traitement du signal et PVT. Nous présentons les différents signaux dans la bande aéronautique, les services associés et les systèmes d'augmentation aéronautiques. Dans ce chapitre, les modules d'un récepteur GNSS, depuis la tête HF jusqu'aux algorithmes de PVT, sont présentés. Nous présentons d'autre part les différents types de perturbations rencontrées pour un récepteur avionique et générant potentiellement des dégradations dans le traitement des signaux reçus. D'autre part, les exigences de l'aviation civile sont décrites en détails et les spécifications à tenir sont rappelées suivant les standards de l'OACI.

2. GNSS applied to Civil Aviation operations

2.1. Introduction

New GNSS signals and constellations are expected to provide operational benefits for civil aviation applications which are in the scope of this thesis work.

The targeted aircraft operations are defined according to [ICAO, 2006] in this chapter. Then, the International Civil Aviation Organization (ICAO) requirements are detailed and used all along this thesis. Indeed, the future embedded combined receivers must comply with these requirements.

Before studying such combined receiver architecture, it is of interest to introduce GNSS. In this chapter, we describe firstly the GNSS principles. The GNSS signals, constellations, services augmentations and their features are then detailed.

Signal processing within the receiver is also described from the receiver front end to the tracking loops. The different kinds of perturbations that can disturb signals processing at the reception are exposed at the end of this chapter.

2.2. Civil Aviation application

2.2.1. Introduction

Future embedded GNSS receivers must comply with ICAO requirements, for all the phases of flight of an aircraft. This section provides the official definitions of the different phases of flight and the underlying requirements. These specifications are referred throughout this thesis work.

Since we focus on approach phases of flight, the definitions provided hereafter are only related to the corresponding aircraft operations, according to the [RTCA, 2006] reference.

2.2.2. Civil aviation operations

2.2.2.1. Phases of flight

Below, we present the definitions of the different phases of flight as provided by ICAO, from Non Precision Approach operation to Cat III.

2.2.2.1.1. Non-precision approach (NPA)

NPA is a standard instrument approach procedure in which no glide slope/glide path is provided [RTCA, 2006].

2.2.2.1.2. Approach and landing operations with vertical guidance (APV)

APV is separated into two broad classes depending on the method retained for the provision of the vertical guidance during the approach, [RTCA, 2006]. The first class relies on GNSS lateral guidance and on barometric vertical guidance generated through a Flight Management System (FMS). However, barometric vertical guidance suffers from limitations in terms of accuracy and from a number of potential integrity failures due to the necessity of manual input of local atmospheric pressure and of temperature compensation. Therefore the ICAO GNSS panel identified two performance levels which are APV-I and APV-II.

2.2.2.1.3. CAT-I, CAT-II, CAT-III precision approach

These phases of flight are more restrictive than the last described ones. The categories are specified by several parameters, which are Decision Height (DH), the distance of visibility (DV) and the Runway Visual Range (RVR), defined in [RTCA, 2006].

The DH is the parameter that determines if a CAT approach can be initiated or not. Otherwise, a Missed Approach is initiated. In that way, DH is the minimal height above the runaway threshold at which a Missed Approach procedure must be executed. In addition, a minimal visual reference is required in order to continue the approach or not and must be established to initiate Cat approach for safety. In case Cat is initiated, the aircraft is flown manually by the pilot using the external visual reference, or automatically by the autopilot under pilot monitoring.

The DV and RVR parameters are taken as visual requirements for such approach categories. DV is expressed in units of length. It is a distance in which it is possible to see and identify, during the day, a dark object and during the night a light source. Obviously, this parameter is strongly dependent upon the atmospheric conditions. The RVR parameter is also a distance. It represents the maximum distance between the pilot and the runway in the direction of the airstrip, in which the pilot is able to see the runway surface markings and lights.

For CAT I, DH have to be greater than 60 m and visual requirements are a visibility greater than 800 m or a RVR greater than 550 m. For CAT II, DH value is taken between 30 m and 60 m and RVR must be greater than 350 m. For CAT III, three levels are defined, the first one (A), while DH is taken between 0 and 30 m, RVR is greater than 200 m, the second one (B) when DH is under 15 m and RVR is between 50 m and 200 m and the last one (C) when these two parameters are null.

2.2.2.1.4. Missed Approach (MA)

The Missed Approach (MA) is an optional procedure between the Cat phases of flight that is initiated when the aircraft cannot land because of too high aircraft dynamics or other problems, primary for safety reasons. This procedure cannot be initiated if the aircraft has a too low altitude at a point of no return. Generally, the pilot determines if an approach point is not in view or when the landing operations cannot be accomplished safely for any reason. In this case, the approach must be stopped immediately. The pilot is expected to inform Air Traffic Control (ATC) by radio of the initiation of the MA as soon as possible. ATC may simply acknowledge the MA call, or modify the MA instructions. ATC may subsequently clear the flight for another approach attempt, depending on the pilot's intentions, as well as weather and traffic considerations.

2.2.2.2. ICAO requirements

Any navigation system has to satisfy a number of performance requirements. In the case of GNSS these requirements concern the Signal-In-Space (SIS), that is to say the aggregate of guidance signals arriving at the antenna of the aircraft. They are based on required navigation performance of the aircraft and are expressed by the ICAO for each phase of flight in terms of accuracy, integrity, availability and continuity of service.

GNSS Signal In Space (SIS) performance requirements are defined for all the operations identified by the ICAO: oceanic and domestic en-route, terminal approach, initial approach, intermediate approach, departure, non-precision approach, and more stringent approaches (APV).

All along this thesis, we will focus on NPA and APV phases of flight and on the transition between NPA and APV. Indeed, APV is the first approach phase of flight that requires vertical guidance after NPA and has restrictive requirements compared to NPA. In addition, the EUROCAE WG 62 needs the results concerning the performances requirements for the future embedded GNSS receivers.

2.2.2.3. Accuracy

The accuracy is the degree of conformance between the estimated or measured position and/or velocity of a platform at a given time and its true position and/or velocity. In order to characterize the accuracy on the estimated quantity, ICAO defines a 95%-confidence level. It means that for any estimated position at a specific location, the probability that the position error is within the former requirement should be at least 95 per cent [RTCA, 2006].

2.2.2.4. Integrity

The integrity is a measure of the trust, which can be placed in the correctness of the information supplied by the total system. The integrity includes the ability of a system to

provide timely and valid warnings (alerts) to the user when the system must not be used for the intended operation. The integrity is defined by the integrity risk, time to alert and alert limits requirements [RTCA, 2006].

Integrity risk

The integrity risk is the probability of an undetectable failure of the specified accuracy. It is expressed per hour or per operation.

Protection levels

The horizontal protection level Fault Detection, HPL, is the radius of a circle in the horizontal plane […] with its centre being at the true position, […] for which the missed alert and false alert requirements are met for the chosen set of satellites when autonomous fault detection is used. It is a function of the satellite and user geometry and the expected error characteristics: it is not affected by actual measurement. Therefore, this value is predictable.

The vertical protection level Fault Detection, VPL, is half the length of a segment in the vertical axis […] with its centre being at the true position, […] for which the missed alert and false alert requirements are met for the chosen set of satellites when autonomous fault detection is used. It is a function of the satellite and user geometry and the expected error characteristics: it is not affected by actual measurement. Therefore, this value is predictable.

Time to alert

It is the maximum allowable time interval between system performance ceasing to meet operational performance limits and the appropriate integrity monitoring subsystem providing an alert [RTCA, 2006].

Alert limits

For each phase of flight, to ensure that the position error is acceptable, alerts limit are defined ([RTCA, 2006]) that represent the largest position error which results in a safe operation.

The Horizontal Alert Limit (HAL) is the radius of a circle in the horizontal plane (the local plane tangent to the WGS 84 ellipsoid), with its centre being at the true position, which describes the region which is required to contain the indicated horizontal position with the required probability for a particular navigation mode […].

The Vertical Alert Limit is half the length of a segment on the vertical axis (perpendicular to the horizontal plane of WGS 84 ellipsoid), with its centre being at the true position, which describes the region which is required to contain the indicated vertical position with a certain probability, for a particular navigation mode […].

While horizontal alert limits (HAL) requirements are defined for all of the phases of flight, vertical alert limits (VAL) are only defined for phases of flight under NPA.

Positioning failure

If the equipment is aware of the navigation mode/alert limit, a positioning failure is defined to occur whenever the difference between the true position and the indicated position exceeds the applicable alert limit. If the equipment is not aware of the navigation mode/alert limit, a positioning failure is defined to occur whenever the difference between the true position and the indicated position exceeds the applicable protection level (either horizontal or vertical as applicable) [RTCA, 2006].

2.2.2.5. Availability

It is the ability of the navigation system to provide the required function and performance at the initiation of the intended operation. It expressed as a percentage of time. The availability of GNSS is characterized by the portion of time the system is to be used for navigation during which reliable navigation information is presented to the crew, autopilot, or other system managing the flight of the aircraft [RTCA, 2006].

2.2.2.6. Continuity of service

It is the capability of the total system (comprising all elements necessary to maintain aircraft position within the defined airspace) to perform its function without interruption during the intended operation. Continuity relates to the capability of the navigation system to provide a navigation output with the specified accuracy and integrity throughout the intended operation, assuming that it was available at the start of the operation. The occurrence of navigation system alerts, either due to rare fault-free performance or to failures, constitute continuity failures. For en-route, since the durations of these operations are variable, the continuity requirement is specified as a probability on a per-hour basis. For approach and landing operations, the continuity requirement is stated as a probability for a short exposure time. Continuity requirement is expressed as the continuity risk, that is to say, the probability that the system to be interrupted during the intended operation [RTCA, 2006].

2.2.2.7. ICAO performance requirements for each phase of flight

Typical Operation	Accuracy Horizontal 95%	Accuracy Vertical 95%	Integrity risk	Time To Alert	Horizontal Alert limit	Vertical Alert limit	Continuity	Availability
En-route	3.7 km (2.0 NM)	N/A	$1 - 1 \times 10^{-7}$/h	5 min	7.4 km	N/A	$1 - 1 \times 10^{-4}$/h to $1 - 1 \times 10^{-8}$/h	0.99 to 0.99999
En-route, Terminal	0.74 km (0.4 NM)	N/A	$1 - 1 \times 10^{-7}$/h	15 s	3.7 km	N/A	$1 - 1 \times 10^{-4}$/h to $1 - 1 \times 10^{-8}$/h	0.99 to 0.99999
Initial approach, Intermediate approach, Non precision approach, Departure	220 m (720 ft)	N/A	$1 - 1 \times 10^{-7}$/h	10 s	556 m	N/A	$1 - 1 \times 10^{-4}$/h to $1 - 1 \times 10^{-8}$/h	0.99 to 0.99999
Approach Operations with vertical Guidance APV I	16 m (52 ft)	20 m (66 ft)	$1 - 2 \times 10^{-7}$ per approach	10 s	40 m	50 m	$1 - 8 \times 10^{-6}$/h in any 15 s	0.99 to 0.99999
Approach Operations with vertical Guidance APV II	16 m (52 ft)	8 m (26 ft)	$1 - 2 \times 10^{-7}$ per approach	6 s	40 m	20 m	$1 - 8 \times 10^{-6}$/h in any 15 s	0.99 to 0.99999
Category I precision approach	16 m (52 ft)	6 m to 4m (20 ft to 13ft)	$1 - 2 \times 10^{-7}$ per approach	6 s	40 m	15.0 m to 10 m	$1 - 8 \times 10^{-6}$/h in any 15 s	0.99 to 0.99999

Table 1: GNSS SIS requirements from [ICAO, 2006].

Table 1 shows ICAO requirements for the different phases of flight.

If combined, GPS, Galileo and augmentation systems are expected to provide sufficient performances for demanding operations. It is thus necessary to:

- identify the most promising combinations that can be used;
- build the architecture of future GNSS combined receivers;
- evaluate the robustness of future combined receivers against all kinds of external perturbations.

That is why, this chapter describes first the GNSS principles and measurements, the GNSS signals, constellations and augmentation systems and the different perturbations affecting the GNSS signals processing.

2.3. Definition and description of GNSS

In this section, the GNSS is described in details. Firstly, the GNSS principles and measurements are exposed. Secondly, the different GNSS signals, constellations, augmentations and services that are in the scope of the EUROCAE WG 62 work are defined according to [RTCA, 2007], and their features are exposed in details. Thirdly, the signal processing in a GNSS receiver is presented.

2.3.1. GNSS principle and measurements

A GNSS receiver provides two main types of measurements called pseudo ranges which are ranges including satellites-receiver clock bias plus different kinds of errors due to signal

propagation from a satellite to the receiver. These errors are due to multipath, troposphere and ionosphere crossing, interferences and residual noise coming from the receiver imperfections. These errors will be defined further in this chapter. Pseudo ranges are code and carrier phase measurements for each satellite. The following models describe these measurements:

$$P^i(k) = \rho^i(k) + c\left(\Delta t_u(k) - \Delta t^i(k)\right) + c\left(I^i(k) + \tau^i(k)\right) + D^i_{mult}(k) + n^i(k) \quad \textbf{(1)}$$

$$\phi^i(k) = \rho^i(k) + c\left(\Delta t_u(k) - \Delta t^i(k)\right) + c\left(-I^i(k) + \tau^i(k)\right) + \Phi^i_{mult}(k) + N^i\lambda^i + n^i(k) \quad \textbf{(2)}$$

Where:

- i denotes a particular satellite
- P is the code pseudorange measurement in meters
- ϕ the carrier phase measurement (in meters)
- ρ is the actual distance between a satellite i and the receiver
- c is the light speed, equal to 299 792 458 m/s
- $\Delta t_u(k)$ is the user clock shift
- $\Delta t^i(k)$ represents the i^{th} satellite clock shift
- I is the ionosphere error
- τ is the troposphere error
- D_{mult} is the multipath error for code measurement
- Φ_{mult} is the multipath error for carrier phase measurement
- N is the ambiguity (random number of cycles)
- λ is the carrier wavelength
- n is the residual noise

2.3.2. GNSS measurements for civil aviation use

A GNSS receiver user position is usually determined by measuring the propagation delay of at least four received satellites signals. Each actual distance between one satellite and the receiver is:

$$\rho^i = \sqrt{(x^i - x)^2 + (y^i - y)^2 + (z^i - z)^2} \quad \textbf{(3)}$$

Where:

- (x,y,z) refers to the receiver location
- (x^i, y^i, z^i) refers to the satellite i position (provided thanks to ephemeris)

Thus, the code pseudorange measurement for the satellite i, can be rewritten:

$$P^i(k) = \sqrt{(x^i(k) - x(k))^2 + (y^i(k) - y(k))^2 + (z^i(k) - z(k))^2} + c\left(\Delta t_u(k) - \Delta t^i(k)\right) + E \quad \textbf{(4)}$$

Where:

- $E = c\left(I^i(k) + \tau^i(k)\right) + D^i_{mult}(k) + n^i(k)$

Making the hypothesis that E is known, $\Delta t^i(k)$ is known, four unknown have to be determined: $\Delta t_u(k)$ and (x(k),y(k),z(k)), which requires four pseudorange measurements at less.

The calculated delays are proportional to the distance the signal travelled from the satellite, and called ranges. But, before calculating the receiver position, the pseudorange measurements are refined according to particular specifications [RTCA, 2006]. The following sections describe this process.

2.3.2.1. Smoothing process and civil aviation requirement

The code and carrier phase measurements models are described in the previous section. It is required in [RTCA, 2006], section 2.1.4.1.1 that the equipment should perform signals carrier smoothing. In the presence of a code-carrier divergence rate of up to 0.018 m/s, the smoothing filter output shall achieve an error less than 0.25 m within 200 seconds after initialization, relative to the steady-state response of the following 100 seconds Hatch filter:

$\tilde{P}(k) = \frac{1}{T_{sm}} P(k) + \left(1 - \frac{1}{T_{sm}}\right)\left[\tilde{P}(k-1) + (\phi(k) - \phi(k-1))\right]$ in steady-state ($k - k_0 \geq T_{sm}$) **(5)**

$\tilde{P}(k) = \frac{1}{T} P(k) + \left(1 - \frac{1}{T}\right)\left[\tilde{P}(k-1) + (\phi(k) - \phi(k-1))\right]$ during convergence ($T = k - k_0 < T_{sm}$) **(6)**

Where:

- $P(k)$ is the raw code pseudorange measurement in meters
- $\phi(k)$ is the raw carrier phase measurement in meters
- $\tilde{P}(k)$ is the smoothed code pseudorange measurement in meters
- T_{sm} is the time smoothing constant in seconds
- k_0 is the time index where the filter is initialized
- during convergence, $T = k - k_0$ is the time since initialization of the filter ($T < T_{sm}$)

The improvement brought by the smoothing process, assuming that the errors affecting the raw pseudorange measurements are independent, is given by [Hegarty1, 1997]:

$$\frac{\sigma_P^2}{\sigma_{\tilde{P}}^2} \approx \frac{\alpha}{2} \quad \textbf{(7)}$$

Where:

- α is the filter weighting coefficient (unit less), equal to the sample interval in seconds divided by the time constant
- $\sigma_{\tilde{P}}$ is the standard deviation of the smoothed pseudorange
- σ_P the standard deviation of the raw pseudorange

2.3.2.2. Least squares position solution

As it is described in details in [Macabiau2, 2005], a GNSS receiver provides n pseudorange measurements collected in a vector noted Y. At least n=4 measurements are required to provide the user position. The measurement vector Y and the state vector X composed of positions and clock bias are linked by:

$$\mathrm{Y} = \mathrm{g}(\mathrm{X}) + \mathrm{E} \quad \textbf{(8)}$$

- $\mathrm{E} = \mathrm{c}\left(\mathrm{I}^{\mathrm{i}}(\mathrm{k}) + \tau^{\mathrm{i}}(\mathrm{k})\right) + \mathrm{D}^{\mathrm{i}}_{\mathrm{mult}}(\mathrm{k}) + \mathrm{n}^{\mathrm{i}}(\mathrm{k})$ is the error due to the multipath, noise and atmospheric effects on the code pseudorange measurements. The same kind of model can be used for carrier phase measurements.
- $X = \begin{bmatrix} x & y & z & b \end{bmatrix}^T$ is composed of positions (x, y and z) and clock bias b.

Let us describe the least squares navigation solution. If $\hat{X}_0$ is an initial estimate of X (the actual position of the aircraft receiver antenna), then X can be noted:

$$\mathrm{X} = \widehat{\mathrm{X}_0} + \Delta\mathrm{X} \quad \textbf{(9)}$$

Where $\Delta\mathrm{X}$ is the deviation between the aircraft position estimation and its actual position. Therefore, the measurement model can be rewritten as:

$$\mathrm{Y} = \mathrm{g}\left(\widehat{\mathrm{X}_0} + \Delta\mathrm{X}\right) + \mathrm{E} \quad \textbf{(10)}$$

This expression may be linearized around $\hat{X}_0$, the initial estimate of X, as follows:

$$\mathrm{Y} = \mathrm{g}\left(\widehat{\mathrm{X}_0}\right) + \frac{\partial \mathrm{g}}{\partial \mathrm{X}}\left(\widehat{\mathrm{X}_0}\right)\Delta\mathrm{X} + \mathrm{E} \quad \textbf{(11)}$$

Where:

$$\frac{\partial \mathrm{g}}{\partial \mathrm{X}}\left(\widehat{\mathrm{X}_0}\right) = \mathrm{G} = \begin{bmatrix} \frac{\partial \mathrm{g}^1}{\partial \mathrm{x}}\left(\widehat{\mathrm{X}_0}\right) & \frac{\partial \mathrm{g}^1}{\partial \mathrm{y}}\left(\widehat{\mathrm{X}_0}\right) & \frac{\partial \mathrm{g}^1}{\partial \mathrm{z}}\left(\widehat{\mathrm{X}_0}\right) & \frac{\partial \mathrm{g}^1}{\partial \mathrm{b}}\left(\widehat{\mathrm{X}_0}\right) \\ \vdots & \vdots & \vdots & \vdots \\ \frac{\partial \mathrm{g}^{\mathrm{n}}}{\partial \mathrm{x}}\left(\widehat{\mathrm{X}_0}\right) & \frac{\partial \mathrm{g}^{\mathrm{n}}}{\partial \mathrm{y}}\left(\widehat{\mathrm{X}_0}\right) & \frac{\partial \mathrm{g}^{\mathrm{n}}}{\partial \mathrm{z}}\left(\widehat{\mathrm{X}_0}\right) & \frac{\partial \mathrm{g}^{\mathrm{n}}}{\partial \mathrm{b}}\left(\widehat{\mathrm{X}_0}\right) \end{bmatrix} \quad \textbf{(12)}$$

The linearized model can be then rewritten as:

$$Y - g(\widehat{X_0}) = G\,\Delta X + E \quad \textbf{(13)}$$

The measurement residual represents the deviation between the measurements made and the predicted noiseless measurements that the receiver would have made if its position and clock delay were $\widehat{X_0}$ and if there were no noise. This residual can be expressed such as:

$$\Delta Y = Y - g(\widehat{X_0}) \quad \textbf{(14)}$$

$$\Delta Y = G\,\Delta X + E \quad \textbf{(15)}$$

Where $\boldsymbol{\Delta Y}$ is the deviation between measurements and noiseless predicted measurements if the position and the clock delay were $\hat{X}_0$.

From this linear relationship between ΔY and ΔX, we deduce the least squares estimate of ΔX :

$$\Delta\widehat{X} = [G^T G]^{-1} G^T\,\Delta Y \quad \textbf{(16)}$$

And

$$\widehat{X} = \widehat{X_0} + \Delta\widehat{X} \quad \textbf{(17)}$$

The residual ΔY considering $\hat{X}$ may be expressed as:

$$\Delta Y = Y - g(\widehat{X}) = g(X) - g(\widehat{X}) + E \quad \textbf{(18)}$$

$$\Delta Y = g(\widehat{X_0} + \Delta X) - g(\widehat{X_0} + \Delta\widehat{X}) + E \quad \textbf{(19)}$$

As it is described in [Macabiau2, 2005], the previous expression is linearized:

$$Y - g(\widehat{X}) \approx G\Delta X - G\Delta\widehat{X} + E = G(\Delta X - \Delta\widehat{X}) + E \quad \textbf{(20)}$$

However,

$$\Delta\widehat{X} = [G^T G]^{-1} G^T\left[Y - g(\widehat{X_0})\right] \quad \textbf{(21)}$$

Therefore:

$$\Delta\widehat{X} = [G^T G]^{-1} G^T[G\Delta X + E] \quad \textbf{(22)}$$

Which is equivalent to:

$$\Delta\widehat{X} = \Delta X + [G^T G]^{-1} G^T E \quad \textbf{(23)}$$

$$\Delta\widehat{X} - \Delta X = [G^T G]^{-1} G^T E \quad \textbf{(24)}$$

Let us note the pseudo inverse matrix A as follows:

$$A = [G^T G]^{-1} G^T \quad \textbf{(25)}$$

Then:

$$\Delta\widehat{X} - \Delta X = AE \quad \textbf{(26)}$$

In this calculation, we assume that, at the end of the iterative process, $\widehat{X}$ and $\widehat{X_0}$ are very close.

The relationship between the measurement residual and the measurement error is:

$$\Delta Y = G\Delta X - G\Delta\widehat{X} + E = G(\Delta X - \Delta\widehat{X}) + E \quad \textbf{(27)}$$

$$\Delta Y = -GAE + E = -G[G^T G]^{-1} G^T E + E = (I - G[G^T G]^{-1} G^T)E \quad \textbf{(28)}$$

For a weighted least squares estimate, ΔY is written as:

$$\Delta Y = (I - G[G^T \Sigma^{-1} G]^{-1} G^T \Sigma^{-1})E \quad \textbf{(29)}$$

Where: $\Sigma = cov(E)$ is the covariance of E.

2.3.3. GNSS components

A GNSS component is identified by EUROCAE WG 62 as a constellation, a frequency, an augmentation system or a service [EUROCAE, 2007]. The GNSS includes several positioning systems. Amongst the constellations, we can quote GLONASS (USSR), GPS (USA), Galileo (Europe) and Beidou (China). But, the WG 62 priority for future GNSS receivers is to track the Galileo and the GPS satellites. As a consequence, only these systems are described in the following.

2.3.3.1. GPS

The GPS is a satellite radio navigation system. Nominally, 24 satellites in orbit round the Earth can be used [GPS SPS, 2008]. These satellites send signals which allow a receiver determining its position velocity and time everywhere on the Earth surface. The GPS infrastructure includes three segments dedicated to specific functions:

- The space segment includes the constellation of GPS satellites, which transmit the signals to the users. It is composed of satellites located in 6 orbital planes; each plane

has a 55 degree inclination from the equator. The revolution period of each GPS satellite is 12 sidereal hours.

- The control segment is responsible for the monitoring and operation of the space segment. Indeed, several ground stations monitor the signals transmitted from GPS satellites. The control segment then uses these signals to estimate and predict the satellite orbits and clock errors. This information gathered in the navigation message is then uploaded to the satellites.

- The user segment includes user hardware and processing software for positioning, navigation, and timing applications.

The GPS modernization plan is resumed in the following. It is divided in three steps:

- The actual basis GPS emitting L1 C/A and L1, L2 P(Y) signals;
- The “IIR-M” block including the L2C signal;
- The “IIF” block including the L5 signal;
- The “III” block including the L1C signal.

2.3.3.2. Galileo

Galileo will be a 27 satellite (+ 3 spare) constellation. The Galileo system provides its own integrity information (INAV message) broadcasted on two different frequencies that are described later in this chapter. A called Galileo Integrity Channel (GIC) will provide integrity information to the user. EUROCAE WG62 is currently working on Galileo receivers specifications to provide Minimum Operational Performance Standards (MOPS) to civil aviation users.

2.3.3.3. Augmentation systems

The augmentation systems are the elements installed on ground, on board satellites and on board the aircraft, which are providing the aircraft with signal and data enabling the aircraft to determine its position and timing. Three types of augmentation systems are used for civil aviation: the ABAS, the SBAS and the GBAS [EUROCAE, 2007].

2.3.3.3.1. Aircraft Based Augmentation System

The ABAS or Aircraft-Based Augmentation System is a system which augments and/or integrates the information obtained from GPS or Galileo with information on board the aircraft. The Receivers Autonomous Integrity Monitoring algorithm is an example of ABAS. Its aim is to verify the integrity of the signals received from the GPS or Galileo constellation. It is also intended to detect local effects which cannot be fully modelled by the SBAS.

2.3.3.3.1.1. Protection levels calculation

The protection levels derive from the smallest bias the RAIM algorithm is able to detect, satisfying the false alarm and the missed detection requirement, by using statistical tests described in [Walter, 1995].

Let us consider the measurement residual ΔY, also called the prediction error vector, which can be expressed thanks to the linear relationship between the measurement error vector E, its covariance matrix: $\sum$ and the observation matrix G:

$$\Delta Y = (I - G[G^T G]^{-1} G^T) E \quad \textbf{(30)}$$

Or for a weighted least square solution:

$$\Delta Y = (I - G[G^T \Sigma^{-1} G]^{-1} G^T \Sigma^{-1}) E \quad \textbf{(31)}$$

Let us define the norm of the measurement residual as:

$$SSE = \Delta Y^T \Delta Y = \|\Delta Y\|^2 \quad \textbf{(32)}$$

Or for a weighted least square solution:

$$WSSE = \Delta Y^T \Sigma^{-1} \Delta Y \quad \textbf{(33)}$$

In literature, classical RAIM statistical tests are built thanks to these norms, as it is described in [Walter, 1995].

If we note:

$$A_\Sigma = [G^T \Sigma^{-1} G]^{-1} G^T \Sigma^{-1} \quad \textbf{(34)}$$

And:

$$B_\Sigma = G[G^T \Sigma^{-1} G]^{-1} G^T \Sigma^{-1} \quad \textbf{(35)}$$

The protection levels are calculated as follows:

The HPL provided by the RAIM algorithm is:

$$HPL = HSLOPE_{max} * p_{bias} \quad \textbf{(36)}$$

And the VPL is:

$$VPL = VSLOPE_{max} * p_{bias} \quad \textbf{(37)}$$

Where:

$$\mathrm{HSLOPE_{max}} = \max_j \left(\frac{\sqrt{{A_{\Sigma 1,j}}^2 + {A_{\Sigma 2,j}}^2}}{\sqrt{1 - B_{\Sigma j,j}}} \right) \quad \textbf{(38)}$$

$$\mathrm{VSLOPE_{max}} = \max_j \left(\frac{A_{\Sigma 3,j}}{\sqrt{1 - B_{j\Sigma,j}}} \right) \quad \textbf{(39)}$$

And:

$$p_{bias} = \mathrm{bias} * \sqrt{1 - B_{\Sigma j,j}} \quad \textbf{(40)}$$

Where bias is the smallest detectable bias on the pseudorange j, corresponding to the satellite j, as it is described in [Walter, 1995].

2.3.3.3.2. Satellite Based Augmentation System

The SBAS stands for Satellite-Based Augmentation System and is designed to improve the accuracy and to ensure the integrity of information coming from GPS, Galileo, GLONASS or other positioning system satellites [EUROCAE, 2007]. Accuracy is improved thanks to differential corrections computed from widely-spaced ground stations and further broadcast by geostationary satellites. They correct for ionospheric disturbances, satellite timing and orbit errors. The quality of navigation signals is also monitored by ground stations and, amongst others, a USE or DON'T USE flag is forwarded to users.

The European Geostationary Navigation Overlay Service (EGNOS) and Wide Area Augmentation System (WAAS) are European and American SBAS. EGNOS is intended to augment GPS on the L1 and future L5 frequencies over the European Civil Aviation Conference (ECAC) airspace using Inmarsat satellites. The WAAS is operational over CONtinental United States (CONUS).

The SBAS systems such as EGNOS require a significant geographically diverse ground infrastructure as well as access to geostationary satellite navigation transponders. Specific SBAS receivers are also required on aircraft to take advantage of the broadcast information.

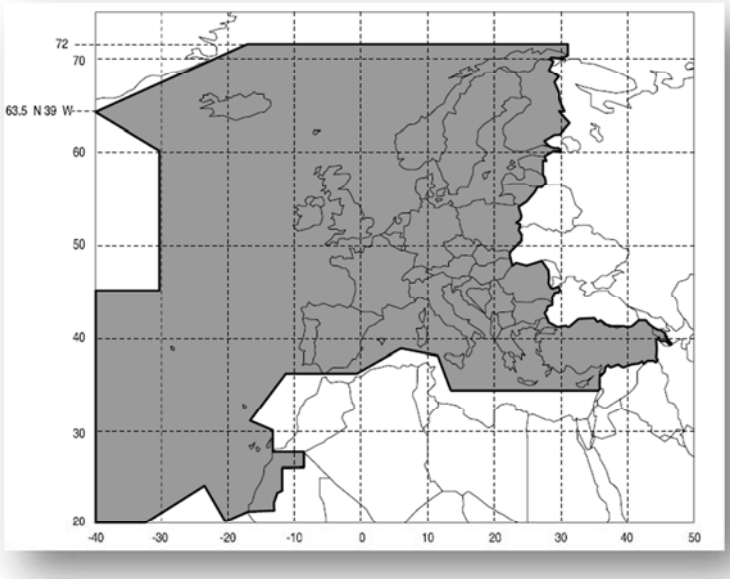

Figure 1: EGNOS theoretical coverage [ESA, 2004].

As it can be seen in figure 1, EGNOS (like other SBAS) is not worldwide and this may be an issue when its use is required to meet the ICAO performances needed to continue or begin a phase of flight. It can be clearly seen that for an EGNOS receiver, this system cannot be used out of its coverage region. For instance, in non-covered airports, approach operations cannot be treated thanks to this augmentation.

The availability of SBAS is determined by confidence bounds on position errors. The error due to the ionospheric delay and satellite errors are corrected according to the SBAS Minimum Operational Performance Standards (MOPS), and local errors such as error due to tropospheric delay, user receiver noise and multipath errors are removed by a standard model described in [RTCA, 2006].

2.3.3.3.2.1. Protection levels calculation

The ICAO normalized protection levels computation for SBAS receivers. We provide hereafter the principles of calculation of the SBAS protection levels.

The corrected range measurements are used to compute the navigation solution, using weighted least squares:

$$\Delta\widehat{X} = [G^T W G]^{-1} G^T W \, \Delta Y \quad \textbf{(41)}$$

Where the weighting matrix is:

$$W^{-1} = \begin{bmatrix} \sigma_1{}^2 & \cdots & 0 \\ \vdots & \ddots & \vdots \\ 0 & \cdots & \sigma_N{}^2 \end{bmatrix} \quad \textbf{(42)}$$

With:

$$\sigma_i^2 = \sigma_{i,flt}^2 + \sigma_{i,UIRE}^2 + \sigma_{i,air}^2 + \sigma_{i,tropo}^2 \quad \textbf{(43)}$$

- $\sigma_{i,flt}$ is the fast and long-term degradation confidence, which is the confidence bound on satellite clock and ephemeris corrections (satellite errors).
- $\sigma_{i,UIRE}$ is the user ionospheric range error confidence, which is the confidence bound on ionospheric delay corrections.
- $\sigma_{i,air} = \sqrt{\sigma_{noise}^2 + \sigma_{multipath}^2}$ is the airborne receiver error confidence. It is the confidence bound on aircraft user receiver error.
- σ_{noise}^2 is the variance of the receiver thermal noise and interferences
- $\sigma_{multipath}^2$ is the variance of multipath
- $\sigma_{i,tropo}$ is the residual tropospheric error model bound, E is the satellite elevation angle

If we note:

$$D = \begin{bmatrix} d_{11} & \cdots & d_{1N} \\ \vdots & \ddots & \vdots \\ d_{41} & \cdots & d_{4N} \end{bmatrix} = [G^T W G]^{-1} G^T W \quad \textbf{(44)}$$

The variance of the horizontal position estimate is:

$$d_H^2 = \frac{\sum_{i=1}^{N} d_{1i}\sigma_i^2 + \sum_{i=1}^{N} d_{2i}\sigma_i^2}{2} + \sqrt{\frac{\sum_{i=1}^{N} d_{1i}\sigma_i^2 - \sum_{i=1}^{N} d_{2i}\sigma_i^2}{2} + \sum_{i=1}^{N} d_{1i}d_{2i}\sigma_i^2} \quad \textbf{(45)}$$

The HPL (Horizontal Protection Level) is:

$$HPL_{SBAS} = 6\, d_H \quad \textbf{(46)}$$

The variance of the vertical position estimate is:

$$d_V^2 = \sum_{i=1}^{N} d_{3i}\sigma_i^2 \quad \textbf{(47)}$$

The VPL (Vertical Protection Level) is:

$$VPL_{SBAS} = 5.33\, d_V \quad \textbf{(48)}$$

5.33 is a multiplier on the standard deviation of the vertical error such that the VPL is only exceeded at most one time in ten million (10^{-7}), according to [Shau-Shiun Jan, 2003].

2.3.3.3.3. Ground Based Augmentation System

The Ground-Based Augmentation System (GBAS) is composed of reference stations located on airports where the GBAS service is intended to be provided. Reference receivers are placed in these stations and produce differential corrections to be applied and also the navigation signal integrity. These informations are then transmitted to the GBAS airborne receiver.

2.3.4. GNSS services

2.3.4.1. Galileo services [ESA, 2004]

2.3.4.1.1. Safety Of Life (SoL)

One of the purposes of the SoL (Safety of Life) service is to satisfy the civil aviation requirements for en route down to APV II phases of flight. It is created to provide integrity information to user with critical and non-critical levels of risk exposure.

Critical levels include critical operations like approach with vertical guidance. Other non-critical levels are less critical operation like en-route. The performance of Galileo airborne receivers processing Galileo SoL signals should allow an aircraft to fly worldwide safe, accurate paths during the phases of flight including en-route, terminal area, NPA and instrument approach with vertical guidance (APV-I and APV-II). For more stringent phases of flight (precision approach CAT-I type up to CAT-II/III type) other configurations will be needed. Such configurations will include the use of Galileo local component or/and Galileo combination with GPS/GBAS or GPS/SBAS. The frequencies used to provide SoL are Galileo E1 and E5b [Hein, 2002]. Their main characteristics and features are described further in this chapter.

2.3.4.1.2. Open Service (OS)

The Open Service (OS) refers to all information (including positioning, velocity and timing) which can be accessed free of charge by all users. The OS will be interoperable with other GNSS systems. Its performance in timing, accuracy and availability will be competitive with respect to existing GNSS systems. It will not provide integrity information. Its signals will be provided on up to three frequencies (E5a, E5b and E1 described latter in this chapter).

2.3.4.1.3. Public Regulated Service (PRS)

The main goal of Public Regulated Service (PRS) is to improve the probability of continuous availability of Signal In Space (SIS), in the presence of jammers. Indeed, it will be capable of using interference mitigation techniques to reduce the threats due to jamming [Hein, 2002]. This service is encrypted and consequently dedicated to private use.

2.3.4.1.4. Commercial Service (CS)

The Commercial Service (CS) will allow the development of professional applications that will be based on broadcasting of two signals, separated in frequency from the OS signals to facilitate advanced applications such as integration of Galileo positioning applications with wireless communications networks, high accuracy positioning and indoor navigation. The CS signals will be the OS signals plus two encrypted signals on the E6 band, presented in 2.3.5.

2.3.4.1.5. Search And Rescue service (SAR)

The Galileo support to the Search And Rescue service (SAR) represents the contribution of Europe to an international cooperative effort on humanitarian search and rescue activities. The SAR transponder on future Galileo satellites will detect the distress alert from a beacon emitting in the 406-406.1 MHz frequency band. Then, it will broadcast this information to the dedicated receiving ground stations in the 1544-1545 MHz band. The SAR data, from SAR operators to distress emitting beacons, will be used for alert acknowledgement and coordination of rescue teams and will be embedded in the OS data of the signal transmitted in the L1-E1 carrier frequency.

2.3.4.2. Conclusion

GPS, Galileo and augmentation systems can be used for civil aviation applications as depicted in [EUROCAE, 2007]. Galileo services rely on new signals features and characteristics. That is why, in the next sections, GPS and Galileo signals main characteristics are described.

2.3.5. Signals characteristics

GPS and Galileo signals are successively described in the next paragraphs. The following figure presents the GPS and Galileo frequency plan and is provided by [GSA, 2008].

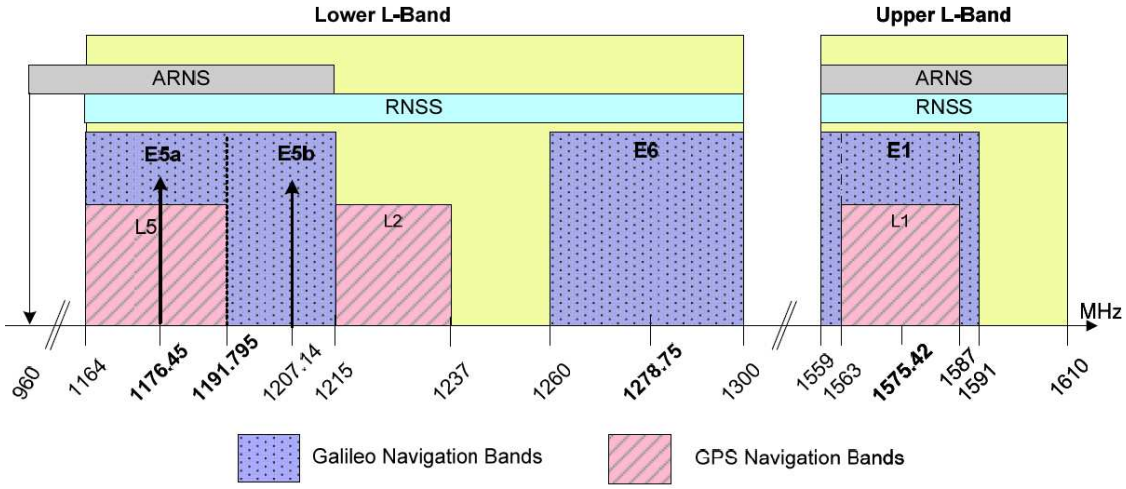

Figure 2: Galileo and GPS frequency plan, [GSA, 2008]

2.3.5.1. GPS L1 signals

The current GPS L1 signal has a central frequency of 1575.42 MHz. It carries a navigation message using two different spreading codes at least: the C/A code, which stands for Coarse/Acquisition, free of charge and available to civilian users and the P (Precise) code available to military users. Note that the P code is usually encrypted into the Y code.

Another new signal on the same band and with the same carrier frequency, denoted GPS L1C will be added in a next future. The L1C signal consists of two main components, one denoted L1 Cp which represents a pilot signal component, free of navigation message data, modulated thanks to a particular Time Multiplexed Binary Offset Carrier modulation, and the other component, denoted L1Cd that is modulated by a data message.

In this thesis, only the GPS L1 C/A signal is used for simulations. The GPS L1 C/A is generated according to the following scheme based on the GPS ICD information.

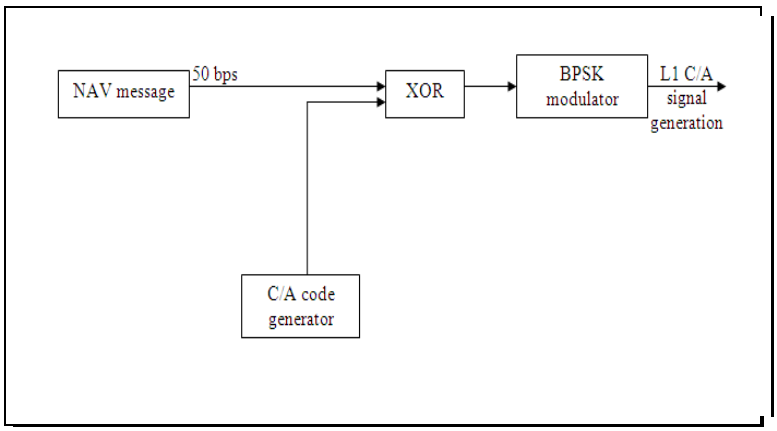

Figure 3: GPS L1 C/A generation

2.3.5.2. GPS L5

L5 is a future GPS signal that will be transmitted with a BPSK (10)[1] modulation and will have the particularity to have two channels: a data channel and a pilot channel. The signal power is equally shared between these two channels. The central frequency is 1176.45 MHz with a code frequency of 10.23 MHz and a length of 10230 (1 ms code period) with a bandwidth of 24 MHz. The minimum received power at the receiver antenna level is – 154 dBW. Each component is modulated thanks to a Neumann-Hoffman code as described in [Bastide1, 2004]. The following scheme illustrates the future GPS L5 signal generation [GSA, 2008].

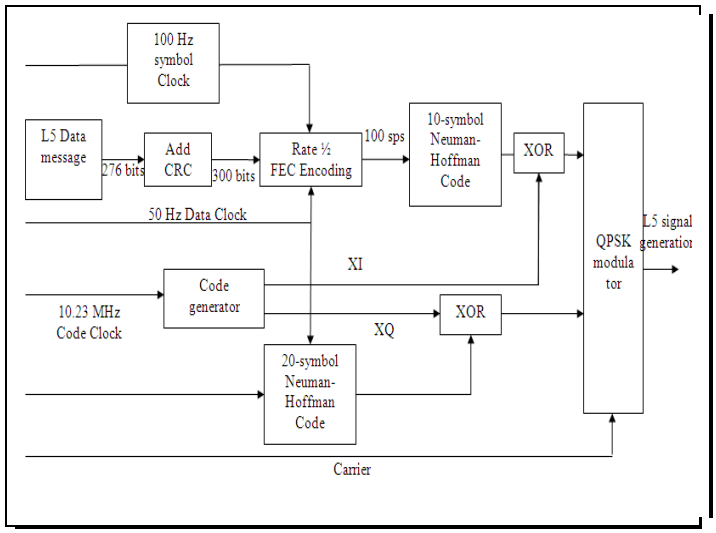

Figure 4: GPS L5 generation

2.3.5.3. Galileo E1

Galileo E1 is broadcasted on the L1 frequency band:

- The Galileo E1 OS signal, free of charge;
- The Galileo E1 PRS signal, which contains encrypted ranging codes, available only for regulated or critical applications by European and sponsoring state members.

In the following, only the E1 OS signal is described since it is studied in this thesis (Chapters 5 and 6). Its specifications are provided in the Galileo SIS ICD [GSA, 2008].

The Galileo E1 OS signal will be available for all equipped civilian users. This signal is composed of two channels:

- The data channel (E1B) which carries the navigation message (INAV);
- The pilot channel (E1C) which is free of data.

The total power of this OS signal is equally distributed between the data and pilot channels. The specified minimum received power with an isotropic antenna of 0 dB gain is -157 dBW.

Note that the navigation message (INAV), will carry an integrity information [GSA, 2008].

[1] The modulations definitions and complete descriptions are not addressed in this thesis dissertation but the interested reader can find more information in [Julien, 2005] or [Rebeyrol, 2007].

The E1 OS signal is modulated thanks to a Composite BOC (CBOC) modulation as it is specified in the Galileo SIS ICD [GSA, 2008]. On both E1B and E1C, the ranging code chip rate will be 1.023 Mcps. The symbol rate for the B component will be 250 symbols/s, as it is detailed in [GSA, 2008]. The primary code length for E1B and C will be 4092 chips. A secondary code also modulates the E1C component. The signal generation is described in the following scheme:

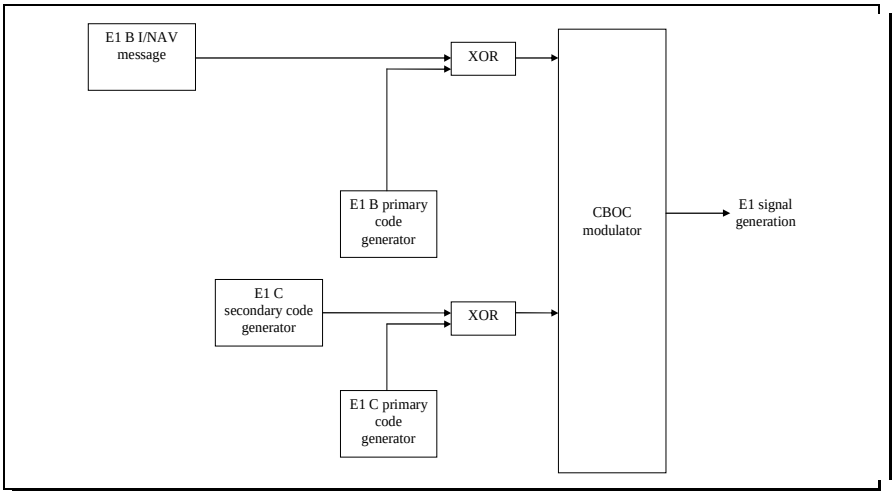

Figure 5: Galileo E1 (B+C) generation

2.3.5.4. Galileo E5a/E5b

Galileo E5a will have the same central frequency as L5 (1176.45 MHz), Galileo E5b central frequency will be 1207.14 MHz. Each signal will carry two different spreading codes in quadrature [GSA, 2008]. The useful power will be equally distributed between components. The minimum received power will be – 155 dBW. An ALTBOC modulation will be used for E5 signals as described in [Rebeyrol, 2006] to build the wideband E5 signal (E5a + E5b). The following schemes represent the E5a and E5b signals generation and are provided according to the Galileo OS SIS ICD ([GSA, 2008]).

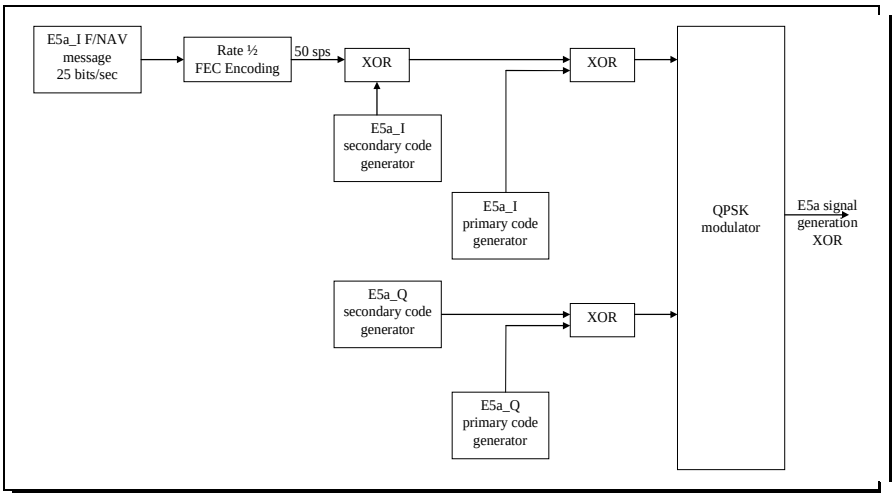

Figure 6: Galileo E5a generation

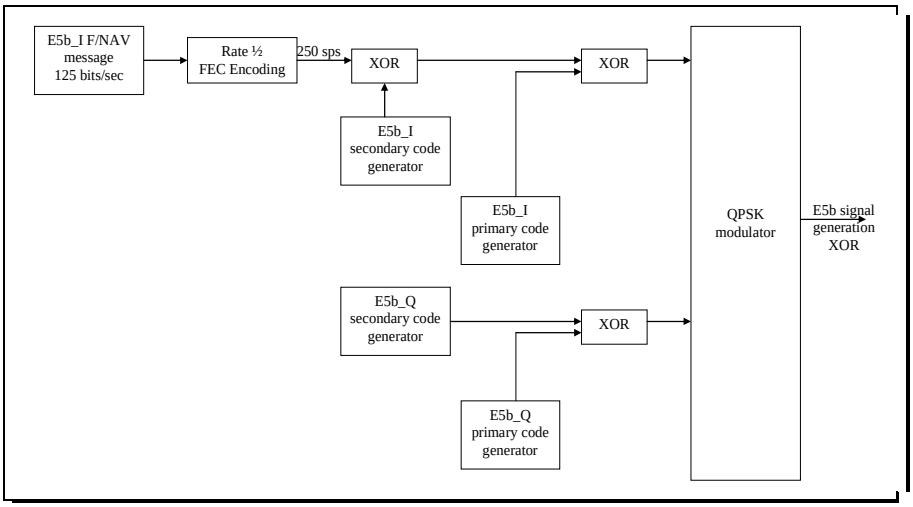

Figure 7: Galileo E5b generation

As it is illustrated in the previous figures, the E5a and E5b signals are generated thanks to primary and secondary codes on both data and pilot channels, each signal is FEC-encoded (rate ½) and QPSK-modulated. The resulting wideband E5 signal is then the combination of the E5a and E5b signals. The E5 composite signal is AltBOC-modulated.

Note that the navigation message broadcasted on the E5b component is a INAV message like for the E1 OS signal. It will carry an integrity information [GSA, 2008].

2.3.5.5. Conclusion

A key characteristic of GPS L1 C/A, L5, Galileo E1, E5a and E5b is that they are (or will be) available worldwide to civil users and transmitted in ARNS bands. These signals are thus of interest for civil aviation community and will be processed by future combined receivers. The existing L1 C/A signal is only composed of a data channel whereas the L5 signal has both a data and a pilot channels. All the E1 OS, E5a and E5b Galileo signals have also a data and a pilot channel. The following paragraphs describe how these signals are processed within GNSS receivers.

2.3.6. Signals reception

In the following, signal processing is described from the front end level to the tracking loops. The goal of this section is not to describe the whole receiver signal processing architecture in details.

2.3.7. RF signal conditioning

The following section presents the RF signal conditioning from the antenna to the baseband processing. A generic conditioning scheme is presented in the following figure. In the future combined GPS-Galileo receivers, the elements presented in the following scheme can be duplicated (for instance two antennas, several amplifiers etc…) to take into account the variety of signals to be received (with different bandwidths).

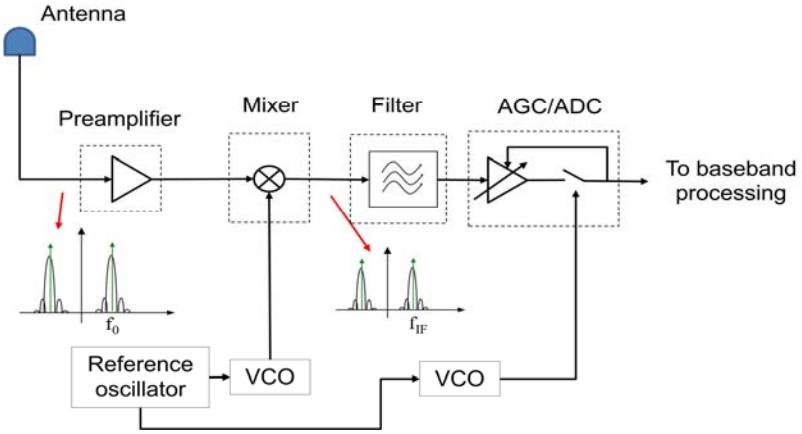

Figure 8: RF signal conditioning until digitalization, VCO stands for Voltage Control Oscillator

2.3.7.1. Antenna

GNSS antenna is the interface with the propagation medium, it is characterized by its frequency selectivity, gain pattern, multipath and interference rejection (these phenomena are described in 2.4). For civil aviation community, the antenna is also adapted to the aircraft design and constraints like shape constraints and high dynamics.

2.3.7.2. Preamplification

Pre amplification is needed to amplify the signal while setting the lowest possible level of noise. It is composed of a low noise amplifier (LNA) designed to achieve a desired level of system noise level. It is defined by three characteristics that are the loss figure, the amplifier noise figure and the gain as mentioned in [Bastide1, 2004].

2.3.7.3. Reference oscillator

A local reference oscillator is used as a basis for generation of all local signals. For civil aviation use, this oscillator has to comply with requirements in terms of power consumption, size, short and long-term stability, sensitivity to high accelerations and phase noise as described in [Bastide1, 2004].

2.3.7.4. Frequency synthesizer

The output of the reference oscillator is used by the frequency synthesizer to derive local oscillators (LO) and clocks needed to achieve certain functions within the receiver. For instance, the LO enables the frequency conversion of the received signals from radio frequency (RF) to intermediate frequency (IF) to ease signal processing as described in [Bastide1, 2004].

2.3.7.5. Down conversion and filtering

Incoming signal down conversion from Radio Frequency to Intermediate Frequency is necessary to ease the amplification of useful signals and the filtering of interference and noise. It is achieved by mixing the incoming amplified signal with Local Oscillators (LO). Generally, the down conversion function is performed by successive down conversion stages towards IF. As the frequency of the incoming signal decreases towards IF, the filtering requirements of the applied successive filters can become more stringent while limiting insertion loss. A mixer is followed by a pass-band filter to suppress the unwanted sideband, LO feed-through and harmonics. Regarding unwanted image, it is filtered at RF before mixing signals.

Filtering at IF is then easier than at RF and it is consequently easier to design sharp filters at lower frequencies. The filters are chosen so that they remove the entire unwanted signal generated by the mixer, they limit the power of the noise entering the IF and they provide a good rejection of out-of-band interference. For future onboard GNSS receivers, these filters will be designed according to interference rejection masks defined by EUROCAE WG 62 in [EUROCAE, 2007] for civil aviation application.

2.3.7.6. Sampling and quantization

The conversion from the analog state to the digital world is accomplished by an Analog-to-Digital Converter (ADC), whose function is to sample then to quantize the incoming signal. Future GNSS combined receivers will probably only have multi bit quantization with uniform law. Anytime a signal is quantized, there is an associated degradation of the system performance. In a GNSS receiver it is classically expressed as Signal to Noise Ratio (SNR) degradation at correlator output described hereafter. Indeed, in a spread spectrum communication system the useful signal power is retrieved at correlator output once the signal has been de-spread.

2.3.7.7. Digital signal processing

In the following, we present the digital signal processing: the acquisition, tracking and correlation processes. These functionalities are duplicated for each receiver channel; each channel being dedicated to a different satellite. Here it is supposed that the satellite PRN to be searched on each channel was already identified.

The first step of the signal processing is the carrier wipe-off which is carried out to translate the received IF signal to baseband. This is done by multiplying the incoming signal with a local IF replica generated using a carrier NCO. It should be noted that the received signal is subject to Doppler frequency due to the relative satellite to aircraft receiver velocity. An estimation of the Doppler frequency is used during the baseband translation. Next, the signal is despread using a locally generated replica of the incoming signal PRN. The dispreading operation is done by correlating the local code replica with the I and Q baseband signal components. The correlation stage is the core of the GNSS CDMA signal processing.

When switched on, a GNSS receiver must first acquire satellites. A successful acquisition enables the receiver to switch on to the tracking process.

2.3.7.7.1. Acquisition

The received signal is delayed because of the emitted signal propagation in the propagation medium, the time offset between satellite and receiver clocks, the payload-induced group delay, the receiver antenna imperfections, the presence of cables and the receiver front end. The acquisition goal is to detect a signal, which implies to find the good pseudorandom noise code used for transmission. The acquisition process also provides a first estimation of the code delay and the carrier Doppler frequency, before the tracking process described in the following section. This research of the good pseudorandom noise code is done testing all the possible codes during sky search.

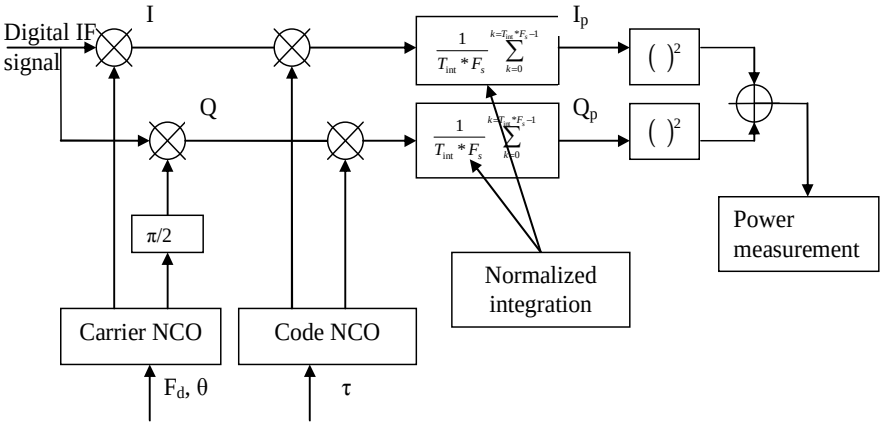

Figure 9: Acquisition process

Where:

- T_{int} (seconds) is the integration time
- F_s (Hertz) is the sampling frequency
- F_d (Hertz) is the Doppler offset
- ???(seconds) is the PRN code delay
- ??(rad) is the phase offset

From the block diagram above, it can be seen that the acquisition unknown parameters are: 1) the PRN code delay ??, 2) the Doppler offset f_d. The acquisition problem can therefore be formulated as a parameter estimation problem where a signal is transmitted from a source with a set of unknown parameters. The traditional acquisition technique consists in visiting all the Doppler and code delay bins.

Thus, the I and Q prompt outputs are summed and squared (summing or squaring steps are realized in different sequences for coherent or non coherent integrations) to build a statistical test criterion. An hypothesis test is then performed by comparing the statistical test to a threshold.

2.3.7.7.2. Acquisition to tracking transition

By the end of the acquisition process, the signal characteristics may have significantly changed. Indeed the acquisition is a relatively long process and may take several tens of seconds per satellite. During this time, and due to the receiver-to-satellite dynamics, the signal Doppler and code delay are continuously modified. In the case where the Doppler and the code delay variations at the end of the acquisition are higher than the tolerated resolution on each of them a second acquisition should be realised based on the results of the first acquisition, the time taken to successfully acquire the signal, and the signal dynamics.

2.3.7.7.3. Tracking

Tracking the IF signal aims at keeping track of the acquired satellite, and subsequently demodulate the navigation message. The tracking process is thus realized in real time, and the signal used is the real incoming signal at each instant. The correlation result is then passed on to the discriminators and next to the loop filters so as to precisely determine the right code delay and carrier phase. These parameters are used to generate the local code and carrier replicas to keep track of the considered satellite. The receiver remains in this stage while the test statistic is higher than a tracking predetermined threshold. Otherwise, it goes back to the acquisition or reacquisition stage. A general block diagram of the tracking process is depicted in the next figure.

The acquired sampled signal (supposing the presence of data and only a primary ranging code, like, for instance the L1 C/A signal) can be expressed by:

$$V(k) = A.D(kT_S - \tau).C(kT_S - \tau).\cos(2\pi f_I kT_S - \theta) + b(k) \quad \textbf{(49)}$$

Where:

- *A* is the magnitude of the incoming signal
- *D* and *C* are waveforms, respectively associated to navigation message and code (C/A for instance)
- f_I is the final intermediate frequency
- T_s is the sample period and $F_s=1/T_s$ is the sampling frequency
- θ is the incoming signal carrier phase shift
- τ is the group propagation time of the signal
- *b* is the additional noise

So, after multiplication by local carrier and code, the output to be integrated is then:

$$\begin{cases} V_I(k) = V(k).\cos\left(2\pi f_I k T_S - \hat{\theta}\right).C(kT_S - \hat{\tau}) \\ V_Q(k) = V(k).\sin\left(2\pi f_I k T_S - \hat{\theta}\right).C(kT_S - \hat{\tau}) \end{cases} \quad \textbf{(50)}$$

In order to track the incoming GNSS signals, two loops have to be used:

- One loop to track the carrier of the incoming signal, called phase lock loop (PLL). The PLL goal is to generate a local carrier as close as possible to the incoming carrier to keep the phase error between the locally generated carrier and the incoming signals close to zero.
- One loop to track the GNSS signals code, called the Delay Lock Loop (DLL) The objective of the DLL is to generate a local code as close as possible to the incoming code to keep the delay error between the locally generated code replica and the incoming signal code.

The following figure illustrates the signal tracking process, which relies on discriminators outputs (and consequently the correlators outputs). The discriminators are defined and described in the next section.

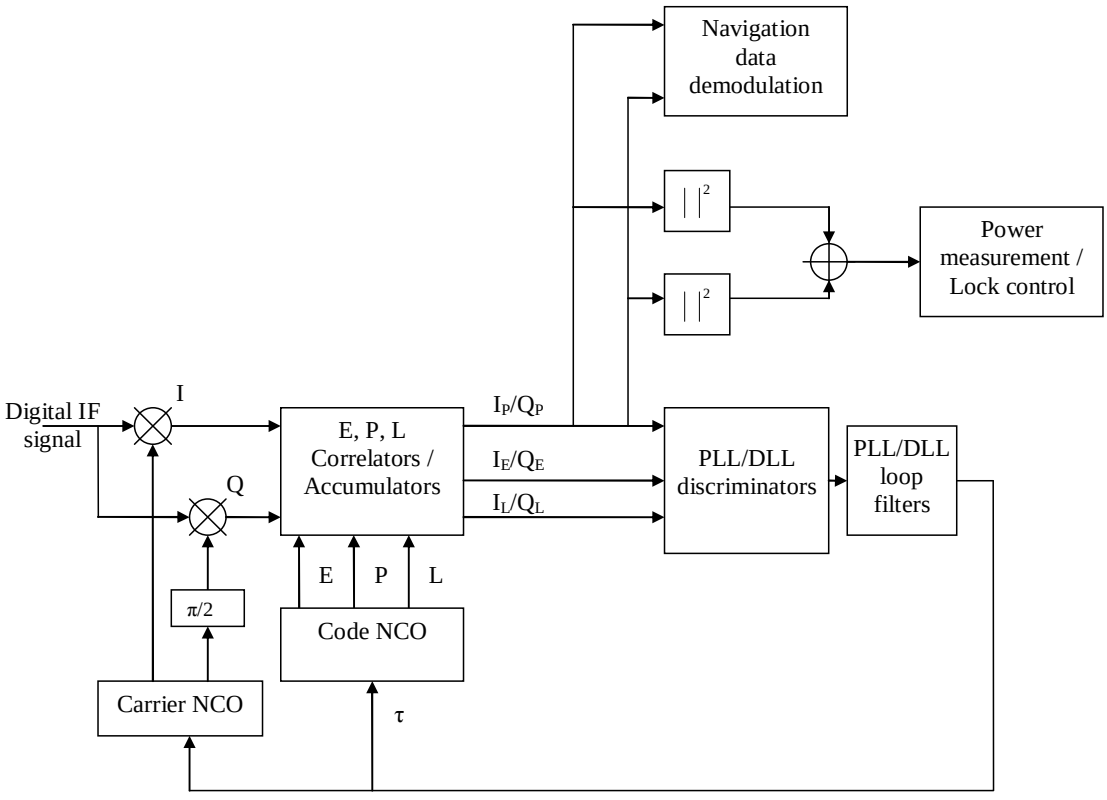

Figure 10: Tracking process

2.3.7.7.4. Correlation

During the tracking of GNSS signals, after signal carrier wipe-off the correlation process consists in the multiplication by a PRN code local replica and then, integration over a certain time. In its strict definition, the correlation is the process of multiplying the incoming signal with the locally generated replica of the received spreading sequence and accumulating (or integrating) the result. The accumulation operation is referred to as the coherent integration. In addition to the effects of external disturbances due to the signal propagation (described latter in this chapter) and frontend filtering (that limits the incoming signal spectrum), the correlation process is greatly affected by the presence of a carrier. For this reason, the correlation process also includes the frequency removal process. Frequency removal, or carrier wipe-off, is performed by multiplying the incoming signal with the locally generated replica of the received carrier. This operation is followed by correlating the resulting incoming signal with a local PRN code replica. It is realized according to the following block diagram.

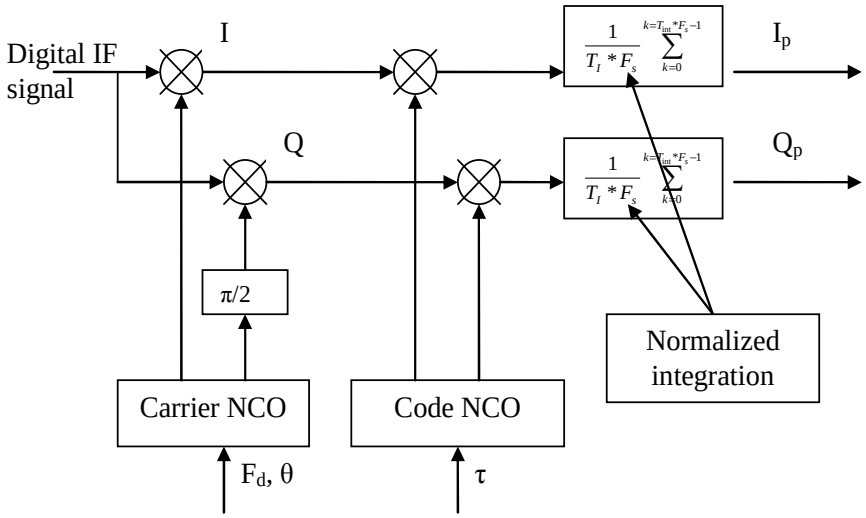

Figure 11: Correlation process

For normal aircraft dynamics, after front end filtering, I and Q channels prompt outputs formal expressions are:

$$\begin{cases} \mathrm{I_p} = \dfrac{\mathrm{A}}{2}\dfrac{\sin(\pi\Delta \mathrm{f T_I})}{\pi\Delta \mathrm{f T_I}}\mathrm{R_{IL}}(\epsilon_\tau)\cos(\epsilon_\theta) + \mathrm{n_I} \\ \mathrm{Q_p} = \dfrac{\mathrm{A}}{2}\dfrac{\sin(\pi\Delta \mathrm{f T_I})}{\pi\Delta \mathrm{f T_I}}\mathrm{R_{IL}}(\epsilon_\tau)\sin(\epsilon_\theta) + \mathrm{n_Q} \end{cases} \quad \textbf{(51)}$$

Where:

- Δf is the frequency offset between received and local carrier
- ϵ_τ is the code tracking error
- ϵ_θ is the phase tracking error
- R_{IL} is the correlation function between the filtered incoming signal and the local replica
- A is the amplitude of the referred signal
- T_I is the integration time
- n_I is the noise at correlator output on the I channel

- n_Q is the noise at correlator output on the Q channel

As it is mentioned in the signals structure description (paragraph 2.3.5), future GNSS signals will be composed of data (with message transmission) and pilot channels. It can be noticed that the maximum coherent integration time is limited to the duration of the data bit on the data channel. This constraint does not exist on the pilot channel. As a consequence, for the Galileo E1 OS data channel and the GPS L1 C/A signal, the coherent integration T_I is limited to 4 and 20 ms respectively. Nevertheless, there are other strong limitations to signal integration time like oscillator stability and dynamics as it is detailed in [Julien, 2005].

2.3.7.7.5. Discriminators

Discrimination is the first step for accurate estimation of code and phase tracking errors. Several discriminators exist and are based on the use of I and Q channels outputs.

The PLL uses phase tracking discriminators that measure the lag between input and local carrier phase. Phase discrimination is dependent upon the presence or absence of data bits on the data and pilot channels. Indeed, the presence of data (data bit transitions) generates changes in phase. It results changes in signal polarity that must be taken into account while discriminating. As a consequence, two types of phase discriminators can be distinguished: on the data channel and on the pilot channel as mentioned in [Julien, 2005].

For the data channel, the discriminator must be insensitive to the phase jumps due to data bit transitions. The most used corresponding phase discriminator is the IQ one [Ward, 2007]. Indeed, the IQ (or Costas) discriminator is based on the product of I and Q channels correlation components. So the sign changes during data bit transitions are compensated, and the discriminator output keeps the same sign.

$$\mathrm{V_e} = \mathrm{I}.\mathrm{Q} \tag{52}$$

$$\mathrm{V_e} = \frac{\mathrm{A}^2}{4}\mathrm{R}_{\mathrm{IL}}^2(\varepsilon_\tau)\ \sin(\varepsilon_\theta)\cos(\varepsilon_\theta) + \ n_e \tag{53}$$

Where:

- $\begin{cases} \varepsilon_\tau = \tau - \hat{\tau} \\ \varepsilon_\theta = \theta - \hat{\theta} \end{cases}$ are respectively, the delay error and the phase tracking error
- $R^2(\varepsilon_\tau)$ is the square of the correlation function between the filtered incoming signal and the local replica
- n_e is the PLL discriminator noise

When the phase loop is locked, the error is then congruent to zero modulo π. The phase is estimated with an error equal to a multiple of π. $\mathrm{V_e}$ is not normalized. This discriminator is

not linear and, in reality, it tracks twice the carrier phase error. Consequently, as depicted in figure 4, the stability domain is reduced to $\left[-\frac{\pi}{2};\frac{\pi}{2}\right]$.

Another well-known discriminator used for the data channel is the arctangent one:

$$V_e = \arctan\left(\frac{Q}{I}\right) \quad \textbf{(54)}$$

Indeed, as for the Costas discriminator, the sign changes are cancelled by the ratio between I and Q channels. This discriminator has the same stability region than the IQ one and has the same uncertainty but it is linear as it can be seen Figure 13 and normalized.

Figure 12: Costas discriminator

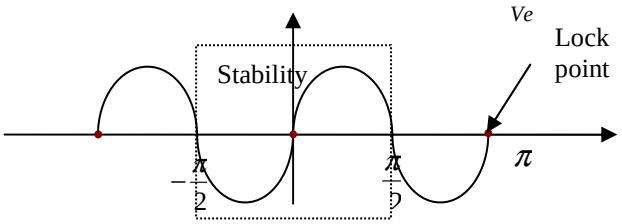

Figure 13: Arctan discriminator

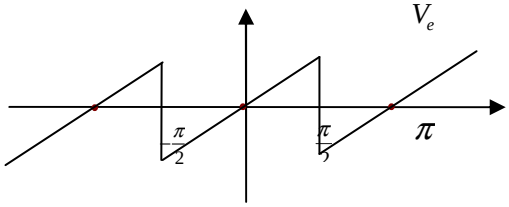

Note that these two discriminators have several lock points separated by π radians. As a consequence, for any reason, if the receiver loses lock of this tracking loop for a certain time (this problem is called cycle slip and is described in details and studied in chapter 6), the minimum slip amplitude is equal to half a cycle. Nevertheless, this is only true before data frame synchronisation.

For the pilot channels, as mentioned in the correlation description (section 2.3.7.7.4), the integration time is not limited by the data bit transitions. Other parameters can limit the integration time like dynamics or local oscillator stability. Thus, the PLL discriminator does not have to be insensitive to data bit transitions. Other discriminators were proposed in literature, for instance, the coherent discriminator [Julien, 2005] with a stability domain twice as large as the Costas stability domain. Another example of discriminator is the extended arctangent discriminator that is described in [Julien, 2005]. It has a wide linear tracking range and is consequently more robust against losses of lock and so cycle slips.

2.3.7.7.6. Loop filters

The purpose of the loop filter is to reduce the power of the noise that affects the discriminator output without cancelling high frequency variations of the error due to the receiver dynamics. A loop filter is usually composed of a sum of digital integrators with different orders. Only two parameters are necessary for the design of a loop filter: the noise bandwidth B_n and the filter order which determines the filter's response to signal dynamics.

The higher the filter order, the higher the loop robustness to dynamic variations of the system, but the lower the loop stability.

The temporal model of pseudoranges variations is used to model the loop robustness against dynamics. There is no tracking error due to dynamics in a first order PLL if the pseudorange has no more than a first order polynomial time variation. The same remark can be made for higher order models. As for PLL, a loop filter is used for DLL. As explained in [Julien, 2005], phase tracking is less robust against dynamics than code phase tracking. So the choice of PLL loop filter order must be higher than the DLL loop filter order. In addition, the DLL is aided by the PLL. Indeed, the DLL DCO command equals the DLL discriminator output plus the filtered PLL discriminator output.

2.3.7.8. Conclusions

From the signal processing described in the previous sections, the receiver provides pseudoranges. In a real world, as described at the beginning of this chapter, pseudorange measurements are affected by signal propagation and several kinds of perturbations identified in [Parkinson, 1996] and described in the next section.

2.4. Perturbations affecting GNSS signals

2.4.1. Introduction

The GNSS measurements are affected by various phenomena due to the receiver environment and capability to track the incoming GNSS signals. Amongst these phenomena are identified the effects due to the signals propagation environment: the ionosphere and troposphere crossing, the signal multipath, and the interferences. Other sources of perturbations are the aircraft dynamics and the receiver noise described in [Julien, 2005] or in [Bastide1, 2004]. The following paragraphs provide a description of each of these phenomena.

2.4.2. Ionosphere

One of the most important effects on the radio navigation signals is the one caused by the ionized layer of the atmosphere, the ionosphere, which causes a delay in the electromagnetic signals that go through it. The GNSS signals used for civil aviation goals are consequently affected by this perturbation. In the following paragraph, we describe the ionosphere and we demonstrate the impact of this atmosphere layer on the electromagnetic wave.

The Earth atmosphere is divided into several layers, one of these is the plasma called the ionosphere. It begins at around 50 km from the Earth surface and ends at around 2000 km [Garcia, 2002]. In this layer of the Earth atmosphere, particles are ionized under the

action of sunlight, cosmic, UV, X radiations and even meteorites falls. At the higher altitudes, there is the layer called magnetosphere.

The ionosphere is produced by the ionization of molecular species as for instance, oxygen, after sun radiations. As this effect is decreasing when approaching the Earth surface, the consequences are different for varying altitudes. That is to say, the electronic content due to the solar radiations varies as a function of altitude. Consequently, several layers in the ionosphere corresponding to different effects on GNSS signals propagation are defined. The layers are the F, E and D regions and are described in [Garcia, 2002]. In the following paragraphs, the characteristics of these layers are recalled.

The F layer (130-150 km) corresponds to the layer where the electrons concentration is between 10^{11} and 10^{12} electrons per m^3. Within this region, ionization effect decreases exponentially with altitude because of the decreasing number of molecules. The ionization of this region of the atmosphere is extremely variable with time and space. Thus, it presents sometimes electronic content irregularities responsible of electromagnetic signals scintillations.

The E layer is located at 90 up to 130 km altitudes and presents more regular fluctuations than the F region. The maximum ionization level, located at 110 km high, is the order of 10^{11} m^{-3}.

The D layer (50 to 90 km) where the molecular density is higher than in the other layers is characterized by collisions between neutral and ionized particles.

The ionospheric code delay is the largest source of ranging error for GNSS signals as mentioned in [Parkinson, 1996]. It is depending upon the Total Electronic Content (TEC) of the medium, which corresponds to the total number of electrons met along one given signal path, considering a 1 m^2-section cylinder around the signal path [Garcia, 2002]. TEC varies as a function of several phenomena such as solar activity (sunspot numbers), the Earth inclination, its rotation around its spin (hours) and around the Sun (seasons).

In the following, we describe the impact of the ionosphere crossing on all GNSS signals. The link between the TEC value and the ionospheric code delay is established. The model proposed in [RTCA, 2006] to estimate ionospheric code delay for any satellite elevation is also provided.

The propagation speed of an electromagnetic wave is proportional to the emission frequency f. More precisely, for a corresponding signal wavelength λ, which depends upon the signal carrier frequency ($\lambda = \frac{c}{f}$), the phase velocity is given by [Garcia, 2002]:

$$v_p = \lambda f \quad \textbf{(55)}$$

The group (where the information is carried) velocity is given by:

$$v_g = -\lambda^2 \frac{df}{d\lambda} \quad \textbf{(56)}$$

Since $f = \frac{v_p}{\lambda}$, these two expressions are related by the following equation:

$$v_g = -\lambda^2 \left[\frac{\frac{dv_p}{d\lambda}\lambda - v_p \frac{d\lambda}{d\lambda}}{\lambda^2} \right] = v_p - \lambda \frac{dv_p}{d\lambda} \quad \textbf{(57)}$$

Since the ionosphere is a dispersive medium, the phase and group speeds are not equal in this medium. Therefore, two refraction indexes to characterize the impact of the ionosphere on the phase and group celerity are defined [Garcia, 2002].

The ionosphere impact on the signal phase is defined thanks to: $n_p = \frac{c}{v_p}$, which is the ratio between the light celerity in the vacuum c (which is also the phase velocity in the vacuum) and the phase velocity in the ionosphere. A development of the refraction index of the phase n_p described in [Garcia, 2002], provides:

$$n_p = \sum_{i=1}^{\infty} \frac{c_i}{f^i} \quad \textbf{(58)}$$

The c_i coefficients depend upon the TEC.

The link between the refraction indexes can be derived:

$$n_g = n_p + f \frac{dn_p}{df} \quad \textbf{(59)}$$

According to [Seeber, 1992], the phase refractive index can be approximated thanks to a series expansion truncated after the quadratic term. A second order truncated development of n_p allows obtaining a significant value of these indexes:

$$n_p = 1 + \frac{c_2}{f^2} - 2f\frac{c_2}{f^3} = 1 - \frac{c_2}{f^2} \quad \textbf{(60)}$$

So, n_g equals to:

$$n_g = 1 + \frac{c_2}{f^2} \quad \textbf{(61)}$$

For ionosphere, the c_2 coefficient is: $c_2 = -40.3 N_e$ **(62),**

where:

- N_e is the electron density in el m^{-3}, it represents the number of electrons in a volume unit;
- 40.3 is expressed in $m^3 s^{-2}$

Along a straight path of an electromagnetic wave, that is to say when the refraction index is equal to 1, the geometric range s_0 (in meters) between a satellite and the receiver is provided by:

$$s_0 = \int_{satellite}^{receiver} ds \tag{63}$$

When the electromagnetic waves cross the ionosphere, then for each satellite in view of the receiver, the path corresponding to phase (s_p) and group (s_g) are then:

$$\begin{cases} s_p = \int_{satellite}^{receiver} n_p \ \ ds \\ s_g = \int_{satellite}^{receiver} n_g \ \ ds \end{cases} \tag{64}$$

As a consequence, the ionosphere error is expressed as a code delay and a phase advance, taking into account the difference between the straight path and the actual path:

$$\begin{cases} \mathrm{I_p = s_p - s_0 = -\frac{40.3}{f^2} \int N_e ds = -\frac{40.3}{f^2} TEC} \\ \mathrm{I_g = s_g - s_0 = +\frac{40.3}{f^2} TEC} \end{cases} \tag{65}$$

Where I_p corresponds to the phase advance and I_g corresponds to the code delay. It is expressed in meters, but it can also be expressed in seconds by dividing by the speed of light in vacuum.

The first equation is synonymous with a phase advance (because of the presence of the minus sign) and the second one, a group delay (sign plus). For instance, for L1, L2, L5, E5a frequencies, the time of arrival of code and phase measurements at the receiver antenna level is:

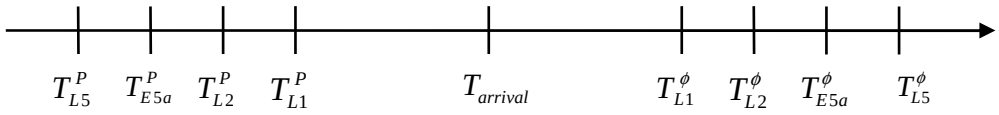

Figure 14: Time of arrival of code and carrier phase of each signal

where the origin represents the theoretical time of arrival of the signal at the receiver level (if the signal followed the s_0 path); T_x^P represents the carrier phase arrival and T_x^ϕ the code arrival with delay for each frequency.

Therefore, the pseudorange measurements can be re-written as:

$$\begin{aligned} \mathrm{P^i(k)} &= \mathrm{\rho^i(k) + c\left(\Delta t_u(k) - \Delta t^i(k)\right) + c\left(I_g{}^i(k) + \tau^i(k)\right) + D^i_{mult}(k) + n^i(k)} \\ &= \mathrm{\rho^i(k) + c\left(\Delta t_u(k) - \Delta t^i(k)\right) + c\left(\frac{40.3}{f^2} TEC^{\,i}(k) + \tau^i(k)\right) + D^i_{mult}(k)} \\ &\quad \mathrm{+ n^i(k)} \end{aligned} \tag{66}$$

$$\phi^i(k) = \rho^i(k) + c\left(\Delta t_u(k) - \Delta t^i(k)\right) + c\left({I_p}^i(k) + \tau^i(k)\right) + \Phi^i_{mult}(k) + N^i\lambda^i + n^i(k) \quad \textbf{(67)}$$

$$= \rho^i(k) + c\left(\Delta t_u(k) - \Delta t^i(k)\right) + c\left(-\frac{40.3}{f^2}\mathrm{TEC}^{\ i}(k) + \tau^i(k)\right) + \Phi^i_{mult}(k) + N^i\lambda^i + n^i(k)$$

Where:

- i denotes a particular satellite
- P is the code pseudorange measurement in meters
- ϕ the carrier phase measurement (in meters)
- ρ is the actual distance between a satellite i and the receiver
- c is the light speed, equal to 299 792 458 m/s
- $\Delta t_u(k)$ is the user clock shift
- $\Delta t^i(k)$ represents the i^{th} satellite clock shift
- I is the ionosphere error
- τ is the troposphere error
- D_{mult} is the multipath error for code measurement
- Φ_{mult} is the multipath error for carrier phase measurement
- N is the ambiguity (random number of cycles)
- λ is the carrier wavelength
- n is the residual noise

The TEC is linked to the behaviour of the ionosphere all along electromagnetic waves path from a satellite to a receiver. It is consequently linked to the receiver and satellites positions. In particular, the TEC value is a function of the considered satellite elevation from the receiver point of view.

The electronic content along an electromagnetic wave path is different if the satellite is at the receiver zenith or near the horizon. In order to take this effect into account, the obliquity factor is defined as the ratio between the real TEC computed between the satellite and the receiver called Slant TEC (STEC) and the Vertical TEC (VTEC) computed when the satellite is at the receiver zenith [Garcia, 2002].

$$Ob = \frac{STEC}{VTEC} \quad \textbf{(68)}$$

As a conclusion, the ionosphere causes the GNSS signals phases to advance and the corresponding codes to delay. The ionosphere can be described thanks to several layers with different electron densities (D, E, F layers) in which the electrons have different densities. In addition, the ionosphere medium has a large variability (in terms of electronic content) depending upon many parameters like for instance the Earth inclination or the solar activity. Thus, the impact of the ionosphere on the GNSS signals is difficult to predict and difficult to model. Nevertheless, some models are built to provide an estimation of the TEC and the corresponding code delay on the GNSS measurements. These models can be based on

single-layer assumptions (Klobuchar) or multi-layer assumptions (NeQuick) and are described in Chapter 6.

Concerning the single-layer models, the assumption made is that the ionosphere can be imagined as a thin shell at 350 km around the reference geoid (WGS 84). Thus, a theoretical derivation of the obliquity factor geometrical value can be made. In the next paragraph, we describe this model proposed in [RTCA, 2006].

2.4.2.1. Thin shell model

Assuming the ionosphere is extremely thin (thin shell model described in [Parkinson, 1996]) and located at 350 km around the Earth reference geoid (WGS 84), the obliquity factor can be modelled geometrically thanks to the elevation angle of the space vehicle, from the model proposed in [RTCA, 2006], assuming the receiver is located near the Earth surface:

$$Ob = \left[1 - \left(\frac{R_e}{R_e + h} \cos(E) \right)^2 \right]^{-\frac{1}{2}} \quad \textbf{(69)}$$

Where:

- R_e is the mean equatorial radius of the Earth,
- h is the altitude of the considered ionosphere,
- E is the elevation angle.

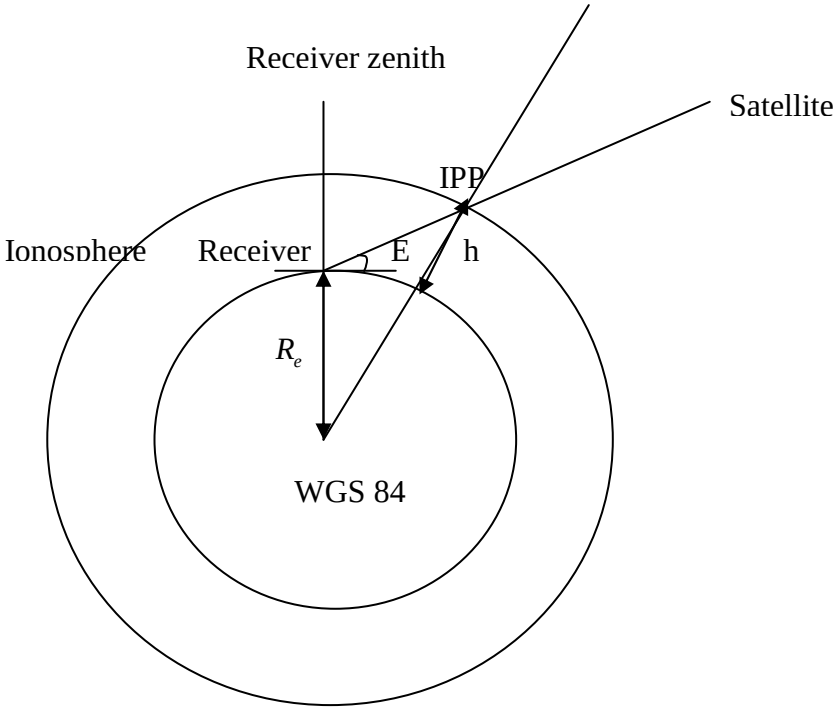

Figure 15: Geometrical parameters for obliquity calculation

Where:

- IPP stands for Ionospheric Pierce Point, it is a theoretical point located at around 350 km high where the electromagnetic wave path from the satellite to the receiver crosses the ionosphere.
- E is the elevation angle of a considered satellite from the receiver point of view taken from the tangent plane to the WGS 84 at the receiver location.

Then, the ionosphere error is given by:

$$\mathrm{I} = \frac{40.3}{\mathrm{cf}^2}\,\mathrm{STEC} \quad \textbf{(70)}$$

It can be seen that it depends upon the TEC computation within an atmosphere column located around an electromagnetic wave path from a satellite to the receiver.

$$\mathrm{I} = \frac{40.3}{\mathrm{cf}^2}.\,\mathrm{VTEC}.\,\mathrm{Ob} \quad \textbf{(71)}$$

2.4.3. Troposphere

Troposphere effects are generated by the non-ionized portion of the atmosphere extending from the surface of the Earth up to an altitude of nearly 40 km. An electromagnetic signal propagating through this neutral layer of the atmosphere is affected by the constituent gases (wet and dry parts) [Parkinson, 1996].

The troposphere causes a refraction of the RF signals because of the larger refractive index than that of vacuum. This index is constant with frequency, non dispersive for frequencies lower than 30 GHz. Thus the group and phase velocities are identical, contrary to ionosphere propagation. The actual path of the RF ray through the troposphere is longer than the straight geometrical line, bent in such a way that the curved path is closer to the zenith than the straight line [Parkinson, 1996].

2.4.4. Multipath

A signal can arrive to the receiver via multiple paths, with different faded power of the replica of the original signal. This phenomenon, attributable to reflections and diffraction on surrounding obstacles (buildings, hard ground, trees etc...) is called multipath and its impact on signals processing is briefly described hereafter.

The reflected signals entering the front end of the receiver are mixed to the original direct signal and entails tracking errors. Indeed, multipath can unshape the correlator outputs used for code and carrier tracking. It can also distort carrier phase as mentioned in [Rebeyrol, 2007].

The amplitudes of multipath signals are frequently less than or equal to the LOS signal. Indeed, the reflectors attenuate the replica of the LOS signal and reflected signals. This fading is thus dependent upon the type of reflecting surface (ground, aircraft fuselage...).

2.4.5. Interferences

The interferences have the particularity to be one of the most feared phenomena affecting GNSS signals and consequently aircraft positioning. Indeed, this phenomenon can affect simultaneously several GNSS components located in the same ARNS band.

Interferences have various and numerous effects on signal processing and consequently on pseudoranges estimation. The impact of the out of band interferences is reduced at the front end level by filters according to maximum interference levels specifications provided by [EUROCAE, 2007].

The main unintentional interference types in the ARNS band are Carrier Waves (CW), Wide Band interferences (WB) and pulsed interferences. In the next paragraphs, a short description of these interferences is provided hereafter.

A CW is a sinusoidal waveform. The mathematical model of a transmitted CW is provided by the following equation:

$$\mathrm{CW}(t) = \sqrt{P_{CW}}.\cos\left(2\pi(f_I + \Delta f_J)t + \theta\right) \quad \textbf{(72)}$$

Where:

- P_{CW} is the power of the CW interference (dBW)
- Δf_J is the frequency offset of the jammer with respect to the considered GNSS signal carrier frequency (Hz)
- $f_I + \Delta f_J$ is the central frequency (Hz)
- θ is the interference phase (rad)

Pulsed interferences can affect GPS L5 and Galileo E5. Indeed, for instance, the DME (Distance Measuring Equipment) system is a pulsed ranging system which provides range measurement from an aircraft to a ground beacon. This system is internationally standardized and operates in the 960-1215 MHz ARNS frequency band. The DME interrogator obtains a distance measurement by transmitting pulse pairs and waiting for reply pulse pairs from the beacon. The aircraft selects a near beacon and an appropriate frequency to measure its distance to ground. Each beacon transmits Gaussian pulses by pairs.

In this thesis, only continuous CW are considered. Indeed, the impact of pulsed interferences has been already conducted in another project and reported in several other publications and in particular in [Raimondi, 2006] for the EUROCAE WG62.

2.4.6. Satellite clock error

The satellite clock error comes from satellite oscillator offset with regard to the GPS or Galileo time. This satellite clock modeling can be done through clock parameters transmitted in the satellite ephemeris [Winkel, 2003].

2.4.7. Receiver dynamics

Aircraft dynamics is another perturbation that can affect GNSS signals processing and consequently, aircraft instantaneous position estimation. The main civil aviation standards ([EUROCAE, 2007], [RTCA, 2006]) provide the onboard receiver dynamics specifications. The maximum dynamics values in terms of ground speed, horizontal and vertical acceleration and total jerk are provided for an aircraft having normal and abnormal maneuvers.

The dynamics values for both normal and abnormal maneuvers are recalled in Table 2:

	NORMAL AIRCRAFT DYNAMICS	ABNORMAL AIRCRAFT DYNAMICS
GROUND SPEED	800 KT	800 KT
HORIZONTAL ACCELERATION	0.58 g	2.00 g
VERTICAL ACCELERATION	0.5 g	1.5 g
TOTAL JERK	0.25 g/s	0.74 g/s

Table 2: Normal and Abnormal aircraft dynamics, [EUROCAE, 2007].
Where: g = 9.81m/s² and Kt are Knots.

The normal dynamics are defined to be manoeuvres whose acceleration and jerk do not exceed the values in the first column. The abnormal dynamics are defined to be manoeuvres whose acceleration and jerk are between the values recalled in the first column and the maximum values in the second column.

The pseudorange measurements model in presence of aircraft dynamics can be re-written as:

$$P^i(k) = \rho^i(k) + v(k).t(k) + 9.81\,a(k).\frac{t(k)^2}{2} + 9.81\,j(k).\frac{t(k)^3}{6} + c\left(\Delta t_u(k) - \Delta t^i(k)\right) + c\left({I_g}^i(k) + \tau^i(k)\right) + D^i_{mult}(k) + n^i(k) \quad \textbf{(73)}$$

$$\phi^i(k) = \rho^i(k) + v(k).t(k) + 9.81\,a(k).\frac{t(k)^2}{2} + 9.81\,j(k).\frac{t(k)^3}{6} + c\left(\Delta t_u(k) - \Delta t^i(k)\right) + c\left({I_p}^i(k) + \tau^i(k)\right) + \Phi^i_{mult}(k) + N^i\lambda^i + n^i(k) \quad \textbf{(74)}$$

Where:

- i denotes a particular satellite

- k denotes the sample time number
- P is the code pseudorange measurement in meters
- ϕ the carrier phase measurement (in meters)
- v is the ground speed of the aircraft (receiver), in m/s
- a is the acceleration of the aircraft, in m/s^2
- j is the jerk of the aircraft in m/s^3
- ρ is the actual distance between a satellite i and the receiver
- c is the light speed, equal to 299 792 458 m/s
- $\Delta t_u(k)$ is the user clock shift
- $\Delta t^i(k)$ represents the i^{th} satellite clock shift
- I is the ionosphere error
- τ is the troposphere error
- D_{mult} is the multipath error for code measurement
- Φ_{mult} is the multipath error for carrier phase measurement
- N is the ambiguity (random number of cycles)
- λ is the carrier wavelength
- n is the residual noise

In the following, the index k, which defines the measurement sample number, will be replaced by the time index only.

2.5. Conclusions

This chapter presents the GNSS applied to civil aviation. It presents the GNSS components studied in this thesis, in compliance with the EUROCAE on-going works [Mabilleau, 2007]. The signal processing within the civil aviation receivers is detailed and the corresponding measurement models (pseudoranges) are described as function of external perturbations in an aircraft environment. All the perturbations affecting the GNSS signals received onboard an aircraft during a phase of flight are also described and their impacts on the measurements are discussed.

The involvement of each perturbation on the performances reached by a receiver located onboard a flying or landing aircraft is described. The resulting GNSS measurements processes to provide the aircraft protection levels are also described. These protection levels have to be compared to civil aviation requirements which are also recalled as function of the phase of flight of the aircraft [RTCA, 2006].

The future onboard GNSS combined receivers have to be compliant with the civil aviation requirements that are defined by means of performances specified in terms of integrity, continuity, availability and accuracy. The different means identified by the EUROCAE WG 62 to provide the required levels of performance during an aircraft flight are identified amongst the components (constellations, frequencies, augmentation systems) presented in this chapter and the different strategies for navigation solution and integrity monitoring will be presented in the next chapter (3).

Chapter 3

Combined use of GNSS components and receivers architecture

Contents

Résumé

Une architecture de récepteur combiné GPS + Galileo + systèmes d'augmentation est proposée dans le chapitre 3. Nous décrivons les modes opérationnels (nominal, alterné et dégradé) et identifions les différentes combinaisons les plus prometteuses d'un point de vue opérationnel et retenues par l'EUROCAE. L'architecture globale des futurs récepteurs combinés est basée sur deux fonctions principales, pour chaque mode opérationnel, qui sont la fonction de navigation qui fournit une position et une intégrité au système et une fonction de détection d'anomalies. Pour chaque mode, la fonction de navigation repose sur l'utilisation de combinaisons GNSS identifiées par l'EUROCAE comme nominales, alternées ou dégradées. Un système de commutation entre les modes opérationnels (ou au sein de combinaisons d'un même mode), permet d'utiliser les combinaisons GNSS disponibles les plus performantes en termes de précision, intégrité, continuité et disponibilité. Les exigences de l'aviation civile pour chaque phase de vol sont satisfaites en mode nominal ou alterné. En mode dégradé, une alerte est automatiquement envoyée au pilote. Dans ce cas, nous abordons la question du maintien des niveaux de performance et de reconfiguration du navigateur. S'il n'est pas possible de maintenir les performances permettant d'effectuer les opérations de vol, d'autres moyens que le GNSS peuvent alors être utilisés.

3. Combined use of GNSS components and receiver architecture

The goal of this chapter is to describe the future civil aviation receiver global architecture. This architecture must comply with the civil aviation needs. So, in order to reach the ICAO requirements for each phase of flight, the most promising GNSS components combinations (in terms of performance) must be identified and used. This identification is made in [EUROCAE, 2007] and summarized in this chapter. Therefore, the global combined receiver architecture relies on these components combinations.

As a consequence, this chapter first recalls the definitions of the modes of operation [EUROCAE, 2007] for each phase of flight addressed in this thesis dissertation. Secondly, the GNSS components combinations identified by the WG 62 are classified by modes of operations, according to the performances that can be reached. Thirdly, the combined receiver architecture is proposed, in coordination with the DTI. This architecture has been approved by the WG 62 during the 22nd meeting.

3.1. Definition of modes of operation

In the following, we provide the official definitions of the operation modes [EUROCAE, 2007].

3.1.1. Nominal mode

A nominal mode is a mode of operation in which the receiver achieves the same level of performance using a pre-described, preferred combination of signals [EUROCAE, 2007].

3.1.2. Alternate mode

An alternative mode is a mode of operation in which the receiver achieves the same level of performance of the nominal mode using alternative means, or an augmentation. A receiver enters into an alternate mode when one or more of the signals of the nominal mode are not available at SIS level, but the remaining signals or augmentations can still meet the level of performance of the nominal mode [EUROCAE, 2007].

3.1.3. Degraded mode

A degraded mode is a mode of operation in which the receiver is unable to achieve the level of performance of the nominal mode. A receiver enters into a degraded mode when one or more of the signals of the nominal mode are not available at SIS level, and the

remaining signals or augmentations are insufficient to meet the level of performance of the nominal mode [EUROCAE, 2007].

3.1.4. Conclusion

When a degradation occurs on one or more GNSS component, the performances reached for aircraft positioning and integrity monitoring can be lower than required by the ICAO to perform an operation. In this case, the combined receiver enters an alternate or a degraded mode. Then, the new mode of operation depends upon the fact the performances reached are sufficient or not to continue the operation. This implies the use of degradation detection functions to monitor the performances reached and thus the availability of the components.

The corresponding degradation detection functions are defined in this chapter with the generic combined receiver architecture. Then, when the degradation is flagged, it is necessary to decide when the receiver enters an alternate or a degraded mode.

When the receiver enters a degraded mode, an alert must be raised to flag the receiver incapability to provide the service required for the aircraft operations.

Note that the detection functions are not only integrity monitoring functions. These functions must allow monitoring all the performances losses. For instance, a detection function can monitor interferences occurrence and impact on the aircraft positioning accuracy.

An on-going development of a reference document called Concept of Operations (ConOps) [EUROCAE, 2008][2], is written by the WG 62 members. In this document, the combinations of GNSS components are classified by modes of operation defined previously. These modes of operation depend upon the level of performance reached by using some specific GNSS components, for a targeted phase of flight. The most promising GNSS components combinations that meet the ICAO requirement corresponding to a given phase of flight are proposed as nominal. The combinations that provide a sufficient level of performance to begin or continue an operation but with non-preferential means are classified as alternate. Finally, in case of loss of GNSS component, the remaining components that are not supposed to match all the performance criteria are classified as degraded. This work is exposed in [EUROCAE, 2007][3] and [EUROCAE, 2008]. These documents are based upon the EUROCAE WG 62 working assumptions.

3.2. GNSS combinations identified by the EUROCAE WG 62

An analysis of the performance reached by GNSS combinations was made upstream this thesis by the WG 62. The following table shows the identified combinations classified as a function of the operation modes and phases of flight by the WG 62 in [EUROCAE, 2008]. The GLONASS constellation is not considered. Indeed, first, the GLONASS MOPS does not exist

[2] Note that this reference document is still under development, the proposed reference is the latest draft version
[3] Note that this is an interim version of MOPS Galileo

anymore, secondly, GLONASS uses only FDMA signals and not CDMA, and thirdly, there is no SIS for civil aviation. Therefore, the EUROCAE WG62 focuses on GPS + Galileo + augmentation systems. Since this thesis follows the evolution of the EUROCAE works, it also focuses on GPS + Galileo + augmentation systems.

	NOMINAL	ALTERNATE	DEGRADED
En route to NPA	• Galileo SoL • Galileo E1 E5b + GPS SBAS • GPS SBAS L1 L5	• GPS single frequency + SBAS • Galileo single frequency + SBAS • Galileo single frequency + SoL • Combination of all available pseudoranges + RAIM	• No integrity information
APV I	• Galileo SoL • Galileo E1 E5b + GPS SBAS • GPS SBAS L1 L5	• GPS single frequency + SBAS • Galileo single frequency + SBAS	• Galileo single frequency + SoL • Combination of all available pseudoranges + RAIM

Table 3: Identified nominal, alternate and degraded modes for en route to NPA and APV I phases of flight [EUROCAE, 2008].

For the Galileo standalone receiver the nominal configuration is E1 + E5b with integrity provided by the Galileo SoL service (see Chapter 2). Note that the Galileo integrity information will be available on two signals navigation message: E1 and E5b I/NAV and on Galileo satellites in view. The use of Galileo provided integrity is the nominal mode of operation for En-Route down to APV.

Concerning the GPS, the nominal configuration is the dual frequency L1 + L5 and the SBAS to provide the required integrity from En-Route down to APV.

There are several possible configurations for the alternate and degraded modes. The alternate and degraded modes to be standardized and used are dependent upon the operational benefits obtained [EUROCAE, 2008].

There are no alternate modes to APV without augmentations. The alternate and degraded modes also include the use of the Galileo E5a signal which is likely to be processed by future receivers [EUROCAE, 2008].

The loss of one frequency implies to use the SBAS to provide the ionospheric corrections usually provided by dual frequency pseudorange measurements combinations as it is described in Chapter 6.

The Receiver Autonomous Integrity Monitoring (RAIM) with a fault detection and exclusion (FDE) capability should also be used to supplement the primary integrity methods (SoL or SBAS).

For En-Route down to NPA operations, the RAIM (+FDE) should be used to provide independent integrity monitoring of the navigation solution whenever SBAS or Galileo provided integrity is not available. When Galileo provided integrity is available, the RAIM is not required [EUROCAE, 2008].

In this report, only GPS SBAS L1/L5 is assumed and not Galileo integrated into an SBAS (e.g. EGNOS).

Galileo Integrity Channel (GIC) is considered in this thesis as there is no specific mismatch between GIC and civil aviation.

3.2.1. Conclusion

A preliminary theoretical study was conducted by the WG 62 and assumptions on potential promising GNSS components combinations are made, in terms of conditions of computation of protection levels and integrity [EUROCAE, 2008]. Thus, the WG 62 identified the components combinations as a function of the performance level reached and classified these combinations as nominal, alternate and degraded means for en-route down to NPA and APV phases of flight. A civil aviation user benefits analysis is on-going within the WG 62 and results in a reference document (ConOps, [EUROCAE, 2008]) which defines the criteria that are mandatory, essential or desirable for future combined receivers' architecture.

Because of a large number of possibilities including other systems like GLONASS, this thesis study is restricted to GPS + Galileo. Then scientific topics are declined from this assumption.

3.3. Global civil aviation combined receivers architecture

3.3.1. Introduction

The goal of this section is to propose a combined receiver architecture, robust against all perturbations described in Chapter 2, with a low complexity and cost and which is compliant with the ICAO requirements for all the phases of flight mentioned in the previous section.

To this end, different strategies have been proposed to define the combined GPS-Galileo receivers. From the operational needs identified by the WG 62, few configurations have been selected as mentioned in [Mabilleau, 2007]. An optimised solution in terms of complexity, robustness and performance for En Route down to APV I operations is proposed and based on a switching logic between dual frequency Galileo SoL and single or dual frequency GPS + SBAS.

The use of the referred components is conditioned by their availability during the operation processed. As a consequence, the receiver global architecture will have to take into account the availability/unavailability of these components and to monitor the degradations that can lead to a loss of GNSS component capability to satisfy the ICAO requirements. In addition, in case of loss of a required component to meet the civil aviation requirement for the on-going operation, the receiver must be able to switch to another

component to maintain the level of performance imposed by the ICAO for the phase of flight.

3.3.2. Global receiver switching architecture

The following scheme represents the global receiver architecture we proposed to the WG 62, in coordination with the DTI. It takes into account the different modes of operation and underlines the link between them thanks to switches driven by detection functions and represented thanks to black arrows. As in table 3, the nominal mode of operation is represented thanks to a green box, alternate mode is represented thanks to an orange box and degraded mode is identified thanks to a red box. On this scheme, blue boxes correspond to functions included in the receiver. Each mode of operation is composed of two functions which are the navigation function and a detection function defined hereafter.

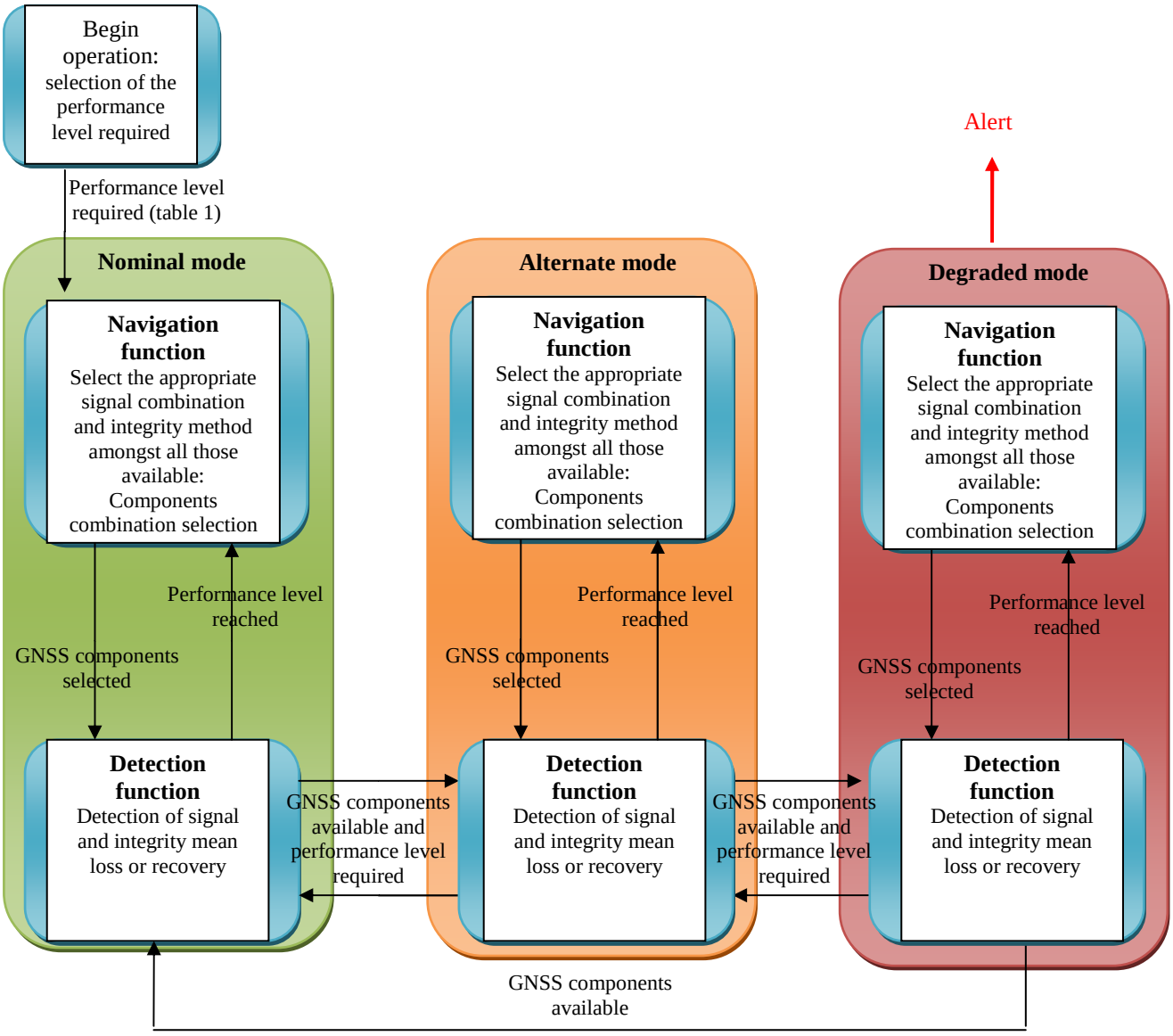

Figure 16: Switching between modes of operation

3.4. The navigation function

The navigation function ensures the provision of the best navigation solution and the corresponding integrity. In the nominal and alternate modes of operation, the navigation function provides outputs compliant with the ICAO requirements (performance criteria).

3.5. The detection function

The detection function allows to determine the components availability and to flag a loss or recovery of component used by the navigation function. Thus, when a component is flagged as unavailable, the receiver can then decide to initiate a switch or not towards other GNSS components combinations.

Amongst the components combinations identified (as function of the operation modes), the receiver must be capable of switching to the best protection level provider (amongst GNSS components), which implies to always compare the protection levels provided by some GNSS components. Nevertheless, the criterion to initiate a switch must not be the lowest protection levels obtained, since, the receiver can switch for a short time to one GNSS component to another. This can imply a jump in the measurements during a short time.

3.5.1. Detection algorithms and civil aviation requirements

To initiate a switch between GNSS components combinations identified in this chapter, the levels of performance reached for each phase of flight obtained after a degradation have to be known and compared to the level of performance required for the current phase of flight. If one of the performance criteria is not reached, then, a switch is initiated.

Therefore, it is necessary to determine the level of performance that can be reached when a component is lost. Then, if the current operation cannot continue or a new phase of flight cannot begin with the current GNSS components, a switch to other components combinations can be initiated. This switching is dependent upon the fact the level of performance is reached or not. The level of performance also determines which nominal, alternate or degraded GNSS components combinations that can be used.

The detection algorithms have to be compliant with continuity and integrity requirements imposed for the current phase of flight. These requirements are synonymous with the false detection, missed detection and false alarm probabilities. These probabilities are defined hereafter.

The false detection probability (P_{FD}) is the probability that the detection algorithm flags an event while nothing occurs.

The false alarm probability (P_{FA}) is the probability that the detection algorithm flags an event and raises an alarm while nothing occurs. The false alarm rate imposed by the operation targeted is the parameter that transcribes the continuity requirements and is recalled for NPA and APV phases of flight in Chapter 2, section 2.2.2.2. The false alarm probability is synonymous with loss of continuity.

The missed detection probability (P_{MD}) is the probability that the detection algorithm does not flag an event (loss of component) whereas this event occurs.

The detection algorithms mentioned here are not built for integrity monitoring but to detect losses of GNSS components capability to provide, when combined with other components, the level of performance required by the ICAO for a targeted phase of flight.

3.5.2. Conclusion

As a conclusion, the detection function must be compliant with the ICAO requirements in terms of integrity and continuity by satisfying missed detection and false alarm probabilities. The detection function is composed of a detection algorithm which indicates a loss or recovery of a given GNSS component. A loss of component is flagged by the detection function when the required level of performance to meet ICAO requirements is not reached for a targeted phase of flight. Then, the unavailable GNSS components are flagged by the detection function and the receiver can then decide to initiate or not a switch to other GNSS components combinations identified by modes of operation in Table 3.

As a consequence, it can be noticed that the detection algorithms allow monitoring each GNSS component availability. Indeed, it allows monitoring the percentage of time the navigation system is capable of providing the required function and performance of the intended phase of flight. A flag of loss or recovery of component is linked to the performances reached thanks to this component. For instance, while using GPS SBAS L1/L5 combination, during APV I, if the SBAS is not able to provide integrity compliant with the ICAO requirements, then, a detection algorithm must flag a loss of the SBAS component availability. The receiver can then decide to switch to other available GNSS combinations, without SBAS.

3.5.3. Detection function and performance levels

The following scheme represents the links between the four performance criteria depicted in [Chatre, 2003] and described in Chapter 2, section 2.2.2. The arrows show that certain performance criteria are dependent upon the others, for instance, the availability of GNSS components is dependent upon the accuracy of the measurements they provide. Indeed, a too large error on the pseudorange values can induce a large bias in the aircraft positioning and a resulting protection level value which may be not compliant with the ICAO

requirements to perform the current phase of flight. The broken arrow shows that continuity limits the risk of losing a component unexpectedly.

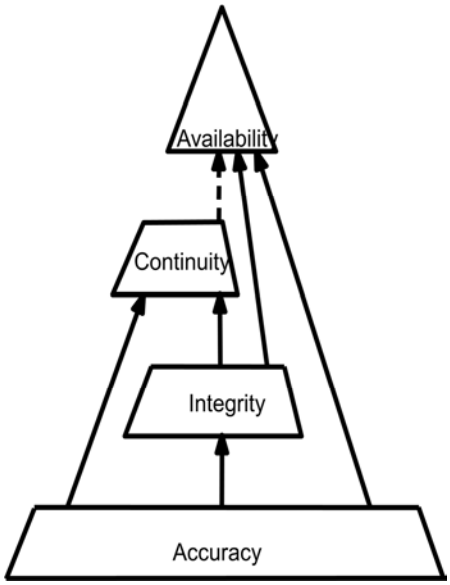

Figure 17: Links between accuracy, integrity, continuity and availability of GNSS components [Chatre, 2003]

The accuracy is the basis of the presented pyramid. The loss of pseudoranges accuracy due to the phenomena described in Chapter 2 (pseudorange measurement model), the bad geometry of satellites from the onboard receiver point of view and the ephemeris error are the three main causes of loss of the accuracy performance level needed to perform a targeted phase of flight.

The availability is at the top of the pyramid, which signifies that all the other performance criteria (accuracy, integrity and continuity) loss have a direct consequence on the availability performance loss for a given GNSS component. Thus, a GNSS component is unavailable when at less one of the accuracy, integrity and continuity performance levels it provides is not compliant with the ICAO requirements for a targeted phase of flight. That is why the detection function is synonymous with GNSS components availability monitoring.

3.6. Conclusion

As a conclusion, operational GNSS components have been identified by the WG 62 and classified by modes of operation for the en route down to the NPA and APV phases of flight. A global receiver architecture is proposed and described in 3.3.2, in coordination with DTI. This architecture relies on a switching logic strategy which was proposed to the Navigation System Panel (NSP) [Mabilleau, 2007]. The global architecture was approved by the WG 62. Two main kinds of functions are part of the presented modes of operation: the navigation and detection functions. It can be noticed that the detection function drives the switches between modes of operation and constitutes one of the main contributions of this thesis (see Chapters 5 and 6) to the WG 62 on-going works. Indeed, the detection function allows flagging the GNSS components availability/unavailability and thus, the availability of the

components combinations identified by the WG 62 (Table 3) as guidelines for future civil aviation combined receivers.

The availability of the GNSS services (Chapter 2) is linked to the GNSS frequencies availability. For instance, considering the Galileo E1 + E5b signals, the availability of the SoL service is linked with the capability of the receiver to demodulate the integrity message carried by both the E1 and E5b signals and the availability of these signals.

If one of the E1 and E5b signals is lost, due to a Radio Frequency Interference (RFI) (Chapter 5), the accuracy of the dual frequency measurements is not ensured because the ionospheric effect is not correctly removed. This problem is addressed in Chapter 6.

If the aircraft is in En-Route down to NPA operations, the single frequency plus SoL solution can be used, since the whole integrity message is broadcasted by both the E1 and E5b signals (I/NAV). The receiver is therefore in an alternate mode.

But, if the aircraft is in APV I phase of flight, the accuracy of the measurements is not sufficient to continue the current operation. An augmentation is thus required to provide the ionospheric code delay estimation (SBAS ionospheric grids) and the receiver is thus in an alternate mode of operation. As a consequence, the Galileo single frequency plus SoL solution is referred to an alternate mode during APV I. In the case the SBAS cannot be used, the receiver reverts to a degraded mode which is the Galileo single frequency mode of operation.

The other main contribution is the study of the degraded mode of operation. In this case, the receiver raises an alert since, by definition, the required level of performance to operate a phase of flight is not reached. As a consequence, it is of interest to propose ways to maintain the required level of performance as long as possible after the switch to the degraded mode of operation. This is done in Chapter 6 for the particular case of single frequency ionospheric code delay estimation.

If the level of performance cannot be maintained, another possibility is to stop using GNSS components for the aircraft operations, until the GNSS components needed to meet the ICAO requirements are available again. The pilot can then use other means to continue or begin a phase of flight, like INS. Nevertheless, the detection function must run during the degraded mode, even if no GNSS component is used. Indeed, in case of component recovery, the receiver can then choose to switch to another mode of operation, so as to provide a sufficient level of performance for the targeted phase of flight.

The aircraft navigator is responsible for troubleshooting problems of the navigation equipment. In the case the level of performance cannot be maintained thanks to the GNSS components, the navigator must be reconfigurated so as to take into account other systems to perform the aircraft operations. Otherwise, the aircraft cannot achieve the current phase of flight or begin a new one.

Chapter 4

Detection of degradations and reconfiguration of the navigator in case of degraded mode

Contents

Résumé

Une architecture de récepteur combiné GPS + Galileo + systèmes d'augmentation est proposée. L'architecture globale des futurs récepteurs combinés est basée sur deux fonctions principales, pour chaque mode opérationnel, qui sont la fonction de navigation qui fournit une position et une intégrité au système et une fonction de détection d'anomalies. Pour chaque mode, la fonction de navigation repose sur l'utilisation de combinaisons GNSS identifiées par l'EUROCAE comme nominales, alternées ou dégradées. Un système de commutation entre les modes opérationnels (ou au sein de combinaisons d'un même mode), permettent d'utiliser les combinaisons GNSS disponibles les plus performantes en termes de précision, intégrité, continuité et disponibilité. Les exigences de l'aviation civile pour chaque phase de vol sont satisfaites en mode nominal ou alterné. En mode dégradé, une alerte est automatiquement envoyée au pilote.
Le chapitre 4 présente les définitions des stratégies possibles : le mode nominal pour les phases de vol « En route » à « NPA », « APV I », le mode alterné, le mode dégradé, en accord avec le groupe de travail 62 de l'EUROCAE.

4. Detection of degradations and reconfiguration of the navigator in case of degraded mode

4.1. Introduction

As proposed in Chapter 3, the global combined receiver architecture relies upon a switching logic strategy. This switching strategy is driven by detection functions.

In this chapter, the combined receiver switching architecture is discussed in details. A further description of the receiver architecture is proposed and the different scenarii that can happen during the en route down to APV I phases of flight are discussed.

The mechanisms that allow switching from degraded modes to alternate modes, from degraded modes to nominal modes or from alternate modes to nominal modes were not addressed in this thesis. Nevertheless, this feature has to be taken into account in order to complete the receiver architecture.

4.2. Strategy for each mode of operation

4.2.1. Nominal mode strategy for en route down to NPA

The following figure shows the nominal mode strategy for the en route down to NPA phases of flight. Two types of schemes are presented: the navigation function and the detection function.

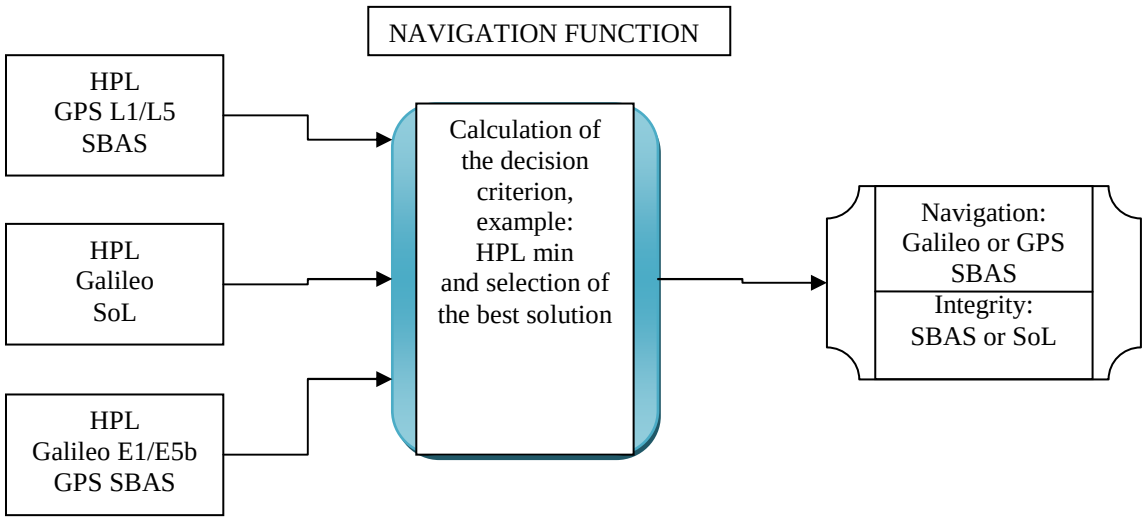

Figure 18: Navigation function for en-route down to NPA operations with nominal mode

For the nominal mode of operation during the en-route down to NPA phases of flight, the horizontal protection level can be provided by:

- Galileo SoL;
- Galileo E1 E5b + GPS SBAS;
- GPS SBAS L1 L5.

These combinations are identified in Table 3, Chapter 3. These component combinations are proposed by the WG 62 and justified in [EUROCAE, 2007].

During en-route down to NPA phases of flight, only the horizontal accuracy requirements are defined, ranging from 3.7 km to 220 meters (Table 1, Chapter 2). Vertical guidance is not required during en route down to NPA. Only horizontal protection levels are computed.

Dual frequency receivers are expected to be compliant with accuracy requirements. Indeed, since the largest source of ranging error is the ionospheric code delay (Chapter 2), the nominal mode of operation relies on dual frequency measurements. The receiver must be capable of providing ionospheric corrections thanks to dual frequency measurements. Therefore, for accuracy purposes, nominal modes must be at least Galileo or GPS dual frequency components. On the one hand, the Galileo E1 (SoL or OS) plus E5b signals can be used in the ARNS bands. On the other hand, the GPS L1 C/A and L5 signals can be used in the ARNS bands.

Since Galileo provides its own integrity information in the I/NAV navigation message, broadcasted on both the E1 SoL (OS) and E5b components, the E1 and E5b signals will be processed in the future combined receivers. Therefore, the Galileo E1 + E5b, with the integrity message is referred as Galileo SoL. If the integrity information is not available (impossibility to demodulate and read the correct I/NAV message or message unavailable), another nominal combination is the E1 + E5b + GPS SBAS when available. Indeed, the SBAS augmentation component will ensure the integrity performance. In the case of GPS L1 C/A + L5, the integrity is only ensured by the SBAS.

The loss of one or more of these components leads to a loss of performance. Thus a switch to other means of navigation in the nominal mode or a switch to alternate or degraded modes is necessary to perform the current operation.

The following figure presents:

- The detection function: the inputs of the detection function allow defining the algorithms detection criteria. These criteria are then compared to detection thresholds compliant with civil aviation requirements. The detection function only provides flags of loss of signals, as it is depicted in Figure 19;
- The event flagged by the detection function;
- The switch to other GNSS combinations.

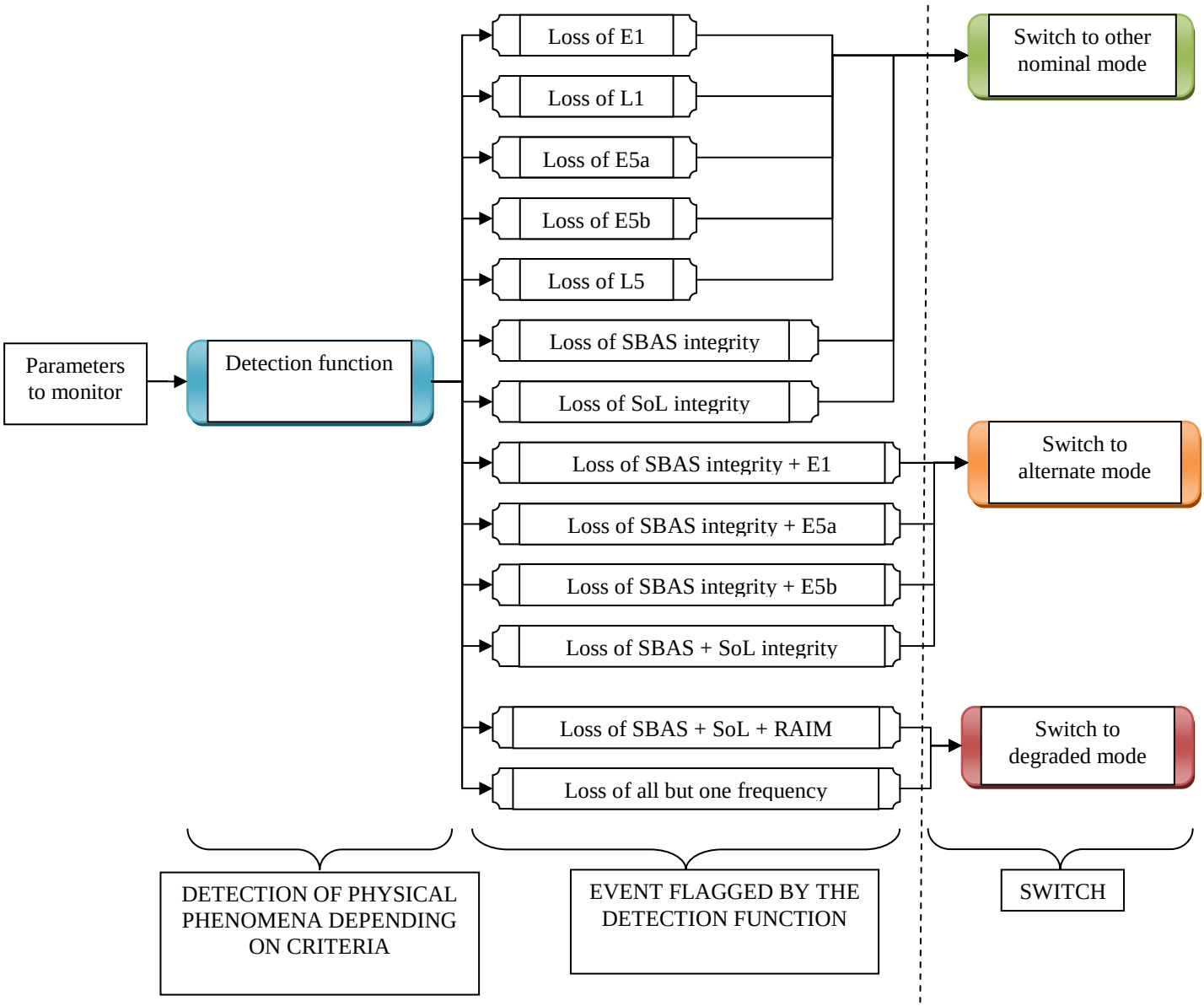

Figure 19: Detection function for en-route down to NPA operations with nominal mode

As a conclusion, during en route down to NPA, the nominal GNSS combinations are Galileo SoL, Galileo E1/E5b + GPS SBAS or GPS SBAS L1/L5. The integrity is provided by SBAS or SoL. As it is depicted in Figure 19, a loss of one of these components may lead to a switch to other nominal combinations, alternate or degraded mode of operation.

4.2.2. Alternate mode strategy for en route down to NPA

Concerning the alternate mode for NPA, the navigation and integrity can be provided by using GPS SBAS single frequency, all available pseudoranges + RAIM, Galileo SoL single frequency, and Galileo + GPS SBAS single frequency. The following figure describes the navigation function during en route down to NPA.

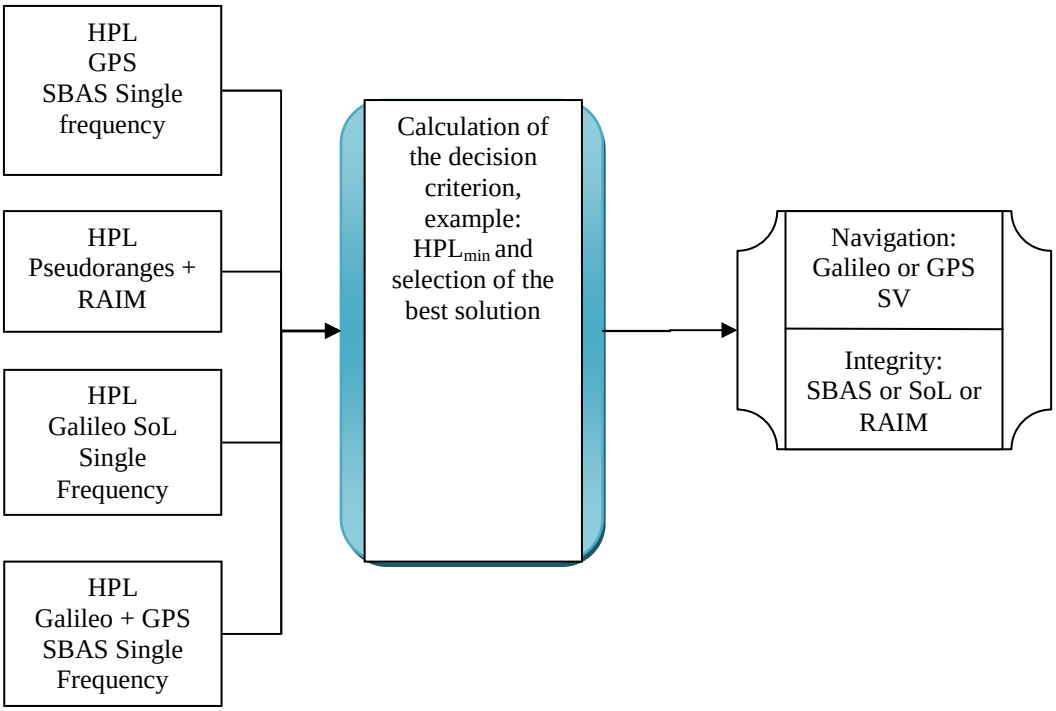

Figure 20: Navigation function for en-route down to NPA operations with alternate mode

Hereafter is represented the detection function. In the alternate mode of operation, the detection function can flag a loss or recovery of GNSS component.

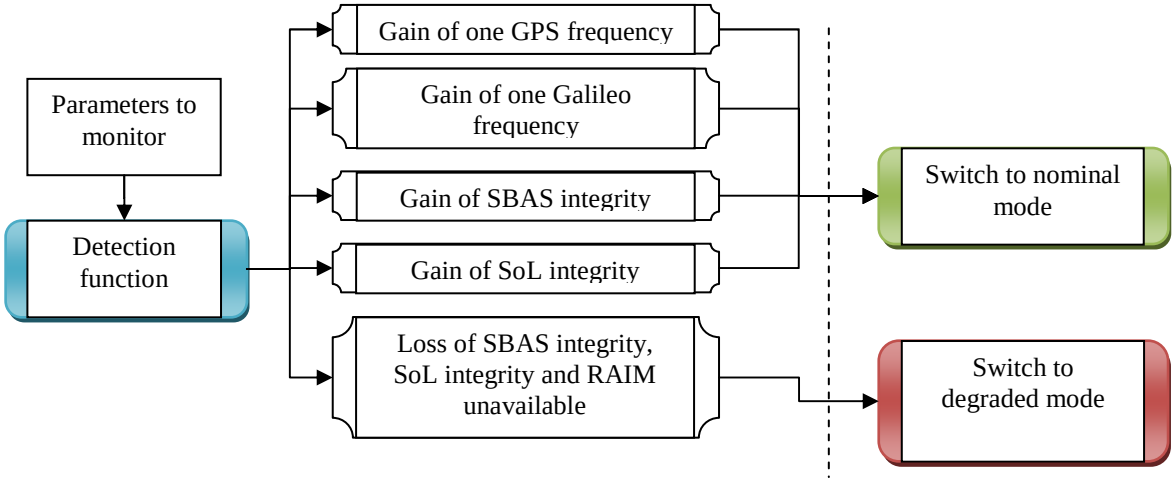

Figure 21: Detection function for en-route down to NPA operations with alternate mode

4.2.3. Degraded mode strategy for en route down to NPA

In case of degraded mode, as described in Figure 22, if the RAIM is not available, integrity is not provided and an alert is raised. The detection function is only used for components recovery. The navigation function provides a position estimate without integrity, with the available components.

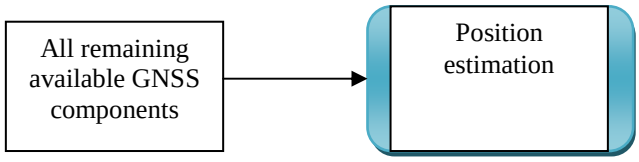

Figure 22: Navigation function for en-route down to NPA operations with degraded mode

For en route down to NPA, GPS or Galileo + RAIM is sufficient to provide the required integrity and accuracy. If the RAIM is not available, only a position estimation can be provided, but without integrity. In this last case, an alert is raised. Thus, as depicted in Figure 23, the corresponding detection function is dedicated to components recovery flag and raises alerts when there is no recovery.

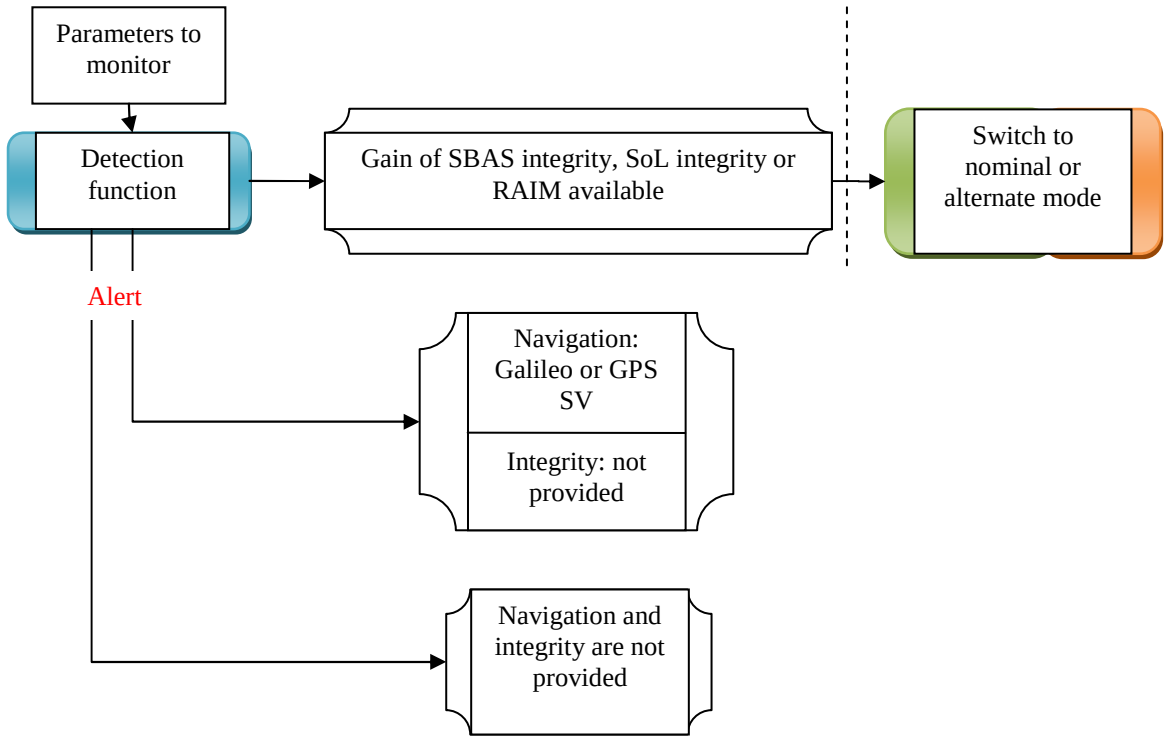

Figure 23: Detection function for en-route down to NPA operations with alternate mode

4.2.4. Nominal mode strategy for APV I

For APV operation, vertical guidance must be taken into account and vertical protection levels are computed. The following schemes describe the navigation function with horizontal and vertical inputs and also illustrate the detection algorithms.

The starting point for nominal mode is the same than for NPA. The parameters to monitor with the detection function are the same than for NPA, only the detection thresholds can be different.

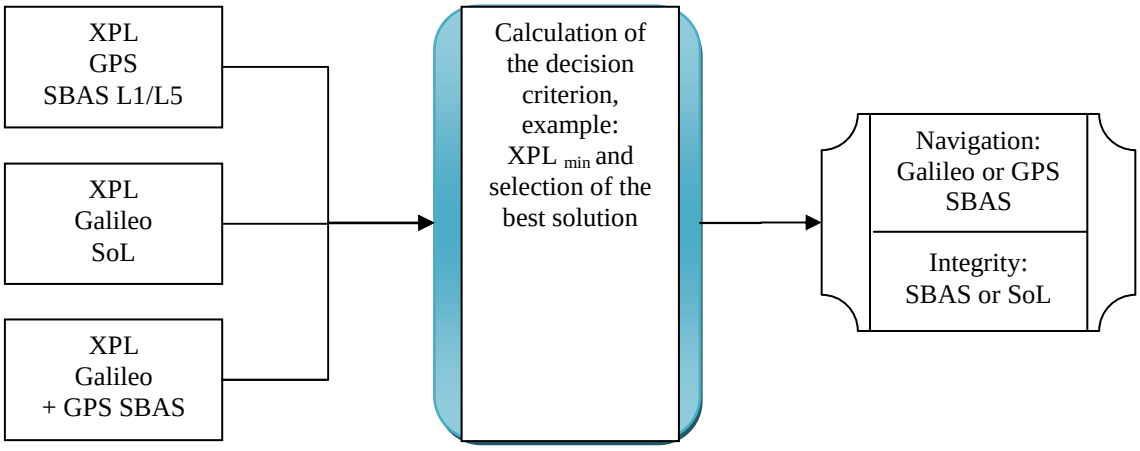

Figure 24: Navigation function for APV I operation with nominal mode

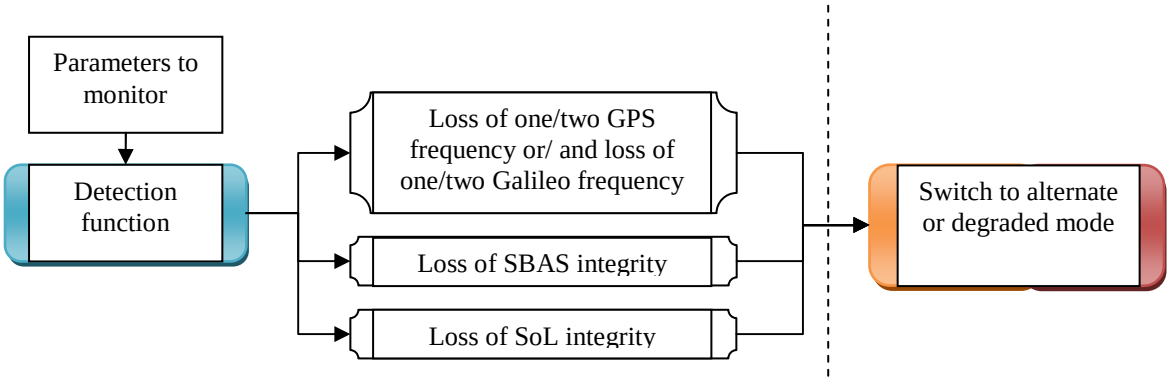

Figure 25: Detection functions for APV I operation with nominal mode

Galileo single frequency + SoL and combinations of all available pseudoranges + RAIM are not alternate combinations but degraded as they are not expected to provide sufficient level of performance, mostly in terms of accuracy.

4.2.5. Alternate mode strategy for APV I

The following figure illustrates the navigation and detection functions included in the alternate mode for APV I.

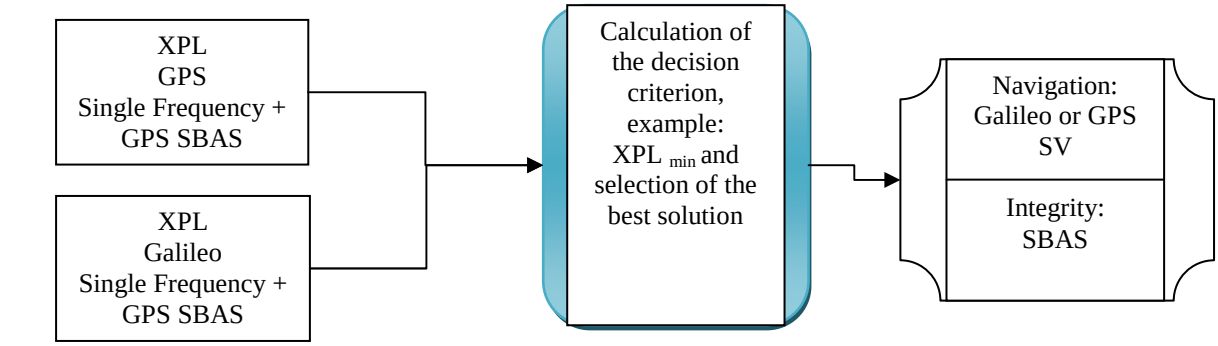

Figure 26: Navigation function for APV I operation with alternate mode

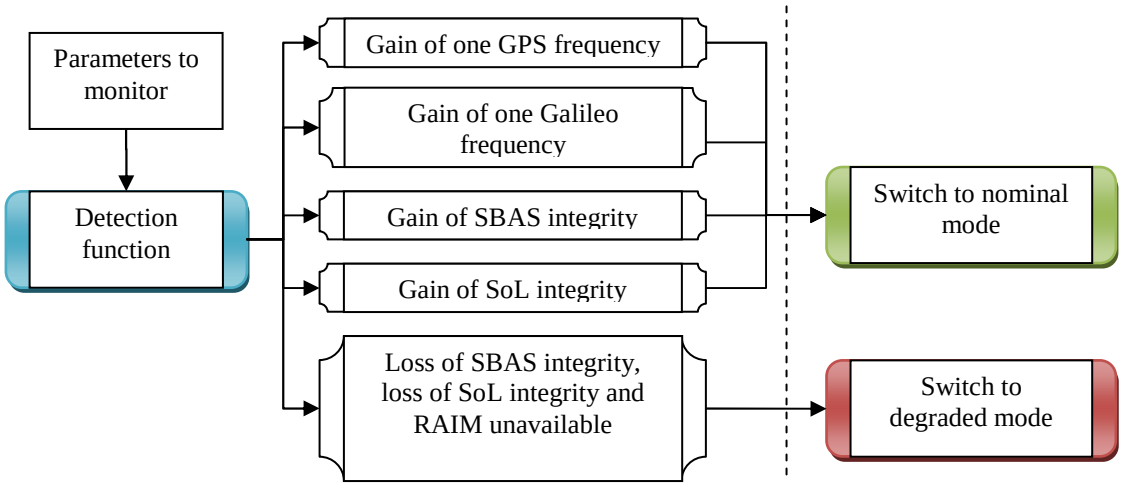

Figure 27: Detection function for APV I operation with alternate mode

4.2.6. Degraded mode strategy for APV I

In Figure 28, the navigation function is presented in case of degraded mode, during APV I.

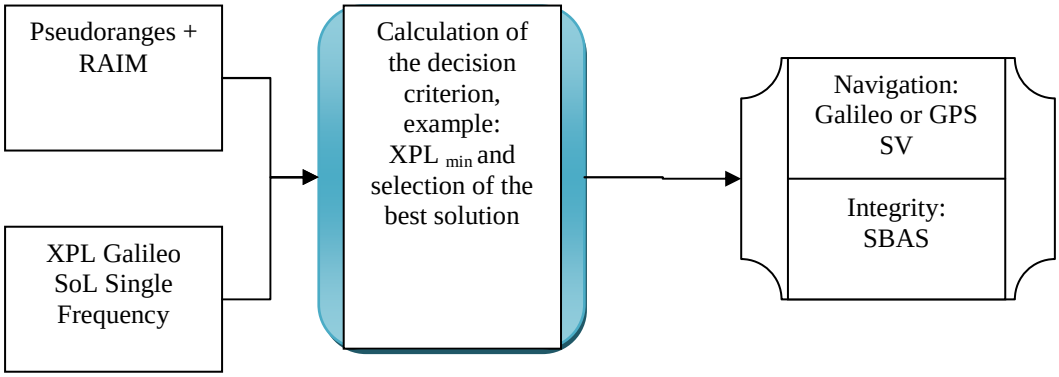

Figure 28: Navigation function for APV I operations with degraded mode

In a degraded mode, the detection function operates as a restoring function, as it is the case for NPA. Indeed, the receiver looks for all available means that could be used after recovery.

In Figure 29, the detection function is presented in case of degraded mode, during APV I.

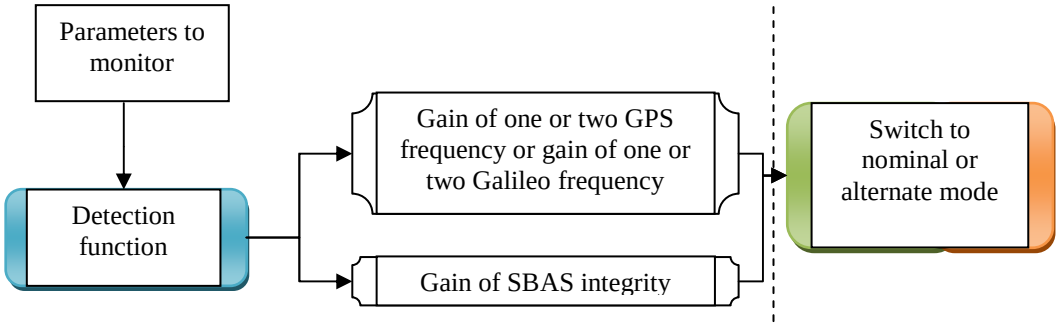

Figure 29: Detection function for APV I operations with degraded mode

The degraded mode of operation implies an alert to the pilot issued by the detection function. However, one must ask whether if it is possible to maintain sufficient levels of performance, compliant with ICAO requirements (Table 1) during a targeted phase of flight. If it is not the case, GNSS cannot be used and the pilot must use other means to achieve the current operation. To consider the above, the navigator reconfiguration in case of degraded mode is discussed in the next section.

4.3. Navigator reconfiguration in case of degraded mode

When the level of performance required is not met during a phase of flight, the receiver switches to degraded mode and raises an alert. As such, it becomes important to properly manage the remaining signals in order to perform the phase of flight. That is why, the main goal of this section is to discuss how to manage the remaining available components during a degraded mode to try to perform the phase of flight.

For instance, it is of interest for civil aviation community to try to maintain the maximum level of performance that can be reached with the remaining available GNSS components, as long as possible after the receiver switched to a degraded mode. The receiver is thus reconfigured.

The reconfiguration does not refer to switching between the different GNSS combinations introduced in this chapter. It concerns the particular case of degraded modes and the means to maintain the best level of performance with the available components and additive algorithms. This terminology is similar to the one used for computers with dynamic device reconfigurations.

Indeed, some algorithms may bridge the gap between the situation before loss of component and after degradation for a given period. In Chapters 5 and 6, repair algorithms are proposed with the detection algorithms for each type of perturbation investigated. In

Chapter 6, a particular algorithm is used to bridge the gap in ionospheric code delay estimations between dual and single frequency modes.

4.4. Conclusion

Navigation and detection functions were described as a function of the operated phase of flight and the operating mode concerned. This is done according to the combinations identified by WG 62 (Table 3). The reconfiguration of the navigator in case of degraded mode was also discussed.

In the following chapters, particular switch cases are studied. The interference detection is detailed. After a loss of frequency due to interference, ionospheric code delay estimation with one frequency is analyzed. The author's choice to investigate these specific cases is justified in the next chapters and is function of the EUROCAE WG 62 needs. Accuracy, integrity, continuity and availability of several proposed detection and repair algorithms are discussed in details in Chapters 5 and 6.

Chapter 5

Performance of Multi correlators GNSS Interference Detection and Repair Algorithms

Contents

Résumé

Le chapitre 5 concerne la détection d'interférence durant une phase de vol APV I. En effet, ce chapitre présente des techniques de détection d'interférence, en particulier des CW, sur les sorties de corrélateur. Nous utilisons pour la détection, de multiples sorties de corrélateurs. Nous détectons les interférences de puissance maximale autorisée par les récepteurs avioniques, les masques d'interférences étant spécifiés dans les MOPS EUROCAE. Un environnement synthétique d'un appareil en phase d'approche est simulé. A partir des sorties de corrélateurs, nous définissons des critères instantanés ou séquentiels permettant de détecter une anomalie sur les sorties de corrélateurs. En effet, comme nous le démontrons dans ce chapitre, une CW impactant le spectre des signaux GNSS (en particulier ici, L1 C/A et E1 OS), génère une sinusoïde sur les sorties de corrélateurs, laquelle est détectable et caractérisable par plusieurs algorithmes. Le premier critère que nous proposons est basé sur le calcul de la FFT des sorties de corrélateurs, la second critère est basé sur une estimation des paramètres d'un modèle autorégressif multi-canal, pour détecter la présence de CW de manière redondante sur toutes les sorties de corrélateur et en temporel. Nous déterminons les performances de tels algorithmes en termes de continuité et intégrité. Un algorithme de correction des sorties de corrélateurs, basé sur une estimation de Prony des paramètres de la CW à détecter (amplitude, fréquence) est aussi proposé afin de réparer les sorties de corrélateur. En cas de détection, les sorties de corrélateurs sont réparées et l'erreur de poursuite résiduelle est analysée. En cas de non détection, l'erreur de poursuite émanant de la CW est alors analysée.

5. Performance of Multi correlators GNSS Interference Detection and Repair Algorithms

5.1. Introduction

Amongst the most feared physical phenomena that can lead to combined receivers performance loss, the interferences are an important issue that is in the scope of the WG 62 studies. From a signal processing point of view, the interferences affect signals reception at front end level and can lead to a loss of lock in tracking loops.

GNSS interference environment includes pure carriers, narrow bands and pulsed interferences signals.

Previous studies focused on pulsed interferences detection, for instance in [Raimondi, 2006] or [Bastide1, 2004]. Some of these pulsed interferences are in the same band than the L5 and E5a signals. As a consequence, these studies are important for the WG 62 purposes. Since pulsed interferences were already studied, we decided to focus our study on pure carriers interferences impacts on GNSS signals processing.

Future combined GNSS receivers will have to be robust against interferences with a certain power. Consequently, it is important to develop robust receivers for civil aviation community.

Future civil aviation combined receivers will be composed of filters ([EUROCAE, 2007]), for resistance to jammers (RF and IF filters). The resulting interference threshold masks provide the characteristics of the interferences mitigation receiver capability.

For civil aviation applications, interferences with power level below the interference masks defined in [EUROCAE, 2007], are expected to generate acceptable tracking errors so that it does not affect significantly the resulting pseudoranges and thus the navigation solution provided by the navigation function.

In this study, it is shown that, even below the Radio Frequency Interference (RFI) masks, with low Doppler rate between the jammer and the incoming signal, the tracking errors induced by a Carrier Wave (CW) interference can be larger than expected in [EUROCAE, 2007]. This is all the more important for highly restrictive approach phases of flight in terms of accuracy. That is why this study focuses on detection of CW during the APV I phase of flight.

In addition, repair algorithms are proposed to remove the effects of interferences (at the correlators outputs level) to perform the receiver tracking process correctly.

5.2. Review of existing interference detection techniques

5.2.1. Detection techniques at the receiver front end level

5.2.1.1. Chi-square test at the ADC Level

Analog to Digital Convertor (ADC) with supplementary bins, may be used to better represent the thermal noise Gaussian distribution through increased resolution. The ADC bins distribution is Gaussian and maintained constant, in the absence of any perturbation, as a result of the Automatic Gain Control (AGC) gain adaptation. Thus it is possible to implement a test on ADC bins distribution changes to detect interference. A straightforward approach is to use the Chi-Square test to decide if two sets of data are consistent. This method has been introduced in [Bastide1, 2004].

5.2.1.2. Temporal blanker and FDIS

The Temporal Blanker was the first pulsed interference mitigation technique proposed to solve the issue of pulsed interference present on the E5a/L5 ARNS band. An analog implementation of the temporal blanker was proposed: a circuitry detecting the beginning and the end of each pulse is implemented before the ADC [Raimondi, 2008].

As it is described in [Raimondi, 2008], the Frequency Domain Interference Suppressor (FDIS) algorithm consists in translating the input signal into the frequency domain using the FFT algorithm. Then, a detection/excision module detects and eliminates interferences, and the signal is calculated back in time domain using the inverse FFT. This processing is performed using the digitalized signal, at the ADC output.

5.2.2. Interference detection within the tracking loops

5.2.2.1. Computation of the Signal to Noise Ratio (SNR)

Signal quality may be assessed by the Signal to Noise Ratio (SNR) estimate at the correlator outputs. This quantity is degraded by imperfect code and carrier tracking and may be directly related to the Bit Error Rate (BER). The receiver declares a signal is present or lost if its estimated SNR at the correlator outputs is respectively above or below a predefined threshold. Such a test on the estimated SNR may be combined with a detection algorithm so as to ensure an in-band interferer is really present. Such a detection algorithm is proposed in [Bastide1, 2004].

5.2.2.2. Detection at the correlators outputs

As it is mentioned in [Bastide2, 2001], CW interferences affect the code and carrier tracking correlator outputs[4], studying the correlator distortions seems to be a good way to determine the presence of interferences and even to model it and remove its effects on tracking.

5.3. GNSS signals studied

The priority here is to be able to detect CW interfering with L1 C/A and E1 signals as it is mentioned in introduction. The CW interferences have different impacts on these two signals since they have different structures as it is mentioned in Chapter 2.

A Binary Phase Shift Keying modulation is used for the L1 C/A signal. This base band signal can be defined as the product between a PRN code sequence represented by an NRZ wave form and a NRZ data sequence (navigation message). This base band is also used for other GNSS signals and can be reduced to a code sequence in case of pilot channel.

A Binary Offset Carrier modulation is used for the Galileo signals since it allows moving signals energy away from the centre band and thus allows the use of a same frequency band for GPS and Galileo signals, like it is the case for the L1 and E1 signals. In addition, it offers a better resistance to noise and multipath because of its light frequency content, and a better robustness against interferences. For instance, the case of the already crowded L1 band is represented in the following figure.

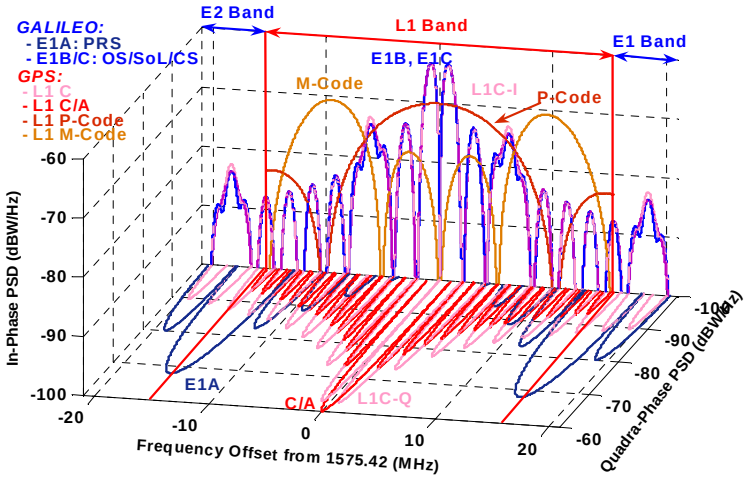

Figure 30: E1 PSD in an already crowded L1 frequency band

A BOC modulation is obtained by multiplying the NRZ spreading code by a subcarrier, which is a NRZ signal, equal to the sign of the sine or cosine waveform. BOC signals are commonly referred to BOC(p,q), where p is the subcarrier rate and q defines the spreading code rate as a multiplier of 1.023 MHz. The E1 OS signal has a data component (B) and a pilot component (C) as it is mentioned in chapter 2. It is modulated thanks to a CBOC [GSA, 2008], which means that the data channel and the pilot channels are both composed of a BOC(1,1) component and a BOC(6,1) component.

[4] The interference impact on tracking loops is studied in details in this chapter. It is shown that interferences distort the correlator outputs.

The different modulation strategies between the L1 C/A and E1 OS signals have a direct impact on the signals spectrum and on the correlators outputs shape. Indeed, the waveforms are different for the two signals: the L1 C/A signal has rectangular waveforms which results in simple triangular correlation peaks, whereas, for the BOC signals, the code materialization is dependant upon the sub-carriers characteristics and the resulting correlation peaks are narrower and presents secondary peaks. This difference is presented in the following figures. As a consequence, the interference detection algorithms must take into account the shape of the correlation peaks and differ for the GPS L1 C/A and Galileo E1 OS signals.

The following figures present the resulting autocorrelation functions of the deterministic binary signal, without noise.

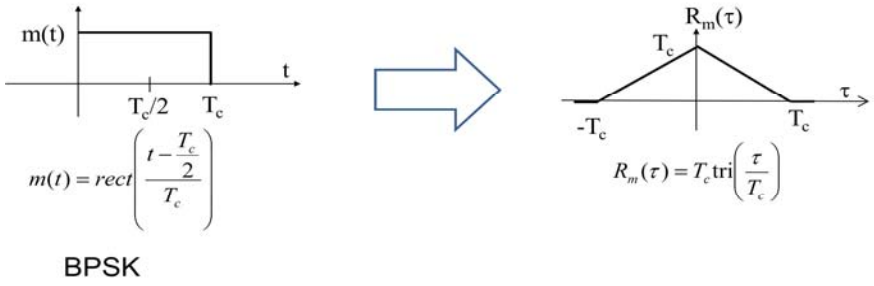

Figure 31: BPSK waveform and corresponding autocorrelation function

The figure below presents the autocorrelation of the deterministic signal, modulated by a sub-carrier.

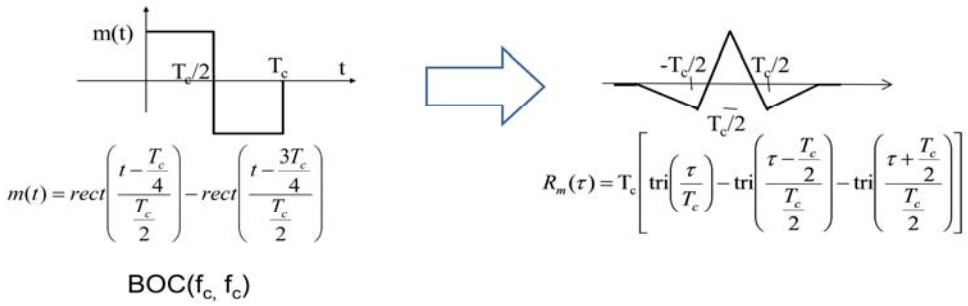

Figure 32: BOC (fs,fc) waveform and corresponding autocorrelation function

Where:

- Tc is the chip period in seconds with the corresponding fc frequency
- fs is the subcarrier frequency
- m(t) represents the binary signal materialization
- Rect is the classical rectangular function
- Tri is the classical triangular function

In the example above, the modulation is a BOC(fs, fc) = BOC(1,1).

The Galileo E1 OS signal is not exactly a BOC signal but a CBOC one, which implies a slightly different shape of the correlator output. The L1 C/A BPSK, E1 OS CBOC and E1 BOC

correlator outputs are presented in the following figure. In the next sections, the assumption is that the E1 OS signal is BOC(1,1)-modulated only. As it is shown in the next figure, the correlator outputs differences between the BOC and CBOC are not significant enough for interference detection study.

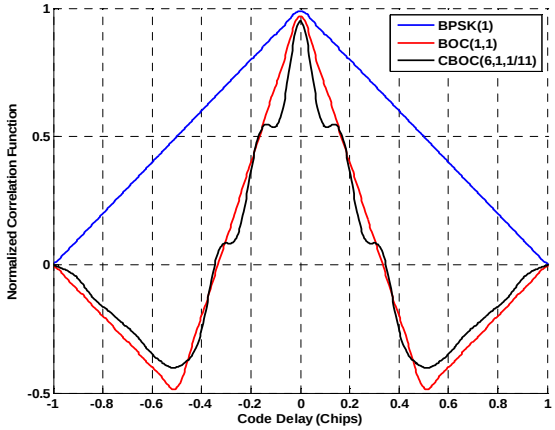

Figure 33: BPSK, BOC and CBOC correlation function

5.3.1. Budget of signals power

In Galileo MOPS ([EUROCAE, 2007]) and DO229 D ([RTCA, 2006]), the specifications for minimum and maximum received power at the antenna output are provided. In the Galileo signals case, only the pilot channel is taken into account. The system noise level is chosen equal to -201.5 or -202.5 dBW/Hz, depending upon the signal received and the correlators properties as described in [EUROCAE, 2007]. Noise resulting from IGNSS is when other satellites from the same constellation are taken into account.

	IGNSS	ANTENNA LOSS OR GAIN (5° ELEVATION)	IMPLEMENTATION LOSS	RECEIVED POWER	SYSTEM NOISE	C/N0
GPS L1 C/A minimum received power	-201.4 dBW/Hz	Loss: 5.5 dB	2 dB	- 158.5 dBW	-201.5 to 202.5 dBW/Hz	32.4 to 32.9 dB Hz
Galileo E1 minimum received power	-204.6 dBW/Hz	Loss: 5.5 dB	2 dB	- 158.5 dBW	-201.5 dBW/Hz	34.8 dB Hz
GPS L1 C/A maximum received power	Not considered	Gain: - 5 dB	2 dB	- 156 dBW	- 202.5 dBW/Hz	49.5 dB Hz
Galileo E1 maximum received power	Not considered	Gain: - 5 dB	2 dB	- 152.5 dBW	- 201.5 dBW/Hz	52 dB Hz

Table 4: Specified received power and carrier to noise ratios required at tracking level, [EUROCAE, 2007].

In the following table, we present the carrier to noise ratio values chosen for simulations, which are compliant with the bounds defined in [EUROCAE, 2007] and recalled in the previous table.

	GPS L1 C/A	GALILEO E1
C/N0	39 dB Hz	35 dB Hz

Table 5 : Carrier to noise ratios for GPS and Galileo signals used during simulations.

5.4. Impact of CW interferences on signals processing

5.4.1. Code spectrum lines correlated with interferences

The spectral position of the interference in the code spectrum lines is analyzed for both GPS L1 C/A and Galileo E1 signals. In particular, the code spectrum lines with the highest amplitudes, have to be considered to protect the user against the most penalizing interference location within signals spectra. The highest amplitude code spectrum lines are called the “worst case” code spectrum lines in the following. Indeed, a CW interference at the same frequency than these code lines can generate a large loss of power. The correlators outputs can be modelled as a function of the useful signal plus the interference spectra as it

is described in the following. As a consequence, it is necessary to identify the worst case code spectrum lines.

The number of spectral lines carrying the incoming signal power influences the weight of each line. Indeed, the more spectral lines are present, the more the total incoming signal power are divided out over these spectral lines. The spacing between two code spectrum lines is the code repetition frequency f_R. In the case of the GPS L1 C/A code for example, the number of code spectrum lines within the main lobe of the signal power spectrum density equals twice the code length. This means that a longer code has an increased number of lines which have a lower power. As a consequence, for the E1 OS signal, spectrum code lines are less powerful than the L1 C/A ones.

The impact of a CW on the E1 and L1 C/A signals processing is dependent upon the useful signals spectra, but also the CW spectrum properties. First, in comparison with the L1 C/A and E1 code spectrum lines spacing, a CW has a very narrow bandwidth and is only expected to strike a single code spectrum line. Secondly, since the impact of a CW on the receiver tracking loops is expected to increase with the impacted code spectrum line power, the Galileo E1 signal is expected to be more robust to CW interferences than the GPS L1 C/A signal.

The following figures illustrate the GPS L1 C/A and Galileo E1 spectra shapes.

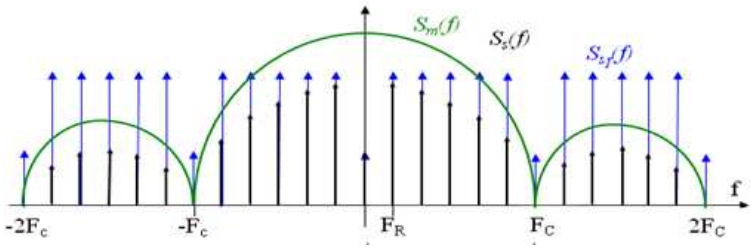

Figure 34: GPS L1 C/A code spectrum

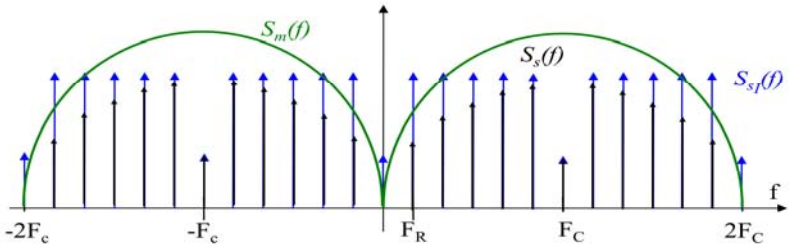

Figure 35: Galileo E1OS code spectrum

In the previous figures, Sm represents the signal modulation (one main centered lobe for the BPSK signal and two shifted main lobes for the BOC signal, due to the multiplication by subcarriers). The code materialization is S_s. F_c is the code frequency and f_R is the separation between each spectral line of the incoming useful signal DSP: $f_R = \frac{fc}{CodeLength}$.

In the following, the worst case code spectrum lines are identified for both L1 C/A and E1 signals.

5.4.1.1. Identified worst case code spectrum lines

The worst line for GPS C/A comes from PRN 24 as it can be seen in Appendix C.2, Table 18. Its frequency is 123 kHz and its magnitude is -21.26 dB (power of the line with regard to the total signal power). However, the frequency of this ray is almost two times lower than the PRN 6 227 kHz-line which has an amplitude of -21.29 dB. Therefore, the PRN 6 is chosen for simulations. For the E1 signal, the worst case code spectrum line is identified on PRN 38, located at 673.5 kHz with an amplitude of -28.81 dB (Galileo E1 OS ICD: [GSA, 2006]).

5.4.1.2. Position of the interference in the code spectrum

An important parameter can influence the spectral position of the jammer: the Doppler shift between the interference and the received signal. In addition, the estimation of the probability of occurrence of a damaging CW is influenced by this Doppler effect. A damaging interference here implies a loss of tracking accuracy which entails an inadequate navigation solution for the targeted phase of flight. Indeed, the Doppler effect generate an additional error on the correlation between the incoming signal and the receiver local replica for tracking.

5.4.2. Model of the influence of interferences on the correlators outputs

After being multiplied by DLL local code and PLL local carrier as described in Chapter 2, the signal is separated into two channels I and Q. The first one corresponds to the multiplication by the in-phase local estimated carrier and the second one the quadra-phase carrier.

[Bastide2, 2001] and [Macabiau, 2002] provide a model of the impact of CW on the correlator outputs. A short mathematical description of this impact on GPS L1 C/A is provided in the following. We assume that the receiver will provide multiple correlators outputs (delayed or advanced with regard to the prompt correlator output).

In presence of noise only, the multiple correlator outputs are modelled as:

$$\begin{cases} \mathrm{I_d} = \dfrac{\mathrm{A}}{2}\mathrm{R}\ \ (\varepsilon_\tau - \mathrm{d})\cos(\varepsilon_\theta) + \mathrm{n_I} \\ \mathrm{Q_d} = \dfrac{\mathrm{A}}{2}\mathrm{R}\ \ (\varepsilon_\tau - \mathrm{d})\sin(\varepsilon_\theta) + \mathrm{n_Q} \end{cases} \quad \textbf{(75)}$$

Where:

- i is the index of the replica
- R is the materialized PRN code autocorrelation function,
- A is the magnitude of the received GNSS signal,
- ε_τ is the code tracking error,

- ε_θ is the carrier phase tracking error,
- d is the delay between the n replica and the prompt,
- n_I and n_Q are additive correlator output noise.

When a CW interferes with the locally generated signal, a sinusoid resulting from the correlation between the local code and the interference appears on the I and Q correlator channels. If that additional correlation product has a frequency greater than the PLL bandwidth B_L^{PLL}, it is then filtered out.

In the case where the GPS L1 C/A input signal is only affected by a CW interference and by noise, the sampled signal is expressed at the output of the RF front-end by [Bastide2, 2001]:

$$\begin{aligned} V(k) = {} & A\, D(kT_s - \tau) C(kT_s - \tau) \cos(2\pi f_I k T_s - \theta) \\ & + A_J \cos\left(2\pi\,(f_I + \Delta f)\, k T_s - \theta_J\right) + n(k) \end{aligned} \quad \textbf{(76)}$$

Where:

- *A* is the magnitude of the incoming signal
- *D* and *C* are P/NRZ/L waveforms associated to navigation message and code (C/A for instance)
- f_I is the final intermediate frequency
- T_s is the sample period and $F_s=1/T_s$ is the sampling frequency
- θ is the incoming signal carrier dephasing
- τ is the group propagation time of the signal
- A_J is the amplitude of the CW jammer
- Δf is the frequency shift of the received jammer signal ,from f_I after the HF
- θ_J is the jammer shift
- *n* is the additional noise

Before integration, on the I and Q channels, V(k) is multiplied by a local replica of the in-phase carrier on I and a quadra-phase carrier replica on Q. Then, these expressions are multiplied by the locally generated code as it is described in Chapter 2, equation **(5)**:

$$\begin{cases} I_I(k) = V(k)\cos\left(2\pi f_I k T_s - \hat{\theta}\right) C(kT_s - \hat{\tau}) \\ V_Q(k) = V(k)\sin\left(2\pi f_I k T_s - \hat{\theta}\right) C(kT_s - \hat{\tau}) \end{cases} \quad \textbf{(77)}$$

As described in [Bastide2, 2001], the outputs of the Integrate and Dump (I&D) filters are then:

$$\begin{cases} I = \frac{A}{2} D.R\ (\varepsilon_\tau)\cos(\varepsilon_\theta) + \frac{A_J}{2M} \sum_{k=(i-1)M}^{iM-1} \cos\left(2\pi\Delta f k T_s - \theta_J + \hat{\theta}\right) C(kT_s - \hat{\tau}) + n_I \\ Q = \frac{A}{2} D.R\ (\varepsilon_\tau)\sin(\varepsilon_\theta) - \frac{A_J}{2M} \sum_{k=(i-1)M}^{iM-1} \sin\left(2\pi\Delta f k T_s - \theta_J + \hat{\theta}\right) C(kT_s - \hat{\tau}) + n_Q \end{cases} \quad \textbf{(78)}$$

Where:

- R is the autocorrelation function
- $\varepsilon_\theta = \theta - \hat{\theta}$ is the phase tracking error

- $\varepsilon_\tau = \tau - \hat{\tau}$ is the code tracking error
- *M* is the number of summed samples by I&D
- n_I and n_Q are the integration of the noise

The second terms in the expressions of I and Q outputs after I&D are the intercorrelation between the jammer (J) and the incoming signal. These intercorrelation functions can be also expressed as:

$$\begin{cases} R_I(\hat{\tau}) = \frac{A_J}{2M} \sum_{k=(i-1)M}^{iM-1} \cos\left(2\pi\Delta f k T_s - \theta_J + \hat{\theta}\right) C(kT_s - \hat{\tau}) = \frac{A_J}{2} c(k) C\left(k - \frac{\hat{\tau}}{T_s}\right) \\ R_Q(\hat{\tau}) = \frac{A_J}{2M} \sum_{k=(i-1)M}^{iM-1} \sin\left(2\pi\Delta f k T_s - \theta_J + \hat{\theta}\right) C(kT_s - \hat{\tau}) = \frac{A_J}{2} s(k)\, C\left(k - \frac{\hat{\tau}}{T_s}\right) \end{cases} \quad (79)$$

Where:

$$\begin{aligned} c(k) &= \frac{1}{M} \sum_{k \epsilon \mathbb{N}} \cos\left(2\pi\Delta f k T_s - \theta_J + \hat{\theta}\right) \text{rect}\left(\frac{kT_s - T_i}{T_I}\right) \\ s(k) &= \frac{1}{M} \sum_{k \epsilon \mathbb{N}} \sin\left(2\pi\Delta f k T_s - \theta_J + \hat{\theta}\right) \text{rect}\left(\frac{kT_s - T_i}{T_I}\right) \end{aligned} \quad (80)$$

Where:

- C is the NRZ PRN code signal
- T_i is the centre of the summing window, $T_i = (i - 0.5)MT_s$
- *rect(x)* is the rectangular window function
- T_I is the integration period of the I&D filter, $f_I = \frac{1}{T_I}$
- $c(k)$ and $s(k)$ are windowed cosine and sine signals.

In the GPS L1 C/A case, a CW interference would only cross one line because of its very low bandwidth (50 Hz) compared to the 1 kHz spacing between two lines.

The expressions of the correlator outputs on the I and Q channels become:

$$\begin{aligned} I &= \frac{A}{2} D.R\ (\varepsilon_\tau)\cos(\varepsilon_\theta) \\ &+ \frac{A_J}{2} \left| \frac{f_R}{f_c} \frac{\sin\left(\pi k \frac{f_R}{f_c}\right)}{\pi k \frac{f_R}{f_c}} C_0(k) \right| \frac{\sin(\pi(k_0 f_R - f_J)T_I)}{\pi(k_0 f_R - f_J)T_I} \cos(2\pi k_0 f_R \hat{\tau} + \varphi) + n_I \end{aligned} \quad (81)$$

$$\begin{aligned} Q &= \frac{A}{2} D.R\ (\varepsilon_\tau)\sin(\varepsilon_\theta) \\ &+ \frac{A_J}{2} \left| \frac{f_R}{f_c} \frac{\sin\left(\pi k \frac{f_R}{f_c}\right)}{\pi k \frac{f_R}{f_c}} C_0(k) \right| \frac{\sin(\pi(k_0 f_R - f_J)T_I)}{\pi(k_0 f_R - f_J)T_I} \sin(2\pi k_0 f_R \hat{\tau} + \varphi) + n_Q \end{aligned} \quad (82)$$

With:

$$\varphi = 2\pi(k_0 f_R - f_J)\frac{T_I}{2} - \left(\theta_J - \theta\right) + \varphi(k_0) \quad (83)$$

Where:

- A is the amplitude of the direct incoming signal, A_J is the amplitude of the jammer
- D represents the incoming signal data value during the integration interval,
- R is the autocorrelation function of the spreading waveform,
- $\hat{\tau}$ is the estimate of the incoming code delay,
- $\hat{\theta}$ is the estimate of the incoming phase,
- ε_τ represents the code tracking error,
- ε_θ represents the phase tracking error,
- T_I is the integration time in seconds,
- f_R is the separation between each spectral line of the local useful signal DSP: $f_R = \frac{fc}{CodeLength}$, where CodeLength is the PRN code length,
- k_0 is chosen so that $k_0 f_R$ is the frequency of the useful signal spectral line closest to f_J,
- n_I and n_Q are the in-phase and quadra-phase correlator's output Gaussian noise supposed uncorrelated and with a variance equal to $\frac{N_0}{4T_I}$, and
- C_0 is the discrete Fourier transform of the tracked PRN code.

The same analysis can be made for the Galileo E1 signal. A sine wave appears on top of the correlation peak when a CW interference occurs. One can mention that the correlation peak has a different shape than in the case of GPS L1 C/A signal (two secondary peaks appear beside the main one which is narrower than for the GPS L1 case).

As a conclusion, when a CW interferes with the incoming GNSS signal, the expressions of the I and Q channels correlator outputs are affected by additive sine waves. The demonstration provided here is valid for GPS L1 C/A signal but can be extended to other signals like Galileo E1 taking into account its characteristics developed in Chapter 2.

In the following, we plot the correlator output affected or not by a CW. The x axis represents the correlators number (66 correlators are used), the y axis represents each correlator output value. The integration time is chosen equal to 20 ms. The CW frequency is 227 kHz and the useful signal is the GPS L1 C/A one, generated with a power of -164 dBW.

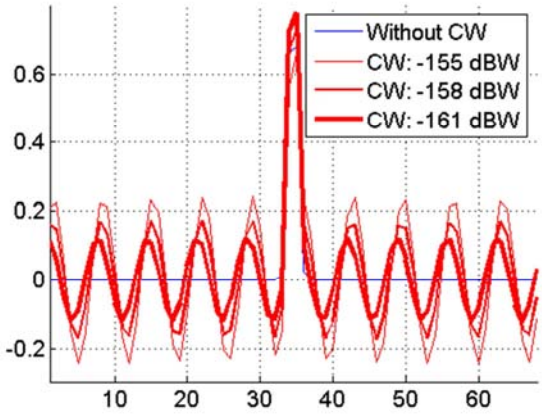

Figure 36 : Simulated correlators outputs on the I GPS L1 C/A channel affected by CW interference.

In the previous figure, it can be seen that the correlator outputs are affected by an additive sinusoidal term, which amplitude depends upon the amplitude of the code line hit by the CW and the power level of the CW interference. Obviously, this is also true for Galileo E1 signal processing.

The correlator output is thus of interest for interference detection. The carrier to noise ratio can be computed at the correlator outputs to detect the presence of an anomaly in the correlation amplitude with regard to background noise. Nevertheless, this estimation is not sufficient to identify the origin of the SNR. Indeed, CW interferences are not the sole reason of such an effect. For instance, multipath can also produce the same effect, as it is demonstrated in [Bastide2, 2001]. However, carrier to noise ratio is an indication of signals tracking degradation and of the impact of potential interferences on the I channel prompt correlator output, we propose the following estimation model:

$$\left(\frac{C}{N_0}\right)_{corr\_output} = \frac{1}{2\,T_S}\frac{mean(I)^2}{std(I)} \quad \textbf{(84)}$$

Where :

- T_S is the sampling period in seconds
- The mean and the standard deviation are estimated over 500 seconds of signal, 50 Hz-sampled

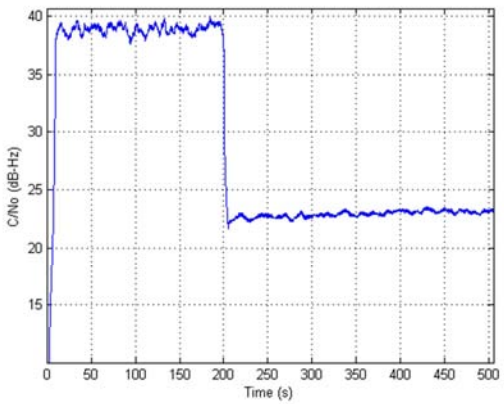

Figure 37 : C/N0 estimated at the correlator output without CW, and with generated interfering CW, 200 seconds after the beginning of the simulation.

On the previous figure, carrier to noise ratio is estimated using prompt correlator output on the I channel. A -155 dBW interference is generated on L1 C/A 200 seconds after the beginning of the tracking process and it can be noticed a loss of 15 dB on the estimated carrier to noise ratio.

Before the CW generation, the estimated carrier to noise ratio is around 39 dBHz as mentioned in table 6.

5.4.3. Observed influence on tracking loops

In order to observe the influence of CW interference on the tracking loops, a tracking simulator was used. Its starting point is the generated correlator outputs and the tracking settings used are summarized in the following table. The description of the discriminators and loop filters are presented in Chapter 2 as well as the L1 and E1 signals characteristics.

	CHARACTERISTICS
DLL	1st order, Bandwidth: 1 Hz, dot product discriminator aided by the PLL
PLL	3rd order, Bandwidth: 10 Hz, arctan discriminator
Integration time	GPS L1 C/A, data: 20 ms Galileo E1, data: 20 ms, pilot: 4 ms.

Table 6 : Simulator tracking characteristics.

Next figures show the impact of a -155 dBW CW interference on the tracking loops accuracy. The worst case GPS L1 C/A PRN 6 code line is impacted. The interference is generated 200 seconds after the beginning of the tracking process. A 100s Hatch filter, described in Chapter 2, is used to smooth raw code measurements.

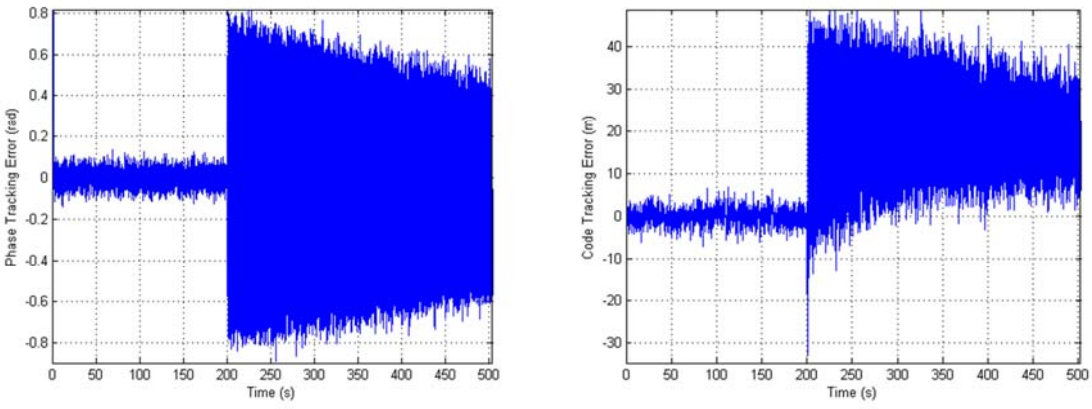

Figure 38 : Phase tracking error with a 10 Hz PLL bandwidth and a dot product discriminator on the left side and raw code tracking error using a 1Hz DLL bandwidth, with CW after 200 seconds simulation, the Doppler shift rate equals 2 Hz/s.

It is clear that the interference occurrence produces large tracking errors on the PLL and DLL outputs. The mean code tracking error value is shifted to 20 meters.

Due to the Doppler shift rate, after the CW occurrence (identified at time = 200 seconds), the code and carrier tracking errors decrease. But it can be noticed that the code and phase tracking errors are large enough during a long time (hundred of seconds whereas the total aircraft approach time is 150 seconds) to induce large pseudoranges errors. The resulting pseudoranges errors are discussed later in this chapter.

The typical value for a phase loop bandwidth used for GPS L1 C/A code is 10 Hz. This value corresponds to the minimum probability of cycle slipping (see [Holmes, 1990] or Chapter 6 of this thesis).

The impact of a CW on code tracking is restricted since a DLL bandwidth is more limited than a PLL one, the chosen value here is 1 Hz because the DLL is aided by the FLL. The impact of a CW on the tracking process is dependent upon the magnitude of the interference compared to the nearest code spectrum line, and its frequency. In addition, the characteristics of the local signal, as well as the amplitude of the Doppler shift between the interference and the amplitude of the CW-hit code spectrum line, the Doppler offset rate, the chip spacing and the DLL discriminator, determine the influence of the interference on code tracking.

The impact of a CW on code tracking is dependent upon the magnitude of the interference. To observe this effect, the raw and smoothed maximum code tracking errors are recorded while generating correlators outputs affected by several CW interferences with varying magnitudes, from – 172 dBW to – 155 dBW (rejection mask defined in [EUROCAE, 2007]). These maximum amplitudes of the correlators outputs affected by CW signals are generated over 300 seconds of simulation of GPS L1 C/A signal tracking and with a 50 Hz sampling. The results are presented in the following figure.

Note that during simulations, the tracking process is carried out over 500 seconds, the CW interference is generated 200 seconds after the beginning of this process. Indeed, since the smoothing filter time constant is 100 seconds, this setting allows the Hatch filter to smooth the first code measurements without perturbation. The tracking errors are consequently affected by the interference during 300 seconds. The approach duration is 150 seconds (<300 seconds). The tracking process time is longer than the APV I duration, which lasts less than 150 seconds. For each CW amplitude, the maximum raw code tracking error standard deviation is plotted, over 300 seconds.

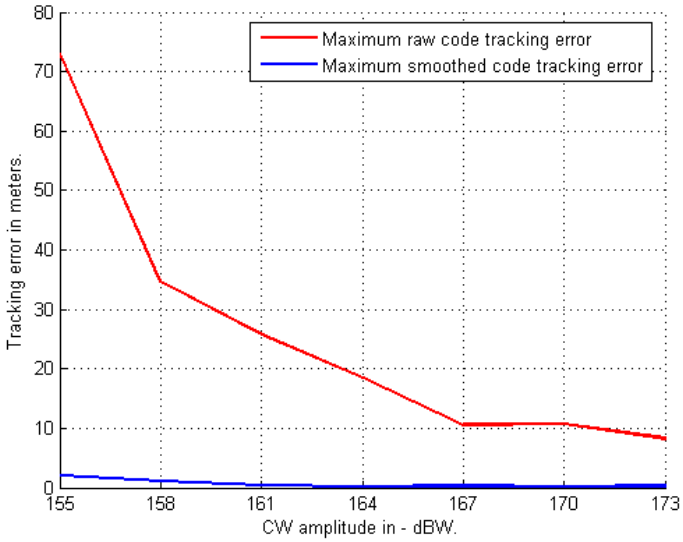

Figure 39 : Impact of the interference power on the code tracking loop accuracy, with the same tracking settings, fighting GPS L1 C/A PRN 6 worst code spectrum line.

As a conclusion, a CW interference affects the two tracking loops and consequently affects the accuracy of the resulting pseudoranges, and thus, the navigation solution. It is consequently important to be able to detect these perturbations in compliance with APV I required accuracy. Since the two loops are affected, the code smoothing process is affected too and the higher the interference power, the higher the resulting pseudorange error as plotted in the previous figure. In the case the interference is not detected, it may generate a penalizing error during the APV I phase of flight without any flag. Indeed, the maximum raw code tracking error is over 70 meters.

5.5. Elaboration of the interferences detection techniques

5.5.1. Multi correlators detection algorithms

GNSS receivers have several reception channels. Each of them specializes in tracking specific satellites. Each reception channel has at least two or three pairs of correlators (E, L, P) for both code and carrier phase tracking.

A multi correlator receiver can compute much more correlator outputs in a same reception channel. If several correlators are available within a same channel, it is possible to observe the code autocorrelation value in several points spaced by a value denoted *d*.

In the following, multiple correlators outputs are monitored to detect the presence of jammers. For instance, while observing the I channel GPS L1 C/A correlator outputs, distortions are used to detect and characterize the potential jamming signal. This algorithm is expected to improve future GNSS receivers robustness against interferences.

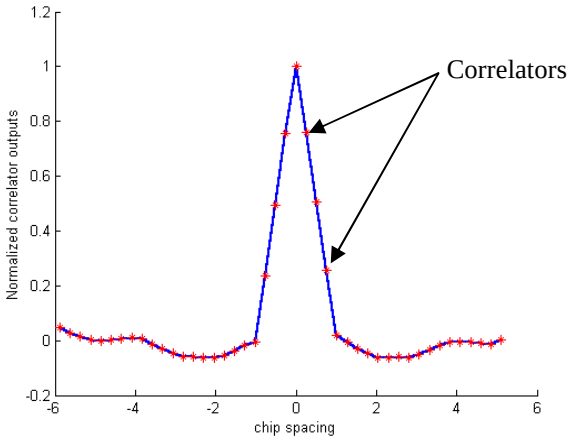

Figure 40 : Normalized GPS L1 C/A correlators outputs.

5.5.2. Proposed detection techniques at the correlators outputs

Two techniques are considered and presented below. They allow monitoring multiple correlator outputs. Their performances are discussed with regards to civil aviation requirements. In addition, their complexity is discussed and depends upon the number of correlators used for detection.

The first proposed algorithm is based upon the calculation of the FFT of the correlator outputs, to detect the presence of a sine wave besides the correlation peak. The second algorithm is a multichannel AR algorithm used to model simultaneously all the correlators outputs.

The objective is to find the most appropriate and promising technique making a trade off between complexity and reached performance. Indeed, detection algorithms with low complexity have to be implemented in order to have the simplest receiver architecture as possible.

5.5.2.1. Computation of the FFT of the correlators outputs

Multiple correlator outputs are monitored and the presence of interferences in the incoming signal is detected thanks to the computation of the Fourier transform of the correlators outputs [Bastide2, 2001]. If undesired carrier sine waves are present, peaks appear in the FFT of the correlator outputs.

The maximum Fourier transform of the correlator outputs is compared to threshold. If a significant sine wave is present in the signal, the maximum Fourier transform of the signal is proportional to the magnitude of the wave, and, in the case the threshold is well chosen, this interference may be detected.

A detection is declared when the following condition is reached [Bastide2, 2001]:

$$\frac{|\max\_fourier_{inst} - mean(max fourier)|}{std(max fourier)} \geq threshold \quad \textbf{(85)}$$

Where :

- $\max\_ fourier_{inst}$ is the maximum of the Fourier transform at a considered instant
- $mean(\max\_ fourier)$ is the mean of maxima of the Fourier transforms during the training stage
- $std(\max\_ fourier)$ is the standard deviation of the maxima of the Fourier transforms during the training stage
- $threshold$ is the chosen threshold for detection

The algorithm can be described in a few points:

1. The mean and the standard deviation of the maximum of the FFT of the correlator outputs are calculated during a training stage, when no interference occurs.

2. Then, the algorithm is launched to detect interferences. At each instant, the maximum of the FFT of the correlator outputs is calculated.

3. Finally, the ratio defined the equation (85) is compared to a detection threshold.

This algorithm was already proposed by [Bastide2, 2001] for interference detection. Nevertheless, its performances were never evaluated for civil aviation compliance. Therefore, the performances assessment of this algorithm is an original contribution of this thesis.

5.5.2.2. Multichannel Autoregressive model of correlator outputs

This proposed algorithm is based on the detection of non regular time variation of the residuals of an AR model of the set of the correlation outputs. The residuals of the model are then monitored. The correlator outputs are supposed to be affected by white Gaussian noise when no interference occurs. Interferences do not cause a constant additive jump on the correlator outputs but they create an additional time-varying error. If a CW interferes with the incoming signal, then the variance of the correlator outputs increases exactly when the interference occurs and varies abnormally during the period the signal is jammed, with a fading due to the Doppler offset variation existing between GNSS signal carrier and jammer. Time variations of each correlator output are modeled thanks to an AR filter and the residuals of the model are monitored. All available correlators are monitored simultaneously to take advantage of the link between their variations in presence of interference. A demonstration of the calculation of the AR parameters (a[k]) is provided in Appendix A.2. The residuals can be modelled as:

$$e[t] = x[t] - \widehat{x[t]} = x[t] + \sum_{k=1}^{p} a[k]x[t-k] \quad \textbf{(86)}$$

Where:

- t is the time index
- e is the model error
- x is the observed sequence of correlator outputs
- $\hat{x}[t]$ is the linear prediction estimate of the sample $x[t]$
- A is the AR coefficient matrix
- p is the AR model order

The major interest of this method is that x is a vector containing the sequence of all the correlators outputs. The multichannel AR model consequently takes into account the existing correlation between the correlators. Indeed, when no interference occurs, the correlators are affected by Gaussian white noise. When an interference occurs, the correlators are affected by sine waves as it is described in the next figure.

In this study, a multichannel AR model is used to model the correlator outputs behaviour, the model parameters are estimated thanks to the technique presented in Appendix A.2. Indeed, in presence of jammer, all correlators are affected by sine waves as it is shown in the next figure.

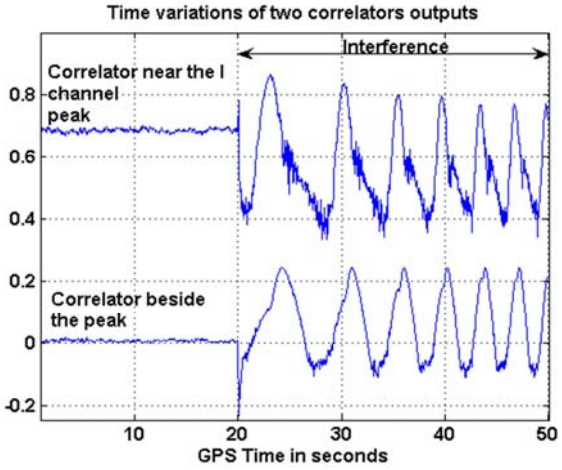

Figure 41 : Time variations of correlators for GPS L1 C/A signal affected by a – 155 dBW CW interference on the PRN 6 worst case line (227 kHz), without Doppler shift. The variations at the top corresponding to a correlator near the peak (0.32 chip away), the bottom correlator variations corresponds to a correlator located 1.6 chip away from the peak.

The main guideline of this detection algorithm is the following:

1. A 3rd order multichannel Auto Regressive model is used to monitor simultaneously all available correlator outputs (not equal to zero) at t, the following formula represents the ith element of the estimation vector:

$$\widehat{x^i[t]} = -\sum_{k=1}^{3} a^i[k]x^i[t-k] \text{ (i^{th} correlator)} \quad \textbf{(87)}$$

2. The multichannel AR model error is determined during a training stage (the index 0 represents the error obtained during the training stage (that is to say without interference), for each component i:

$$e_0^i[t] = x_0^i[t] - \widehat{x_0^i[t]} = x_0^i[t] + \sum_{k=1}^{3} a_0^i[k] x_0^i[t-k] \quad \textbf{(88)}$$

3. And then during test simulations, on studied samples and for each component, the error is:

$$e^i[t] = x^i[t] - \widehat{x^i[t]} = x^i[t] + \sum_{k=1}^{3} a^i[k] x^i[t-k] \quad \textbf{(89)}$$

4. The following detection criterion is finally calculated and compared to a threshold (E and E_0 are the norm of the error vectors including all the available correlator outputs errors):

$$\log \frac{E[t]}{E_0[t]} \quad \textbf{(90)}$$

This algorithm is derived from the theory developed in [Marple, 1987]. To our knowledge, it has never been used for such an application. As a consequence, the application of this algorithm as well as its performances assessment are original contributions to the EUROCAE WG 62 works.

5.6. Detection algorithms performances evaluation process

In this section, the performance evaluation methodology used for the previously proposed detection algorithms, is proposed in a few steps:

1. A detection criterion is defined from correlators output characteristics.
2. The detection algorithm is launched using the detection criterion over non-jammed simulated measurements. Detection criterion parameters are set during a training stage without interference under APV phase of flight conditions (dynamics, multipath).
3. Varying the criterion threshold, the APV continuity-compliant threshold is chosen when the false alarm rate is lower or equal to P_{FA} ($1.6\ 10^{-5}$ from ICAO continuity requirements for APV I [ICAO, 2002]).
4. Then the P_{MD} value is determined, generating interferences and using the defined criterion and threshold.
5. The impact of non-detected interferences on tracking error at any time is then discussed.

The obtained P_{MD} value must be multiplied by the interference probability of occurrence to compare the performance obtained to the integrity risk allowed for APV. Nevertheless, this probability of occurrence is unknown, as a consequence, no assessment about the integrity risk induced by the interference can be made.

5.7. Simulations assumptions

5.7.1. Simulation of actual aircraft approach conditions

The interference detection algorithms are tested taking into account the aircraft environment and dynamics during APV I. Indeed, aircraft dynamics and multipath were generated at the correlators outputs level, in compliance with the APV I phase of flight. This is explained and detailed in the next paragraphs.

5.7.1.1. Aircraft dynamics

Aircraft dynamics is modelled as described in Appendix B.1, taking into account the maximum values of ground speed, acceleration and jerk of the aircraft for both normal and abnormal manoeuvres recalled in [EUROCAE, 2007] or [RTCA, 2006]. These values are recalled in Chapter 2, paragraph 2.4.7.

5.7.1.2. Doppler shift rate between aircraft, satellites in view and interference source

The Doppler shift between the interference and the code spectrum lines is assumed to have a variation with time due to satellites and aircraft dynamics. The following figure shows an assumed satellite-aircraft-jammer configuration during the aircraft approach, near the airport, because the focus is given on the performances assessment of detection algorithms during APV I. The jammer is assumed located on the ground.

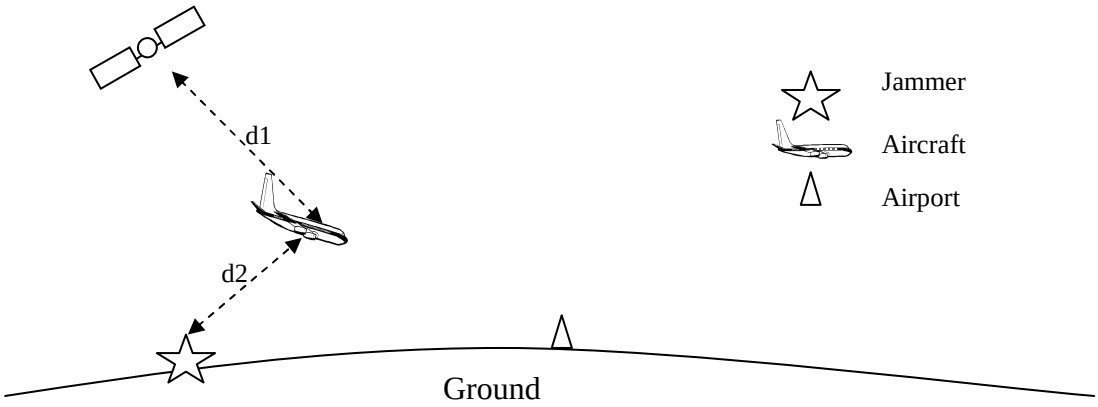

Figure 42: Satellite-aircraft-jammer configuration

The line of sight vector between each satellite and the aircraft antenna can be calculated thanks to the following ratio:

$$V_{\text{lign of sight}} = -\frac{\text{Pos}_{\text{satellite}} - \text{Pos}_{\text{aircraft}}}{\|\text{Pos}_{\text{satellite}} - \text{Pos}_{\text{aircraft}}\|} \quad \textbf{(91)}$$

Where:

- $\text{Pos}_{\text{satellite}}$ is the satellite position in space in the local reference frame (3 by 1 vector)
- $\text{Pos}_{\text{aircraft}}$ is the aircraft location vector in the same reference frame

Therefore the radial velocity is provided by:

$$v_{radial(Satellite \rightarrow Aircraft)} = (Velocity_{satellite} - Velocity_{aircraft}).V_{lign\ of\ sight} \quad \textbf{(92)}$$

Where:

- $Velocity_{satellite}$ is the considered satellite velocity vector
- $Velocity_{aircraft}$ is the aircraft ground velocity vector

If $\|Pos_{satellite} - Pos_{aircraft}\|$ denotes the distance between the receiver (aircraft GNSS antenna) and a satellite in meters, depending upon the satellite and receiver dynamics, with a linear variation, the distance between the satellite and the aircraft is then:

$$d_1 = \|Pos_{satellite} - Pos_{aircraft}\| + v_{radial(Satellite \rightarrow Aircraft)}.\Delta t \quad \textbf{(93)}$$

Where: $V_{radial(Satellite \rightarrow Aircraft)}$ is the radial initial speed between satellite and receiver. Identically,

$$d_2 = \left\|Pos_{jammer} - Pos_{aircraft}\right\| + v_{radial(Jammer \rightarrow Aircraft)}.\Delta t \quad \textbf{(94)}$$

Where: $\left\|Pos_{jammer} - Pos_{aircraft}\right\|$ is the distance between the jammer and the receiver onboard the aircraft, and $V_{radial(Jammer \rightarrow Aircraft)}$ the corresponding radial velocity, depending upon the receiver dynamics.

In the following, the index i = 1 if we consider the Doppler effect between the satellite and the aircraft and i=2 if we consider the Doppler effect between the jammer and the aircraft.

Considering the GPS L1 C/A or the Galileo E1 signal, the signal phase can be described as:

$$\varphi(t) = 2\pi ft - \theta(t) = 2\pi ft - 2\pi f\tau_i + \theta_0 \quad \textbf{(95)}$$

Where:

- f is the transmitted signal carrier central frequency (L1 C/A or E1)
- $\theta(t)$ is the phase offset due to the Doppler effect
- θ_0 is the phase initial offset
- $\tau_i = \frac{d_i}{c}$ is the time delay

So the corresponding instantaneous frequency is provided by a first order derivative of the cosine phase:

$$f_i = \frac{1}{2\pi}\frac{d\varphi}{dt} = f - f\,\frac{1}{c}\frac{d(d_i)}{dt} \quad \textbf{(96)}$$

Where:

- f is the signal carrier central frequency (L1 C/A or E1)
- c is the light speed equal to 299 792 458 m/s

The Doppler shift frequency between the satellite and the aircraft or between the jammer and the aircraft is thus defined as:

$$F_{di} = -\frac{f}{c}\frac{d(d_i)}{dt} \quad \textbf{(97)}$$

Consequently:

$$f_i = f + F_{di} \quad \textbf{(98)}$$

Moreover, the carrier wavelength is related to the carrier frequency of the considered GNSS signal by:

$$\lambda = \frac{c}{f} \quad \textbf{(99)}$$

So the corresponding Doppler frequency is:

$$F_{di} = -\frac{1}{\lambda}\frac{d(d_i)}{dt} \quad \textbf{(100)}$$

Finally, using (30) and (31):

$$\begin{cases} F_{d1} = -f\frac{d\tau_1}{dt} = -\frac{V_{radial(Satellite\rightarrow Aircraft)}}{\lambda} \\ F_{d2} = -f\frac{d\tau_2}{dt} = -\frac{V_{radial(Jammer\rightarrow Aircraft)}}{\lambda} \end{cases} \quad \textbf{(101)}$$

The Doppler shift obtained with the transmitted frequency L_1 (can be replaced by E1), from one given satellite to the aircraft receiver is thus:

$$Dopp_{L_{1(Satellite\rightarrow Aicraft)}} = -V_{radial(Satellite\rightarrow Aicraft)} \cdot \frac{L_1}{c} \quad \textbf{(102)}$$

The same result is obtained for the Doppler shift between the jammer and the aircraft:

$$Dopp_{L_{1(Jammer\rightarrow Aircraft)}} = -V_{radial(Jammer\rightarrow Aircraft)} \cdot \frac{L_1}{c} \quad \textbf{(103)}$$

The following table shows the obtained Doppler shift rate through simulations, taking into account the GPS L1 C/A signal. The presented values are the maximum and minimum Doppler shift rate obtained, taking into account the whole GPS L1 C/A signal coming from the whole constellation (with Yuma ephemeris), during one day. The aircraft normal

maneuvers maximum acceleration and jerk defined in [RTCA, 2006] and recalled in Chapter 2 (Table 2) were simulated to calculate the radial speed between the aircraft and a jammer located 8 kilometers away around the aircraft location.

	MINIMUM	MAXIMUM
Doppler shift rate	2.3 Hz/s	4.1 Hz/s

Table 7 : Doppler shift rate values obtained through simulations.

According to [Rollet, 2008], the resulting Doppler shift rate from satellites movement is between 2.9 and 3.1 Hz per second. The distance between the aircraft and the jammer is supposed negligible in comparison with the distance between each satellite and the aircraft. The radial speed between the aircraft and the jammer is supposed negligible compared to the radial speed between the aircraft and each satellite. As a consequence, the Doppler shift rate between the useful signal and the jammer can be approximated as the Doppler shift rate from satellites movement.

During our simulations, the Doppler shift rate was set to **2 Hz per second**. This means that when the interference affects one given code spectrum line, it stays a long time near this code spectrum line, which is damaging for code tracking and pseudoranges estimation. More precisely, during a whole aircraft approach, that is to say during 150 seconds ([RTCA, 2006]), the interference can move 300 Hz around a code spectrum line impacted. We considered a worst case where the aircraft does not accelerate, since when the aircraft accelerates, the jammer sweep the band.

This case is not representative of the actual aircraft dynamics because the jerk related to aircraft manoeuvers has not been taken into account, but it allows providing worst case simulation results. The actual aircraft dynamics would create a variable jerk in reality that could more probably improve the situation by increasing the satellite jammer aircraft shift rate, thus the situation described here is a worst case.

5.7.1.3. Multipath

As it is described in Chapter 2, multipath have an influence on the correlators outputs and will unshape the outskirts of the correlation peak.

Since the detection algorithms proposed are based upon the monitoring of the correlators outputs, it is necessary to take into account the impact of multipath on it. Indeed, due to multipath, a deformation of the correlation peak may be flagged instead of a CW while using one of the proposed interference detection criteria described in this chapter.

The model used for multipath is the DLR aeronautical channel model proposed by [Lehner, 2007]. A 10 degree satellite elevation is chosen to perform simulations and the model is launched during the 500 seconds of tracking. This elevation corresponds to the elevation mask angle for future Galileo satellites provided by Galileo [EUROCAE, 2007]. It is higher than the GPS elevation mask angle which is 5° as mentioned in [RTCA, 2006]. See Appendix B.2 for a further description of the multipath model used for simulations.

The model used here simulates multipath on the Graz Airport (Austria) where empirical tests were conducted to set the model. It is obvious that multipath impact on the correlator outputs is dependent upon the targeted airport geometry but this is the only setting available for simulations.

5.7.2. Generated signals power

In the following table, we present the carrier to noise ratio values chosen for simulations, which are compliant with the bounds defined in [EUROCAE, 2007]:

	GPS L1 C/A	GALILEO E1
C/N0	39 dB Hz	35 dB Hz

Table 8 : Carrier to noise ratios for GPS and Galileo signals used during simulations.

5.7.3. Receiver settings

5.7.3.1. Tracking loops

The following table recalls the simulation assumptions concerning the tracking loops settings:

	CHARACTERISTICS
DLL	1st order, Bandwidth: 1 Hz, dot product discriminator aided by the PLL
PLL	3rd order, Bandwidth: 10 Hz, arctan discriminator
Integration time	GPS L1 C/A, data: 20 ms Galileo E1, data: 20 ms, pilot: 4 ms.

Table 9 : Simulator tracking characteristics.

5.7.3.2. Multiple correlators settings

Multiple correlator outputs are generated for both GPS L1 C/A and Galileo E1 signals on the I and Q channels. The number of correlators, their spacing and span is dependent upon the signal processed since BPSK and BOC signals do not present the same correlation shape.

The correlators spacing *d* and the correlators window size around the main peak for both GPS and Galileo signals have to be set. For GPS L1 C/A, with a classical BPSK (1) modulation, the maximum CW frequency is 1.023 MHz, which corresponds to the main lobe

of the signal spectrum, where the highest amplitude spectrum lines are located (see Appendix C.2). The problem of detection out of this lobe is thus not addressed here. The larger the delay range used for correlators, the better the detection of a CW. Indeed, the variations of a sinusoid are visible on a larger delay window in this case. So low frequency CWs can be detected and estimated more easily than if the delay range is restricted. The maximum CW frequency is set to f_{CW} = 1.023 MHz to take into account the worst case C/A code spectrum lines within the main signal spectrum lobe. In simulations, the total number of correlators used is 2*34 =68. The chip-spacing is 0.32.

The impact of CW on the correlator outputs for GPS L1 C/A and Galileo E1 signals has the same shape, that is to say a sine wave appears in the autocorrelation.

Galileo E1 code spectrum is different than GPS L1 C/A spectrum (two main lobes between -2 MHz and 2 MHz appear in the code spectrum whose lines are 250 Hz-spaced [GSA, 2008], if the primary code only is considered and not the secondary one). The worst PRN code lines are located on the main lobes of the spectrum, the CW frequency is f_{CW} = 2 MHz. The total number of correlators is 2*36 =72. The chip-spacing is 0.125.

5.8. Simulation results

5.8.1. Obtained PMD and undetected errors induced in pseudoranges measurements by using the first FFT-based algorithm

The P_{MD} is calculated as the following ratio: the number of tests where the detection criterion is under the pre-defined threshold over the total number of tests conducted with the interference injected.

The obtained P_{MD} value for the worst case CW power (one jammer at -155 dBW) impacting the GPS L1 C/A signal on the worst case PRN 6 code spectrum line (227 kHz), is 6.7 10^{-5} using the snapshot FFT algorithm. On the next figures are represented **the maximum raw and smoothed code tracking error values generated by undetected CW**. The smoothed code error never exceeds 15 meters in the GPS L1 C/A case.

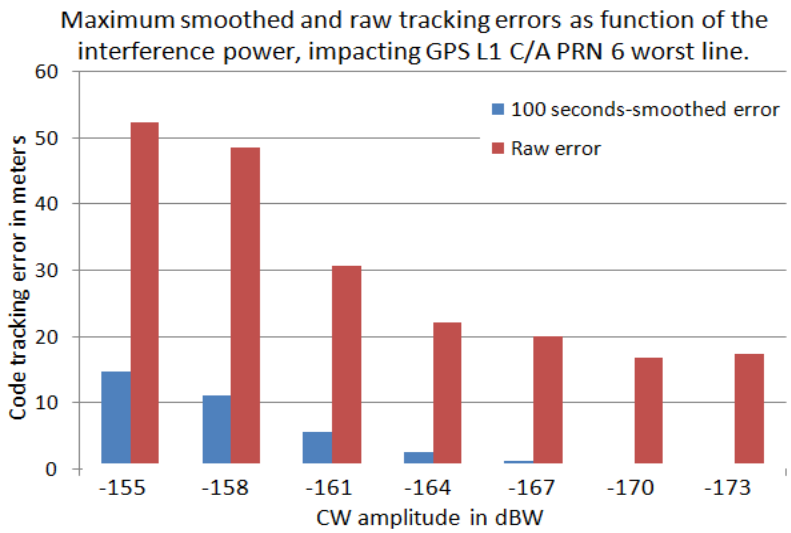

Figure 43 : Amplitude of maximum tracking error as a function of interference power resulting from non-detected CW on the GPS L1 C/A code, PRN 6 (227 kHz), the useful signal power is -158.5 dBW.

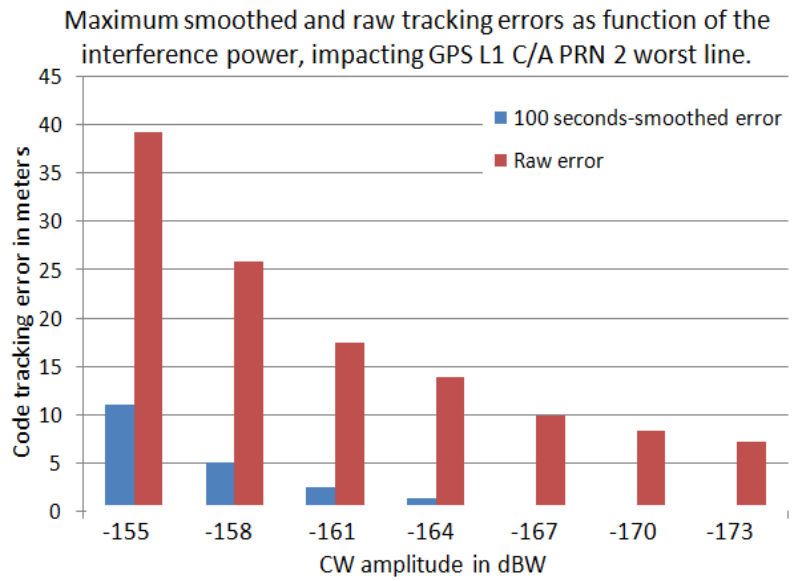

Figure 44 : Amplitude of maximum tracking errors as a function of interference power resulting from non-detected CW on the GPS L1 C/A code, PRN 2, the useful signal power is -158.5 dBW.

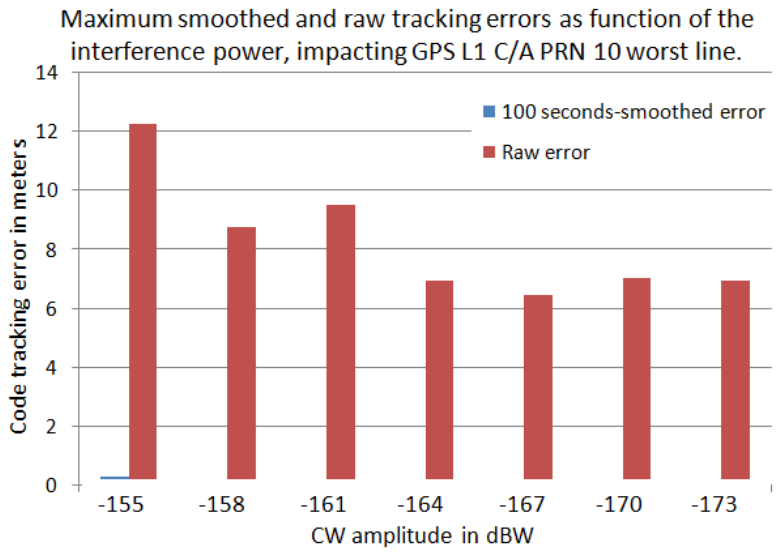

Figure 45 : Amplitude of maximum tracking errors as a function of interference power resulting from non-detected CW on the GPS L1 C/A code, PRN 10, the power of the useful signal is -158.5 dBW.

The obtained P_{MD} value for the worst case CW impacting the Galileo E1 signal is 10^{-5}. Hereafter is represented the maximum raw and smoothed code tracking errors obtained for undetected CW. The smoothed error never exceeds 1.5 meters as it can be observed in the following figure.

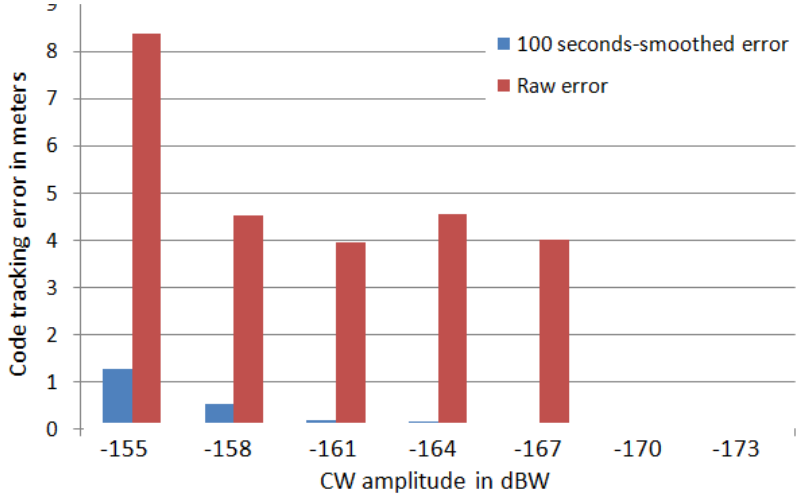

Figure 46 : Amplitude of maximum tracking errors as a function of interference power resulting from non-detected CW on the Galileo E1 code, PRN 38, the power of the useful signal is -160 dBW.

The obtained missed detection probability is weighted by the probability of having each error amplitude amongst all experienced amplitudes and represented in the next Figure 47. The results are represented over 3 10^6 tests of the resulting raw tracking errors distribution. These results have been obtained for GPS L1 C/A PRN 6 highest code spectrum line impacted by a -155 dBW CW interference.

As the algorithm missed detection probability is low, the number of examples of tracking errors obtained during missed detection is low in our simulation results (only 200 values). As a consequence, the following results have to be taken with care. The maximum tracking errors are obtained amongst the available measurements.

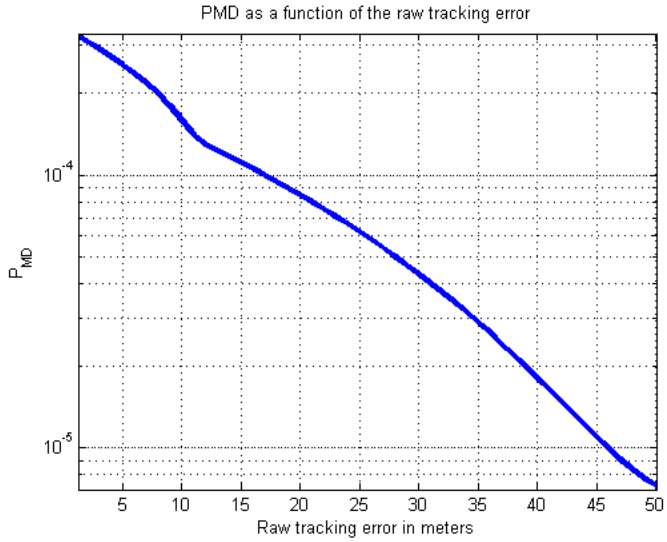

Figure 47 : Obtained missed detection classified by resulting raw tracking errors for GPS L1 C/A PRN 6 highest code spectrum line impacted by one -155 dBW CW interference.

With a larger number of tests, it would be interesting in future works to plot the distribution of the tracking errors resulting from the non-detected CW.

5.8.2. Obtained PMD by using the second AR-based algorithm

The P_{MD} obtained for the worst case CW amplitude using the multichannel AR model is comparable to the P_{MD} obtained thanks to the FFT algorithm. Indeed, when the GPS L1 C/A PRN 6 worst code spectrum line is impacted by a -155 dBW CW, the multichannel AR detection algorithm P_{MD} is 10^{-5}.

5.9. Discussion about the obtained results

A first remark is that if one wants to implement the FFT detection technique or the AR one within future receivers, the detection criteria parameters and thresholds under actual normal aircraft conditions of dynamics and multipath have to be previously saved.

As shown in the figure 40, the impact of jammers on the correlator outputs differs with the amplitude of the interference. Indeed, the larger the amplitude of the interference, the larger the amplitude of the sine wave. The two techniques have different approaches, considering the instantaneous behaviour of the correlators' outputs in the Fourier domain or considering the time evolution of these ones.

It seems that for Galileo signal case (PRN 38), the maximum smoothed error generated by an undetected interference is smaller than for GPS L1 C/A, this is due to the fact Galileo code spectrum lines have a lower amplitude than GPS L1 C/A ones. Indeed, the maximum amplitude code spectrum lines identified for the GPS L1 C/A signal are between -25 dB and -21 dB, whereas for the Galileo E1 OS signal, they are included between -32 dB and -28 dB. In particular, the worst case spectrum line of the L1 C/A signal is -21.29 dB whereas it is -28.81 for the E1 signal (see the appendix C.2 for all amplitude values).

It can be also clearly seen that the impact of CW on the raw pseudorange errors in terms of worst case code lines is larger than for other lines as PRN 10 worst case code line for instance.

With a larger number of tests, it will be interesting for future works, to plot the distribution of the tracking errors resulting from the non-detected CW.

5.10. Conclusion and future works on interference detection

In our simulations, worst cases in terms of interference power: -155 dBW CW and code spectrum lines impacted were considered: -21.29 dB PRN 6 line for the C/A signal and -28.81 dBW PRN 38 for the E1 OS signal.

Each CW interference is generated using a Doppler variation rate (between code lines and interference) of 2Hz/s for each 300 seconds tracking trial. So, interference does not permanently strike exactly the worst spectrum lines.

Two algorithms are proposed: a snapshot one (FFT) and an AR model-based one. Such detection algorithms are expected to alleviate and complete the detection made by RAIM-type algorithms in the case where CW interferences hit PRN code spectrum lines. The obtained P_{MD} are between 6 10^{-5} and 10^{-5} for the worst case -155 dBW CW. These results concern the worst case GPS L1 C/A PRN 6 and Galileo E1 PRN 38 code spectrum lines using each of the two proposed detection algorithms.

The resulting maximum error on smoothed pseudoranges when such a CW is not detected, is 15 meters for GPS L1 C/A and 1 meter for Galileo E1. For the sake of comparison, in presence of a -155 dBW CW, without any detection algorithm, the maximum smoothed tracking error obtained during simulations is near 30 meters when tracking the L1 C/A signal. The presented techniques are consequently useful when an interference occurs during approach phases of flight like APV because, it will allow detecting a degradation due to a CW with a low P_{MD} (integrity) and in case of failure in the detection, the resulting error is not expected to exceed 1 meter while using Galileo E1 for positioning as shown by simulations.

In this study, the delay for interference detection was not evaluated.

The minimum number of correlators required to obtain the same performances was not evaluated and should be evaluated to reduce further the algorithms complexity.

5.10.1. Discussion about the proposed algorithms and civil aviation requirements

Civil aviation requirements for APV I phase of flight in terms of accuracy and integrity are recalled in Chapter 2, Table 1. TTA which stands for Time To Alert, is the maximum allowable time interval between system performance ceasing to meet operational performance limits and the appropriate integrity monitoring subsystem providing an alert. It is important to obtain a low time of detection with regards to TTA to maintain integrity. The two proposed detection algorithms latency durations are much lower than the APV I time to alert which is 10 seconds, as the FFT algorithm is snapshot and the AR algorithm only requires 3 time samples, 20 ms-spaced and a maximum time of latency lower than one second.

The P_{MD} value obtained during our simulations must be multiplied by the interference probability of occurrence to evaluate the corresponding integrity risk requirement. Unfortunately, the probability of occurrence of interferences cannot be estimated to our knowledge. It is consequently not possible to evaluate the integrity risk. The obtained missed detection probabilities must be weighted by the probability for a CW to hit a given worst case code line, so this decreases the risk induced by CW in terms of integrity.

The proposed algorithms, elaborated here for interference detection, are expected to alleviate the burden of RAIM-type algorithms. As a consequence, future works can consist in taking into account both detection capability within tracking loops using the proposed techniques and the RAIM capability to detect failures due to interferences.

For future civil aviation combined receivers, the FFT-based detection technique seems to be the best algorithm to choose. Indeed, it provides slightly worse results than the AR technique in terms of missed detection probability, but it is the simplest solution. Therefore, we recommend the FFT algorithm as detection mean for future receivers. The FFT solution could be implemented in hardware or software parts of the receiver.

When a detection is made and when there is an impact on the performances, it is possible to characterize the interferences with a Prony-like model for instance and thus to clean out the correlator outputs from the interference.

After detection, the next step consists in two options:

- initializing a switch to other GNSS components within the same mode of operation or to another mode to perform the current phase of flight;
- or removing the incoming interference to continue using the affected GNSS component.

5.11. Use of a model to characterize each interference

It is of interest to know the performance of a repair algorithm: that is to say an algorithm which cleans out the correlators outputs, when the interference is flagged. As a consequence, a preliminary study of an estimation and repair algorithm is provided in the

following. It seems this algorithm provides promising results as it can be seen in the following.

In order to repair the correlators outputs, interferences characteristics have to be determined. Parametric models allow representing physical phenomena like CW interfering signals. Such models provide, with a small number of parameters, the main characteristics of a CW. In the following, a third order Prony model ([Castanié, 2003]) is used to characterize the CW interferences. This model is described in Appendix A.3.

The results are presented in the following and concern the estimation and correlators output repair when a CW hits the identified worst case GPS L1 C/A PRN 6 code spectrum line, located at 227 kHz. In the following figure, the estimation of the CW frequency (227 kHz) is represented over 100 tests, thanks to the Prony model. The obtained estimations are between 226.84 kHz and 227 kHz. The obtained resolution of the algorithm is consequently better than 200 Hz.

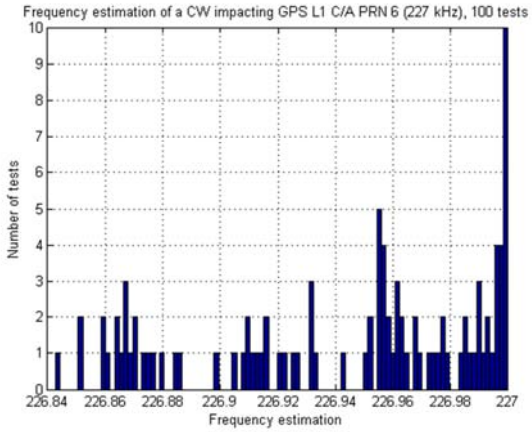

Figure 48 : Estimation of a -155 dBW CW frequency impacting GPS L1 C/A PRN 6 (227 kHz) using a third order Prony model on 68 correlators outputs.

The CW frequency estimation is acceptable as it can be seen in the previous figure. Indeed, over 100 tests, the frequency estimation error never exceeds 160 Hz. The tests are made here for GPS L1 C/A signal. The spacing between two code spectrum lines is 1 kHz. For Galileo E1 signal, the spacing between two lines is 250 Hz.

But the most important result is the resulting tracking error after clean out of the correlators outputs. Indeed, it can be noticed in the following figure that this algorithm can provide significant improvement in tracking robustness and avoid a loss of tracking lock. Simulations show that the standard deviation of the code tracking error (always for GPS PRN 6), is reduced from 80 meters (in red) to 6 meters (in blue) in this case as it can be seen in the next figure.

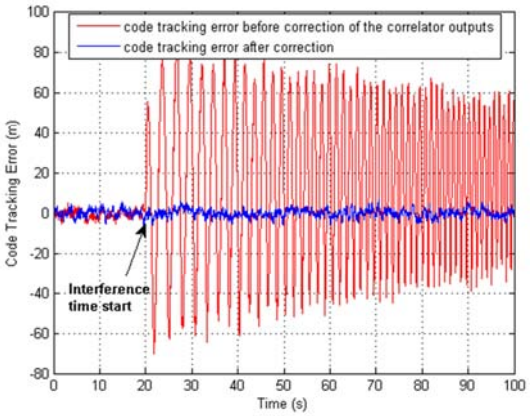

Figure 49 : Raw code tracking error with and without one -155 dBW CW interference estimation and correction, the impacted code spectrum line is the PRN 6 (227 KHz) of the L1 C/A signal.

The raw and smoothed pseudoranges, before and after correction are provided in the following table, over 4000 samples, that is to say during 80 seconds:

	ESTIMATED STATISTICS	VALUE WITHOUT CORRECTION	VALUE WITH CORRECTION
Raw code tracking error	Mean	19.9 m	$-9\ 10^{-3}$ m
	Standard deviation	10.5 m	1.9 m
Smoothed code tracking error	Mean	13.7 m	$3\ 10^{-2}$ m
	Standard deviation	5.3 m	$4\ 10^{-2}$ m

Table 10: Raw and smoothed code tracking error with and without interference removal at the correlator output level, over 80 seconds (4000 samples).

Note that the smoothing filter used here is the one presented in Chapter 2, 2.3.2.1.

5.12. Conclusion

This study focuses on CW interference detection because this kind of interference can stay a long time near high amplitude code spectrum lines and can thus generate damaging code tracking errors which can result in a biased navigation solution during APV I. Indeed, high level interference, at the limit of the interference rejection masks defined in [EUROCAE, 2007] and recalled in this chapter, can stay a sufficiently long time near high amplitude GPS L1 C/A or Galileo E1 code spectrum lines to generate large code tracking errors. This is due to low Doppler shift rate between interference and code spectrum lines. Nevertheless, the hypotheses of having such interferences are related to the worst cases that can occur in civil aviation applications, the probability of having such CW near the rejection mask is expected to be low.

Two detection algorithms are proposed here and are expected to alleviate and complete the detection made by RAIM-type algorithms. The obtained P_{MD} are 10^{-5} using the AR

algorithm and 6.67 10^{-5} using the FFT one, for the worst case generated CW (-155 dBW). These results concern GPS L1 C/A PRN 6 and Galileo E1 PRN 38 worst case code spectrum lines.

The resulting maximum error on smoothed pseudoranges when the algorithms do not detect the CW, is 15 meters for GPS L1 C/A and 1 meter for Galileo E1.

The presented techniques are consequently useful when an interference occurs during approach phases of flight like APV I, because they allow detecting degradation due to a CW with a low P_{MD} (integrity), and, in case of failure in the CW detection, the resulting error due to the CW, does not exceed 1 meter on Galileo E1 OS code-carrier smoothed pseudorange. These results show that the threat due to the interferences is eliminated at the input of RAIM detection algorithms.

The strategies proposed in Chapter 4 include a switch after interference detection. In case of interference detection on GPS L1 C/A or Galileo E1, the receiver can switch to single frequency alternate or degraded modes identified in Chapter 3. When a detection is made and when there is an impact on performances, it is possible to repair the correlator outputs thanks to the characterization of the interferences affecting GPS L1 C/A and Galileo E1 signals. In this chapter, a 3rd order Prony model is proposed for CW characterisation in order to clean out the correlator outputs. The repair algorithm provides good results as the maximum code tracking error on GPS L1 C/A processing, is reduced from 80 meters to 6 meters as shown in the figure 49. Thus, the receiver can continue using GPS L1 C/A or Galileo E1 when a damaging CW occurs and affects these GNSS components. Indeed, it is demonstrated that the proposed correlators outputs repair algorithm can maintain the level of performance reached when no CW occurs, in terms of tracking accuracy during APV I.

5.12.1. Scenarii with regard to the combined receiver architecture

According to the schemes described in Chapter 4, the interference detection function presented here relies on the monitoring of the correlators outputs. The detection is based on the FFT or AR detection criteria defined in this chapter. If a significant loss of performance (not sufficient to perform a targeted phase of flight, APV I for instance) results from the interference occurrence, then, the monitored GNSS component is declared lost (unavailable). The receiver can then switch to other available GNSS components combinations within modes of operations described in the following figure.

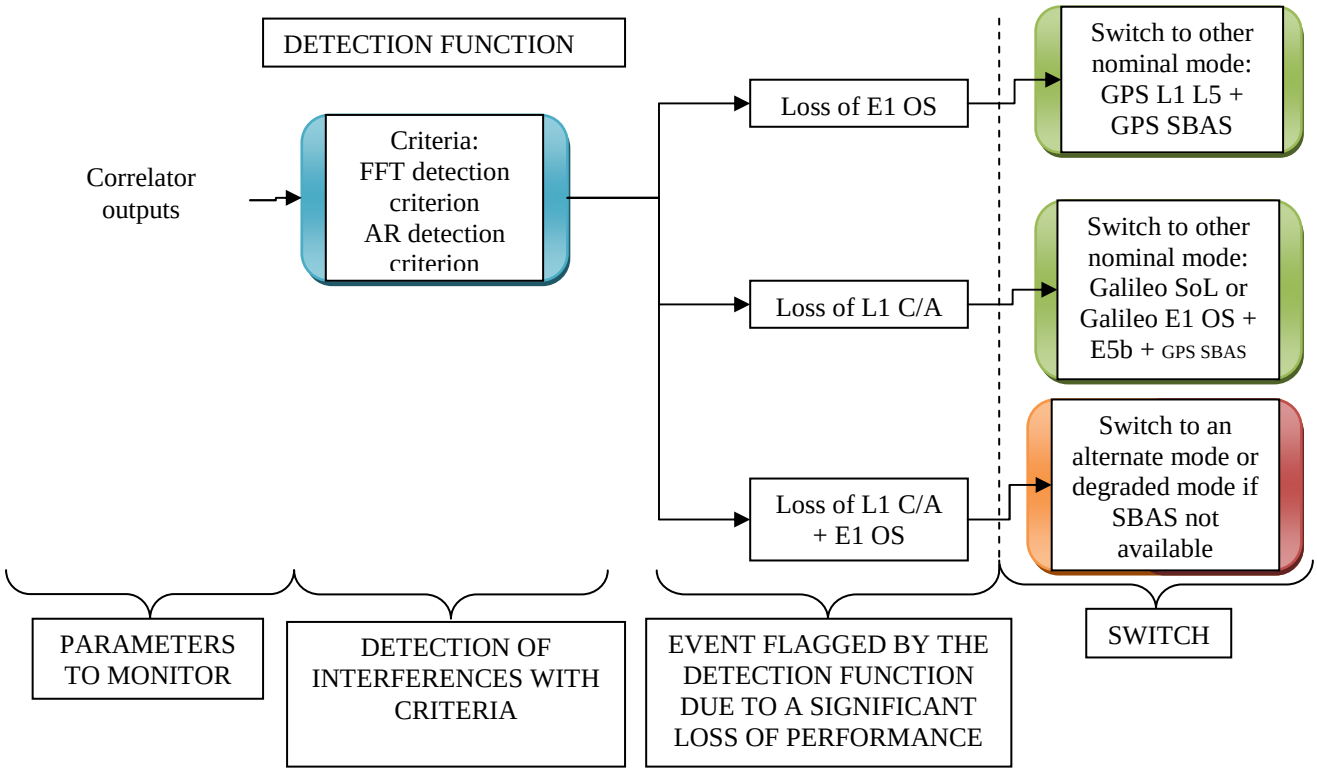

Figure 50: Interference detection function based on correlators outputs monitoring

Another solution can consist in estimating the interference characteristics. The correlators outputs can be repaired after the interference detection. Thus, a correct digital signal processing can be performed to provide accurate tracking loops outputs and pseudoranges measurements. A technique to model the interferences at the correlators outputs, based on a Prony model, was presented in this chapter and showed encouraging results. After correction, the resulting errors due to a CW on tracking outputs are negligible.

As it is described in Chapter 2, if no interference occurs, the most contributing error in pseudoranges is the error due to the ionosphere, if left uncorrected. As mentioned in Chapter 2, this error is well determined thanks to a combination of pseudoranges at two different frequencies to provide a composite ionospheric-free pseudorange.

In case of loss of dual frequency measurements for instance, when the aircraft crosses a Radio Frequency Interference (RFI) area, the receiver must revert to a single frequency mode (alternate or degraded as mentioned in Chapter 3) and ionospheric code delay is not yet provided as in a nominal dual frequency mode. Other alternatives to estimate ionospheric code delay are SBAS ionospheric grids, TEC estimation models, which input parameters are broadcasted by the remaining GPS or Galileo signal, and code minus carrier measurements as described in the next chapter. However, these techniques do not allow reaching the performances required by the ICAO for restrictive approach phases of flight. The receiver cannot rely on these techniques in case of single frequency mode. Indeed, most of them are not accurate enough or do not comply with integrity requirements. That is why, single frequency ionospheric code delay estimation techniques are discussed, studied and improved in the next chapter. New algorithms are proposed and their capabilities are evaluated in terms of continuity, integrity, accuracy and availability.

Chapter 6

Ionospheric code delay estimation in case of single frequency degraded mode

Contents

Résumé

Le chapitre 6 concerne l'estimation de l'erreur ionosphérique en mode dégradé mono fréquence. En effet, dans ce chapitre est abordée la problématique du maintien des niveaux de performance lors d'un passage en mode dégradé en APV I. Pour cela, nous étudions d'abord tous les algorithmes monofréquence permettant d'estimer l'erreur ionosphérique sur les mesures de pseudodistances et comparons leurs performances en termes de précision. Nous dressons de plus un bilan des avantages et inconvénients liés à chaque algorithme. Nous retenons finalement la technique de divergence code-porteuse, prometteuse en précision, mais sujette à des perturbations de type sauts de cycles dans les mesures de phase de la porteuse du signal traité. En cela, nous décidons d'investiguer différentes techniques de détection de sauts de cycles et nous évaluons leurs performances pour satisfaire les exigences de l'aviation civile en termes d'intégrité et de continuité. Ainsi, nous déterminons le plus petit biais détectable sur les mesures de pseudodistance, dans un environnement hypothétique le plus contraignant possible. Ce biais se répercutant sur les mesures de pseudodistances, il est nécessaire d'évaluer l'impact d'un tel biais dans l'estimation de position de l'avion (à l'intérieur d'un cylindre de protection). Pour cela, nous décidons de projeter l'erreur obtenue sur le plan horizontal de l'appareil en approche, ainsi que sur l'axe vertical, de manière à comparer les valeurs obtenues aux limites d'alerte définies par l'aviation civile pour l'APV I. Ainsi, lorsque les résultats obtenus sont en deçà des limites d'alerte, l'algorithme considère que les mesures sont disponibles (avec ou sans saut de cycle). Ce procédé est utilisé pour les constellations GPS et Galileo. En ce qui concerne la précision des mesures, les paramètres de la technique de divergence code porteuse (erreur ionosphérique et ambiguités de porteuse) sont estimés à l'aide d'un filtre de Kalman, initialisé en mode bifréquence (nominal), c'est-à-dire, avant dégradation. Ceci, afin de créer un pont de passage entre mode nominal et mode dégradé, ce qui permet de maintenir le niveau de performance en précision, le plus longtemps possible après la dégradation conduisant au mode opérationnel dégradé.

6. Ionospheric code delay estimation in case of single frequency degraded mode

6.1. Introduction

The ionosphere is a dispersive medium that can strongly affect GPS and Galileo signals. It is the larger source of ranging error, if left uncorrected. In addition, this perturbation is difficult to model and thus difficult to predict. Indeed, it is dependent upon the signal path from the satellite to the aircraft and the ionization of the atmosphere as it is described in Chapter 2.

A multi-frequency receiver can identify and correct errors induced by the ionosphere. Indeed, two pseudorange measurements on two different frequencies enable to determine precisely the ionospheric code delay. However, if affected by a Radio Frequency Interference (RFI), a receiver can lose one or more frequencies leading to the use of only one frequency to estimate the ionospheric code delay. Therefore, it is identified by [NATS, 2003] and [Shau-Shiun Jan, 2003] as an important task to investigate techniques aimed at sustaining multi-frequency performance when a multi-constellation receiver installed onboard an aircraft is suddenly affected by RFI, during critical phases of flight.

When only one frequency is available, one way to use single frequency measurements is to use code and carrier phase measurements to deduce ionospheric code delay from the dispersive behavior of the medium and the derived properties on electromagnetic waves as described in Chapter 2 and depicted in Figure 14. This method is called code-carrier divergence technique.

In the case of a loss of all GNSS components but one frequency, the technique analyzed is the code-carrier divergence technique, consisting in computing the difference between the signal code and carrier phase measurements. This difference is twice the ionospheric delay plus the carrier phase ambiguity plus errors, from which the ionospheric code delay can be extracted. If a cycle slip occurs on phase measurements, the integer ambiguity appearing as a constant offset in the code-carrier difference can cause this technique not to be accurate enough to meet APV I requirements. That is why, it is necessary to be able to detect cycle slips. The cycle slip detection algorithm used must be compliant with APV I integrity and continuity requirements.

A Kalman filter can also be used to estimate ionospheric code delay and ambiguities of all satellites in view as mentioned in [Lestarquit, 1997]. This Kalman filter can be initialized in the dual frequency mode, and left running when only one frequency is left.

Another way to estimate ionosphere thanks to only one frequency, is to use the broadcasted parameters provided in GPS and Galileo messages for ionosphere modeling to calculate the Total Electronic Content (TEC) defined in Chapter 2. But this technique has strong accuracy limitations as described in [NATS, 2003].

Another solution can consist in using other available GNSS components such as SBAS as it is proposed in [Shau-Shiun Jan, 2003]. Indeed, through a ionospheric threat model technique described in [Shau-Shiun Jan, 2003], the receiver can use a ionospheric grid that can provide an estimation of a bound on the corresponding error, depending upon the aircraft position around the reference geoid. However, this system is only regional as depicted in figure 1. The SBAS coverage is not sufficient to protect the user everywhere on the Earth. Furthermore, the case when an aircraft flies in border line of the SBAS coverage has to be studied in details to know the availability of the component. In addition, this system is not robust against ionosphere irregularities generated by storms. Indeed, magnetic storms are characterized by abnormal variations in the magnetic field of the Earth. It causes free electrons distributions to be disturbed (mostly in F layer as described in Chapter 2, paragraph 2.4.1). The use of a storm detector is consequently required as mentioned in [Shau-Shiun Jan, 2003].

In this chapter, the problem of maintaining dual frequency measurements performances is addressed without use of SBAS. The use of SBAS corrections has already been studied in [Shau-Shiun Jan, 2003].

Several configurations can be considered due to a loss of frequency after an RFI crossing. For example, for a dual frequency GPS L1 C/A / L5 receiver, the loss of L1 tracking due to a CW implies the use of the remaining L5 frequency. The same remark can be made for the Galileo E1 and E5 signals.

As mentioned in Chapter 3, a single frequency GNSS combination is classified as an alternate mode of operation if an augmentation is used for en route down to NPA. It is the case of GPS or Galileo single frequency plus GPS SBAS, Galileo single frequency plus SoL combinations (integrity carried by both E5b and E1).

In the APV I case, only the combinations using SBAS are expected to allow reaching a sufficient level of performance. Galileo single frequency plus SoL is classified as a degraded mode of operation. In that way, the study conducted and described in this chapter concerns this degraded combination (even if actual measurements used to analyze the performances of the algorithms proposed are only GPS measurements).

The case when GPS single frequency is used in standalone mode, without SBAS, is not considered by the WG 62.

This chapter can be viewed as a study aimed at maintaining the nominal modes level of performance during degraded modes. The cycle slip detection algorithm can also be viewed as detection mean useful to detect anomalies in carrier phase measurements in nominal modes of operation. Indeed, in dual frequency modes of operation, phase measurements are used to smooth code measurements and cycle slips affect carrier phase measurements.

6.2. Dual frequency ionospheric code delay estimation

So as to get rid of ionospheric effect on pseudoranges measurements, a combination of dual frequency measurements is used. Indeed, for future civil aviation GNSS receivers complying with EUROCAE requirements, dual frequency measurements are combined into a single composite measurement called the "ionospheric-free" measurement, corrected from ionospheric code delay. This can be done by using future GPS or Galileo signals.

In a nominal mode of operation (see section 3.1.1), the pseudorange measurements that are available to the aircraft receiver are the GPS L1, GPS L5, Galileo L1, Galileo E5a, Galileo E5b code and phase measurements. These frequencies can be combined to build ionospheric-free measurements.

For two frequencies, the ionospheric-free measurements are expressed thanks to:

$$P = \frac{f_1^2}{f_1^2 - f_2^2} P_1 - \frac{f_2^2}{f_1^2 - f_2^2} P_2 \quad \textbf{(104)}$$

$$\phi = \frac{f_1^2}{f_1^2 - f_2^2} \phi_1 - \frac{f_2^2}{f_1^2 - f_2^2} \phi_2 \quad \textbf{(105)}$$

Where:

- f_1 and f_2 are two different signals central frequencies
- P_1 and P_2 are the corresponding code pseudorange measurements
- Φ_1 and Φ_2 are the carrier phase measurements
- P is the code "ionospheric-free" pseudorange measurement
- Φ is the carrier phase "ionospheric-free" measurement

A demonstration of the ionospheric-free estimation model is provided in Appendix B.3.

6.2.1. Application to future GNSS signals

Only the combined E1/E5b ionospheric-free measurements are protected by the Galileo ground integrity information. Therefore, from GPS L1/L5, and from Galileo E1/E5b, two distinct ionospheric-free code-carrier measurements can be built.

This is based on:

$$P_{L1-L5}(k) = \frac{f_{L1}^2}{f_{L1}^2 - f_{L5}^2} P_{L1}(k) - \frac{f_{L5}^2}{f_{L5}^2 - f_{L1}^2} P_{L5}(k) \text{ (GPS)} \quad \textbf{(106)}$$

$$P_{E1-E5b}(k) = \frac{f_{E1}^2}{f_{E1}^2 - f_{E5b}^2} P_{E1}(k) - \frac{f_{E5b}^2}{f_{E5b}^2 - f_{E1}^2} P_{E5b}(k) \text{ (Galileo)} \quad \textbf{(107)}$$

$$\phi_{L1-L5}(k) = \frac{f_{L1}^2}{f_{L1}^2 - f_{L5}^2} \phi_{L1}(k) - \frac{f_{L5}^2}{f_{L5}^2 - f_{L1}^2} \phi_{L5}(k) \text{ (GPS)} \quad \textbf{(108)}$$

$$\phi_{E1-E5b}(k) = \frac{f_{E1}^2}{f_{E1}^2 - f_{E5b}^2} \phi_{E1}(k) - \frac{f_{E5b}^2}{f_{E5b}^2 - f_{E1}^2} \phi_{E5b}(k) \text{ (Galileo)} \quad \textbf{(109)}$$

With:

$$\frac{f_{L1}^2}{f_{L1}^2-f_{L5}^2} \approx 2.261 \quad \frac{f_{L5}^2}{f_{L5}^2-f_{L1}^2} \approx -1.261 \quad \frac{f_{E1}^2}{f_{E1}^2-f_{E5b}^2} \approx 2.422 \quad \frac{f_{E5b}^2}{f_{E5b}^2-f_{E1}^2} \approx -1.422$$

These values show that the weighting factor applied to GPS L5 or Galileo E5b is half the weighting factor applied to L1 or E1. More precisely, it is 55% for GPS and 58% for Galileo.

The statistics of the combined composite ionospheric-free measurements are related to the quality of the resulting position estimation. The standard deviation of the error affecting the smoothed composite ionospheric-free measurements can be modeled as:

$$\sigma_{L1-L5} = \sqrt{\left(\frac{f_{L1}^2}{f_{L1}^2-f_{L5}^2}\right)^2 \sigma_{L1}^2 + \left(\frac{f_{L5}^2}{f_{L5}^2-f_{L1}^2}\right)^2 \sigma_{L5}^2} = \sqrt{2.261^2\sigma_{L1}^2 + 1.261^2\sigma_{L5}^2} \quad \textbf{(110)}$$

$$\sigma_{E1-E5b} = \sqrt{\left(\frac{f_{E1}^2}{f_{E1}^2-f_{E5b}^2}\right)^2 \sigma_{E1}^2 + \left(\frac{f_{E5b}^2}{f_{E5b}^2-f_{E1}^2}\right)^2 \sigma_{E5b}^2} = \sqrt{2.261^2\sigma_{E1}^2 + 1.261^2\sigma_{E5b}^2} \quad \textbf{(111)}$$

Ionospheric-free measurements affected by multipath are shown in [Eissfeller, 2005]. Due to the high chipping rate of 10.23 MHz used for the GPS L5 and Galileo E5b signals, noise and multipath errors are statistically higher for the measurements from higher central frequencies like GPS L1 or Galileo E1 signals than for GPS L5 or Galileo E5b. Therefore, the ionospheric-free measurements are more affected by the noise and multipath errors on L1/E1 than on L5/E5b. Indeed, the error induced by multipath affects each code and carrier phase measurement on GPS L1, GPS L5, Galileo E1, and Galileo E5b. The impact of multipath propagation is different on code tracking and on carrier tracking; it is also dependent upon the signals processed and the modulations. The effect of noise and multipath on the previously mentioned signals is mainly due to thermal noise, antenna design and obstacles encountered around the antenna. However, the perturbations on the measurements are different because of the design of PRN codes which differ from one signal to another one. Similarly, if advanced code and carrier phase tracking techniques are used, the carrier phase measurements can benefit from the signal structure adopted for GPS L5 and Galileo E5b [Bastide1, 2004], and noise and multipath errors are also reduced for these two frequencies compared to GPS L1 or Galileo L1 phase measurements.

6.2.2. Conclusion

Smoothed ionospheric-free range measurements are used for civil aircraft operations. However, in case of loss of one frequency due to radiofrequency interference (RFI) for instance, another way to estimate ionospheric code delay must be used. Models are also proposed to estimate the ionospheric code delay, like the Klobuchar model described latter in this chapter. They could be used in case of loss of dual frequency estimations, but, as it is

described in the next paragraphs, the accuracy of these models is not sufficient for some civil aviation operations, for instance during APV I.

6.3. Estimation of the ionospheric code delay thanks to estimation models

6.3.1. GPS Klobuchar model

The first existing model described in this dissertation is proposed by Klobuchar and the corresponding algorithm is detailed in [Parkinson, 1996]. The input parameters of this model are provided by the GPS satellites signals navigation message. It is a single layer model. Indeed, the TEC is supposed to be concentrated in an infinitely thin layer at an altitude of 350 km. Since the electronic content depends upon the solar activity (Chapter 2), the ionospheric code delay is chosen constant and equal to 5 ns during the nights. During the days, a cosine function models this delay; it is a function of the receiver position.

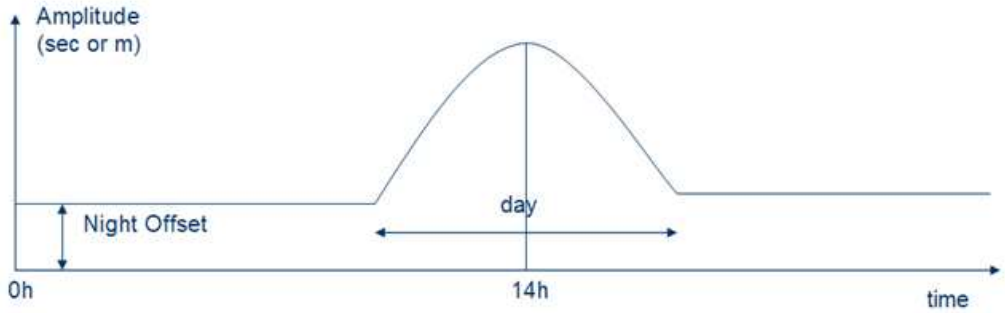

Figure 51: Klobuchar function: evolution of single atmospheric layer located at 350 km high

This cosine function provides the ionospheric code delay due to the signal propagation through the ionosphere, along the satellite to receiver path. It is described by [Parkinson, 1996]:

$$\mathrm{T} = \mathrm{Ob}\left[\frac{\mathrm{DC}+\mathrm{A}\cos\left(2\pi(\mathrm{t}-\phi)\right)}{\mathrm{P}}\right] \quad \textbf{(112)}$$

Where:

- DC is the night offset which corresponds to the error related to the TEC estimation without sunlight
- A is the amplitude of the error
- t is the current time (sec)
- ϕ is the origin phase
- Ob is the obliquity factor, equal to the ratio between the vertical TEC and the slant TEC (that is to say for a satellite elevation different of 90°, from the receiver point of view)

The carried information in GPS L1 C/A navigation message is divided into two sets of parameters which are the coefficients of the third order development of the amplitude and period of the model presented above respectively:

$$A \approx \sum_{i=0}^{3} a_i \varphi \quad \textbf{(113)}$$

$$P \approx \sum_{i=0}^{3} b_i \varphi \quad \textbf{(114)}$$

Where φ is the geomagnetic latitude of the aircraft (receiver), in semi-circles (rad/pi).

6.3.2. Galileo NeQuick model

Another model is the NeQuick one which was proposed more recently and which parameters will be broadcasted in the Galileo signals navigation message. It is a multilayer model. The electronic content estimation is provided by an Epstein estimator [Garcia, 2002] of the number of electron in each layer defined in Chapter 2. The Epstein estimator is provided by the following formula:

$$N_{Epstein}(h, h_{max}, N_{max}, B) = \frac{4\, N_{max}}{\left(1+\exp\left(\frac{h-h_{max}}{B}\right)\right)^2} \exp\left(\frac{h-h_{max}}{B}\right) \quad \textbf{(115)}$$

Where:

- h is the altitude of the layer (which can vary along time, for instance this altitude differs between nights and days)
- h_{max} is the maximum altitude of the layer
- B is the characteristic of the layer [Garcia, 2002]
- N_{max} is the maximum number of electrons in the layer

The NeQuick model relies on the estimation of the number of electrons contained within the layers E and F (detailed in two sub layers F1 and F2) described in Chapter 2, paragraph 2.4.1. Therefore, the Epstein formulation is used for each representative layer:

$$N_E(h) = \frac{4\, N_{maxE}}{\left(1+\exp\left(\frac{h-h_{maxE}}{B_E}\right)\right)^2} \exp\left(\frac{h-h_{maxE}}{B_E}\right) \quad \textbf{(116)}$$

$$N_{F1}(h) = \frac{4\, N_{maxF1}}{\left(1+\exp\left(\frac{h-h_{maxF1}}{B_{F1}}\right)\right)^2} \exp\left(\frac{h-h_{maxF1}}{B_{F1}}\right) \quad \textbf{(117)}$$

$$N_{F2}(h) = \frac{4\, N_{maxF2}}{\left(1+\exp\left(\frac{h-h_{maxF2}}{B_{F2}}\right)\right)^2} \exp\left(\frac{h-h_{maxF2}}{B_{F2}}\right) \quad \textbf{(118)}$$

Then, the estimation of the total number of electrons is provided by the sum of each layer electronic content:

$$N(h) = N_E(h) + N_{F1}(h) + N_{F2}(h) \quad \textbf{(119)}$$

A complete description of this model is provided in [Garcia, 2002]. The future Galileo signals navigation messages will provide three parameters a_0, a_1, a_2 which are the coefficients of the effective ionisation level parameter [Radicella, 2003]. These parameters represent the maximum number of electrons in each layer between each satellite in view and the aircraft.

In the following figure, an estimation of the TEC, provided by the NeQuick model is represented as a function of the altitude. The TEC can be then converted into an ionospheric code delay as it is described in Chapter 2, taking into account, the emitted signal carrier frequency.

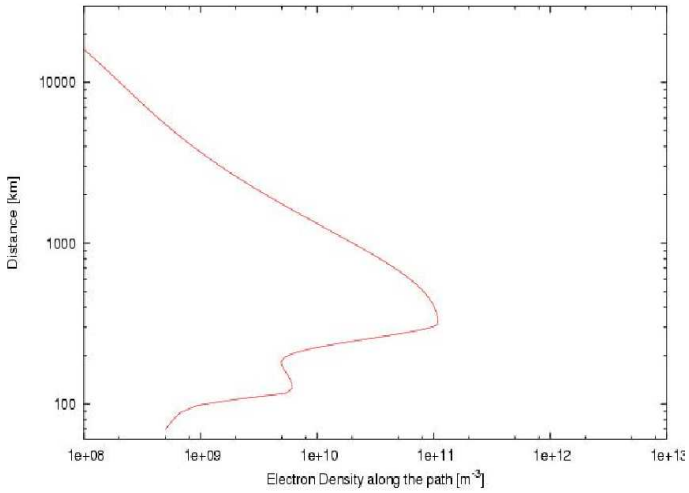

Figure 52: Variations of the electronic density estimated with the NeQuick model as a function of the altitude at the zenith of Toulouse (position: latitude: 43.56475924°N, longitude: 1.48171036°E, altitude: 203.845 m).

6.3.3. Advantages and drawbacks of the estimation models

The Klobuchar model provides a good estimate of the attributes of the actual ionospheric code delay, but in general, tends to underestimate the ionospheric delay as depicted in [NATS, 2003]. Indeed, this model has wide limitations for civil aviation applications. Indeed, this algorithm is only optimized for middle latitudes user aircraft locations. As a consequence, it does not represent properly the behavior of the ionosphere all over the world. It can only correct 50% of the global ionospheric code delay.

The NeQuick model will be the standard ionospheric model for single frequency Galileo receivers. However, even if the estimations provided by this model are better than for GPS model (80% of the global ionosphere error), for accuracy purposes, this one cannot be used in single frequency modes of operation for civil aviation as it is described in [NATS, 2004].

Both of the above models represent the standard single frequency ionospheric delay estimation algorithm for GPS and Galileo respectively. [Belabbas, 2005] compares the models by using two statistical figures: the mean and the variance of the residuals of the ionospheric code delay estimations. It shows the distribution of residual errors of Klobuchar and NeQuick models. Since the NeQuick model takes into account seasonal effects and is based on multiple layers TEC estimations, this one has a residual error distribution closer to a Gaussian distribution than Klobuchar residual error.

Furthermore, the presented models cannot represent the behavior of the ionosphere during important deviations from its average behavior (geomagnetic storms).

As a conclusion, neither the Klobuchar nor the NeQuick model represents the true ionospheric delay. As a consequence, these models cannot be used to support APV I operations as it is described in [NATS, 2003]. The following table summarizes the two models main characteristics.

	KLOBUCHAR MODEL	NEQUICK MODEL
Model type	Single layer model	Multiple layer model
Percentage of ionospheric error estimated over the world during one year	50% of the error estimated	80% of the error estimated
Constellation concerned	GPS	Galileo
Accuracy	Long term (> 1 year)	Seasonal (4 months)
Seasonal variations	No	Yes
Spatial variations	Medium	Good except near the Equator
Complexity	Simple cosine function: low complexity	Epstein formulation of different layers and seasonal variations, sunspots number: high complexity

Table 11: Comparison between Klobuchar and NeQuick models [Belabbas, 2005] and [NATS, 2003].

In the case of loss of one frequency, an estimation of the ionospheric delay can be provided by the Klobuchar model for GPS or the NeQuick one for Galileo. But, the use of these models implies the use of large σ_{UERE} values that do not allow supporting flight operations that require vertical protection levels computation. Another way to compute ionospheric code delay is the use of SBAS ionospheric grids but these one are not available everywhere as depicted in Figure 1.

In the following, the Code Minus Carrier (CMC) divergence technique is described. The advantage of this technique is that it does not need an ionospheric model but rather uses code and carrier phase measurements.

6.4. Single frequency Code Minus Carrier divergence technique to estimate ionospheric code delay

6.4.1. Method

After a loss of several frequencies leading to a single frequency degraded mode, resulting from a perturbation like an interference, a receiver may only be able to use code and carrier phase pseudoranges from only one carrier frequency. To estimate the ionospheric code delay, the difference between code and carrier phase measurements can provide good measurements. This is modelled as:

$$P_x - \phi_x = 2\,I_x - N_x\lambda_x + w_x + v_x \quad \textbf{(120)}$$

Where:

- P is the code pseudorange measurement in meters
- ϕ is the phase measurement in meters
- I is the ionospheric delay in meters
- N is the integer ambiguity
- λ is the carrier wavelength in meters
- w is the code multipath and noise error
- v is the phase multipath and noise error
- x denotes the used carrier frequency

6.4.2. Accuracy of the method

The difference between code delay and phase advance provides us twice the shift caused by the propagation of the electromagnetic waves through the ionosphere. The ionospheric delay can therefore be extracted from this difference assuming the ambiguity N is known and constant. This is the so-called code minus carrier divergence technique (CMC).

A comparison between single and dual frequency estimations of the ionospheric delay was made in [NATS, 2003] for a user located at Gatwick and Swanwick (UK). It appears that code carrier technique has a high level of performance in terms of accuracy. The resulting standard deviation for dual frequency estimations is compared to the resulting code carrier standard deviation and reported in the following table.

IONOSPHERIC ESTIMATION TECHNIQUE	GATWICK (UK)	SWANWICK (UK)
σ_{L1-L2_code}	0.93 m	0.65 m
$\sigma_{L1-L2\_carrier}$	0.41 m	0.33 m
$\sigma_{code\_carrier}$	0.39 m	0.38 m

Table 12: Comparison between dual and single frequency ionosphere estimation standard deviations at Gatwick and Swanwick (UK), [NATS, 2003].

In this study, only raw code and carrier phase measurements are used for simulations to estimate ionospheric code delay. This delay is extracted from code minus carrier, provided no cycle slip occurs.

6.4.3. Cycle slips

Carrier phase measurements are taken from the carrier phase lock loop. The capability of this loop to closely track the evolution of the GNSS signals carrier phase conditions the quality of the carrier phase measurements. Without external perturbations like dynamics of the receiver, multipath or interferences, this tracking loop is able to quickly follow the evolutions of the carrier phase when the elevation angle is above the mask angles.

However, in case of perturbations, the loop may lose lock from one instant to another for a certain time and then re-acquire the signal and lock around a new stability point of the carrier phase loop, as it is described in details in [Kaplan, 1996]. This phenomenon is called “cycle slip” or “phase slip”. In particular, cycle slips occur when the signal is blocked by an obstacle, when dynamics of the receiver are too high for the tracking loop to follow or during ionospheric scintillations.

A third order phase tracking loop is robust against many kinds of dynamics for instance for pedestrian or car applications when jerk values are not too high. For civil aviation operations, maximum dynamics values provided by [EUROCAE, 2007] must be taken into account. With normal aircraft manoeuvres, such a tracking loop is able to follow the signal carrier phase evolution as it is shown in chapter 5 and Appendix B.1.

A cycle slip produces a jump in carrier phase measurements that can be modelled like a sudden change in the ambiguity of the affected satellite signal phase. Consequently, this phenomenon may have a disastrous effect on carrier phase measurements and can lead to a loss of performance in terms of accuracy as well as in terms of integrity since it can generate large errors in carrier phase measurements, with a certain probability of occurrence.

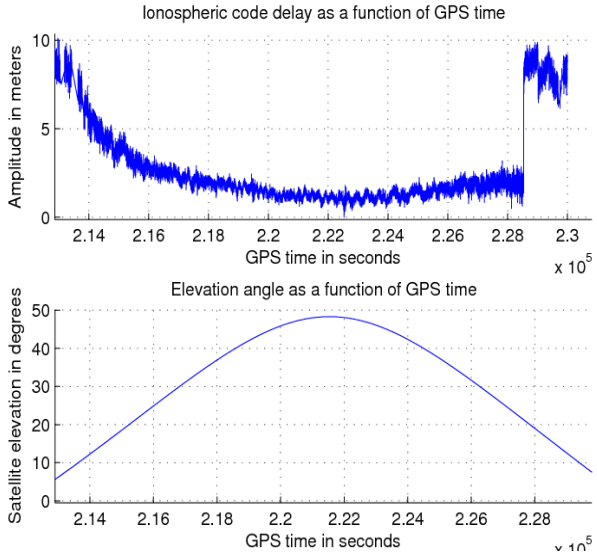

Figure 53: L1slant ionospheric delay estimated thanks to the CMC technique, for a receiver located at ENAC, Toulouse, France, on 14/03/2006. A cycle slip occurs for a low elevation angle of about 20 degrees, which may correspond to a multipath.

Figure 53 shows the estimation of ionospheric code delay using CMC estimation on L1 C/A. It can be noticed that a cycle slip occurs for a low elevation angle. It can also be noticed that the estimation is dependent upon the satellite elevation.

6.4.3.1. Cycle slip occurrence rate

The focus is given here on the estimation of the occurrence of cycle slips in the carrier phase measurements provided by the receiver. The probability of occurrence of a cycle slip during a given time period Δt is ([Holmes, 1990]):

$$P_{occ} = 1 - \exp\left(-\frac{\Delta t}{\overline{T}}\right) \quad \textbf{(121)}$$

Where $\overline{T}$ is the cycle slip mean time.

Therefore, the probability of having K cycle slips during Δt is:

$$P_{occ}(K, \Delta t) = \left(\frac{\Delta t}{\overline{T}}\right)^K \frac{\exp\left(-\frac{\Delta t}{\overline{T}}\right)}{K!} \quad \textbf{(122)}$$

The cycle slip mean time is calculated by using the following formula:

$$\overline{T} = \frac{\pi}{2 W_L \gamma} \tanh\left(\frac{2\pi\gamma}{\sigma_\phi^2}\right) \left[I_0^2\left(\frac{1}{\sigma_\phi^2}\right) + 2\sum_{n=1}^{\infty} (-1)^n \frac{I_n^2\left(\frac{1}{\sigma_\phi^2}\right)}{1 + \left(\frac{n\sigma_\phi^2}{\gamma}\right)^2} \right] \quad \textbf{(123)}$$

Where:

- I_n are Bessel functions of order n. See [Holmes, 1990] for a complete demonstration. γ represents the tracking error of the phase linked to the receiver dynamics (rad), correlated with the aircraft dynamics.
- W_L is the PLL one-sided loop bandwidth in Hz.
- σ_ϕ is the phase loop noise, its value depends on the type of loop employed:
  - For a Costas loop :

$$\sigma_\phi = \sqrt{\frac{W_L}{\frac{C}{N_0}} \left(1 + \frac{1}{2\frac{C}{N_0} T_I}\right)} \quad \textbf{(124)}$$

  - For a classical PLL,

$$\sigma_\phi = \sqrt{\frac{W_L}{\frac{C}{N_0}}} \quad \textbf{(125)}$$

Where:

- C/N_0 is the carrier to noise density ratio
- T_I is the coherent integration time
- W_L is the PLL one-sided loop bandwidth

We can note that σ_ϕ does not depend on the integration time for a classical PLL. According to [Holmes, 1990], the maximum value of γ (γ_{max}) depends on the maximum expected aircraft jerk $j_{\max}$ in g/s and the PLL one sided loop bandwidth in Hz. According to RTCA, 2006], for precision approach, the maximum expected jerk for normal manoeuvres is 0.25g/s and 0.74g/s for abnormal manoeuvres. The corresponding γ_{max}values are 2.7 and 7.9 degrees respectively for a 10 Hz PLL loop bandwidth.

The cycle slip rate is then defined as the inverse of the cycle slip mean time $\overline{T}$.

The probabilities of occurrence of cycle slips using a Costas loop and a classical PLL are compared hereafter. These probabilities are estimated for the GPS L1 C/A signal, with carrier to noise ratios respectively equal to 30 dB Hz and 40 dB Hz. The results are presented in Figure 55.

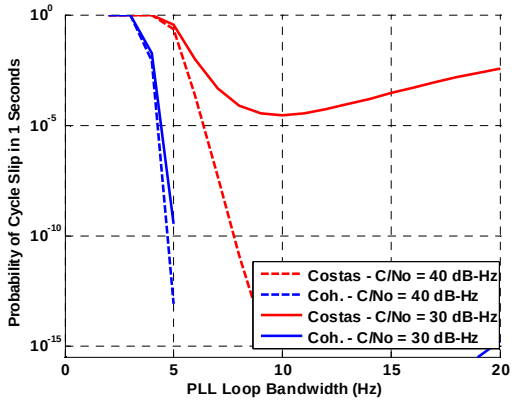

*Figure 54: Cycle slip occurrence probability using different phase tracking loops for maximum normal dynamics, calculated for 1 second, with a **20 ms integration time** for GPS L1 C/A, Coh stands for coherent and corresponds to a classical PLL.*

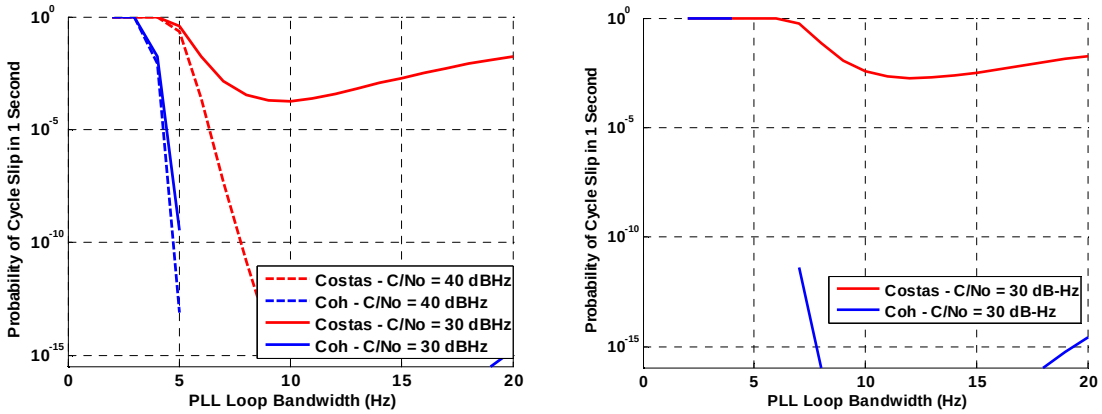

*Figure 55: Cycle slip occurrence probability using different phase tracking loops for maximum normal dynamics on the left side and abnormal aircraft dynamics on the right side, calculated for 1 second, with a **4 ms integration time** for GPS L1 C/A, Coh stands for coherent and corresponds to a classical PLL.*

Note that future Galileo E1, E5a and E5b will include both data and pilot (dataless) channels as it is described in chapter 2.

On the data channel, the presence of data is responsible of 180 degrees phase shifts during the tracking process. Costas loops are designed for data channel processing.

Concerning the pilot channel, no navigation data will modulate the incoming signal, a traditional PLL can hence be employed. In this case, the value of σ_ϕ will not vary as a function of integration time in the probability of occurrence computation.

Otherwise, it can be clearly seen that the optimal loop bandwidth is around 10 Hz for both normal and abnormal cases. This is the value chosen for simulations all along this thesis.

As it is mentioned in chapter 3, this thesis focuses on the APV I phase of flight. As a consequence, since a total approach mean time is 150 seconds ([RTCA, 2006]), the probability of occurrence is calculated for a whole approach time. The results are provided for each signal from maximum normal aircraft dynamics to maximum abnormal dynamics defined in [EUROCAE, 2007], through the jerk variation.

In Table 13, this probability of occurrence of cycle slip is calculated for different signals and integration times, for a Costas loop.

SIGNAL	T_I	PROBABILITY OF OCCURRENCE WITHIN 150 SECONDS	
		Normal manœuvres	Abnormal manoeuvres
GPS L1 C/A or Galileo E1	4 ms	$1.0\ 10^{-3}$	$9.2\ 10^{-2}$
	10 ms	$7.5\ 10^{-4}$	$6.1\ 10^{-2}$
	20 ms	$4.7\ 10^{-4}$	$3.8\ 10^{-2}$
GPS L5 or Galileo E5a	4 ms	$9.1\ 10^{-4}$	$9.0\ 10^{-2}$
	10 ms	$6.8\ 10^{-4}$	$6.0\ 10^{-3}$
	20 ms	$2.4\ 10^{-4}$	$3.4\ 10^{-2}$
Galileo E5b	4 ms	$9.1\ 10^{-4}$	$9.0\ 10^{-2}$
	10 ms	$6.9\ 10^{-4}$	$6.0\ 10^{-3}$
	20 ms	$2.4\ 10^{-4}$	$3.4\ 10^{-2}$

Table 13: Probability of cycle slip occurrence for a Costas PLL, with 10 Hz bandwidth and coherent integration time T_I.

As a conclusion, the probability of a cycle slip occurrence is not negligible for civil aviation purposes.

6.4.3.2. Cycle slip and integrity for APV

Integrity risks induced by cycle slips are integrity risks allocated to the manufacturer since cycle slips are due to the difficulty of the receiver to closely track the evolution of signals carrier phase with the phase tracking loop. The corresponding requirement in terms of integrity risk is 10^{-7}.

As it can clearly be seen in 6.4.3.1, cycle slip occurrence probability is low, even taking into account maximum normal aircraft dynamics. Therefore, to test detection algorithms capability (missed detection probability, false alarm rate), it is needed to have a large number of measurements. Only a few cycle slips can be experienced while using actual onboard GPS measurements. In addition, the amplitude of these cycle slips cannot be mastered. Another possibility may be to use actual measurements from data collection with a static receiver. But on one hand, these measurements do not match with actual aircraft conditions (and in particular with APV I conditions), as the dynamics are low, so the cycle slip probability is low. And, multipath components do not comply with aircraft approach conditions. On the other hand, the set of experienced cycle slips may not contain a good cycle slip amplitude range to test the detection algorithms capability. As a consequence, the best solution to test the next proposed algorithms is to generate pseudoranges and to generate cycle slips with known magnitudes.

The cycle slip occurrence probability can be estimated as it is described in 6.4.3.1. However, the probability of having a cycle slip over a given period of time with a given amplitude cannot be estimated since cycle slip amplitudes do not follow a well-known statistical law. As it is described in the next paragraphs, the approach for estimating the detection algorithms capability is first to determine a detection threshold compliant with the

false alarm rate imposed by the targeted phase of flight (APV I) for continuity requirement. Then, with regard to this threshold, the missed detection probability of the algorithms is determined. Finally, by multiplying this probability by the probability of occurrence of cycle slip, the resulting product probability can be compared to the integrity risk to know if the algorithms are compliant or not with ICAO integrity requirement for APV I. This is done for varying cycle slip amplitudes, and the minimum amplitude that allows reaching the integrity requirement is then recorded for each detection algorithm. This provides its capability to detect small cycle slips in compliance with continuity and integrity requirements for the targeted phase of flight.

6.4.3.3. Cycle slip detection methods

Different cycle slip detection methods can be proposed. One method consists in calculating the derivatives of carrier phase measurements. In theory, for high aircraft dynamics, and for detection threshold setting, a third order derivative of carrier phase is needed, which implies a heavy detection algorithm in term of calculation time cost.

Another method can consist in comparing raw and phase-smoothed code measurements (Hatch filter). The difference between raw and smoothed measurements is not expected to exceed a certain threshold which can be determined in compliance with continuity requirements for APV I. This technique has been tested and the results are discussed as a conclusion and it seems not to be the most promising technique.

A third technique is the monitoring of carrier phase measurements using Doppler predicted phase as described in next paragraph. This technique has a low complexity and is robust against high aircraft dynamics, which is of interest for civil aviation community. In addition, this technique seems to provide promising performances as it is described in the following.

The scope of this study is not to repair the impact of cycle slips on the measurements but to be able to detect it to comply with ICAO integrity requirements for APV I.

6.4.3.3.1. Cycle slip detection using Doppler measurements

This algorithm is based on a prediction of future phase measurements with Doppler measurements:

$$\widehat{\phi}(t) = \phi(t - \Delta t) + F_d(t - \Delta t).\Delta t \quad \textbf{(126)}$$

Where:

- F_d is the Doppler frequency
- Δt is the time delay between the previous and the current measurement
- ϕ is the carrier phase measurement (in meters)
- $\widehat{\phi}$ is the estimated carrier phase measurement (in meters)

Then the difference between phase measurements and predicted phase measurements is compared to a threshold which has to be fixed:

$$\left|\widehat{\phi}(t) - \phi(t)\right| > Threshold \quad \textbf{(127)}$$

The choice of a threshold is a function of false alarm probability with regards to APV phase of flight requirement and depends on the receiver dynamics.

6.4.3.4. Smallest detectable cycle slip

We launch simulations to determine the smallest detectable bias with the required P_{MD}, to determine the performance of some cycle slip detection algorithms.

Different magnitudes of cycle slips must be simulated, and we have to compute non-detection probability and to determine whether the obtained values are acceptable as a function of the magnitude of cycle slips.

6.4.3.4.1. Measurements simulator

Due to the low probability of cycle slipping, the number of actual available measurements is too low to assess the performances of our algorithms. As a consequence, the measurements are generated taking into account the aircraft dynamics:

$$P(t) = \rho_0 + v.t + 9.81\ a.\frac{t^2}{2} + 9.81\ j.\frac{t^3}{6} + c(\Delta t_u - \Delta t^i) + c\left(I_g{}^i + \tau^i\right) + D^i_{mult} + n^i \quad \textbf{(128)}$$

$$\phi(t) = \rho_0 + v.t + 9.81\ a.\frac{t^2}{2} + 9.81\ j.\frac{t^3}{6} + c\left(\Delta t_u - \Delta t^i\right) + c\left(I_p{}^i + \tau^i\right) + \Phi^i_{mult} + N^i\lambda^i + n^i \quad \textbf{(129)}$$

Where:

- ϕ is the phase measurement in meters
- P is the code pseudorange measurement in meters
- ρ_0 is a typical constant range (for instance 20200 km for GPS satellites and 23258 km for Galileo, but this distance depends on the satellites orbitography)
- v is the range rate, taken here to be 800 + 70 m/s (worst case range rate due to satellite and aircraft movement during an approach).
- a is the acceleration.
- j is the jerk.
- $c\left(\Delta t_u - \Delta t^i\right)$ is the clock bias generated as a function of the clock imperfections described in [Winkel, 2003].

6.4.3.4.1.1. Doppler

The Doppler measurements are generated as a first order derivative of the previously defined phase except that the additive noise is provided by Gaussian random values multiplied by a FLL sigma value defined in [Kaplan, 1996] instead of a PLL sigma value:

$$\sigma_{FLL} = \frac{1}{2\pi T_I}\sqrt{\frac{8\,W_L}{\frac{C}{N_0}}\left(1+\frac{1}{T_I\frac{C}{N_0}}\right)}\,(Hz) \qquad \textbf{(130)}$$

6.4.3.4.1.2. Clock bias

In a real world, GNSS relies on accurate time to provide accurate measurements to civil aviation users. However, the satellites and receiver oscillators are not perfect and the imperfections must be taken into account. Actually, the satellites and receiver times must be as close as possible to the reference time (i.e. GPS or Galileo time) or the offset to this reference must be evaluated.

As it is described in [Julien, 2005], the oscillator timing error is linked to the oscillator deviation from its original frequency. It is called the oscillator frequency noise. It can be modelled thanks to three main components which are a random walk, white frequency noise and Flicker as described in [Winkel, 2003]. These components are evaluated by Winkel and can be used to characterize five different types of oscillators: Quartz, TCXO (Temperature Compensated Crystal Oscillator), OCXO (Oven Controlled Crystal Oscillator), Rubidium and Caesium. The three components have different effects on the Allan variance of the oscillator as depicted in [Winkel, 2003]. The Allan variance represents half the root mean square of the timing error and is given by:

$$\sigma^2_{Allan}(\Delta t) = \frac{h_0}{2\,\Delta t} + 2.h_{-1} + \frac{2\pi^2}{3}\Delta t.h_{-2} \qquad \textbf{(131)}$$

The set of parameters h_0 (seconds), h_{-1}, and h_{-2} (Hz), determines the categories of oscillators. These parameters are provided in [Winkel, 2003] and their values are recalled in the following table:

	H_0 (SEC)	H_{-1}	H_{-2} (HZ)
Quartz	$2\ 10^{-19}$	$7\ 10^{-21}$	$2\ 10^{-20}$
TCXO	$\mathbf{10^{-21}}$	$\mathbf{10^{-20}}$	$\mathbf{2\ 10^{-20}}$
OCXO	$8\ 10^{-20}$	$2\ 10^{-21}$	$4\ 10^{-23}$
Rubidium	$2\ 10^{-20}$	$7\ 10^{-24}$	10^{-29}
Caesium	10^{-19}	10^{-25}	$2\ 10^{-23}$

Table 14: Oscillators characteristics, [Winkel, 2003].

Pseudoranges are simulated by using a TCXO for the generation of the clock error through differential equations as described in [Winkel, 2003].

6.4.3.4.1.3. Multipath

The multipath error for code measurements is generated by drawing successive independent Gaussian random values with a standard deviation corresponding to the worst case value at 5° elevation (for Galileo, this value of mask angle is 10 degrees), so our choice for simulations corresponds to a worst case for both GPS and Galileo constellations using [SARPs, 2006] formula:

$$\sigma_{\text{multipath}} = 0.13 + 0.53 \exp\left(-\frac{E}{10}\right) \text{(m)} \quad \textbf{(132)}$$

Where: E is the elevation angle of the considered satellite in view (deg).

The maximum carrier phase multipath error due to one reflected signal does not exceed one quarter of a carrier cycle. Indeed, the quarter wavelength corresponds to the phase tracking error due to a $\frac{\pi}{2}$ reflected path, if we suppose there is only one signal replica with a magnitude of 1. The corresponding chosen sigma value is set to this maximum of a quarter wavelength.

6.4.3.4.1.4. Troposphere

The troposphere effect is generated by drawing successive independent Gaussian random values with standard deviations obtained thanks to the model defined in [RTCA, 2006]:

$$\sigma_{\text{troposphere}} = \frac{0.12 * 0.001}{\sqrt{0.002001 + \sin(E)^2}} \text{(m)} \quad \textbf{(133)}$$

with an elevation angle E of 5 degrees (assuming a minimum mask angle for a GPS satellite orbitography).

6.4.3.4.1.5. Ionosphere

The ionosphere impact is generated by drawing successive independent Gaussian random values. The ionospheric code delay is generated by using a standard deviation value of 0.83 meter. The standard deviation value on carrier phase measurements is set to 0.23 meter to comply with the values obtained in [Shau-Shiun Jan, 2003].

6.4.3.4.1.6. Noise

The noise is generated by drawing successive independant Gaussian values with the standard deviation of the tracking error due to noise (PLL and DLL), defined in [Julien, 2004].

6.4.3.4.2. Estimation of the smallest detectable cycle slip with the proposed detection algorithm

The methodology used to determine the smallest detectable bias with the proposed detection algorithm can be summarized in a few steps:

1. The pseudoranges and Doppler measurements are generated without cycle slips. The detection criterion is compared to varying thresholds. For each threshold, the false alarm rate of the algorithm is recorded. When the false alarm rate imposed for APV I is reached, the corresponding threshold is kept in memory as the detection threshold.

2. Then, the pseudoranges and Doppler measurements are generated again with varying cycle slip amplitudes. The missed detection probability is estimated for each cycle slip amplitude.

3. The integrity risk due to cycle slip can be expressed as the product of the algorithm missed detection probability by the cycle slip probability of occurrence. A theoretical missed detection probability is estimated by dividing the integrity risk by the obtained cycle slip probabilities. The integration time is set to 4 ms to take into account a pilot channel (dataless). The P_{MD} is estimated for maximum normal and abnormal aircraft dynamics. Indeed, the maximum cycle slip occurrence rate is bounded to 10^{-3} for normal aircraft dynamics and 10^{-1} for abnormal aircraft dynamics. The integrity risk is not only allocated to cycle slips, this risk is due to manufacturing[5] as seems to indicate [RTCA, 2006]. The integrity risk is chosen equal to 10^{-8} (lower than the actual value since this part of the integrity tree is not only allocated to cycle slips). Therefore, the required missed detection probabilities for integrity compliance are respectively 10^{-5} for the normal manoeuvre case and 10^{-6} for the abnormal manoeuvre case.

4. The experienced missed detection probabilities are compared to the theoretically derived ones for normal (10^{-5}) and abnormal dynamics (10^{-6}). Once the experienced missed detection probability is lower than the theoretical P_{MD} value, the cycle slip amplitude corresponding to the obtained P_{MD} is then recorded as the minimum detectable bias.

Figure 56 shows the obtained P_{FA} as a function of the generated cycle slip amplitude in meters.

[5] Note that this risk can be viewed as a SIS integrity risk ($2*10^{-7}$), but these results were proposed to the EUROCAE WG 62 which decided to consider this risk as a manufacturer one.

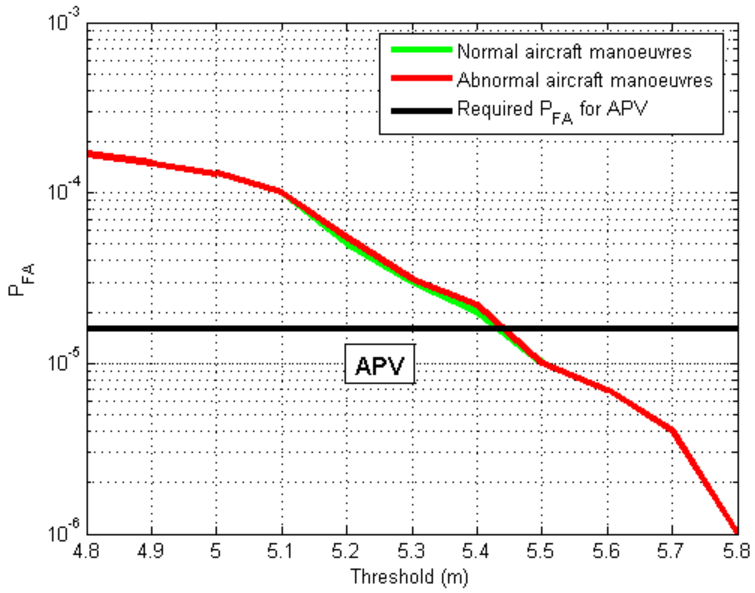

*Figure 56: Probability of False Alarm obtained through simulations as a function of detection thresholds for both **maximum** normal and abnormal manoeuvres (step 1).*

The previous figure is obtained by simulating varying detection thresholds. The false alarm rate values are recorded and compared to the required P_{FA} from the APV I continuity requirements (step 1). In this simulation, no cycle slip is generated to obtain the false alarm rates. In this figure, it can be noticed that the threshold is between 5.4 and 5.5 meters for both the maximum normal and abnormal aircraft dynamics.

For APV I, the maximum integrity risk equals 10^{-7} per approach. As the integrity risk is not only allocated to cycle slips, we choose to overbound the required probability of missed detection of the cycle slip detection algorithm with a value of 10^{-5} for normal manoeuvres and 10^{-6} for the abnormal case.

Indeed, since the maximum cycle slip probability of occurrence is 10^{-3} for normal dynamics, the corresponding integrity risk allocated to cycle slips is $10^{-5} * 10^{-3} = 10^{-8} < 10^{-7}$. For the abnormal case, the integrity risk is supposed allocated to cycle slips only. The risk must be weighted by the probability to have abnormal manoeuvres. In this case, the maximum probability of occurrence is 10^{-1}, the integrity risk is consequently $10^{-1} * 10^{-6} = 10^{-7}$.

Now we have to determine the smallest detectable cycle slip with this required P_{MD}. These values are represented respectively in green and red in the following figure.

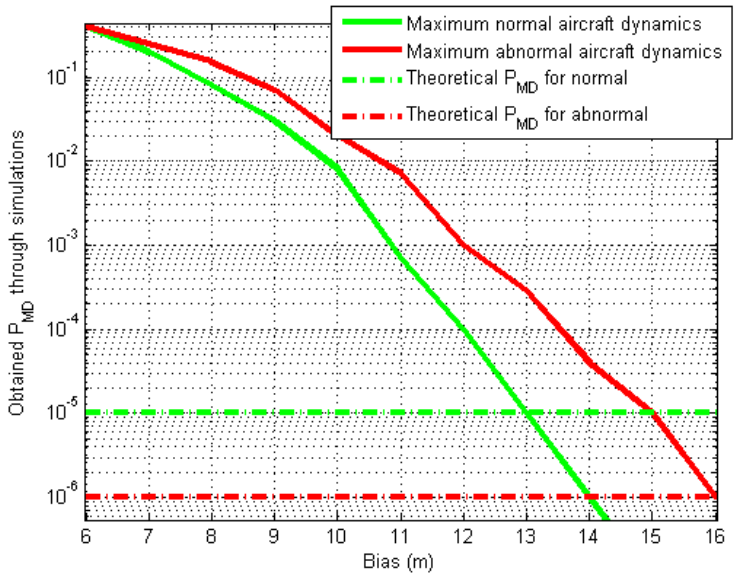

Figure 57: Probability of Missed Detection of the cycle slip detection algorithm with regards to integrity requirements for APV, obtained by simulating different cycle slip amplitudes (bias), the P_{MD} are recorded for each cycle slip amplitude and compared to theoretical P_{MD} values for both normal and abnormal aircraft manoeuvres (step 2).

As it can be seen in Figure 57, the smallest detectable cycle slip with Doppler-based detection algorithm, has an amplitude of 13 meters for normal dynamics and 16 meters for abnormal manoeuvres, choosing a maximum jerk for these two cases.

It is understood that the normal (resp. abnormal) aircraft manoeuvres correspond to the maximum dynamics values defined in [EUROCAE, 2007] or [RTCA, 2006]. As a consequence, the results obtained allow protecting the user against all kinds of aircraft dynamics.

The tests to determine the minimum detectable bias were made using 10^5 samples.

It is important to notice that for simulations, assumptions on pseudoranges take into account the worst case values. More precisely, multipaths are generated by assuming the corresponding satellite in view has the lowest elevation angle (equal to the mask angle), ionosphere and troposphere errors are generated by multiplying theoretical maximum standard deviation values by successive independent Gaussian random values rather than taking into account the actual correlation of this error along a satellite course for instance. Indeed, the generated values are not used for accurate estimation of ionosphere error, but for cycle slip detection over a sufficient number of tests.

These smallest detectable cycle slips imply a bias on position error depending on geometry. Since integrity requirements are expressed in the position domain, we need to switch from the pseudorange domain to the position domain. The availability of protection against cycle slip compatible with APV depends on geometry and must be computed at every second. This is described in the next paragraph.

6.4.3.4.3. Cycle slip detection availability calculation

Tests are made over Europe for both GPS and Galileo constellations, considering the worst-positioned satellites.

As it is described in details in [Macabiau2, 2005], the assumption is that the receiver makes n pseudorange measurements collected in a vector noted Y. The measurement vector Y and the state vector X composed of positions coordinates and clock bias are related by:

$$\mathrm{Y} = \mathrm{g}(\mathrm{X}) + \mathrm{E} \quad \textbf{(134)}$$

E is the measurement error, due to multipath, noise, possible cycle slips, atmospheric effects and satellite clock residuals. $X = [x \quad y \quad z \quad b]^T$ is composed of positions coordinates (x, y and z) and clock bias b.

Let us describe the least squares navigation solution.
If $\hat{X}_0$ is an initial estimate of X , then X can be noted:

$$\mathrm{X} = \widehat{\mathrm{X}_0} + \Delta\mathrm{X} \quad \textbf{(135)}$$

The measurement model can be rewritten as:

$$\mathrm{Y} = \mathrm{g}\left(\widehat{\mathrm{X}_0} + \Delta\mathrm{X}\right) + \mathrm{E} \quad \textbf{(136)}$$

This expression may be linearized around $\hat{X}_0$, the estimate of X :

$$\mathrm{Y} = \mathrm{g}\left(\widehat{\mathrm{X}_0}\right) + \frac{\partial \mathrm{g}}{\partial \mathrm{X}}\left(\widehat{\mathrm{X}_0}\right)\Delta\mathrm{X} \; + \mathrm{E} \quad \textbf{(137)}$$

Where:

$$\frac{\partial \mathrm{g}}{\partial \mathrm{X}}\left(\widehat{\mathrm{X}_0}\right) = \mathrm{G} = \begin{bmatrix} \frac{\partial \mathrm{g}^1}{\partial \mathrm{x}}\left(\widehat{\mathrm{X}_0}\right) & \frac{\partial \mathrm{g}^1}{\partial \mathrm{y}}\left(\widehat{\mathrm{X}_0}\right) & \frac{\partial \mathrm{g}^1}{\partial \mathrm{z}}\left(\widehat{\mathrm{X}_0}\right) & \frac{\partial \mathrm{g}^1}{\partial \mathrm{b}}\left(\widehat{\mathrm{X}_0}\right) \\ \vdots & \vdots & \vdots & \vdots \\ \frac{\partial \mathrm{g}^\mathrm{n}}{\partial \mathrm{x}}\left(\widehat{\mathrm{X}_0}\right) & \frac{\partial \mathrm{g}^\mathrm{n}}{\partial \mathrm{y}}\left(\widehat{\mathrm{X}_0}\right) & \frac{\partial \mathrm{g}^\mathrm{n}}{\partial \mathrm{z}}\left(\widehat{\mathrm{X}_0}\right) & \frac{\partial \mathrm{g}^\mathrm{n}}{\partial \mathrm{b}}\left(\widehat{\mathrm{X}_0}\right) \end{bmatrix} \quad \textbf{(138)}$$

The linearized model can then be rewritten as:

$$\mathrm{Y} - \mathrm{g}\left(\widehat{\mathrm{X}_0}\right) = \mathrm{G}\,\Delta\mathrm{X} \; + \mathrm{E} \quad \textbf{(139)}$$

$$\Delta\mathrm{Y} = \mathrm{G}\,\Delta\mathrm{X} \; + \mathrm{E} \quad \textbf{(140)}$$

$$\Delta\mathrm{Y} = \mathrm{Y} - \mathrm{g}\left(\widehat{\mathrm{X}_0}\right) \quad \textbf{(141)}$$

is the deviation between measurements and noiseless predicted measurements if position and clock delay were $\hat{X}_0$.

From this linear relationship between ΔY and ΔX, we deduce the least squares estimate of ΔX :

$$\Delta\widehat{\mathrm{X}} = [\mathrm{G}^{\mathrm{T}}\mathrm{G}]^{-1}\mathrm{G}^{\mathrm{T}}\,\Delta\mathrm{Y} \quad \textbf{(142)}$$

And

$$\widehat{\mathrm{X}} = \widehat{\mathrm{X}_0} + \Delta\widehat{\mathrm{X}} \quad \textbf{(143)}$$

The residual ΔY considering $\hat{X}$ may be expressed as:

$$\Delta\mathrm{Y} = \mathrm{Y} - \mathrm{g}(\widehat{\mathrm{X}}) = \mathrm{g}(\mathrm{X}) - \mathrm{g}(\widehat{\mathrm{X}}) + \mathrm{E} \quad \textbf{(144)}$$

$$\Delta\mathrm{Y} = \mathrm{g}(\widehat{\mathrm{X}_0} + \Delta\mathrm{X}) - \mathrm{g}(\widehat{\mathrm{X}_0} + \Delta\widehat{\mathrm{X}}) + \mathrm{E} \quad \textbf{(145)}$$

As described in [Macabiau2, 2005], the previous expression is linearized:

$$\mathrm{Y} - \mathrm{g}(\widehat{\mathrm{X}}) \approx \mathrm{G}\Delta\mathrm{X} - \mathrm{G}\Delta\widehat{\mathrm{X}} + \mathrm{E} = \mathrm{G}(\Delta\mathrm{X} - \Delta\widehat{\mathrm{X}}) + \mathrm{E} \quad \textbf{(146)}$$

However,

$$\Delta\widehat{\mathrm{X}} = [\mathrm{G}^{\mathrm{T}}\mathrm{G}]^{-1}\mathrm{G}^{\mathrm{T}}\left[\mathrm{Y} - \mathrm{g}(\widehat{\mathrm{X}_0})\right] \quad \textbf{(147)}$$

Therefore:

$$\Delta\widehat{\mathrm{X}} = [\mathrm{G}^{\mathrm{T}}\mathrm{G}]^{-1}\mathrm{G}^{\mathrm{T}}[\mathrm{G}\Delta\mathrm{X} + \mathrm{E}] \quad \textbf{(148)}$$

Which is equivalent to:

$$\Delta\widehat{\mathrm{X}} = \Delta\mathrm{X} + [\mathrm{G}^{\mathrm{T}}\mathrm{G}]^{-1}\mathrm{G}^{\mathrm{T}}\mathrm{E} \quad \textbf{(149)}$$

$$\Delta\widehat{\mathrm{X}} - \Delta\mathrm{X} = [\mathrm{G}^{\mathrm{T}}\mathrm{G}]^{-1}\mathrm{G}^{\mathrm{T}}\mathrm{E} \quad \textbf{(150)}$$

If the pseudo inverse matrix is denoted:

$$\mathrm{A} = [\mathrm{G}^{\mathrm{T}}\mathrm{G}]^{-1}\mathrm{G}^{\mathrm{T}} \quad \textbf{(151)}$$

Then:

$$-\Delta\mathrm{X} + \Delta\widehat{\mathrm{X}} = \mathrm{AE} \quad \textbf{(152)}$$

The difference between X and its estimate is thus described as a function of the measurement error E.

The horizontal and vertical projections factors of the previous relation are estimated by using the following equations:

$$\begin{cases} H(i) = \sqrt{A_{1i}^2 + A_{2i}^2} \\ H_{max} = \max_i(H(i)) \end{cases} \quad \textbf{(153)}$$

$$\begin{cases} V(i) = A_{3i} \\ V_{max} = \max_i(V(i)) \end{cases} \quad \textbf{(154)}$$

for $i = 1 \ldots n$. where n is the number of raws of the matrix A.

The relationship between the aircraft position error and the measurement error can be drawn horizontally and vertically thanks to the following figure. The minimum detectable bias due to cycle slips can be then projected on the horizontal plane and on the vertical axis to compare the impact of the bias induced by cycle slip detection capability in the position domain to the alert limits imposed for the APV I phase of flight (table 1).

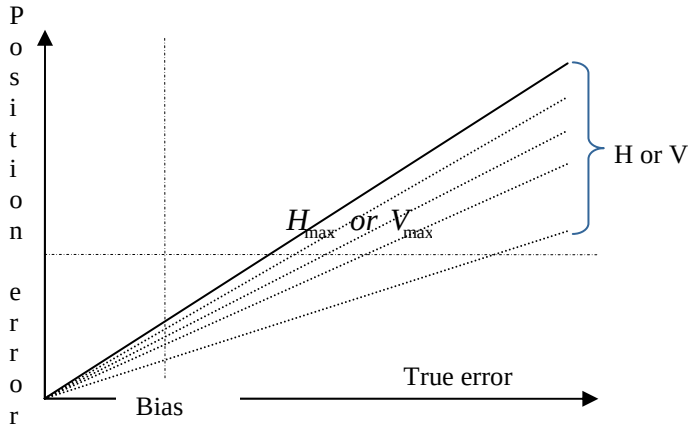

Figure 58: Computed position error for all satellites in view.

As we can see in Figure 58, the more important the geometrical factor is, the higher the position error. The maximum geometrical factor is considered in the following so as to study the worst satellite position case.

The horizontal impact of the undetected bias induced by a cycle slip is thus modelled by:

$$H_{impact} = H_{max} \cdot bias \quad \textbf{(155)}$$

A similar relationship can be used to define the vertical one:

$$V_{impact} = V_{max} \cdot bias \quad \textbf{(156)}$$

$H_{\max}$ and $V_{\max}$ are the horizontal and vertical projection factors that induce the maximum position errors in horizontal and vertical planes respectively, considering all the satellites in view.

$H_{\max}$ ($V_{\max}$) is the horizontal (vertical) value of the position error induced by the largest undetectable cycle slip on the worst case satellite.

When the computed impacts (H_{impact}, V_{impact}) are above alert limits (horizontally and vertically), the CMC + detection algorithm is declared unavailable. When these impacts are under or equal to alert limits, it is declared available.

The code minus carrier divergence (CMC) technique alone does not satisfy integrity requirements for the APV I phase of flight. Indeed, carrier phase measurements can be affected by cycle slips with a certain probability of occurrence. As a consequence, the cycle slip detection algorithm is required. The availability of this algorithm (and therefore the availability of the CMC measurements to estimate the ionospheric delay to correct the pseudorange measurements and finally to calculate the protection levels) is evaluated in the following paragraphs.

6.4.3.4.4. Maps of availability of cycle slip detection algorithm for GPS and Galileo constellations

The following maps are drawn for the APV I phase of flight. The availability maps of detection algorithms over Europe for normal maximum dynamics are drawn. Simulations are made over 24 hours for GPS and over 10 days for Galileo. These plots show that using GPS or Galileo constellations in standalone mode, the availability of cycle slip Fault Detection (FD) function is not sufficient for normal aircraft dynamics when using only detection based on Doppler measurements. It is also consequently the case for abnormal dynamics, but during abnormal manoeuvres, the accuracy of the measurements is not required as it is specified in [RTCA, 2006].

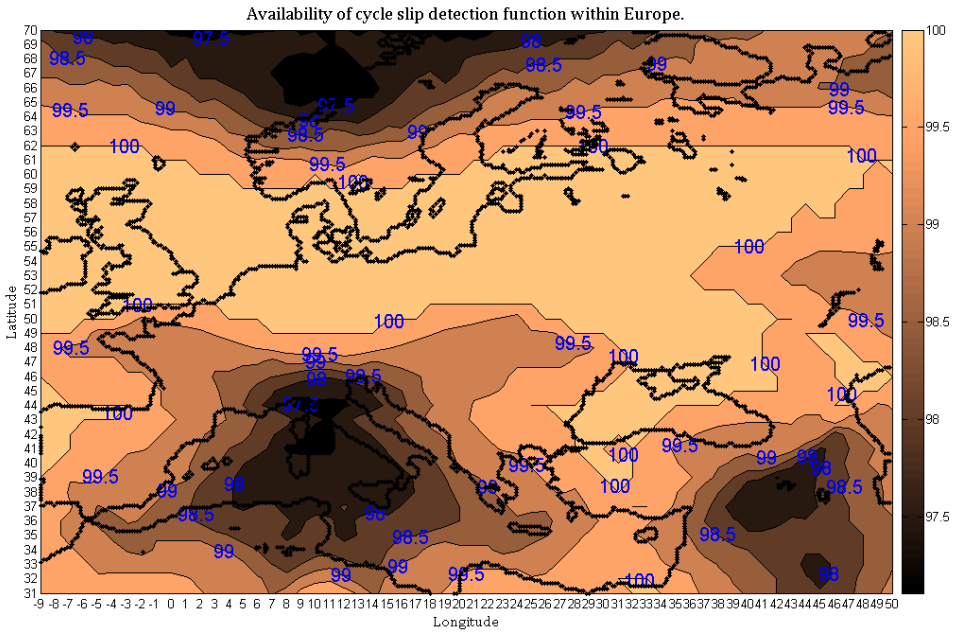

Figure 59: Availability of proposed cycle slip detection algorithm over Europe considering GPS constellation only and normal aircraft dynamics, for APV 1 alert limits.

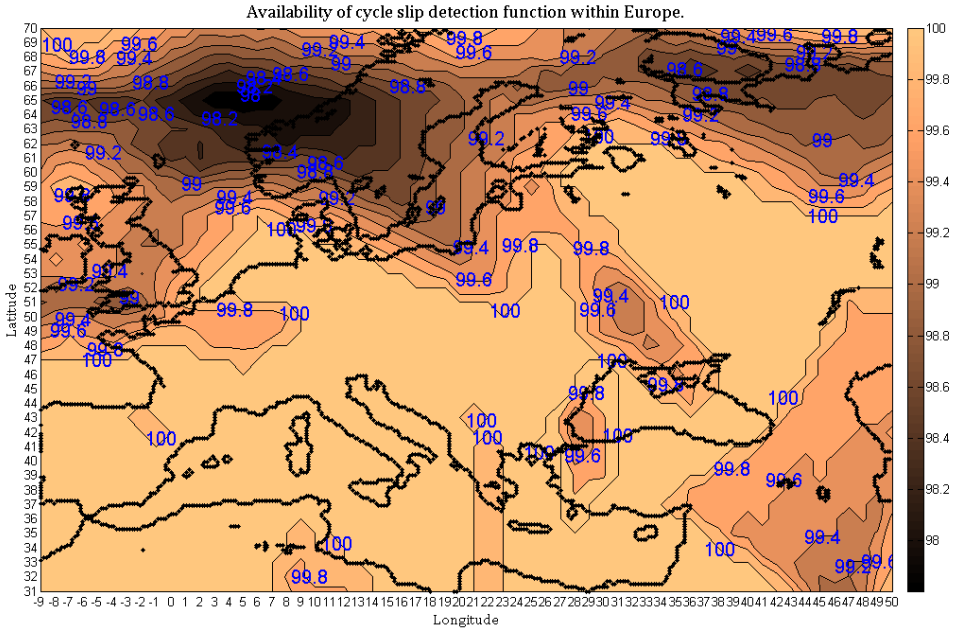

Figure 60: Availability of proposed cycle slip detection algorithm over Europe considering Galileo constellation only and normal aircraft dynamics for APV 1 alert limits.

As it can be seen in Figure 59, for GPS, a maximum value of 100% availability is reached but only in Northern Europe. The minimum value obtained is 97.1%. The mean value is 99.5%. This means that single frequency GPS measurements corrected from ionospheric delay through CMC technique plus cycle slip detection cannot be used in standalone mode, as the minimum required continuity value during APV I phase of flight is 99.99%.

As seen in Figure 60, for the Galileo constellation, assuming normal dynamics, the results obtained show that availability is sufficient over a large part of Europe but not enough over Norway for instance. The minimum availability is 97.8%, the mean value is 99.63% and the maximum is 100%.

Note that, this lack of availability for GPS and Galileo single frequency ionospheric correction plus cycle slip detection is mainly due to the largest impact of the bias on the vertical axis. This is due to the fact that the geometrical factor $(G^T G)^{-1} G^T$ is larger on the vertical axis than on the horizontal plane.

Recall that the bias included in the availability computation is calculated for the higher value of dynamics. That is to say, the availability is calculated for maximum jerks and accelerations of an aircraft in a normal dynamics case. We thus considered the least favourable case for each calculation of availability.

The availability of this detection algorithm is not so low for each constellation. Indeed, the risk induced by cycle slips affecting single frequency ionospheric delay estimate must be weighted by the unavailability of dual frequency ionospheric code delay estimation. More precisely, it must be weighted by the probability of falling into single frequency mode (degraded), for instance, after a RFI area crossing, as described in equations written in Appendix A.4.

6.5. Ionospheric delay estimation using Kalman filter on CMC observables

6.5.1. Filter settings and characteristics

As proposed in [Euler, 1991], a classical Kalman filter is used in order to evaluate the ionospheric code delay and to follow the evolution of ambiguities of all satellites in view. The observation and state propagation models are described in the following. The acquisition and loss of each satellite are taken into account in the estimation algorithm by updating the states according to the different satellites in view. When a cycle slip occurs, the ambiguity on the corresponding phase measurement is affected by a jump.

The ambiguity of each satellite carrier phase measurement of a same constellation is estimated thanks to the filter and is taken into account in the state vector. Each ambiguity is not expected to vary along each corresponding satellite course.

As a consequence, the state vector is defined in the following:

$$X = (I_0 \quad N_1 \quad \dots \quad N_n)^T \qquad \textbf{(157)}$$

The filter is initialized thanks to dual frequency ionospheric delay estimation. Indeed, in reality, the filter will not have to run before loss of frequency, only dual frequency ionospheric delay estimation must be kept in memory, for each satellite in view. In case of

loss of frequency, this value is then used to initialize the states of the Kalman filter. Each state is thus initialized as described in the following.

I_0 is the ionospheric delay at the Ionospheric Pierce Point (IPP), it is calculated as:

$$I_0 = \frac{\sum_{k=1}^{Nb\_sat} \frac{I_k}{Ob_k}}{Nb\_sat} \quad \textbf{(158)}$$

Where:

- Nb_sat is the number of satellites in view
- Ob_k is the obliquity factor corresponding to the k[th] satellite in view
- I_k is the slant ionospheric estimation provided by the CMC technique and considering the k[th] satellite in view

The ionospheric delay (I) at the zenith of the aircraft antenna can be then deduced by removing the ionospheric delay variations modeled by spatial gradients (A, B) around the IPP location, from the ionospheric delay (I_0) obtained at the IPP. As it is modelled in [Lestarquit, 1997], the ionospheric delay is:

$$I = I_0 - A * \Delta lat - B * \Delta lon \quad \textbf{(159)}$$

Where:

- Δlat (in degrees) is the coordinate of the subionospheric IPP along an axis that points to the North direction
- A is the linear gradient constant along the South-North axis
- Δlon (in dergrees) is the coordinate of the subionospheric IPP along an axis that points to the East direction
- B is the linear gradient constant along the West-East axis

In order to test the ionospheric code delay estimation algorithm performances, the spatial gradients A and B can be set to 0 as it is mentioned in [Lestarquit, 1997]. In that way, we consider only a uniform ionospheric model.

N_1 … N_n are the carrier phase measurements ambiguities of all the acquired n satellites in view.

The initial ambiguity for each satellite in view is derived from the difference between dual frequency and single frequency code minus carrier estimations. The mean of this difference over the first measurements is used as initial value for each satellite in view.

The obliquity factor, which is a ratio between slant and vertical electronic content at an ionospheric pierce point, depends upon the transmitting satellite elevation. It is a function of elevation of each considered satellite in view [RTCA, 2006]:

$$\mathrm{Ob} = \left[1 - \left(\frac{\mathrm{R_e}}{\mathrm{R_e} + \mathrm{h}}\cos(\mathrm{E})\right)^2\right]^{-\frac{1}{2}} \quad \textbf{(160)}$$

Where: R_e is the Earth equatorial radius, h the altitude of the ionospheric pierce point (350 km) and E the elevation angle at the ionospheric pierce point (thin shell model) as it is described in chapter 2.

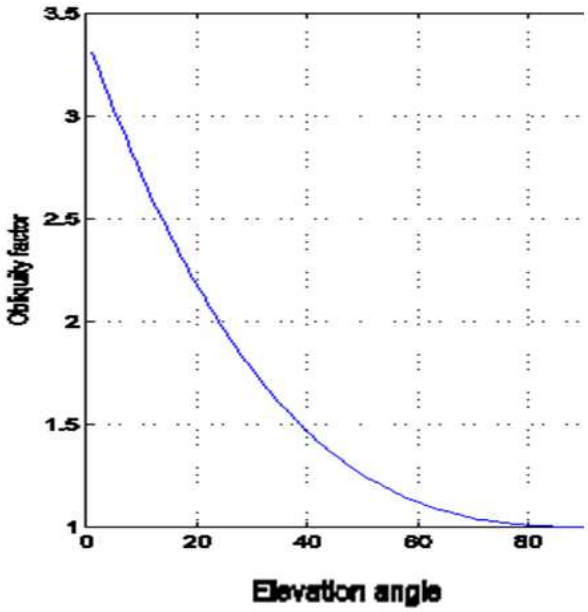

Figure 61: Obliquity factor as a function of the elevation in degrees

Here, for a position of a space vehicle at the zenith of the IPP, the obliquity factor equals 1, its values are 3 for GPS mask angle (5 degrees) and 2.7 for Galileo mask angle (10 degrees).

The Kalman filter provides real time estimation of the ionospheric delay thanks to measurements from all satellites in view and of ambiguities for these satellites for the same frequency. The relationship between observation vector Y and state vector X at the instant t is assumed to be:

$$\mathrm{Y_t} = \mathrm{H_t X_t} + \mathrm{V_t} \quad \textbf{(161)}$$

Where:

- Y_t is the observation vector, composed of the difference between code and carrier phase measurements for all satellites in view. Note that the obliquity factor is multiplied by two in the algorithm for the construction of the matrix H so as to obtain two times the ionospheric code delay for each satellite. The measurements used are the raw code and carrier phase measurements, the code measurements are not smoothed.
- V_t is the observation noise
- H_t is the observation matrix

$$H_t = \begin{pmatrix} Ob'_1 & 1 & \dots & 0 \\ \vdots & \vdots & \ddots & \vdots \\ Ob'_{Nb\_sat} & 0 & \dots & 1 \end{pmatrix} \quad \textbf{(162)}$$

Where :

$$Ob'_i = 2 * Ob_i, i = 1, \dots, Nb\_sat$$

The local model states are considered constant between measurements periods, except the ionospheric delay that is affected by the West-East gradient [Lestarquit, 2007]. Nevertheless, we consider that the parameter B (linear gradient constant along the West-East axis) is equal to zero in the model.

The covariances are propagated according to the Kalman equations.

An extensive study of the state noise covariance values has already been performed in [Lestarquit, 1997]. In this study, the same values are used and recalled in the following.

W is the state noise process. It is used here to model random fluctuations in linear prediction model imperfections. The covariance matrix of W is Q:

$$Q = \begin{pmatrix} \left(\frac{5\Delta t}{3600}\right)^2 & 0 & \dots & 0 \\ 0 & 10^{-4} & \dots & 0 \\ \vdots & \vdots & \ddots & \vdots \\ 0 & 0 & \dots & 10^{-4} \end{pmatrix} \quad \textbf{(163)}$$

Q_{11} is in m². Note that the covariance matrix assumes correlation time of ionospheric which corresponds to the nominal behaviour of the ionosphere, in case of ionospheric scintillations, this model must not be applied.

The covariance matrix of the measurement noise V is:

$$R = 3.5^2 \begin{pmatrix} \left(\frac{Ob_1}{\Delta t}\right)^2 & \dots & 0 \\ \vdots & \ddots & \vdots \\ 0 & \dots & \left(\frac{Ob_{Nb\_sat}}{\Delta t}\right)^2 \end{pmatrix} \quad \textbf{(164)}$$

Where Δt is the measurement interval, 3.5 is a multiplicative empirical term used in [Lestarquit, 1997]. The measurement rate is one second. When the receiver loses track of one satellite signal, its corresponding state in the state vector of the Kalman filter is suppressed, its ambiguity is not kept in memory.

As proposed, the code minus carrier calculation is based on raw measurements and thus, the remaining noise and multipath components still affect the measurements. It is consequently of interest to discuss the sensitivity of the filter to multipath. During calculation of raw code minus carrier, multipath effects on both code and carrier phase measurements are accumulated as these effects are not the same on code and on carrier

phase. It must be noticed that the multipath and noise on the carrier phase measurements are lower than on the code measurements. As a consequence, the multipath and noise on code measurements dominate the resulting errors in the CMC estimations. However, as this study focuses on APV phases of flight, the multipath are not strong and their impact on the filter is not expected to be significant.

6.5.2. Receiver ionospheric error estimation

6.5.2.1. Validation with actual measurements: GPS L1 C/A

Code and carrier phase measurements on GPS L1 and L2 signals were collected during a flight around Toulouse-Blagnac airport (France), which path is drawn in the following figures.

Figure 62: Aircraft path, data collected from Airbus campaign, zoom on the Blagnac Airport (Toulouse, France), ©Airbus.

Figure 63: Aircraft path, data collected from Airbus campaign around Blagnac Airport (Toulouse, France), ©Airbus.

Dual frequency measurements were collected during these flights around Blagnac airport (France), on both GPS L1 C/A and L2. The objectives of having such measurements are multiple. First, it is convenient to test the algorithm on real measurements during aircraft flight to experience aircraft approaches with actual conditions. Indeed, aircraft dynamics and multipaths allow testing the filter robustness against these types of perturbations during APV and even during other phases of flight. Secondly, even if the goal is to estimate single frequency ionospheric delay, a dual frequency basis is necessary to compare the performances of the estimation algorithm. As a consequence, dual frequency measurements are needed. Nevertheless, these measurements are carried out on L1/L2. The dual frequency measurements in nominal modes will be on L1/L5 for GPS and E1/E5a or E1/E5b for Galileo. Since L5 is still not available at the time of the data collection, this study will be based on L1/L2 frequency measurements. Pegasus software (Eurocontrol) is used to process the collected data.

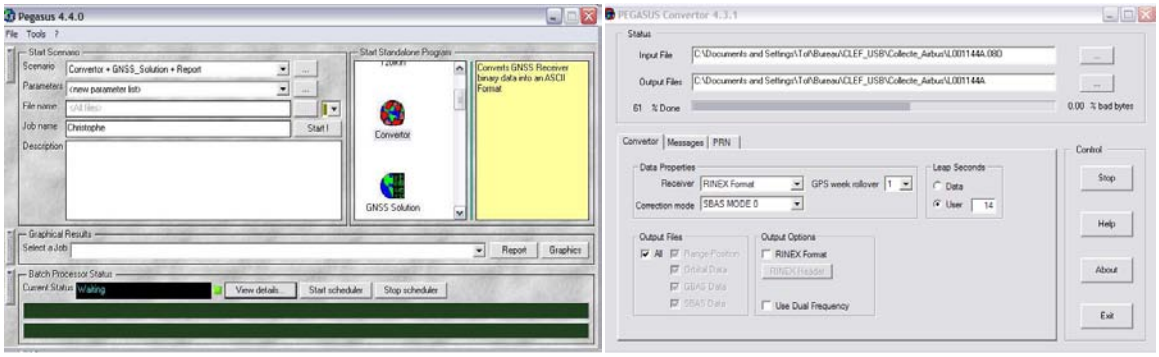

Figure 64: Eurocontrol Pegasus Software

Dual and single frequency ionospheric delays are calculated for all satellites in view over the data file. The scenario presented here is the loss of GPS L2 leading to single GPS L1 C/A frequency mode.

The Airbus collect was made during 2h20, the measurements available are provided each 0.2 second. In the following, all figures are plotted as a function of the number of samples, where 5 samples are available each second. The total number of time samples is 42000.

Note that the number of satellites tracked varies along time as it is presented in next paragraph.

The minimum number of satellites tracked equals 7 for short periods of time that can be identified in Figure 65. This graph allows identifying the onset or the loss of satellites from the receiver point of view.

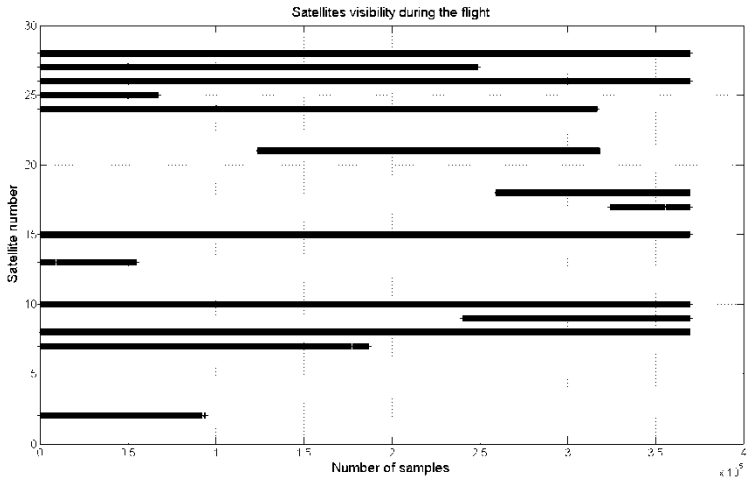

Figure 65: Number of satellites tracked as a function of time samples

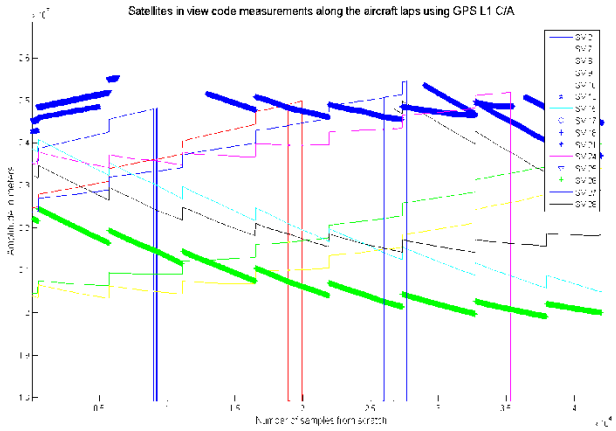

Figure 66: GPS L1 C/A code measurements for all tracked satellites over the entire file

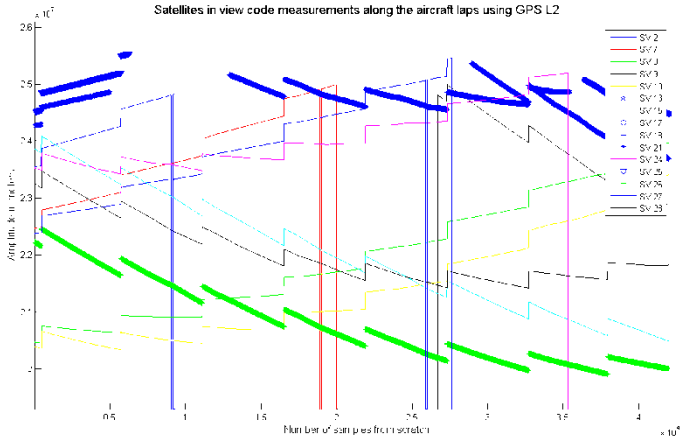

Figure 67: GPS L2 code measurements for all tracked satellites over the entire file

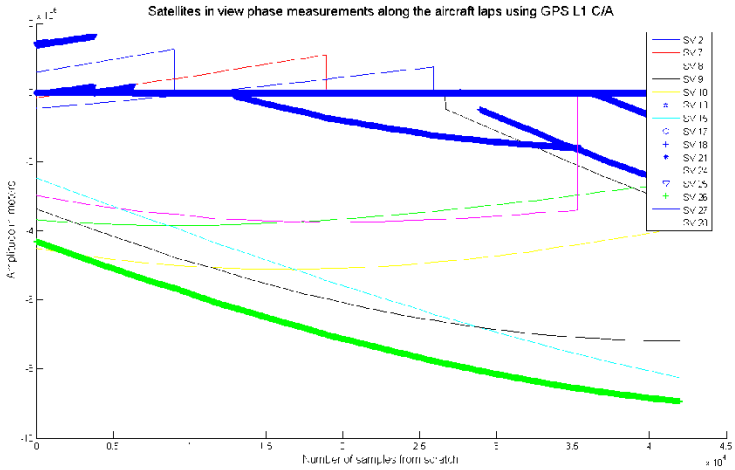

Figure 68: GPS L1 C/A carrier phase measurements for all tracked satellites

The abrupt changes that appear in code and phase measurements are clock shifts or losses of satellites (they are correlated with the number of tracked satellites and can be observed for both frequencies and on code and carrier phase measurements).

6.5.3. Kalman filter estimation in single frequency mode

Before presenting the Kalman filter estimations of the ionospheric code delay, we present the ionospheric code delay obtained thanks to the classical dual frequency method for each satellite. The results are plotted hereafter during the data collection onboard the Airbus aircraft.

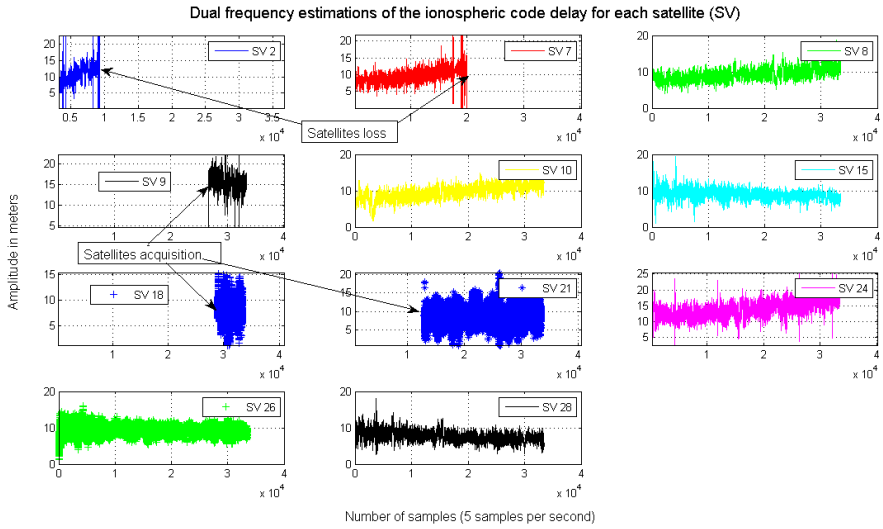

Figure 69: Ionospheric code delay estimated thanks to dual frequency measurements during the aircraft flight, the presented results are weighted by the obliquity factors.

In Figure 70, the mean dual frequency estimation of zenith ionospheric code delay for all tracked satellites is plotted in green. The red curve represents the Kalman estimation as described in the previous section. This estimation concerns the mean ionospheric code delay taking into account all the satellites in view (if acquired). The filter is initialized with dual

frequency measurements. Indeed, it is assumed that the loss of frequency occurs after the filter has started.

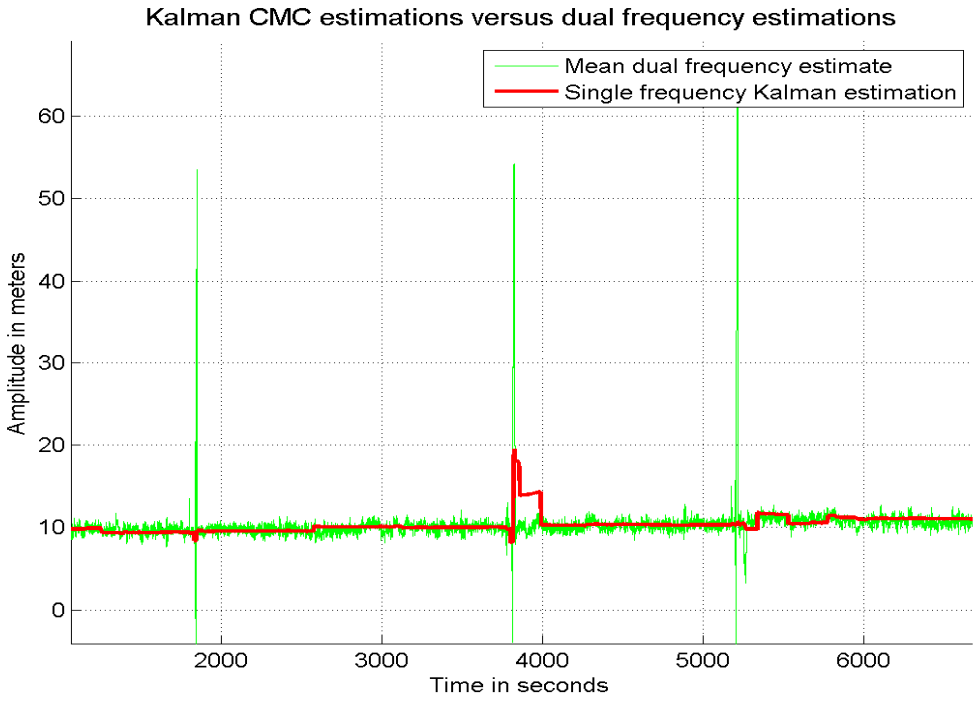

Figure 70: Ionospheric code delay estimated by the Kalman filter (in red) versus mean dual frequency estimation over all the acquired satellites (in green).

The accuracy of the filter is evaluated by comparing the mean and the standard deviations (STD) of dual and single frequency estimations over all the available measurements.

	N_{sample}	Mean vertical ionospheric delay over all tracked satellites measurements	
		Mean	Standard deviation (STD)
Dual frequency	$3\ 10^4$	11.09 m	3.31 m
Single frequency	$3\ 10^4$	10.89 m	1.49 m

Table 15: Mean and STD of dual and single frequency estimations of mean ionospheric code delay over all the tracked satellites.

Note that the figures presented in this table are obtained by processing GPS L1 C/A measurements in single frequency mode and thanks to L1 C/A + L2 measurements in dual frequency mode.

Some cycle slips were experienced during the data collection; these cycle slips can be identified thanks to the Kalman filter innovations. An example of significant cycle slip in the measurements is plotted in the figure below.

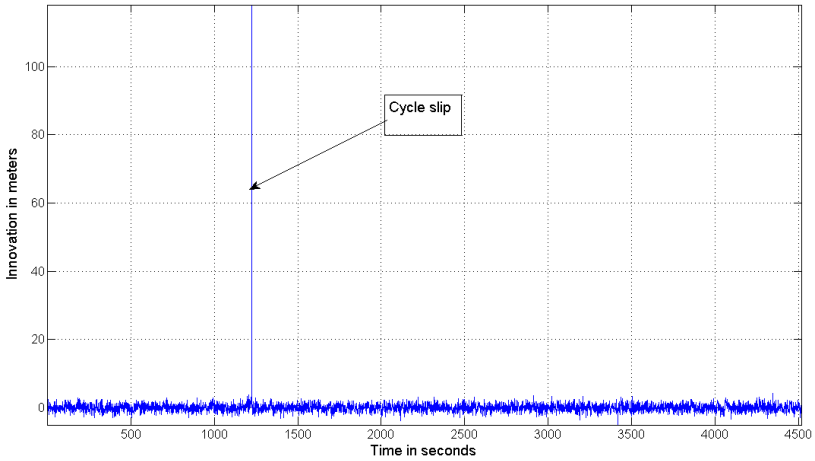

Figure 71: Innovation plotted for the SV 7.

6.6. Conclusion and future works

The performances of an algorithm capable of estimating single frequency ionospheric code delay have been estimated for civil aviation application.

Two parameters are taken into account for the accuracy: the mean and the standard deviation of the ionospheric code delay estimation error (and other percentiles in case of satellites loss or acquisition). It appears from this processing of the 2h20 data set that the estimation provided by the Kalman filter can allow keeping the accuracy of dual frequency estimations after a loss of frequency, with the cycle slip detector described in this chapter, to ensure the integrity required for APV I.

Thus, if cycle slips are detected, integrity is maintained as mentioned in [Ouzeau2, 2006]. But in this study, only a few significant cycle slips were experienced. Further investigations can estimate the filter resistance to cycle slips, with varying amplitudes.

Other types of algorithms may be used to detect cycle slips, like comparing raw and smoothed code measurements using the Hatch filter described in chapter 2 or using a Generalized Likelihood Ratio test (GLR) at the output of the Kalman filter which estimates the ambiguities of all tracked satellites.

The same performance analysis was conducted while comparing the Hatch filter inputs and outputs to detect cycle slips. It appears that the minimum detectable bias induced by cycle slips in normal aircraft dynamics conditions is 14.8 meters, slightly higher than the minimum bias obtained while using Doppler measurements (13 meters).

Concerning the GLR algorithm at the output of the Kalman filter, it is expected to have a much higher complexity than the two other detection algorithms. The actual performances of this algorithm in terms of cycle slip amplitude estimation must be evaluated through intensive future tests.

Ionospheric scintillations are not addressed in this study. However, it would be interesting to evaluate the behavior of the Kalman filter under ionospheric scintillations for further investigations, since the time constant for the ionospheric state is 3600 seconds as described in the equation (163).

The Kalman filter can be initialized thanks to SBAS dual frequency data, but simulations must be launched to evaluate the performances of the algorithm in this case.

Chapter 7

Conclusion and future works

7. Conclusion and future works

7.1. Global goals and combined receiver architecture

In this thesis, some key elements of the architecture of future combined receivers are proposed and discussed. A switching-based strategy between nominal, alternate and degraded modes of operation is described. The switching strategy depends on the targeted operation. In this thesis, in particular, we focused on the APV I phase of flight.

When a degradation occurs on one ore more GNSS components, the performances reached may be not sufficient to perform a phase of flight. This implies the use of degradation detection functions to monitor the performances reached and thus, the availability of the GNSS components. Degradation detection algorithms also allow to initiate a switch between modes of operation.

The detection functions are not only integrity monitoring functions. These functions must allow monitoring all the performances losses.

Another important point discussed in this thesis work, is how to maintain as long as possible the performance level required during degraded modes of operation.

In the following paragraphs, conclusions and way forward for future investigations are provided.

7.2. Interference threat

7.2.1. Interference detection for integrity and continuity

Amongst the perturbations that can lead to a loss of performance, interference is one of the most feared events. It can affect simultaneously several GNSS signals (GPS L1 C/A and Galileo E1 for instance) and can generate large tracking errors. As described in chapter 5 the interference can lead to pseudoranges measurements errors. In this study, we focus on the CW detection. Indeed, a CW can stay a long time near high-power code spectrum lines due

to low Doppler shit rate between the interference and the GNSS signals (2 Hz/s), leading to abnormal code tracking errors as described in chapter 5.

The impact of CW on GPS L1 C/A and Galileo E1 is studied in details in chapter 5. The maximum amplitude code spectrum lines within main lobes of GPS L1 C/A and Galileo E1 spectra are located respectively on PRN 6, 227 kHz and PRN 38, 673.5 kHz.

In [EUROCAE, 2007], the maximum CW power with proposed receiver design is -155 dBW. Under maximum aircraft dynamics conditions defined in [EUROCAE, 2007], the raw code tracking error can reach 50 meters and 22 meters after 100 s carrier smoothing as depicted in Chapter 5.

Two interference detection algorithms are proposed and based on multi correlator outputs monitoring: on the one hand, calculating the FFT of the correlators outputs on the I channel; on the other hand, by comparing the residuals of multichannel autoregressive model of all correlators outputs time variations. The FFT algorithm provides a missed detection probability of 6.7 10^{-5} when generating correlators outputs affected by CW interferences and impacting the GPS L1 C/A PRN 6. The resulting maximum tracking error is 15 meters when the interference is not detected, after carrier-smoothing. In the case of Galileo E1 PRN 38, the obtained missed detection probability is 10^{-5}. The resulting maximum smoothed tracking error is 1 meter. The multichannels AR algorithm provides a missed detection probability of 10^{-5} for both GPS L1 C/A and Galileo E1 worst code spectrum lines impacted.

As a trade-off must be made between detection algorithms complexity and the detection capability, the minimum number of useful correlators used without loss of detection capability can be evaluated in future studies for manufacturing. Between the two detection methods, the FFT algorithm is a simple one, which is easy to be implemented with low cost. The resulting missed detection probability was evaluated in this study, however a final discussion about the algorithm capability compared to required integrity cannot be made for a targeted phase of flight, and in particular for APV I. In fact, to compare the obtained results to the ICAO specifications about integrity risk, the obtained missed detection probabilities must be multiplied by the CW probability of occurrence and the probability of hitting one given code spectrum line to cause large tracking errors. The probability of occurrence of interferences cannot be evaluated precisely when the potential jammers locations, powers, etc are not known.

7.2.2. Interference removal for accuracy

Two options can then be considered when a CW is detected. As proposed in chapters 3 and 4, the receiver can switch to another available GNSS component to continue the current operation. Another solution can consist in estimating the CW characteristics and removing the interference effects from the correlators outputs. A 3rd order Prony model is thus proposed in chapter 5 and it results in our simulations that the interference impact on code tracking is completely removed as depicted in Chapter 5. The accuracy is consequently maintained when a CW occurs, by using this algorithm.

7.2.3. Recommendations and future works on interference threat

Future works may consist in studying other interference detection algorithms and other types of interferences. Some types of interferences like wide band or pulsed ones for instance, are not studied here. Other detection algorithms must be proposed to take into account these interferences. The actual performances of these algorithms must be assessed and compared to civil aviation requirements.

7.3. Single frequency degraded mode

7.3.1. Ionospheric code delay estimation for accuracy

After a loss of one frequency due to interferences for instance, ionospheric delay cannot be estimated through dual frequency measurements. This particular case is also addressed in this study. Indeed, the resulting position estimation is not accurate enough to provide aircraft position during critical phases of flight in particular. A Code Minus Carrier Kalman-aided algorithm is proposed to estimate the ionospheric code delay. The performances of such algorithm are tested through simulations and also validated thanks to actual aircraft measurements. The integrity is maintained with the help of a cycle slip detection algorithm.

7.3.2. Cycle slip detection for integrity

For cycle slip detection, some algorithms are proposed in this study and the one using Doppler measurements seems to be adequate. Indeed, the minimum detectable bias amplitude obtained is 13 meters while simulating normal aircraft dynamics and 16 meters for abnormal aircraft dynamics. The difference between these results is only 3 meters, which indicates that the detection algorithm is robust against high aircraft dynamics. In addition, these results were obtained while generating pseudoranges with unfavorable conditions: minimum satellite elevation angle (5 degrees), low carrier to noise ratio (30 dB Hz), and maximum dynamics values as described in chapter 6.

The cycle slip detection technique is interesting since detection can be made on single frequency raw measurements. It can protect the user against cycle slip integrity risk. On the one hand, it improves the code carrier smoothing with a 100 seconds Hatch filter. On the other hand, in case of single frequency mode, it can allow the user to maintain integrity while estimating ionospheric code delay with CMC divergence technique for instance as proposed in chapter 6. Nevertheless, Doppler measurements must be available for the receiver to use this technique.

7.3.3. Availability of the algorithm

In case of single frequency mode, the availability of the cycle slip detection technique is evaluated over Europe and is not complying with the requirements for APV I as depicted Figure 59 and Figure 60. However, the obtained results are dependent upon the fact that simulated pseudoranges are generated with the worst conditions (multipath, atmosphere, dynamics, satellite position…). In addition, the probability of falling into a single frequency mode due to aircraft RFI crossing for instance, reduces the corresponding integrity risk and thus augments the availability of the algorithm. The probability of losing all but one frequency is expected to be very low as mentioned in [RTCA, 2006].

7.3.4. Recommendations and future works for single frequency ionospheric delay estimation

Further investigations may consider the dynamics parameters in the Kalman states to take into account the high aircraft dynamics that can generate frequent cycle slips in carrier phase measurements ([Holmes, 1990]). If dynamics parameters are added, the number of states increases. A trade-off must be made between the filter robustness, the impact of aircraft high dynamics and the number of states.

The ambiguities are also estimated thanks to the Kalman filter. The estimations can be used by a GLR algorithm to monitor cycle slips and estimate cycle slips amplitudes. Further works may consist in studying the impact of the improvements of these estimations on the resulting pseudoranges accuracy, if these estimations are used to repair the measurements in case of cycle slip occurrence. In addition, the amplitudes of cycle slips can also be estimated thanks to the code carrier smoothing or the Doppler measurements.

7.4. Recommendations and future works

Even if the major risks leading to GNSS components performances degradations are addressed in this study, other phenomena deserve to be studied in details, like multipath during final approaches, with different airport environments.

This thesis work focuses only on the approach phases of flight. The objective of such a study is to converge towards a final architecture of receiver for each aircraft operation. The switch between components must be driven by monitoring algorithms with low costs and good capabilities. The goal is not to over-equip future combined receivers but to minimize the risks induced for each configuration.

The navigator reconfiguration should also be further discussed in case of degraded mode. Indeed, the possibility to maintain the level of performance in terms of continuity, integrity, accuracy and availability for APV I operations is discussed in this thesis for both interferences and ionosphere perturbations. But, EUROCAE WG 62 must decide if it is preferable to use algorithms to maintain the required level of performance during degraded modes of operation or not.

The detection algorithms proposed in this thesis focus on interferences (CW) and cycle slips detection. It is of interest to combine them with RAIM-type algorithms in future investigations to evaluate precisely the performance of the combined algorithms for using in civil aviation.

This thesis focuses on the detection function and not on the navigation function. However, future works may include a complete simulator of protection levels computation, by taking into account all components described in Chapter 2 and the architectures presented in Chapters 3 and 4.

References

[Akos, 2005] A Prototype Platform for Multi-Frequency GNSS Receivers, *Akos D.M., Ene A., Institute Of Navigation, GNSS 2005.*

[Alcantarilla, 2006] The Benefits of Multi-constellation GNSS Augmentations, *I. Alcantarilla, D. Porras, A. Tajdine, N. Zarraoa (GMV), JL. Damidaux, D. Flament, JC. Levy (Alcatel Alenia Space), Institute Of Navigation, GNSS, 19th international Technical Meeting of the Satellite Division, 26-29 September 2006, Fort Worth, TX.*

[Basseville, 1993] Detection Of Abrupt changes, Theory and Application, *Michèle Basseville, IRISA/CNRS, Rennes, France, Igor V. Nikiforov, Institute of Control Sciences, Moscow, Russia, Prentice Hall Information And System Sciences Series, Thomas Kailath, Series Editor, 1993.*

[Bastide, 2006] Civil Aviation Galileo E5 Receivers Architecture, *Frédéric Bastide, Benoît Roturier, DTI, O. Julien, C. Macabiau, E. Rebeyrol, M. Raimondi, C. Ouzeau, D. Kubrak, ENAC, First Galileo Workshop CNES, 12-13 October 2006, Toulouse, France.*

[Bastide1, 2004] Analysis of the Feasibility and Interests of Galileo E5a/E5b and GPS L5 for Use with Civil Aviation, *Frederic Bastide, PhD dissertation, 2004.*

[Bastide2, 2001] GPS interference detection and identification using multicorrelator receivers, *F.Bastide, E.Chatre, C.Macabiau ION GPS 2001.*

[Belabbas, 2005] Impact of NeQuick Correction Model to Positioning and Timing Accuracy using the Instantaneous Pseudo Range Error of Single Frequency Absolute Positioning Receivers, *B. Belabbas, S. Schlueter, M.Z. Sadeque, Deutsches Zentrum f¨ur Luft- und Raumfahrt (DLR), Germany, ION GNSS 2005.*

[Betz, 2001] Effect of Partial-Band Interference on Receiver Estimation of C/N_0: *Theory, J. W. Betz, ION NTM 2001.*

[Burnham, 2004] Multimodel Inference: Understanding AIC and BIC in Model selection, *Kenneth P.Burnham, David R. Anderson, Colorado State University, 2004.*

[Castanié, 2003] Analyse Spectrale, Traitement du Signal et de l'Image, *sous la direction de Francis Castanié, Hermès Science Publications, 2003.*

[Castro, 2006] A New Unambiguous Low-Complexity BOC Tracking Technique, David de Castro, *Deimos Space*, José Diez, *Deimos Space*, Antonio Fernández, *Deimos Space*, Jean-Marie Sleewaegen, *Septentrio Satellite Navigation, proceedings of the Institute Of Navigation, International Technical Meeting of the Satellite Division, 26-29 September 2006, Fort Worth, TX.*

[Chatre, 2003] GNSS Development Status and Future Works, *Eric Chatre, EC/ESA, rapporteur, technical WG, GNSS Panel, Agenda, Item 6, Eleventh Air Navigation Conference, ICAO, 22th of September to 3rd of October 2003.*

[Coco, 1991] Variability of GPS Satellite Differential Group Delay Biases, *David S. Coco, Clayton Coker, Scott R. Dahlke, IBM, James R.Clynch, Naval Postgraduate School, IEEE transactions on aerospace and electronic systems, Vol. 27, N° 6, November 1991.*

[Dassaud, 2007] Contribution to GALILEO signals, IAC-07-B2.1.07, Daniel Dassaud, Jean-Luc Issler, Lionel Ries, Antoine Richard De Latour, Laurent Lestarquit, CNES, Toulouse, France, *58th International Astronautical Congress, Hyberabad, India, 24-28 September 2007 (Copyright IAF/IAA).*

[Dellago, 2003] Galileo-GPS Interoperability And Compatibility, *R. Dellago, JM. Pieplu, R. Stalford, Galileo Industries, 9-12 September 2003, Portland OR.*

[Driscoll, 2005] Performance Analysis of an FFT Based Fast Acquisition GPS Receiver, Cillian O'Driscoll and Colin C. Murphy *Department of Electrical and Electronic Engineering University College Cork Ireland, proceedings of the Institute Of Navigation, National Technical Meeting, 24-26 January 2005, San Diego, CA.*

[Ducasse, 1998] Ducasse A., Mailhes C., Castanié F., Estimation de fréquences : panorama des méthodes paramétriques, frequency estimation : survey of parametric methods. *Traitement du signal, ISSN, 1998, vol. 15, n° 2, pp. 149-162. Groupe de recherche et étude de traitement du signal et des images, Saint Martin d'Hères, France.*

[EUROCAE, 2008] Concept Of Operations For Combined Galileo/GPS Receivers,

prepared by Galileo/GPS Ad-Hoc group within EUROCAE WG-62, Issue 3, Version 1.0, 2 June 2008. ***Note that it is an interim version.***

[EUROCAE, 2007] Minimum Operational Performance Standards for Galileo, *EUROCAE, WG 62, 2007.* ***Note that it is an interim version.***

[ESA, 2004] Galileo Mission Requirements Document, *Issue 6, 11th July 2004, ESA.*

[Esbri, 2006] Antenna-based Multipath and Interference Mitigation for Aeronautical Applications: Present and Future, *O. Esbri-Rodriguez, DLR German Aerospace Center, Germany, M. Philippakis, ERA Technology (Cobham PLC), U.K., A. Konovaltsev, DLR German Aerospace Center, Germany, F. Antreich, DLR German Aerospace Center, Germany, C. Martel, ONERA, France (formerly with ERA Technology (Cobham PLC), U.K.), D. Moore, ERA Technology (Cobham PLC), U.K, 2006.*

[Eissfeller, 2005] Implementation and Simulation of a Mass-Market GPS-Galileo Single Point Positioning Receiver, Bernd Eissfeller, G. Hein, Roland Kaniuth, Andrea Pósfay and Thomas Pany *Institute of Geodesy and Navigation, University FAF Munich, Germany, Proceedings of the Institute Of Navigation, National Technical Meeting, 24-26 January 2005, San Diego, CA.*

[Euler, 1991] On Optimal Filtering of Dual Frequency Observations without using Orbit Information, Euler, H-J, Goad, C.C, Bulletin Géodésique (1991, Vol. 65.

[FAA, 2008] Wide Area Augmentation System (WAAS) – Program Status, Deborah Lawrence, WAAS Program Manager, *Federal Aviation Administration (FAA), ION GNSS 2008 – Program Updates, September 18, 2008.*

[Garcia, 2002] Contributions to the 3D ionospheric sounding with GPS data, Miquel Garcia Fernandez, *PhD thesis, Reseach group of Astronomy and Geomatics, Departments of Applied Mathematics IV and Applied Physics, Universitat Politecnica de Catalunya, Spain, 2002.*

[Grewal, 2001] Kalman Filtering, Theory and Practice Using Matlab, *Second Edition, Mohinder S. Grewal, Angus, P. Andrews, 2001.*

[GJU, 2006] EGNOS Mission Requirement Document, *Version 2.0, 8th May*

2006, Galileo Joint Undertaking.

[GSA, 2008] Galileo Open Service, Signal In Space, Interface Control *Document, OS SIS ICD, Draft 1, European Space Agency, European GNSS Supervisory Authority, 2008.*

[Hegarty1, 1997] Analytical Derivation of the Maximum Tolerable In-Band Interference Levels for Aviation Applications of GNSS, *C. Hegarty, Navigation: Journal of the Institute Of Navigation, Vol. 44, N°1, Spring, pp 25-34.*

[Hegarty2, 1999] Evaluation of the Proposed Signal Structure for the New Civil GPS Signal at 1176.45 MHz, *C. Hegarty, June 1999, Working Note, MITRE Corporation.*

[Hein, 2002] Status of Galileo Frequency and Signal Design, *Guenter W. Hein, Jeremie Godet, Jean-Luc Issler, Jean-Christophe Martin, Philippe Erhard, Rafael Lucas-Rodriguez and Tony Pratt, Members of the Galileo Signal Task Force of the European Commission, Brussels, Galileo European Satellite Navigation System, Technical documents, 25th September 2002.*

[Holmes, 1990] Coherent spread Spectrum Systems, *Krieger, 1990.*

[ICAO, 2006] Annex 10, Volume I, *ICAO.*

[Ilir, 2006] GPS L5 Signal Acquisition and Tracking under Unintentional Interference or Jamming, *Ilir F. Progri, California State Polytechnic University (Cal Poly), Pomona, CA, proceedings of the Institute Of Navigation, National Technical Meeting 2005,18-20 January 2006, Monterey, CA.*

[Issler, 2004] Probabilistic approach of frequency diversity as interference mitigation means, *J.L Issler, L. Ries, J.M. Bourgeade, L. Lestarquit, CNES (French space agency), C. Macabiau, ENAC, Proceedings of the ION NTM, January 2004, Long Beach, CA.*

[Julien, 2005] PhD thesis: Design of Galileo L1F Receiver Tracking Loops, *Olivier Julien, July 2005.*

[Jun, 2006] A New Technology for GNSS Signal Fast Acquisition within Three Seconds, Applicable to Current GNSS Receivers, *Haeyoung Jun, Seoul National University, Changdon Kee, Seoul National University, proceedings of the Institute Of Navigation, National Technical Meeting 2005,18-20 January 2006, Monterey, CA.*

[Kaplan, 1996] Understanding GPS, Principles And Applications, *Elliott D.Kaplan, Artech House, Boston, London, 1996.*

[Kubrak, 2005] Analysis of a Software-based A-GPS Acquisition Performance Using Statistical Processes, *Damien Kubrak, Ecole Nationale de l'Aviation Civile, France, Christophe Macabiau, Ecole Nationale de l'Aviation Civile, France, Michel Monnerat, Alcatel Space, France, proceedings of the Institute Of Navigation, National Technical Meeting 2005, 24-26 January 2005, San Diego, CA.*

[Lehner, 2007] Multipath Channel Modelling for Satellite Navigation Systems, *Andreas Lehner, Shaker Verlag, 2007.*

[Lestarquit, 1997] Iono-GPS software: determination of the ionospheric error using only L1 frequency GPS receiver, *Laurent Lestarquit, Norbert Suard, Jean-Luc Issler, DGA, CNES, AI 1997.*

[Lyn, 2002] GALILEO.s SERVICES, *Lyn Dutton, Thales Avionics Limited, UK, David Rumens, Thales ATM, UK, William Forrest, Thales ATM, UK, Luis Ruiz, ESA Galileo Interim Support Structure, Belgium, proceedings of the Institute Of Navigation, GPS 2002, 24-27 September 2002, Portland, OR.*

[Mabilleau, 2007] Combined GALILEO-GPS receiver based on a switching logic *presented by Paul Flament, prepared by Mikaël Mabilleau (DTI), Paul Nisner (NATS), Laurent Azoulai (Airbus), Jean Pierre Arenthens (Thales), Gerard Alcouffe (Thales), Christophe Ouzeau (ENAC), Navigation System Panel, New Delhi, India, March, 2007.*

[Macabiau, 2002] Use Of Multicorrelator Techniques for Interference Detection, *C. Macabiau, O. Julien, E. Chatre, Proceedings of the Institue Of Navigation, National Technical Meeting, Long Beach, CA, Jan 22-24, 2002.*

[Macabiau1, 1997] Analysis of the Feasibility of Using GPS Carrier Phase Ambiguity Resolution Techniques for Precision Approaches, *PhD thesis, C. Macabiau, 29th of September 1997.*

[Macabiau2, 2005] RAIM Performance in Presence of Multiple Range Failures, *Christophe Macabiau (ENAC), Bertrand Gerfault (Thales), Igor Nikiforov, Lionel Fillatre (UTT), Benoît Roturier (STNA), Eric Chatre (GJU), Mathieu Raimondi, Anne-Christine Escher (ENAC), proceedings of the Institute Of Navigation, National Technical Meeting, San Diego, CA, 24-26 January 2005.*

[Marple, 1987] Digital Spectral Analysis With Applications, *S. Lawrence Marple, Jr., Prentice Hall, Signal Processing Series, 1987.*

[Mongrédien, 2006] Testing GPS L5 Acquisition and Tracking Algorithms Using a Hardware Simulator, *C. Mongrédien, G. Lachapelle and M.E. Cannon Position, Location and Navigation (PLAN) Research Group Department of Geomatics Engineering Schulich School of Engineering University of Calgary, proceedings of the Institute Of Navigation, International Technical Meeting of the Satellite Division, 26-29 September 2006, Fort Worth, TX.*

[Moreno, 1999] Ionospheric delay using only L1: validation and application to GPS receiver calibration and to inter-frequency biases estimation, *Richard Moreno, Norbert Suard, Centre National d'Etudes Spatiales (CNES), proceedings of the ION, GPS, September 1999.*

[NATS, 2003] Degraded Modes – Maintaining Dual Frequency Navigation Performance in the Presence of Interference, *Agenda Item 8: Concept of Operations, Information Paper prepared by National Air Traffic Services Limited, NATS, EUROCAE WG 62, 8/9 July 2003.*

[Nisner, 1996] GPS Ionosphere Determination Using L1 Only, *Paul Nisner, Mike Trethewey, proceedings of the Institute Of Navigation National Technical Meeting, 1996.*

[Ouzeau1, 2006] Etude du retard de code ionosphérique pour un récepteur mono fréquence, *C. Ouzeau, C. Macabiau, AC. Escher, EDIT, avril 2006.*

[Ouzeau2, 2006] Ionospheric Code Delay Estimation In Case Of Radio Frequency Interference For Civil Aviation, *Christophe Ouzeau, Frederic Bastide, Christophe Macabiau, Benoît Roturier, Proceedings of the Institute Of Navigation, Global Navigation Satellite System, Fort Worth, Texas, September, 2006.*

[Ouzeau3, 2007] Compliance Of Single Frequency Ionospheric Delay Estimation And Cycle Slip Detection With Civil Aviation Requirements, *Christophe Ouzeau, Christophe Macabiau, Anne-Christine Escher, Benoît Roturier, Proceedings of the Institute Of Navigation, National Technical Meeting, San Diego, California, January, 2007.*

[Ouzeau4, 2008] Performance of a Multicorrelator GNSS Interference

Detection Algorithms for Civil Aviation, *Proceedings of the Institute Of Navigation, National Technical Meeting, San Diego, California, January, 2008*.

[Ouzeau5, 2008] Performance assessment of Multi Correlator Interference Detection and Repair Algorithms for Civil Aviation, *Christophe Ouzeau, Christophe Macabiau, Benoît Roturier, Mikaël Mabilleau, ENC GNSS, Toulouse Space Show, April 2008.*

[Ouzeau6, 2008] Ionospheric Error Estimation in a Degraded Single Frequency Mode for Civil Aviation**,** *C. Ouzeau, TeSA/ENAC/DTI, France; C. Macabiau, ENAC, France; B. Roturier, DSNA-DTI, France; M. Mabilleau, Sofreavia, France; J. Levan, F. Besse, ENAC, France, Proceedings of the Institute Of Navigation, GNSS, Savannah, Georgia, September, 2008.*

[Parkinson, 1996] Global Positioning System: Theoy and Applications, *Volume I, edited by Bradford W. Parkinson, James J. Spilker, associate editors Penina Axelrad, Per Enge. Progress in Astronautics, Paul Zarchan, Editor-in-Chief, Volume 163, second printing, 1996.*

[Radicella, 2003] Ionospheric model for single frequency receivers, *S. Radicella, R. Leitinger, B. Arbesser-Reitsburg, R. Lucas-Rodriguez, ESA-APPNG-SPEC/00344-BAR, 2003.*

[Raimondi, 2006] Mitigating Pulsed Interference Using Frequency Domain Adaptive Filtering, *Mathieu Raimondi, Olivier Julien, Christophe Macabiau (ENAC), Frédéric Bastide (Sofreavia/DTI), proceedings of the Institute Of Navigation, GNSS, Fort Worth, TX, September 2006.*

[Rebeyrol, 2006] Signal Distorsions At Payload Level, *Emilie Rebeyrol, Christophe Macabiau, Olivier Julien, ENAC/TéSA, Lionel Ries, Jean-Luc Issler, CNES, Michel Bousquet, SUPAERO, Marie-Laure Boucheret, ENSEEIHT, Proceedings of the Institute Of Navigation, Global Navigation Satellite System, Fort Worth, Texas, September, 2006.*

[Rollet, 2008] EUROCAE WG 62 ANASTASIA results and recommendations, *Thales, aerospace, NAV/08/xxx, working presentation by S. Rollet, meeting 25.*

[RTCA, 2002] Assessment of Radio Frequency Interference Relevant to the GNSS, *DO-235A, RTCA SC-159 Inc, 2002.*

[RTCA, 2004] Minimum Aviation System Performance Standards for Local Area Augmentation System (LAAS), *RTCA WG SC-159. LAAS MASPS, 2004.*

[RTCA, 2006] Minimum Operational Performance Standards For Global Positioning System/ Wide Area Augmentation System Airborne Equipment, *RTCA DO-229D, Paper No. 093-06/SC-159-939, 2006.*

[Shau-Shiun Jan, 2003] Aircraft Landing Using a Modernized Global Positioning System And The Wide Area Augmentation System*, Shau-Shiun Jan, PhD thesis, Department of Aeronautics and Astronautics and the Committee on Graduate Studies of Standford University, 2003.*

[Simsky, 2006] Performance Assessment of Galileo Ranging Signals Transmitted by GSTB-V2 Satellites, *Andrew Simsky, Jean-Marie Sleewaegen, Septentrio Satellite Navigation, Belgium Martin Hollreiser, Massimo Crisci, ESA/ESTEC, Netherlands, proceedings of the Institute Of Navigation, International Technical Meeting of the Satellite Division, 26-29 September 2006, Fort Worth, TX.*

[Steingass, 2004] Alexander Steingaß, Andreas Lehner, F. Pérez-Fontán, Erwin Kubista, M.J. Martín, Bertram Arbesser-Rastburg, "*The High Resolution Aeronautical Multipath Navigation Channel*", ION NTM 2004, San Diego, USA, January 26-28, 2004

[Stephens, 1993] Controlled-Root Formulation For Digital Phase-Locked Loops, *S. A. Stephens, J. B. Thomas, 1993.*

[Verhoef, 2008] European GNSS programmes Update, *Paul Verhoef, European Commission, Directorate-General for Energy and Transport, ION 2008, Savannah, Georgia, 16 September 2008.*

[Walter, 1995] Weighted RAIM for Precision Approaches, Walter T., P. Enge, Proceedings of the Institute Of Navigation, GPS 1995, September.

[Willsky, 1976] A generalized likelihood ratio approach to the detection and estimation of jumps in linear systems*, A.S. Willsky and H. L. Jones (1976), IEEE Trans. Aut. Control, 21, pp. 108-112.*

[Winkel, 2003] Modelling and Simulating GNSS Signal Structures and Receivers*, Winkel, J.O. PhD Thesis, 2003, University FAF Munich, Neubiberg.*

[Younes, 1998] Sequential RAIM: theory and application to civil aviation needs, *A. Younes, B. Bakhache, I. Nikiforov, A. Benhallam 1998.*

Author publications presented for this PhD Thesis

1. Etude du retard de code ionosphérique pour un récepteur mono fréquence, Christophe Ouzeau, Christophe Macabiau, Anne-Christine Escher, EDIT, avril 2006.

2. Ionospheric Code Delay Estimation In Case Of Radio Frequency Interference For Civil Aviation, Christophe Ouzeau, Frederic Bastide, Christophe Macabiau, Benoît Roturier, *Proceedings of the Institute Of Navigation, Global Navigation Satellite System, Fort Worth, Texas, September, 2006.*

3. Compliance Of Single Frequency Ionospheric Delay Estimation And Cycle Slip Detection With Civil Aviation Requirements, Christophe Ouzeau, Christophe Macabiau, Anne-Christine Escher, Benoît Roturier, *Proceedings of the Institute Of Navigation, National Technical Meeting, San Diego, California, January, 2007.*

4. Performance of a Multicorrelator GNSS Interference Detection Algorithms for Civil Aviation, *Proceedings of the Institute Of Navigation, National Technical Meeting, San Diego, California, January, 2008*.

5. Performance assessment of Multi Correlator Interference Detection and Repair Algorithms for Civil Aviation, Christophe Ouzeau, Christophe Macabiau, Benoît Roturier, Mikaël Mabilleau*, ENC GNSS, Toulouse Space Show, April 2008.*

6. Ionospheric Error Estimation in a Degraded Single Frequency Mode for Civil Aviation C. Ouzeau, TeSA/ENAC/DTI, France; C. Macabiau, ENAC, France; B. Roturier, DSNA-DTI, France; M. Mabilleau, Sofreavia, France; J. Levan, F. Besse, ENAC, France, *Proceedings of the Institute Of Navigation, GNSS, Savannah, Georgia, September, 2008*.

7. Civil Aviation Galileo E5 Receivers Architecture, Frederic Bastide, Benoît Roturier, DTI, Olivier Julien, Christophe Macabiau, Emilie Rebeyrol, Mathieu Raimondi, Christophe Ouzeau, Damien Kubrak, ENAC, First Galileo signal processing CNES Workshop, October 2006.

8. Combined GALILEO-GPS receiver based on a switching logic, Mikaël Mabilleau (DTI), Paul Nisner (NATS), Laurent Azoulai (Airbus), Jean Pierre Arenthens (Thales), Gerard Alcouffe (Thales), Christophe Ouzeau (ENAC), Navigation System Panel, New Delhi, India, March 2007.

Appendix A: Mathematical models

Appendix A.1: ARMA model

We assume that a sampled stationary random signal x(n) can be modeled as the output of a numerical ARMA (Auto-Regressive Moving Average) filter F(z), excited by a centered white noise e(n):

$$F(z) = \frac{\sum_{k=0}^{q} b_k \, Z^{-k}}{\sum_{k=0}^{p} a_k \, Z^{-k}} \text{with } a_0 = 1 \quad \textbf{(165)}$$

We assume that the expectation ($\mathbb{E}$) of the noise is:

$$\mathbb{E}[e(n)] = 0 \quad \textbf{(166)}$$

And:

$$\mathbb{E}[e(n)e^*(n-k)] = \sigma_e^2 \delta_k^n \quad \textbf{(167)}$$

Where:

- σ_e^2 is the noise variance (power)
- $\delta_k^n = \begin{cases} 1 \; if \; n = k \\ 0 \; otherwise \end{cases}$

The signal x can be written by means of an ARMA(p,q) model:

$$x(n) = -\sum_{k=1}^{p} a_k \, x(n-k) + \sum_{k=0}^{q} b_k \, e(n-k) \quad \textbf{(168)}$$

- The order of the AR model is p and corresponds to the $\{a_k\}_{k=1,\dots,p}$ coefficients.
- The order of the MA model is q and corresponds to the $\{b_k\}_{k=0,\dots,q}$ coefficients.

The goal of the ARMA model is to determine the p+q $\{a_k\}_{k=1,\dots,p}$ and $\{b_k\}_{k=0,\dots,q}$ coefficients plus the input noise power.

The Auto-Regressive (AR) and Moving Average (MA) models are particular cases of an ARMA model:

- The AR model is:

$$x(n) = -\sum_{k=1}^{p} a_k \, x(n-k) + e(n) \quad \textbf{(169)}$$

The transfer function is:

$$F(z) = \frac{1}{1 + \sum_{k=1}^{p} a_k \, Z^{-k}} \quad \textbf{(170)}$$

The estimation of the modeled signal is:

$$\hat{x}(n) = -\sum_{k=1}^{p} a_k \, x(n-k) \quad \textbf{(171)}$$

Therefore, e(n) is:

$$e(n) = x(n) - \hat{x}\ (n) \quad \textbf{(172)}$$

- The MA model is:

$$x(n) = \sum_{k=0}^{q} b_k\ e(n-k) \quad \textbf{(173)}$$

The AR model coefficients can be linearly solved, whereas the MA model induces non linearity. The AR model is widely used and we only use this model in this thesis for interference detection at the correlators' outputs. Since the detection is made over all the available correlators, we decided to use a multichannel version of this algorithm to take advantage of the existing correlation between the correlators' outputs time variations in presence of CW. This multichannel version of the AR model is presented in the next appendix.

AR coefficients estimation

Several methods to estimate the AR coefficients are described in the literature, for instance in [Castanié, 2003]. For instance, the AR parameters can be found by minimizing the following criterion (quadratic prediction error):

$$E = \sum_n |e(n)|^2 = \sum_n |x(n) - \hat{x}(n)|^2 = \sum_n \left|x(n) + \sum_{k=1}^{p} a_k x(n-k)\right|^2 \quad \textbf{(174)}$$

$$E = \sum_n \left|\sum_{k=0}^{p} a_k x(n-k)\right|^2 \quad \textbf{(175)}$$

In order to find the AR coefficients that minimize the criterion, the most popular techniques are based on Yule-Walker equations solving. We do not describe these techniques here, since our goal is to propose a multichannel resolution described in the next appendix.

Appendix A.2: Multichannel Autoregressive model

In the following, h is the filter model, x is the filter output, e represents the filter input. $\mathbb{E}$ is the classical mathematical expectation. _ represents a block matrix.

In this appendix, we describe how the multichannel AR coefficients are calculated, on the basis of the theory developed in [Marple, 1987].

Multichannel AR model

A multichannel AR(p) model is almost like a classical AR model described in [Castanié, 2003]. The main difference is that it represents the output of a multichannel filter which inputs are noise processes.

The objective here is to determine the coefficients which define the model filter. The assumption here is that the signal is the result of a stationary random input white noise process filtered by a filter H on several channels. Each channel corresponds to a correlator output in our application.

The problem is to determine the filter coefficients that model as accurately as possible the correlator outputs behaviour. To this end, we select the AR estimates that induce the minimum norm of the estimation error:

$$E = \sum_{k=1}^{N} \left| e[n] \right|^2 \quad \textbf{(176)}$$

Where: $e[n] = x[n] - \hat{x}[n]$ **(177)** is the estimation error

$$E = r_{xx}[0] + \begin{pmatrix} r_{xx}[1] \\ \vdots \\ r_{xx}[p] \end{pmatrix}^T a + a^H \begin{pmatrix} r_{xx}[1] \\ \vdots \\ r_{xx}[p] \end{pmatrix}^* + a^H R^* a \quad \textbf{(178)}$$

Where r is a correlation matrix (relative to the model order) and a represents the AR coefficients, R is the global correlation matrix.

This expression of the error E depends upon the AR coefficients, and as a consequence, the best estimation of these coefficients is provided by minimizing the error, i.e. finding $E_{\min}$, solving the following equation:

$$\begin{pmatrix} r & r^H \\ r & R \end{pmatrix} \begin{pmatrix} 1 \\ -a \end{pmatrix} = \begin{pmatrix} E_{\min} \\ 0 \end{pmatrix} \quad \textbf{(179)}$$

Proof:

The estimation of x is provided by:

$$\hat{x}[n] = a_1 x_1[n] + \ldots + a_p x_m[n] \quad \textbf{(180)}$$

$$x - \hat{x}a = e \quad \textbf{(181)}$$

$$\begin{pmatrix} x & \hat{x} \end{pmatrix} \begin{pmatrix} 1 \\ -a \end{pmatrix} = e \quad \textbf{(182)}$$

$$\hat{x} = \begin{pmatrix} x_1[1] & \cdots & x_p[1] \\ \vdots & \ddots & \vdots \\ x_1[n] & \cdots & x_p[n] \end{pmatrix},\ a = \begin{pmatrix} a_1 \\ \vdots \\ a_p \end{pmatrix},\ x = \begin{pmatrix} x[1] \\ \vdots \\ x[n] \end{pmatrix},\ e = \begin{pmatrix} e[1] \\ \vdots \\ e[n] \end{pmatrix} \quad \textbf{(183)}$$

$$E = e^H e = x^H x - x^H \hat{x} a - a^H \hat{x}^H x + a^H \hat{x}^H \hat{x} a \ (*) \quad \textbf{(184)}$$

$$E = e^H e = x^H x - x^H \hat{x} (\hat{x}^H \hat{x})^{-1} \hat{x}^H x + (\hat{x}^H x - \hat{x}^H \hat{x} a)^H (\hat{x}^H \hat{x})^{-1} (\hat{x}^H x - \hat{x}^H \hat{x} a) \quad \textbf{(185)}$$

As it can be seen, only the second term of the previous expression is dependent upon the AR coefficients. Since $E2 = (\widehat{x^H} x - \widehat{x^H} \widehat{x}\ a)^{\mathsf{H}}\ (\widehat{x^H} \widehat{x})^{-1}\ (\widehat{x^H} x - \widehat{x^H} \widehat{x}\ a)$ (the second term) is positive, it has to be minimized as a function of a.

As a consequence, a must verify the following conditions:

$$\hat{x}^H x = \hat{x}^H \hat{x} a \quad \textbf{(186)}$$

From (*), and the previous condition, E becomes:

$$E_{\min} = e^H e = x^H x - x^H \hat{x} a \quad \textbf{(187)}$$

In other words:

$$\begin{pmatrix} x^H x & x^H \hat{x} \\ \hat{x}^H x & \hat{x}^H \hat{x} \end{pmatrix} \begin{pmatrix} 1 \\ -a \end{pmatrix} = \begin{pmatrix} x^H x - a x^H \hat{x} \\ \hat{x}^H x - a \hat{x}^H \hat{x} \end{pmatrix} = \begin{pmatrix} E_{\min} \\ 0_m \end{pmatrix} \quad \textbf{(188)}$$

Estimation of the AR coefficients of the multichannel model

If a block column vector of multichannel data vectors is defined as:

$$\underline{E}_p(n) = \begin{pmatrix} E(n) \\ \vdots \\ E(n-p) \end{pmatrix} \quad \textbf{(189)}$$

where p is the order of the AR model, the stationary m-channel AR process (with model coefficients represented by A) may be expressed as the block vector inner product:

$$err_p^f(n) = \underline{A}_p \underline{E}_p(n) \quad \textbf{(190)}$$

Similarly, the following product is defined with backward coefficients [Marple, 1987]:

$$err_p^b(n) = \underline{C}_p \underline{E}_p(n) \quad \textbf{(191)}$$

Where:

$\underline{C}_p = \begin{pmatrix} C(p) & \cdots & C(1) & I \end{pmatrix}$ is built in the same way than A.

It describes respectively the forward and backward linear prediction error (f and b superscripts).

Indeed, in the single channel AR model case, the Hermitian Toepliz structure of the correlation matrix is sufficient to ensure the conjugate relationship between the A and C coefficients: $a_p(k) \neq c_p^*(k)$, but it is not the case for the multichannel model [Marple, 1987].

In the theory developed in [Marple, 1987], in order to estimate the A and C coefficients, the linear prediction errors are multiplied by the Hermitian transpose of $\underline{E}_p(n)$ and the expectation of the obtained expression is calculated:

$$\mathbb{E}[err_p^f(n)\underline{E}_p^H(n)] = \mathbb{E}[\underline{A}_p\underline{E}_p(n)\underline{E}_p^H(n)] = \underline{A}_p\,\mathbb{E}[\underline{E}_p(n)\underline{E}_p^H(n)] = \underline{A}_p\ \underline{R}_p \quad \textbf{(192)}$$

Where: $\underline{R}_p$ is defined as the block matrix:

$$\underline{R}_p = \begin{pmatrix} R_{EE}(0) & \cdots & R_{EE}(p) \\ \vdots & \ddots & \vdots \\ R_{EE}(-p) & \cdots & R_{EE}(0) \end{pmatrix} \quad \textbf{(193)}$$

$\mathbb{E}[err_p^f(n)\underline{E}_p^H(n)] = \delta_k^n P_\omega$ **(194)** is the model noise power P multiplied by $\delta_k^n = \begin{cases} 1\ if\ n = k \\ 0\ otherwise \end{cases}$.

$$\mathbb{E}[err_p^f(n)\underline{E}_p^H(n)] = \mathbb{E}[err_p^f(n)(err_p^{fH}(n) - \sum_{k=1}^{p}\underline{E}_p^H(n)A_p^H(k)] = \begin{pmatrix} P_p^f & 0 & \cdots & 0 \end{pmatrix} \quad \textbf{(195)}$$

$$\boxed{\underline{A}_p}\,\underline{R}_p = \begin{pmatrix} P_p^f & 0 & \cdots & 0 \end{pmatrix} \square \textbf{(196)}$$

With:

$$P_p^f = \mathbb{E}[err_p^f(n)err_p^{fH}(n)] = P_\omega \quad \textbf{(197)}$$

And similarly:

$$\boxed{\underline{C}_p}\,\underline{R}_p = \begin{pmatrix} 0 & \cdots & 0 & P_p^b \end{pmatrix} \square \textbf{(198)}$$

The resolution of the two framed equations should be made using the following methodology.

We define the (p+1)-block Toepliz matrix:

$$\underline{R}_{p+1} = \begin{pmatrix} R_{EE}(0) & r_{p+1} \\ r_{p+1}^H & \underline{R}_p \end{pmatrix} = \begin{pmatrix} \underline{R}_p & s_{p+1}^H \\ s_{p+1} & R_{EE}(0) \end{pmatrix} \quad \textbf{(199)}$$

Where:

$$\underline{r}_{p+1} = \begin{pmatrix} R_{EE}(1) & \cdots & R_{EE}(p+1) \end{pmatrix} \quad \textbf{(200)}$$

$$\underline{s}_{p+1} = \begin{pmatrix} R_{EE}(-(p+1)) & \cdots & R_{EE}(-1) \end{pmatrix} \quad \textbf{(201)}$$

In this way, the AR coefficients are calculated in a recursive manner:

$$\begin{pmatrix}\underline{A}_p & 0\end{pmatrix}\underline{R}_{p+1} = \begin{pmatrix}P_p^f & 0 & \cdots & 0 & \Delta_{p+1}\end{pmatrix} \quad \textbf{(202)}$$

$$\begin{pmatrix}0 & \underline{C}_p\end{pmatrix}\underline{R}_{p+1} = \begin{pmatrix}\nabla_{p+1} & 0 & \cdots & 0 & P_p^b\end{pmatrix} \quad \textbf{(203)}$$

With:

$$\Delta_{p+1} = R_{EE}(p+1) + \sum_{k=1}^{p} A_p(k) R_{EE}(p+1-k) = \underline{A}_p \underline{s}_{p+1}^H \quad \textbf{(204)}$$

$$\nabla_{p+1} = R_{EE}(-(p+1)) + \sum_{k=1}^{p} C_p(k) R_{EE}(-(p+1-k)) = \underline{C}_p \underline{r}_{p+1}^H \quad \textbf{(205)}$$

The update of the AR coefficients is then ensured by:

$$\underline{A}_{p+1} = \begin{pmatrix}\underline{A_p} & 0\end{pmatrix} + A_{p+1}(p+1)\begin{pmatrix}0 & \underline{C}_p\end{pmatrix} \quad \textbf{(206)}$$

$$\underline{C}_{p+1} = \begin{pmatrix}0 & \underline{C}_p\end{pmatrix} + C_{p+1}(p+1)\begin{pmatrix}\underline{A_p} & 0\end{pmatrix} \quad \textbf{(207)}$$

Therefore, the coefficients of the linear prediction filter for k from 1 to p can be derived:

$$A_{p+1}(k) = A_p(k) + A_{p+1}(k) + A_{p+1}(p+1) C_p(p+1-k) \quad \textbf{(208)}$$

$$C_{p+1}(k) = C_p(k) + C_{p+1}(k) + C_{p+1}(p+1) A_p(p+1-k) \quad \textbf{(209)}$$

And:

$$A_{p+1}(p+1) = -\Delta_{p+1}(P_p^b)^{-1} \quad \textbf{(210)}$$

$$C_{p+1}(p+1) = -\nabla_{p+1}(P_p^f)^{-1} \quad \textbf{(211)}$$

The noise prediction error covariance is given by:

$$P_{p+1}^f = P_p^f + A_{p+1}(p+1)\nabla_{p+1} \quad \textbf{(212)}$$

$$P_{p+1}^b = P_p^b + C_{p+1}(p+1)\nabla_{p+1} \quad \textbf{(213)}$$

And:

$$P_{p+1}^f = (I - A_{p+1}(p+1) C_{p+1}(p+1)) P_p^f \quad \textbf{(214)}$$

$$P_{p+1}^b = (I - C_{p+1}(p+1) A_{p+1}(p+1)) P_p^b \quad \textbf{(215)}$$

The normalized cross-correlation is defined by:

$$\Lambda_{p+1} = (P_p^{f\,1/2})^{-1}(P_p^{fb})(P_p^{b1/2})^{-H} \quad \textbf{(216)}$$

as mentioned in [Marple, 1987].

One can also deduce:

$$A_{p+1}(p+1) = -(P_p^{f1/2})(\Lambda_{p+1})(P_p^{b1/2})^{-1} \quad \textbf{(217)}$$

$$C_{p+1}(p+1) = -(P_p^{b1/2})(\Lambda_{p+1}^{H})(P_p^{f1/2})^{-1} \quad \textbf{(218)}$$

Conclusion:

The application of this model is made on the correlators' outputs as it is described in Chapter 5. The model errors are then compared to determine if jammers are present or not in the signal. Each channel corresponds to a correlator output. Without interference, the correlator outputs are only affected by noise. In presence of jammer, and in particular, in presence of a CW, all the correlators' outputs present sine waves. By comparing the model error e in the case when no interference occurs (during a training stage) by the error when an interference occurs, it is possible to detect the presence of the jammer in the signal. Indeed, the correlators' outputs are correlated when an interference (CW) occurs whereas it is not the case in presence of noise only.

The multichannel AR model is an extension of the classical model. In our application, it takes into account multiple correlator outputs. Therefore, it takes advantage of the existing correlation between the outputs in presence of interference.

Appendix A.3: Prony model

We assume that the discrete interfering signal x(n) that has to be modeled, can be written like [Castanié, 2003]:

$$x(n) = \sum_{k=1}^{p} \beta_k \, Z_k^n + e(n) \quad \textbf{(219)}$$

With :

- $\beta_k = A_k e^{j\theta_k}$
  - A_k is the amplitude of the k^{th} mode
  - θ_k is the phase in radian
- $Z_k = e^{(\alpha_k + j2\pi f_k)T}$
  - α_k is the damping coefficient
  - f_k is the frequency in Hertz
  - T is the sampling period in seconds
- p is the model order, for a real signal, the order must be even, whereas for a complex signal, the order can be odd or even. In our case, the signal (I+Q correlators outputs) is complex and the CW affects both the I and Q correlator outputs.
- $e(n)$ corresponds to the model error

The Prony model is an ARMA(p,p) model with $b_k = a_k$, $\forall\, k \in [|0; p|]$.

$$x(n) = -\sum_{k=1}^{p} a_k \, x(n-k) + \sum_{k=0}^{p} a_k \, e(n-k) \quad \textbf{(220)}$$

Proof:

If we note the model estimation:

$$\hat{x}(n) = \sum_{k=1}^{p} \beta_k \, Z_k^n \quad \textbf{(221)}$$

We can deduce:

$$\sum_{k=0}^{p} a_k \, \hat{x}(n-k) = \sum_{m=1}^{p} \beta_m \sum_{k=0}^{p} a_k \, Z_m^{n-k} = \sum_{m=1}^{p} \beta_m Z_m^n \sum_{k=0}^{p} a_k \, Z_m^{-k} \quad \textbf{(222)}$$

$$\sum_{k=0}^{p} a_k \ \hat{x}(n-k) = \sum_{m=1}^{p} \beta_m \ Z_m^n A(Z_m) \quad \textbf{(223)}$$

Where:

$$A(Z) = \sum_{k=0}^{p} a_k \ Z^{-k} = \prod_{k=1}^{p} (1 - Z^{-1} Z_k) \quad \textbf{(224)}$$

Z_m is defined as a root of A(Z), $\forall\ m \in [|0; p|]$, we have:

$$\sum_{k=0}^{p} a_k \ \hat{x}(n-k) = \sum_{m=1}^{p} \beta_m \ Z_m^n A(Z_m) = 0 \quad \textbf{(225)}$$

Therefore:

$$\sum_{k=0}^{p} a_k \ \hat{x}(n-k) = x(n) + \sum_{k=1}^{p} a_k \ x(n-k) - \sum_{k=0}^{p} a_k \ e(n-k) = 0 \quad \textbf{(226)}$$

QED.

The error criterion to minimize is [Castanié, 2003] (extended Prony model):

$$\frac{1}{N-p} \sum_{n=p}^{N-1} |E(n)|^2 = \frac{1}{N-p} \sum_{n=p}^{N-1} \left| x(n) + \sum_{k=1}^{p} a_k \ x(n-k) \right|^2 \quad \textbf{(227)}$$

Where:

- N is the number of samples

The damping and frequency coefficients are determined thanks to the following relationships:

$$\alpha_k = \frac{\ln(Z_k)}{T} \quad \textbf{(228)}$$

$$f_k = \frac{atan\left(\frac{Im(Z_k)}{Re(Z_k)}\right)}{2\pi T} \quad \textbf{(229)}$$

The β_k coefficients are provided by the following least square solution:

$$\beta = (V^H V)^{-1} V^H X \quad \textbf{(230)}$$

Where:

$$\beta = \begin{pmatrix} \beta_1 \\ \vdots \\ \beta_p \end{pmatrix} \quad \textbf{(231)}$$

$$X = \begin{pmatrix} x(0) \\ \vdots \\ x(n-1) \end{pmatrix} \quad \textbf{(232)}$$

$$V = \begin{pmatrix} 1 & 1 & \dots & 1 \\ Z_1 & Z_2 & \dots & Z_p \\ \vdots & \vdots & \ddots & \vdots \\ Z_1^{N-1} & Z_2^{N-1} & & Z_p^{N-1} \end{pmatrix} \quad \textbf{(233)}$$

V is a N by p Van der Monde matrix.

The amplitudes and phases of the modes k, are respectively:

$$A_k = |\beta_k| \quad \textbf{(234)}$$

$$\theta_k = atan\left(\frac{\mathrm{Im}(\beta_\mathrm{k})}{\mathrm{Re}(\beta_\mathrm{k})}\right) \quad \textbf{(235)}$$

Appendix A.4: Probability of interference occurrence

As it is described in Chapter 5, the interference detection algorithms can reach sufficient performances in terms of continuity. The obtained results in terms of P_{MD} cannot be discussed with regard to the integrity risk required during APV I because the probability of occurrence of interferences cannot be calculated or estimated precisely. Nevertheless, a theoretical derivation of the interference probabilities of occurrence is provided hereafter.

The probability of interference occurrence depends upon the frequency band of the signals. A frequency is said lost when the signals in the corresponding frequency band cannot be processed with the civil aviation required performances.

If H_1 denotes the event that no signal can be tracked within the corresponding frequency band B_i (in our case L_i or E_i), the probability that tracking is impossible is noted: $P(H_1|B_i)$. The opposite hypothesis, within the same band, is H_0, no interference occurs or, more precisely, no interference causes the loss of signal tracking receiver capability within this band. The probability of having such an event is thus noted: $P(H_0|B_i)$.

In a first theoretical approach, it can be assumed that tracking thresholds (different for each signal as justified in [Bastide1, 2004]) are the same for all the considered bands and that the number of potential interferers is not dependent upon the frequency band. In other words, each band has the same probability to be impacted by a jammer, that is: $P(H_1|B_i) = P(H_1|B_j)$, for i and j that indicate different frequency bands.

As proposed in [Issler, 2004], one can then derive the following relationships:

$$P(H_0|B_i) = 1 - P(H_1|B_i) = P(H_0|B_j) = 1 - P(H_1|B_j) = 1 - p_{1i} \quad \textbf{(236)}$$

$$P(H_1|B_i, H_1|B_j) = P(H_1|B_i)^2 = p_{1i}^2 \quad \textbf{(237)}$$

The events $(H_1|B_i)$ and $(H_1|B_j)$ can be supposed completely independent. Thus, in this case, the probability of jamming of B_i whereas B_j is not jammed is:

$$P(H_1|B_i, H_0|B_j) = P(H_1|B_i).P(H_0|B_j) = P(H_1|B_i).[1 - P(H_1|B_i)] \quad \textbf{(238)}$$

Another hypothesis that can be made is that GNSS frequencies have a low probability to be jammed:

$$p_{1i} \ll 1$$

Therefore:

$$P(H_1|B_i, H_0|B_j) = p_{1i} - p_{1i}^2 \# p_{1i} \quad \textbf{(239)}$$

In this thesis, the baseline is GPS L1 and L5 and Galileo E1, E5a and E5b signals. In the following, standalone GPS L1/L5 and Galileo E1/E5a/E5b are considered. Indeed, the theoretical values of the probabilities of loss of one frequency for dual and triple frequency users will be provided.

The probability to lose the dual frequency navigation in dual frequency GPS (this study do not rely on L2C) is provided by:

$$P\left(H_1 \middle| L_{15|single}\right) = P(H_1|L_1, H_0|L_5) + P(H_0|L_1, H_1|L_5) + P(H_1|L_1, H_1|L_5) \quad \textbf{(240)}$$

$$= 2\, p_{15}\,(1 - p_{15}) + p_{15}^2 = 2\, p_{15} - p_{15}^2 \;\#\; 2\, p_{15} \quad \textbf{(241)}$$

As described in [Issler, 2004], the probability of simultaneous loss of two frequencies in two different bands is negligible.

In the case of Galileo E1/E5a/E5b, the probability to have a single frequency mode can be described by:

$$\begin{aligned} &P\left(H_1 \middle| E_{15ab|single}\right) \\ &\quad = P\left(H_1 \middle| E_{1,} H_1 \middle| E_{5a}, H_0 \middle| E_{5b}\right) + P\left(H_1 \middle| E_{1,} H_0 \middle| E_{5a}, H_1 \middle| E_{5b}\right) \\ &\quad + P\left(H_0 \middle| E_{1,} H_1 \middle| E_{5a}, H_1 \middle| E_{5b}\right) + P\left(H_1 \middle| E_{1,} H_1 \middle| E_{5a}, H_1 \middle| E_{5b}\right) \end{aligned} \quad \textbf{(242)}$$

$$\begin{aligned} = P(H_1|E_1)P(H_1|E_{5a})[1 - P(H_1|E_{5b})] \\ + P(H_1|E_{5b})P(H_1|E_{5a})[1 - P(H_1|E_1)] \\ + P(H_1|E_1)P(H_1|E_{5b})[1 - P(H_1|E_{5a})] \\ + P(H_1|E_1)P(H_1|E_{5a})P(H_1|E_{5b}) \end{aligned} \quad \textbf{(243)}$$

$$= 3\, p_{15ab}^2(1 - p_{15ab}) + p_{15ab}^3 = 3\, p_{15ab}^2 - 2\, p_{15ab}^3 \;\#\; 3\, p_{15ab}^2 = 3\, p_{15ab}{}^2 \quad \textbf{(244)}$$

As for GPS L1/L5, the simultaneous total loss of the three E1, E5a, E5b frequencies is negligible.

Appendix B: Aircraft environment

Appendix B.1: Model of aircraft dynamics

Introduction

To comply with actual aircraft conditions, the embedded combined receiver is supposed to be affected by dynamics that depends on the aircraft manoeuvres. The maximum dynamics parameters are provided in [RTCA, 2002] for normal and abnormal aircraft manoeuvres (see Chapter 2). According to these figures, the aircraft dynamics are simulated during our tests, in Chapter 5, by using the following model.

Principle of the model

At the output of the correlator, the non-filtered DCO command voltage V_p is computed. This function depends on the type of discriminator used. In the case of a classical arctangent discriminator:

$$V_e(k) = \arctan\left(\frac{Q(k)}{I(k)}\right) \quad \textbf{(245)}$$

A third-order 10 Hz PLL was used in the following simulations. It is characterised by the coefficients K1, K2 and K3 which are defined in [Stephens, 1993] from the product between the PLL filter bandwidth and the time of integration.

The filtered command voltage V_{ec} is thus defined as following:

$$V_{ec}(k+1)T_S = K_1 . V_e(k) + K_2 \sum_{i=1}^{k} V_e(i) + K_3 \sum_{i=1}^{k} \sum_{j=1}^{i} V_e(j) \quad \textbf{(246)}$$

Finally, the estimated phase at the next instant is provided by:

$$\hat{\theta}(k+1) = K_{phase} . V_{ec}(k+1) + \hat{\theta}(k) \quad \textbf{(247)}$$

And the next tracking error is:

$$\varepsilon_\theta = \hat{\theta}(k+1) - \theta(k+1) \quad \textbf{(248)}$$

With:

$$\theta(k+1) = 2\pi f \tau(k+1) \quad \textbf{(249)}$$

The range is assumed to have the following variation:

$$\tau(k+1) = a_0 + a_1 . t_{k+1} + \frac{a_2}{2} . t_{k+1}^2 + \frac{a_3}{6} . t_{k+1}^3 \quad \textbf{(250)}$$

a_0, a_1, a_2, a_3 being the dynamics parameters corresponding respectively to the position of the aircraft, its ground speed, acceleration and jerk. The variations of the acceleration and jerk as a function of time are represented in the following figures.

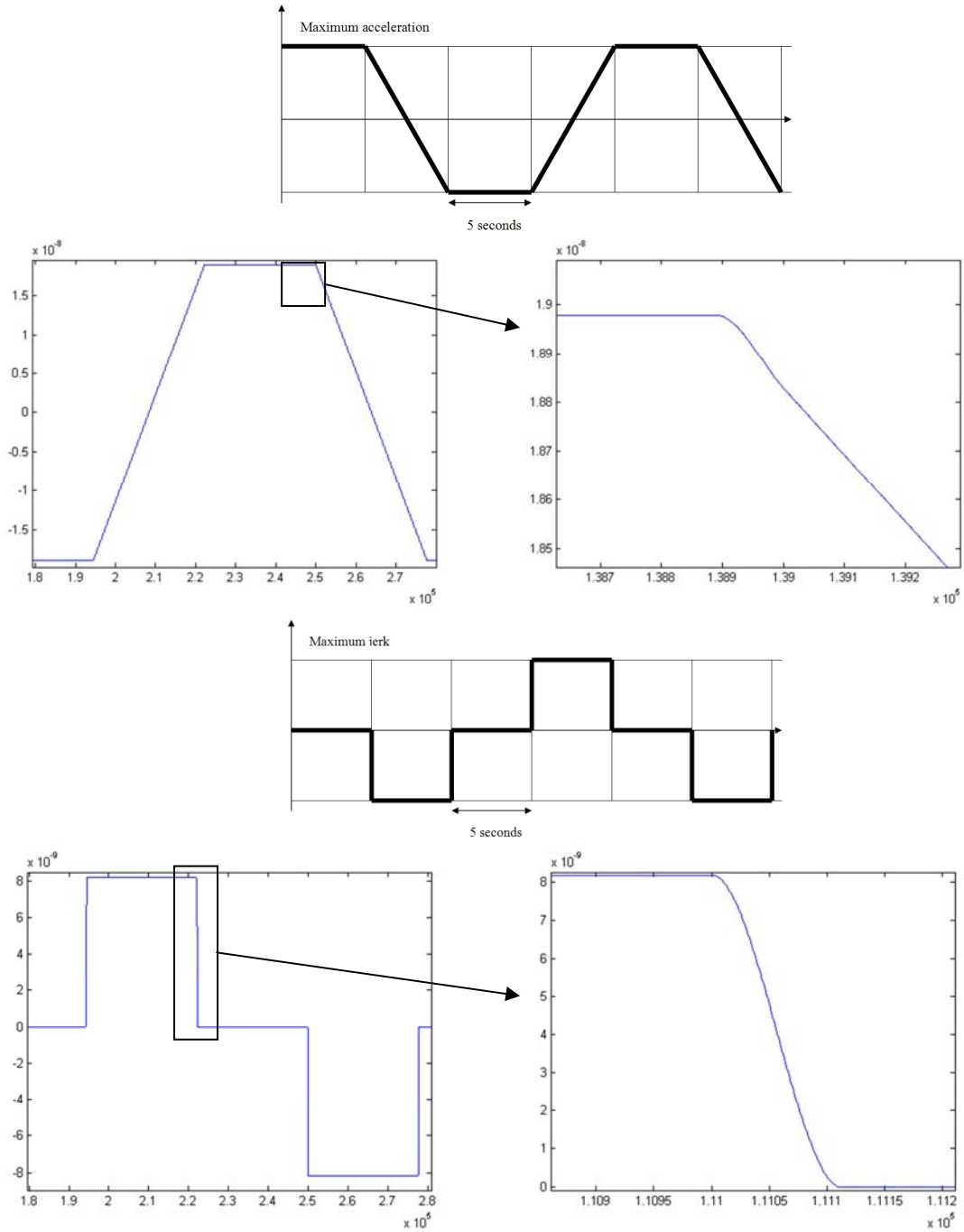

Figure 72 : Dynamics generation according to the acceleration and jerk values (divided by the speed of light)

The receiver outputs the raw code and phase tracking errors ε_τ and ε_φ. The 100 seconds code-carrier smoothed pseudorange is computed.

The code tracking loop is a 1 Hz first order DLL pushed by the PLL.

The filtered command voltage Vcc is defined by:

$$V_{cc}(k+1) = K_1 . V_e(k) + V_{ec}(k+1) . \frac{f_c}{f} \quad \textbf{(251)}$$

Finally, the time delay then becomes:

$$\hat{\tau}(k+1) = K_{code} . V_{cc}(k+1) + \hat{\tau}(k) \quad \textbf{(252)}$$

And the tracking error:

$$\varepsilon_\tau = \hat{\tau}(k+1) - \tau(k+1) \quad \textbf{(253)}$$

Where:

- $\tau(k+1) = a_0 + a_1.t_{k+1} + \frac{a_2}{2}.t_{k+1}^2 + \frac{a_3}{6}.t_{k+1}^3$
- $K_{code} = \frac{T_C}{T_S}$ is the DCO coefficient of the DLL.

In this way, the receiver outputs the raw code and phase tracking errors ε_τ and ε_θ, 100 seconds smoothed pseudorange is then estimated with the error on the smoothed pseudorange.

Appendix B.2: Multipath generation

Introduction

This appendix is dedicated to the multipath generation during the simulations presented in Chapter 5. Indeed, to comply with actual aircraft conditions, the interference detection algorithms were tested by generating interferences obviously, but also multipath. Indeed, since multipath are faded replica of the incoming useful LOS signal, it can affect the correlators outputs (secondary peaks). The model used for simulations is the aeronautical DLR model presented hereafter.

The aeronautical DLR model

For an in-flight aircraft, it has been demonstrated in [Steingass, 2004] that the wings reflection power level is very low and that the probability of occurrence of such a reflection is extremely low, so it is not considered in the model. Only the fuselage and ground reflections are taken into account.

As shown in [Steingass, 2004], a quite strong reflection close to the direct signal was identified, when analyzing the impulse response of the high resolution aeronautical channel model. It is one to two nanoseconds delayed from the direct path. This reflection has been identified and located near the antenna, on the aircraft fuselage. It was called fuselage echo. The power of this echo is estimated to -14.2 dB. Consequently, the multipath model will be composed of a ground reflection, a fuselage reflection and echo.

Fuselage:

It was noticed by the DLR that the fuselage echo is approximated very well by an exponential function: $P_{proc}(dB) = k + b_2.e^{b_3|f|}$. The DLR decided to filter out White Gaussian Noise with a transfer function filter equal to the fuselage power spectrum, this transfer function will be noticed h.

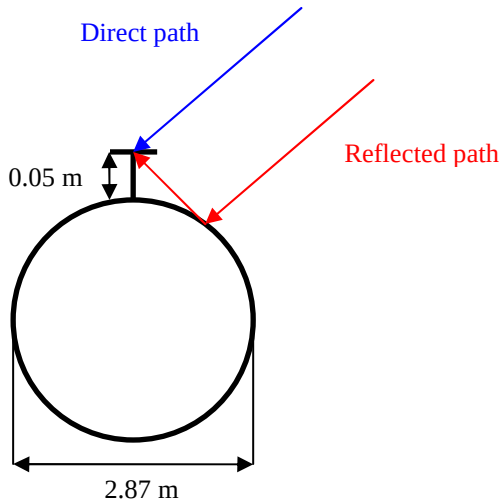

Figure 73: Multipath aircraft fuselage

Ground:

Assuming a Gauss distributed ground reflection amplitude with zero mean, the spectrum of the ground reflection is modelled by: $P_{Gr(dB)} = 20 \cdot \log\left(k \cdot e^{-\frac{f^2}{2\sigma^2}} \right)$ with a standard deviation of 3.8 Hz. The ground echo delay is depending on satellite elevation and aircraft altitude as demonstrated below:

If we consider d1 and d2 the distances shown on the figure hereafter, the delay of the ground reflection is provided geometrically by: $d_1 - d_2 = 2h\sin(\theta)$.

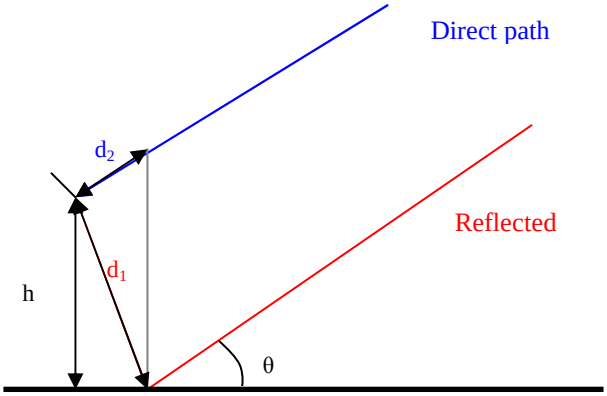

Figure 74: Multipath ground reflection

The correlator outputs depend on the multipath parameters:

- α1, α2, α3 are respectively the relative amplitudes of the ground echo, the fuselage refracted signal and the fuselage reflected signal.
- Δτ1, Δτ2, Δτ3 are the code delays of the ground echo, the fuselage refracted signal and the fuselage reflected signal.
- $\Delta\theta$1, $\Delta\theta$2, $\Delta\theta$3 are the phase shifts of the ground echo, the fuselage refracted signal and the fuselage reflected signal.

Expressions used when deriving the code and phase tracking error envelopes are only valid if the multipath parameters do not vary very fast compared to the tracking loops bandwidth.

The correlator outputs with multipath are provided for PLL by:

$$\begin{aligned} I(k) = {} & \frac{A}{2}.D(k).R(\varepsilon_\tau).\cos(\varepsilon_\theta) \\ & + A.\frac{\alpha_1}{2}.D(k).R(\varepsilon_\tau + \Delta\tau_1).\cos(\varepsilon_\theta + \Delta\theta_1) \\ & + A.\frac{\alpha_2}{2}.D(k).R(\varepsilon_\tau + \Delta\tau_2).\cos(\varepsilon_\theta + \Delta\theta_2) \\ & + A.\frac{\alpha_3}{2}.D(k).R(\varepsilon_\tau + \Delta\tau_3).\cos(\varepsilon_\theta + \Delta\theta_3) \end{aligned} \quad \textbf{(254)}$$

$$Q(k) = \frac{A}{2}.D(k).R(\varepsilon_\tau).\sin(\varepsilon_\theta)$$
$$+A.\frac{\alpha_1}{2}.D(k).R(\varepsilon_\tau + \Delta\tau_1).\sin(\varepsilon_\theta + \Delta\theta_1)$$
$$+A.\frac{\alpha_2}{2}.D(k).R(\varepsilon_\tau + \Delta\tau_2).\sin(\varepsilon_\theta + \Delta\theta_2)$$
$$+A.\frac{\alpha_3}{2}.D(k).R(\varepsilon_\tau + \Delta\tau_3).\sin(\varepsilon_\theta + \Delta\theta_3) \quad \textbf{(255)}$$

And for the DLL, the correlator outputs are:

$$I(k) = R(\varepsilon_\tau).\cos(\varepsilon_\theta) + \alpha_1.R(\varepsilon_\tau + \Delta\tau_1).\cos(\varepsilon_\theta + \Delta\theta_1) + \alpha_2.R(\varepsilon_\tau + \Delta\tau_2).\cos(\varepsilon_\theta + \Delta\theta_2) + \alpha_3.R(\varepsilon_\tau + \Delta\tau_3).\cos(\varepsilon_\theta + \Delta\theta_3) \quad \textbf{(256)}$$

$$Q(k) = R(\varepsilon_\tau).\sin(\varepsilon_\theta) + \alpha_1.R(\varepsilon_\tau + \Delta\tau_1).\sin(\varepsilon_\theta + \Delta\theta_1) + \alpha_2.R(\varepsilon_\tau + \Delta\tau_2).\sin(\varepsilon_\theta + \Delta\theta_2) + \alpha_3.R(\varepsilon_\tau + \Delta\tau_3).\sin(\varepsilon_\theta + \Delta\theta_3) \quad \textbf{(257)}$$

In [Steingass, 2004], the approach is divided into three different zones of altitude (high, mid and low altitude) in order to characterize the ground reflection which is characterized in each zone by a Markov state model. The Markov model described here is specific at Graz airport.

The multipaths were generated using a DLR model based on a measurement campaign taking into account ground and fuselage reflections. Let us describe in a few paragraphs the model in the following.

The model is composed of a direct path, plus a refractive component on this direct path, plus a strong echo on the fuselage changing very slowly and a quickly changing ground echo. The estimated parameters to inject in correlator outputs computation are the time delay, reflection power amplitude and phase of the signal replicas. Time delay and reflection power of each ray is determined from the measurement campaign.

Each approach is divided into three different zones: high, mid and low altitudes. The ground reflection is thus characterized by a Markov state in each zone. This Markov model is specific to one given airport (Graz) and must be changed for further studies.

The Markov parameters are power values, the transition matrix containing the probability of changing from each power state determined for each altitude region independently:

```
MarcovProbs = {[0.9866 0.0087 0.0047 0 ; ...
0.6087 0.3043 0.0870 0 ; ...
0.2143 0.3571 0.4286 0 ; ...
0.3333 0.3333 0.3334 0 ] ...
,...
[0.9842 0.0130 0.0028 0 ; ...
0.6667 0.2222 0.0889 0.0222; ...
0.0667 0.1167 0.5000 0.3166; ...
0 0 0.3279 0.6721] ...
,...
[0.9645 0.0310 0.0045 0 ; ...
0.7308 0.1538 0.1154 0 ; ...
```

```
0.6250 0.1250 0.2500 0 ; ...
0.3333 0.3333 0.3334 0 ] ...
,...
[1 0 0 0 ; ...
1 0 0 0 ; ...
1 0 0 0 ; ...
1 0 0 0 ]};

MarkovAtten = {[-50 -23 -19 -15],... %state 1
[-50 -23 -19 -15],... %state 2
[-50 -23 -19 -15],... %state 3
[-50 -23 -19 -15]}; %state 4 in dB

MarkovAtten = {[-18 -15 -12 -9],... %state 1
[-18 -15 -12 -9],... %state 2
[-18 -15 -12 -9],... %state 3
[-18 -15 -12 -9]}; %state 4 in dB
```

Moreover, the occurring power levels are quantized into four power levels:

	POWER IN DB	COMMENT
State 1	-15	
State 2	-19	
State 3	-23	
State 4	<-25	≈ no ground reflection

Table 16: States of the ground fading Markov model

The following figures present the multipath generation on an A 340, during landing, including the APV phase of flight.

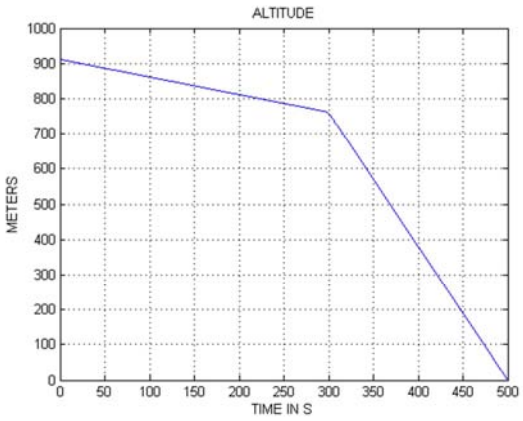

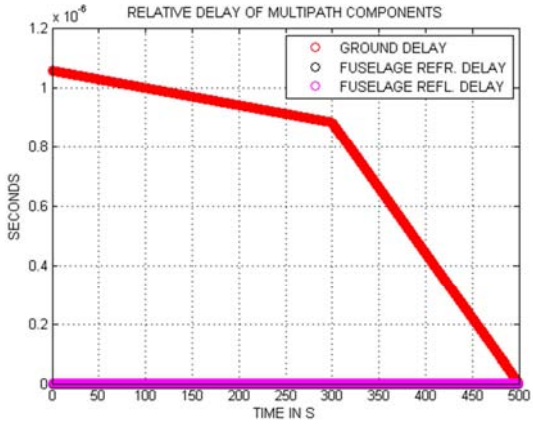

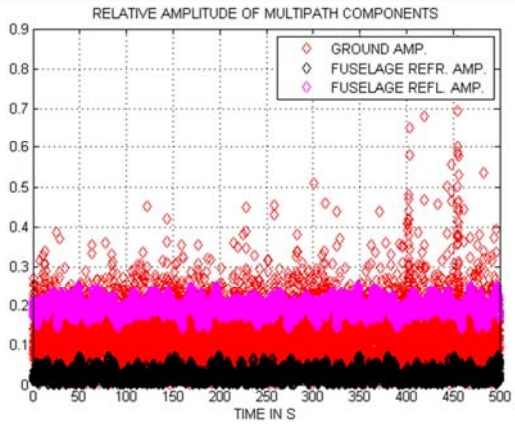

Figure 75 : Multipath generation on an A 340 over 500-seconds simulation during landing, taking into account fuselage and ground reflections

Appendix B.3: Dual frequency ionospheric error estimation

Dual frequency ionosphere-free measurements can be provided by code or carrier phase measurements on two frequencies:

$$P = \frac{f_1^2}{f_1^2 - f_2^2} P_1 - \frac{f_2^2}{f_1^2 - f_2^2} P_2 \quad \textbf{(258)}$$

$$\phi = \frac{f_1^2}{f_1^2 - f_2^2} \phi_1 - \frac{f_2^2}{f_1^2 - f_2^2} \phi_2 \quad \textbf{(259)}$$

Indeed, two code pseudorange measurements at two different frequencies can be modeled as:

$$P_1 = \rho + c(\Delta t_u - \Delta t) + c(I_1 + \tau) + D_{mult} + n \quad \textbf{(260)}$$

$$P_2 = \rho + c(\Delta t_u - \Delta t) + c(I_2 + \tau) + D_{mult} + n \quad \textbf{(261)}$$

And then:

$$P_1 - P_2 = c(I_1 - I_2) \quad \textbf{(262)}$$

The ionospheric code delay can be modeled as a function of the signal carrier frequency as it is described in Chapter 2:

$$I_1 = + \frac{40.3}{f_1^2} TEC \quad \textbf{(263)}$$

$$I_2 = + \frac{40.3}{f_2^2} TEC \quad \textbf{(264)}$$

As a consequence:

$$I_1 . f_1^2 = I_2 . f_2^2 \quad \textbf{(265)}$$

And so:

$$P_1 . f_1^2 - [\rho + c(\Delta t_u - \Delta t) + c(\tau) + D_{mult} + n]. f_1^2 = P_2 . f_2^2 - [\rho + c(\Delta t_u - \Delta t) + c(\tau) + D_{mult} + n]. f_2^2 \quad \textbf{(266)}$$

Then:

$$P = \rho + c(\Delta t_u - \Delta t) + c(\tau) + D_{mult} + n = \frac{f_1^2}{f_1^2 - f_2^2} P_1 - \frac{f_2^2}{f_1^2 - f_2^2} P_2 \quad \textbf{(267)}$$

The same demonstration can be made with carrier phase measurements.

Appendix C: Receivers and signals characteristics

Appendix C.1: Receivers classes

EUROCAE WG-62 is tasked with developing MOPS for Galileo receivers. EUROCAE WG-62 is also pursuing the objective to define jointly with RTCA SC-159 a combined GPS/Galileo receiver MOPS which will include SBAS and ABAS, and in conjunction with EUROCAE WG-28, to consider the existing standards related to precision approach and if appropriate update these standards to take account of GALILEO use (including joint GALILEO/GPS/SBAS use).
Under this context, a combined GPS/Galileo receiver can have different definitions according to ones vision.

Operational classes [EUROCAE, 2007]

The Class 1 equipment supports oceanic and domestic en-route, terminal, non-precision approach, approach with vertical guidance (APV-I and II), and departure operations.

The Class 2 equipment supports oceanic and domestic en-route, terminal, non-precision approach, approach with vertical guidance (APV-I and II), Category I precision approach, and departure operations.

The Class 3 equipment supports precision approach operation for Category I/II/IIIA/IIIB operations. This class of equipment is intended to serve as an alternative to existing precision approach equipment such as ILS but may also provide enhanced capabilities such as curved or segmented approaches.

Functional classes [EUROCAE, 2007]

Class Beta equipment consists of a GNSS sensor that determines position (with integrity) and provides position and integrity data to an integrated navigation system (such as flight management system and multi-sensor navigation system). The following figure illustrates the class beta architecture described in [EUROCAE, 2007].

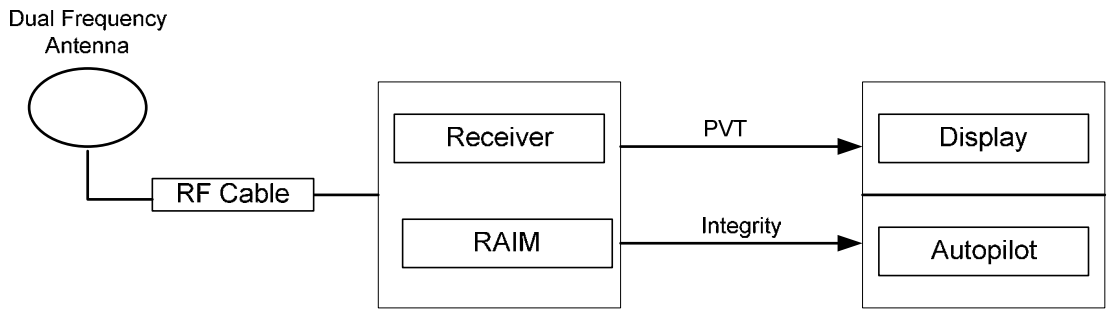

Figure 76: Class Beta Architecture [EUROCAE, 2007]

Class Delta equipment consists of both the GNSS position sensor (defined by Class Beta) and a navigation function, so that the equipment provides path deviations relative to a selected path. Class Delta does not provide a database or direct pilot controls. The Delta class of equipment is only applicable to Class 2 and Class 3 precision approach, providing an alternative to Instrument Landing System (ILS). The figure below illustrates the class delta architecture described in [EUROCAE, 2007].

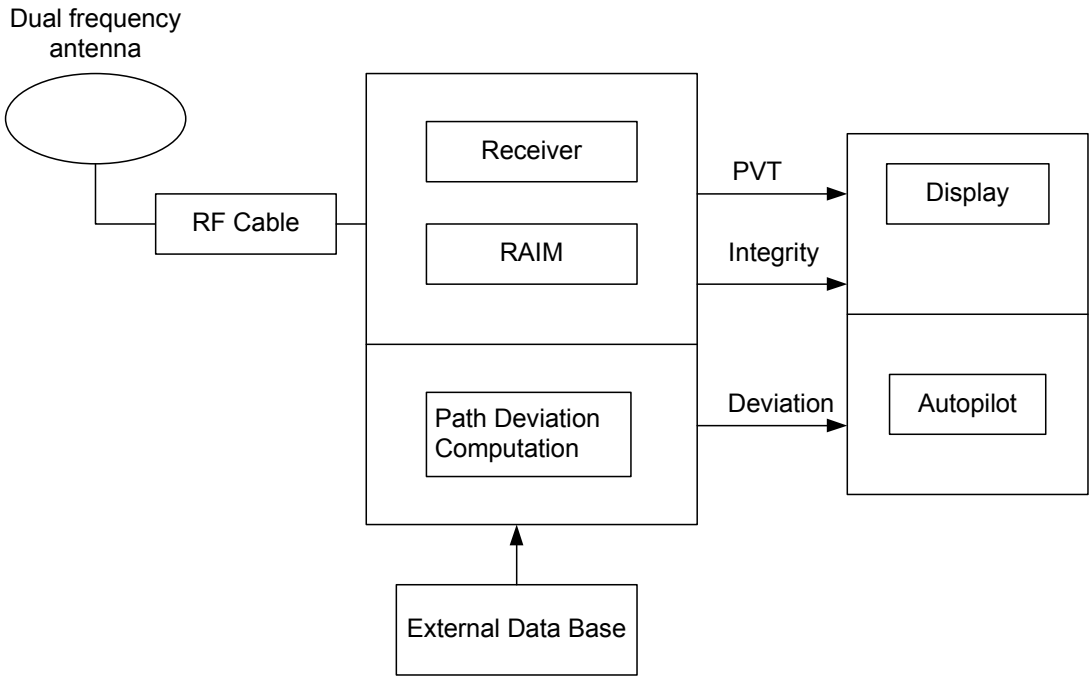

Figure 77: Class Delta Architecture [EUROCAE, 2007]

The Class Gamma functional class, incorporating the navigation function, data base, displays and controls is not covered by [EUROCAE, 2007]. Receivers which combine these functions with the sensor may be developed but the navigation function will be covered by a separate MOPS, such as that developed by RTCA SC-181.

As recalled in chapter 3, table 3, the operational GNSS components combinations are identified by mode of operation and for en route down to APV I phases of flight. Based on the expected levels of performance that can be achieved with different signal combinations, the following combinations are defined in [EUROCAE, 2007]:

	FUNCTIONNAL CLASS ALPHA	FUNCTIONNAL CLASS DELTA
OPERATIONAL CLASS 1	Mode A: Galileo only	
OPERATIONAL CLASS 2	Mode B: GPS only + GPS SBAS Mode C: Galileo + GPS + GPS SBAS	Mode D: Galileo + GPS + GPS SBAS

Table 17: Combinations to be standardized [EUROCAE, 2007].

In [RTCA, 2006], some receiver classes are only simple sensors as depicted in the following figure.

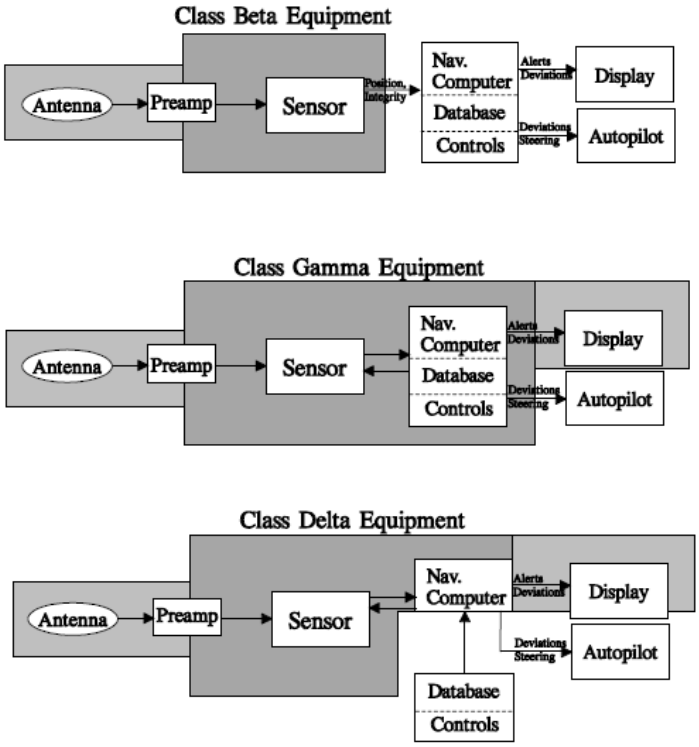

Figure 78: Receivers functional classes as defined in [RTCA, 2006].

Appendix C.2: L1 C/A and E1 OS high amplitude code spectrum lines

The worst code spectrum lines in terms of power level, for each signal are given hereafter and provided for each PRN. These power levels take into account the PRN code FFT and the Fourier transform of the materialization waveform. These values are obtained by generating PRN code values, then computing the spectrum of the transmitted waveforms and comparing all code spectrum lines of GPS L1 C/A and future Galileo E1 OS signals.

Below are identified the amplitudes (AMPL) and frequency (FREQ) of the worst code spectrum lines for each PRN of GPS L1 C/A and Galileo E1 OS code. The amplitude values presented are the power level with regard to the full signal power level.

C/A CODE PRN N°	WORST LINE FREQ (KHZ)	WORST LINE AMPL (DB)	C/A CODE PRN N°	WORST LINE FREQ (KHZ)	WORST LINE AMPL (DB)
1	42	-22.71	20	30	-22.78
2	263	-23.12	21	55	-23.51
3	108	-22.04	22	12	-22.12
4	122	-22.98	23	127	-23.08
5	23	-21.53	24	123	-21.26
6	227	-21.29	25	151	-23.78
7	78	-23.27	26	102	-23.06
8	66	-21.50	27	132	-21.68
9	173	-22.09	28	203	-21.73
10	16	-22.45	29	176	-22.22
11	123	-22.64	30	63	-22.14
12	199	-22.08	31	72	-23.13
13	214	-23.52	32	74	-23.58
14	120	-22.01	33	82	-21.82
15	69	-21.90	34	55	-24.13
16	154	-22.58	35	43	-21.71
17	138	-22.50	36	23	-22.23
18	183	-21.40	37	55	-24.13
19	211	-21.77			

Table 18 : Worst line characteristics for each PRN for GPS C/A code.

CODE PRN N°	WORST LINE FREQ (KHZ)	WORST LINE AMPL (DB)	C/A CODE PRN N°	WORST LINE FREQ (KHZ)	WORST LINE AMPL (DB)
1	697.75	-30.06	26	808	-29.43
2	768	-30.25	27	859.5	-31.43
3	729	-31.00	28	729.25	-29.59
4	815.5	-29.75	29	827	-30.47
5	587.25	-30.89	30	732.5	-30.87
6	734	-29.91	31	930.25	-30.53
7	634.75	-31.02	32	854	-30.25
8	921.25	-30.04	33	726	-30.06
9	618.75	-31.02	34	746.25	-31.04
10	647.5	-31.05	35	558.25	-30.60
11	855.25	-30.71	36	579.75	-30.17
12	823	-30.67	37	593.75	-30.25
13	884	-30.91	38	673.5	-28.81
14	802.75	-30.48	39	866.75	-30.33
15	562.5	-29.87	40	617.75	-29.50
16	565	-29.91	41	580.75	-30.92
17	776	-31.26	42	690.25	-30.69
18	685.75	-30.86	43	714.75	-31.29
19	979.5	-31.16	44	812	-30.04
20	100.525	-30.91	45	663.75	-29.64
21	602	-31.11	46	751	-30.01
22	871.25	-30.35	47	745.5	-30.52
23	740.75	-30.40	48	854.5	-30.73
24	722.25	-30.97	49	522.75	-30.10
25	827.25	-31.24	50	629.75	-29.71

Table 19: Worst line characteristics for each PRN for GALILEO E1 code.

END OF DOCUMENT